THE JOURNAL
OF
CHEMICAL PHYSICS

VOLUME 19, NUMBER 10 OCTOBER, 1951

The Compressibility of Gaseous Xenon. I. An Equation of State for Xenon and the Weight of a Liter of Xenon

JAMES A. BEATTIE, ROLAND J. BARRIAULT, AND JAMES S. BRIERLEY
Department of Chemistry, Massachusetts Institute of Technology, Cambridge, Massachusetts
(Received June 4, 1951)

The compressibility of xenon containing 0.14 mole percent of krypton has been measured from 16.65° (the critical temperature) to 300°C and over the density range 1 to 10 mole per liter. The constants of the Beattie-Bridgeman equation of state for the sample used and for pure xenon have been determined from these measurements. The constants for pure xenon are $R=0.08206$, $A_0=4.6715$, $a=0.03311$, $B_0=0.07503$, $b=0$, $c=30.02\times10^4$ in units of normal atmos, liter per mole, and °K (T°K$=t$°C$+273.13$). The weight of one liter of Xe at a pressure of one standard atmosphere is calculated from its molecular weight (131.3) and the above parameters to be 5.897 g per liter at 0°C and 5.467 g per liter at 70°F.

RECENTLY the noble gases have become available in quantity and in a state of high purity. When the present investigation of the compressibility of xenon was begun the details of final purification and especially of accurate analysis had not been worked out to as successful conclusion as at the present time. However the xenon used in the present investigation contained far less impurity than any heretofore available.

Ramsay and Travers[1] studied the compressibility of Xe at 11.2°C to 50 atmos and at 237.3°C to 100 atmos. The present measurements were made on a sample of Xe containing 0.14 mole percent Kr and cover the temperature range 16.65° (the critical temperature) to 300°C and the density range 1 to 10 mole per liter, the maximum pressure being 406 atmos.

We are greatly indebted to Dr. John M. Gaines, Dr. Roger H. Gillette, and the Linde Air Products Company for the gift of the sample of Xe used in the present investigation, and to the Linde Air Products Company for a grant-in-aid that made the work possible.

The procedure for controlling the temperature and density of the gas and the method of measuring mass, volume, pressure, and temperature have been described elsewhere[2] and are the same as those employed for the study of the compressibilities of a number of hydrocarbons and their mixtures.[3] For the measurements on Xe the all-steel bomb having a volume of about 200 ml was used.

In our procedure we inject sufficient mercury into the bomb holding the gas so that at each temperature the pressures are read for the same molar density of gas. This compressor setting depends then on the mass of gas in the bomb and its molecular weight. The latter is affected by the purity of the gas. The sample of Xe used in the present work weighed 22.28615 grams. The measurements were completed on the assumption that the gas was pure Xe and had a molecular weight of 131.3. When $B(V, T)$ defined by the relation,

$$B(V, T)=V(pV-RT),$$

was plotted at each temperature against molar density $(1/V)$ the curves for xenon (and to a greater extent those for krypton) did not approach linearity as the density approached zero. This indicated an error in RT or in V, the molar volumes used. Since RT was calculated for the absolute thermodynamic (not the International) temperature scale we suspected the molecular weight used. This could be in error because of an incorrect atomic weight for Xe, or because of an impurity in the gas.

In the meantime Dr. Gillette made an analysis of the gas in one of the unused ampules on a mass spectrometer

[1] W. Ramsay and M. W. Travers, Phil. Trans. Royal Soc. (London), **A197**, 47 (1901).
[2] J. A. Beattie, Proc. Am. Acad. Arts and Sci. **69**, 389 (1934).
[3] For the last reports on this work see Beattie, Marple, Jr., Edwards, J. Chem. Phys. **18**, 127 (1950); J. A. Beattie and S. Marple, Jr., J. Am. Chem. Soc. **72**, 4143 (1950).

TABLE I. Comparison of the pressures calculated from the equation of state with the observed pressures for gaseous xenon.

(For each temperature the first line gives the observed pressure and the second line gives the observed pressure minus the pressure calculated from the equation given in Table II. The critical constants of xenon are approximately: $t_c = 16.65$°C, $p_c = 57.89$ atmos, $d_c = 8.32$ mole per liter.)

Density, mole/liter		1.0	1.5	2.0	2.5	3.0	3.5	4.0	4.5	5.0	6.0	7.0	8.0	9.0	10.0
Temp., °C (Int.)		Pressure, standard atmosphere													
16.65	obsd.	20.667	28.817	35.652	41.292	45.853	49.467	52.224	54.226	55.720	57.29	57.78	57.88	57.91	58.02
	obsd.-calc.	−0.067	−0.150	−0.257	−0.367	−0.465	−0.518	−0.534	−0.472	−0.303	0.38	1.37	3.16	4.67	5.46
25	obsd.	21.443	30.040	37.366	43.537	48.670	52.872	56.282	59.000	61.140	64.12	65.97	67.32	68.60	70.38
	obsd.-calc.	−0.045	−0.111	−0.193	−0.277	−0.345	−0.391	−0.376	−0.300	−0.151	0.40	1.23	2.17	2.83	3.00
50	obsd.	23.731	33.652	42.418	50.131	56.909	62.864	68.086	72.691	76.776	83.79	89.82	95.58	101.69	109.39
	obsd.-calc.	−0.007	−0.025	−0.049	−0.079	−0.099	−0.101	−0.097	−0.073	−0.035	0.07	0.11	−0.05	−0.59	−1.10
75	obsd.	26.007	37.223	47.387	56.619	64.959	72.575	79.550	85.989	91.970	103.01	113.41	123.93	135.57	149.13
	obsd.-calc.	0.029	0.041	0.051	0.076	0.051	0.040	0.020	−0.007	−0.067	−0.26	−0.64	−1.30	−2.07	−2.98
100	obsd.	28.268	40.759	52.290	62.957	72.880	82.128	90.837	99.071	106.952	122.03	136.87	152.36	169.60	189.82
	obsd.-calc.	0.056	0.087	0.115	0.129	0.143	0.121	0.092	0.015	−0.094	−0.46	−1.05	−1.82	−2.53	−2.79
125	obsd.	30.512	44.262	57.152	69.262	80.702	91.573	101.983	112.008	121.753	140.87	160.19	180.76	203.63	230.35
	obsd.-calc.	0.072	0.113	0.159	0.186	0.189	0.168	0.303	0.022	−0.136	−0.59	−1.23	−1.89	−2.35	−1.93
150	obsd.	32.741	47.744	61.973	75.505	88.460	100.918	113.000	124.814	136.446	159.60	183.45	208.98	237.61	270.92
	obsd.-calc.	0.076	0.127	0.180	0.204	0.211	0.173	0.102	−0.001	−0.160	−0.64	−1.21	−1.75	−1.71	−0.38
175	obsd.	34.967	51.211	66.754	81.710	96.150	110.161	123.943	137.533	151.014	178.22	206.49	237.25	271.61	311.41
	obsd.-calc.	0.081	0.133	0.174	0.208	0.197	0.120	0.067	−0.034	−0.208	−0.64	−1.18	−1.27	−0.66	1.60
200	obsd.	37.194	54.673	71.552	87.883	103.838	119.458	134.892	150.195	165.564	196.78	229.62	265.35	305.38	351.84
	obsd.-calc.	0.089	0.140	0.196	0.197	0.207	0.157	0.086	−0.061	−0.196	−0.59	−0.89	−0.72	0.47	3.92
225	obsd.	39.412	58.127	76.308	94.056	111.473	128.683	145.733	162.810	179.984	215.23	252.54	293.30	338.70	391.86
	obsd.-calc.	0.090	0.144	0.184	0.200	0.184	0.150	0.035	−0.085	−0.250	−0.55	−0.68	−0.13	1.40	6.16
250	obsd.	41.637	61.584	81.082	100.208	119.118	137.871	156.634	175.428	194.476	233.74	275.57	321.39	372.92	
	obsd.-calc.	0.099	0.154	0.196	0.193	0.188	0.130	0.076	−0.065	−0.180	−0.37	−0.24	0.76	3.44	
275	obsd.	43.860	65.026	85.825	106.346	126.709	147.015	167.371	187.963	208.811	252.06	298.51	349.18	406.15	
	obsd.-calc.	0.108	0.153	0.184	0.181	0.151	0.085	−0.022	−0.095	−0.225	−0.32	0.20	1.46	4.66	
300	obsd.	46.057	68.457	90.557	112.456	134.290	156.129	178.146	200.418	223.184	270.43	321.16	377.08		
	obsd.-calc.	0.092	0.143	0.166	0.148	0.116	0.026	−0.060	−0.176	−0.196	−0.16	0.43	2.39		
Av. dev. (atmos)		0.070	0.117	0.162	0.188	0.196	0.168	0.144	0.108	0.169	0.42	0.82	1.45	2.28	2.93
Av. percent dev.		0.21	0.25	0.28	0.29	0.28	0.23	0.20	0.14	0.15	0.31	0.69	1.15	1.71	2.23

Total average deviation (atmos), 0.611; total average percent deviation, 0.546.
Total average deviation (atmos) from 1 to 8 mole/liter, 0.334; total average percent deviation from 1 to 8 mole/liter, 0.349.

and found that the sample of Xe contained 0.105 mole percent Kr but Ne, A, O_2, and N_2 were not detected although looked for. At this time we were using 83.8 as the molecular weight of Kr since we believed that the atomic weight of Kr was too small by 0.1 unit. This gave 131.250 (=0.99895×131.3+0.00105×83.8) for the average molecular weight of the sample, a difference of 0.050 from the value used in computing the mercury compressor settings to give integer and half-integer gas densities in the bomb. Subsequently a second analysis of a sample of the gas actually used in the compressibility runs was found by Dr. Gillette to contain 0.14±0.01 mole percent Kr. If we use the accepted atomic weight for Kr, 83.7, we find the molecular weight of the sample of Xe to be 131.233 (=0.9986×131.3 +0.0014×83.7). The accepted atomic weight of Kr is used here since the measurements of the compressibility of Kr were reasonably well correlated on this basis, the earlier discrepancies in the values of $B(V, T)$ for Kr being explained by the presence of some Xe.

The original pressures were measured for gas densities computed on the basis of a molecular weight of 131.3 for Xe. From these a value of $B(V, T)$ was computed for each point the corresponding molar volume being computed on a basis of a molecular weight of 131.250 for the gas in the bomb, that is, each density was multiplied by the factor 131.3/131.250=1.00038095. The values of $B(V, T)$ corresponding to integer and half-integer densities at each temperature were then obtained by interpolation without smoothing. This was possible since the change in any one density was only 0.038 percent. The pressures so obtained are listed in Table I.

On the basis of the latest analysis the molecular

TABLE II. Constants of the Beattie-Bridgeman equation of state for xenon.

$p=[RT(1-\epsilon)/V^2][V+B]-A/V^2$, $A=A_0(1-a/V)$, $B=B_0(1-b/V)$, $\epsilon=c/VT^3$

Units: standard atmosphere, liter per mole, °K(T°K = t°C + 273.13)

Composition in mole percent	R	A_0	a	B_0	b	c	Molecular weight
99.86 percent Xe, 0.14 percent Kr	0.08206	4.6678	0.03310	0.07500	0	30.00×10^4	...
100 percent Xe	0.08206	4.6715	0.03311	0.07503	0	30.02×10^4	131.3

weight of the sample was 131.233 which would change each density by 0.013 percent and the corresponding pressure from 0.01 percent to 0.02 percent at a maximum. This is well within the accuracy of the measurements which may be placed in the range 0.05 percent to 0.10 percent.

The constants of the Beattie-Bridgeman equation of state for the mixture are given in Table II. We used the value 273.13 for the Kelvin temperature of the ice point for the purpose of fitting the equation to the measurements because it has been used for all of the other gases to which the equation has been applied. From these equation of state constants, the final analysis of the mixture, and the constants for krypton[4] we computed the constants for pure Xe from the relations[5]

$$\begin{aligned}
A_{0m}&=(x_1A_{01}^{\frac{1}{3}}+x_2A_{02}^{\frac{1}{3}})^2\\
B_{0m}&=\tfrac{1}{4}(x_1B_{01}+x_2B_{02})\\
&\quad+\tfrac{3}{4}(x_1B_{01}^{\frac{1}{3}}+x_2B_{02}^{\frac{1}{3}})(x_1B_{01}^{\frac{2}{3}}+x_2B_{02}^{\frac{2}{3}}) \qquad (1)\\
c_m&=(x_1c_1^{\frac{1}{3}}+x_2c_2^{\frac{1}{3}})^2\\
a_m&=x_1a_1+x_2a_2\\
b_m&=x_1b_1+x_2b_2,
\end{aligned}$$

where the subscripts m, 1, 2 denote the mixture, Xe, Kr, respectively; and x is the mole fraction of a constituent. The constants for pure Xe are also listed in Table I. In this computation we took $x_1=0.9986$ and $x_2=0.0014$, the values given by the latest analysis of the gas sample.

WEIGHT OF A LITER OF XENON AT ONE ATMOSPHERE PRESSURE

The results of the calculation of the weight of one liter of Xe under a pressure of one standard atmosphere at 0°C and at 70°F are given in Table III. The molar volume V at 1 atmos was computed from the equation

$$V=RT+\beta/V+\gamma/V^2 \quad (p=1 \text{ atmos}), \qquad (2)$$
$$\beta=RTB_0-A_0-Rc/T^2,$$
$$\gamma=A_0a-RB_0c/T^2,$$

the virial coefficients being evaluated from the values of the constants listed in Table I. Two separate calculations were made. One was based on RT and T_0 obtained from $R=0.08206$ and $T_0=273.13$. In the second the same values of the virial constants were used but the leading term RT was evaluated from Birge's[6] value

TABLE III. Weight of one lifter of xenon at a pressure of one standard atmosphere.

See Eq. (2) β atmos.-l²/mole²	γ atmos.-l³/mole³	V^a liter/mole	m^a g/liter	V^b liter/mole	m^b g/liter
		$t=0$°C			
−3.3201	+0.130	22.2642	5.897	22.2652	5.897
		$t=70$°F			
−3.1444	+0.133	24.0147	5.467	24.0150	5.467

Molecular weight of Xe = 131.3 g/mole.
[a] Based on $RT=22.4130$ at 0°C and $RT=22.4154$ at 70°F.
[b] Based on $RT=22.4140$ at 0°C and $RT=24.1457$ at 70°F.

$RT_0=22.4140$ liter-atmos per mole and the Kelvin temperature derived from the work of this laboratory

$$T°K=273.16+t+(t/100)(t/100-1)(0.04217-7.481\times10^{-5}t), \quad t=t°C \text{ (Int)}, \quad 0°<t<450°C$$

and mentioned by Stimson[7] in his report on the International Temperature Scale of 1948. The two values of the weight of a liter agree to 3×10^{-4} g at 0° and 1×10^{-4} g at 70°F.

[4] Beattie, Brierley, and Barriault, to be published.
[5] See J. A. Beattie, Chem. Phys. 44, 141 (1949).
[6] R. T. Birge, Revs. Modern Phys. 13, 233 (1941).
[7] H. F. Stimson, J. Research Natl. Bur. Standards 42, 209 (1949).

The Compressibility of Gaseous Xenon. II. The Virial Coefficients and Potential Parameters of Xenon

JAMES A. BEATTIE, ROLAND J. BARRIAULT, AND JAMES S. BRIERLEY
Department of Chemistry, Massachusetts Institute of Technology, Cambridge, Massachusetts

(Received June 4, 1951)

The second and third virial coefficients of xenon have been determined from our compressibility measurements over the temperature range 16.65° (the critical temperature) to 300°C. They are listed in Table II. The parameters of the Lennard-Jones (6, 12) potential for xenon are $\mu=5.583\times10^{-58}$ erg-cm^6, $\lambda=2.514\times10^{-102}$ erg-cm^{12}, $\epsilon=309.9\times10^{-16}$ erg, $b_0=84.65$ cm^3 per mole, $\theta=224.5$°K, $\sigma=4.064\times10^{-8}$ cm, $r_0=4.561\times10^{-8}$ cm. The representation of the second virial coefficient is quite satisfactory. The third virial coefficients agree moderately well with the theoretical values for the Lennard-Jones (6, 12) potential tabulated by Bird, Spotz, and Hirschfelder for $(T/\theta)>1.5$ but diverge rapidly as the temperature approaches the critical. The observed second virial coefficients agree moderately well with the values tabulated by Buckingham and Corner for an inverse sixth power attractive and an exponential repulsive potential when the calculated values are read from the table for the parameters given by Kane from data on the solid state of xenon and from Born and Mayer's value of the exponent derived for neon.

IN the first paper[1] of this series we presented the results of a study of the compressibility of gaseous xenon from 16.65° (the critical temperature) to 300°C and over the density range 1 to 10 moles per liter. The gas contained 0.14 mole percent krypton, and all of the results reported in the present paper refer to this mixture.

From each observation we computed the quantity,

$$B(V, T)=V(pV-RT), \tag{1}$$

which is listed under the heading "observed" in Table I. As explained in the earlier paper these values of $B(V, T)$ yield the pressures given in Table I of Part I to the number of significant places retained in the pressure, but the converse is not necessarily true. In the application of Eq. (1) the value of RT used was[2]

$$RT=22.4140T/T_0 \text{ liter-atmos/mole}, \tag{2}$$

where T_0 is 273.16° and T is on the Kelvin scale, which is related to the International temperature t through the relation,

$$T=t+273.16+(t/100)(t/100-1)(0.04217 -7.481\times10^{-5}t) \quad 0°<t<450°, \tag{3}$$

found in this laboratory.[3]

The virial form of the equation of state of one mole of a gas may be written in the approximate, closed form:

$$pV=RT+B(T)/V+C(T)/V^2+D(T)/V^4, \tag{4}$$

where $B(T)$ and $C(T)$ are the second and the third virial coefficients, respectively; and the rest of the series is summed by the single term in the fourth power of the density. Comparison of Eqs. (1) and (4) gives

$$B(V, T)=B(T)+C(T)/V+D(T)/V^3. \tag{5}$$

We determined $B(T)$, $C(T)$, and $D(T)$ from the entries in Table 1 for each isotherm by the method of least squares. These parameters are entered in Table II, and the deviations of the values of $B(V, T)$ calculated by Eq. (5) with these parameters from the observed values are given in Table I. Although all the deviations are positive at the lowest density, they are within the experimental error of the measurements. Thus at 25° and 1 mole per liter the observed pressure is 21.443 atmos while that computed from Eqs. (4) and (1) is 21.428 atmos, a deviation of 0.015 atmos or 0.07 percent which is just about the limit of the precision of the measurements. The accuracy of the results is affected also by the uncertainty in the atomic weight of xenon and in the analysis of the sample used.

SECOND AND THIRD VIRIAL COEFFICIENTS FROM THE LENNARD-JONES (6,12) POTENTIAL

Classical statistical mechanics gives for the pV product of one mole of a gas an expansion containing all powers of the density:

$$pV=RT(1+B'(T)/V +C'(T)/V^2+D'(T)/V^3+\cdots). \tag{6}$$

The second virial coefficient $B'(T)$ of a gas composed of molecules of spherical symmetry is given by

$$B'(T)=2\pi N\int_0^\infty (1-e^{-u(r)/kT})r^2dr, \tag{7}$$

where N is Avogadro's number, $u(r)$ the mutual potential energy of a pair of molecules of separation r, and k is Boltzmann's constant. Corrections for quantum effects in the case of xenon are negligibly small for temperatures above the critical point.

One expression for $u(r)$ that has received considerable attention is the Lennard-Jones[4] (6, 12) potential:

[1] Beattie, Barriault, and Brierley, J. Chem. Phys. **19**, 1227 (1951).
[2] R. T. Birge, Revs. Modern Phys., **13**, 233 (1941).
[3] See the report on the International Temperature Scale of 1948 by H. F. Stimson, J. Research Natl. Bur. Standards **42**, 209 (1949).
[4] J. E. Lennard-Jones, Proc. Roy. Soc. (London), **A106**, 463 (1924); Physica, 4, 941 (1937); R. H. Fowler, *Statistical Mechanics* (The Macmillan Company, New York, 1936), Chapter X.

TABLE I. Values of $B(V, T)$ for xenon. $B(V, T)=V(pV-RT)$ (observed), $B(V, T)=B(T)+C(T)/V+D(T)/V^3$ (calculated, see Table II).

Temp., °C(Int.)		16.65	25	50	75	100	125	150	175	200	225	250	275	300
Temp., °K		289.804	298.152	323.150	348.153	373.160	398.170	423.183	448.198	473.214	498.231	523.248	548.264	573.278
RT, liter-atmos/mole		23.7797	24.4647	26.5159	28.5675	30.6194	32.6716	34,7241	36.7767	38.8293	40.8821	42.9348	44.9875	47.0400
Density, mole/liter							$B(V, T)$, liter²-atmos/mole²							
1	obs.	−3.11246	−3.02180	−2.78489	−2.56046	−2.35134	−2.15942	−1.98288	−1.80935	−1.63492	−1.47085	−1.29824	−1.12780	−0.98317
	obs.-calc.	+0.01325	+0.01441	+0.00708	+0.00616	+0.00840	+0.00823	+0.00561	+0.00704	+0.00903	+0.00848	+0.01183	+0.01883	+0.01003
1.5	obs.	−3.04539	−2.95874	−2.72064	−2.50152	−2.29766	−2.10912	−1.92973	−1.75739	−1.58692	−1.42052	−1.25232	−1.09117	−0.93444
	obs.-calc.	+0.00494	+0.00331	+0.00106	−0.00112	−0.00107	−0.00280	−0.00180	−0.00101	−0.00234	−0.00070	−0.00055	−0.00220	+0.00078
2	obs.	−2.97673	−2.89091	−2.65334	−2.43692	−2.23719	−2.04781	−1.86883	−1.69989	−1.52671	−1.36412	−1.19698	−1.03759	−0.88084
	obs.-calc.	−0.00173	−0.00295	−0.00185	−0.00277	−0.00390	−0.00305	−0.00177	−0.00393	−0.00199	−0.00411	−0.00429	−0.00709	−0.00453
2.5	obs.	−2.90511	−2.81991	−2.58535	−2.36791	−2.17473	−1.98632	−1.80887	−1.63710	−1.47640	−1.30394	−1.14068	−0.97962	−0.82313
	obs.-calc.	−0.00539	−0.00592	−0.00398	−0.00004	−0.00491	−0.00344	−0.00311	−0.00209	−0.00620	−0.00450	−0.00800	−0.00865	−0.00697
3	obs.	−2.83182	−2.74709	−2.51537	−2.30484	−2.10868	−1.92368	−1.74581	−1.57561	−1.40555	−1.24144	−1.07627	−0.91710	−0.75889
	obs.-calc.	−0.00731	−0.00695	−0.00400	−0.00328	−0.00257	−0.00307	−0.00187	−0.00224	−0.00269	−0.00352	−0.00476	−0.00700	−0.00444
3.5	obs.	−2.75612	−2.67384	−2.44420	−2.23770	−2.04405	−1.85943	−1.68293	−1.51488	−1.34243	−1.17584	−1.01231	−0.85236	−0.69480
	obs.-calc.	−0.00674	−0.00740	−0.00269	−0.00251	−0.00193	−0.00155	−0.00144	−0.00395	−0.00191	−0.00058	−0.00335	−0.00473	−0.00391
4	obs.	−2.68093	−2.59857	−2.37359	−2.17003	−1·97752	−1.79397	−1.61856	−1.44772	−1.27661	−1.11220	−0.94409	−0.78621	−0.62585
	obs.-calc.	−0.00659	−0.00564	−0.00177	−0.00125	+0.00029	+0.00063	−0.00026	−0.00018	+0.00042	−0.00092	+0.00070	−0.00292	−0.00071
4.5	obs.	−2.60456	−2.52303	−2.30274	−2.10196	−1.91190	−1.72909	−1.55282	−1.38086	−1.21172	−1.04490	−0.87798	−0.71510	−0.55615
	obs.-calc.	−0.00514	−0.00341	−0.00044	+0.00034	+0.00123	+0.00160	+0.00145	+0.00220	+0.00049	+0.00087	+0.00080	+0.00170	+0.00077
5	obs.	−2.52715	−2.44736	−2.23212	−2.03470	−1.84597	−1.66420	−1.48698	−1.31476	−1.14332	−0.97705	−0.80792	−0.64507	−0.48062
	obs.-calc.	−0.00253	−0.00081	+0.00088	+0.00105	+0.00206	+0.00188	+0.00231	+0.00261	+0.00259	+0.00151	+0.00277	+0.00284	+0.00528
6	obs.	−2.37181	−2.29632	−2.09172	−1.89987	−1.71361	−1.53213	−1.35399	−1.17900	−1.00544	−0.83503	−0.66314	−0.49613	−0.32802
	obs.-calc.	+0.00363	+0.00481	+0.00340	+0.00253	+0.00279	+0.00230	+0.00209	+0.00280	+0.00274	+0.00321	+0.00430	+0.00572	+0.00622
7	obs.	−2.21791	−2.14857	−1.95484	−1.76649	−1.58084	−1.39811	−1.21668	−1.03982	−0.86086	−0.68645	−0.50968	−0.33468	−0.16579
	obs. calc.	+0.00900	+0.00853	+0.00350	+0.00220	+0.00171	+0.00093	+0.00114	−0.00009	+0.00167	+0.00236	+0.00323	+0.00827	+0.00188
8	obs.	−2.06809	−2.00627	−1.82098	−1.63450	−1.44677	−1.25959	−1.07519	−0.89009	−0.70754	−0.52750	−0.34506	−0.16753	+0.01189
	obs.-calc.	+0.01105	+0.00818	+0.00189	+0.00003	−0.00066	−0.00033	−0.00151	±0.00000	+0.00008	+0.00125	+0.00050	+0.00155	−0.00440
9	obs.	−1.92730	−1.87138	−1.69081	−1.50046	−1.30835	−1.11628	−0.92483	−0.73315	−0.54421	−0.36093	−0.16659	+0.01556	
	obs. calc.	+0.00495	+0.00207	−0.00193	−0.00058	−0.00165	−0.00179	−0.00202	−0.00136	−0.00207	−0.00440	−0.00317	−0.00634	
10	obs.	−1.79772	−1.74262	−1.55773	−1.36543	−1.16375	−0.96362	−0.76319	−0.56356	−0.36458	−0.16957			
	obs.-calc.	−0.01138	−0.00831	−0.00116	−0.00076	+0.00022	+0.00047	+0.00117	+0.00019	+0.00018	+0.00107			

$$u(r)=\lambda r^{-12}-\mu r^{-6}, \tag{8}$$

$$=4\epsilon[(\sigma/r)^{12}-(\sigma/r)^{6}], \tag{9}$$

$$=\epsilon[(r_0/r)^{12}-2(r_0/r)^{6}], \tag{10}$$

where

$$\epsilon=\mu^2/4\lambda=\text{the depth of the potential well,} \tag{11}$$

$$\sigma=(\lambda/\mu)^{1/6}$$
$$=\text{separation of a pair of molecules at } u(r)=0, \tag{12}$$

$$r_0=(2\lambda/\mu)^{1/6}$$
$$=\text{separation of a pair of molecules at } u(r) \text{ a minimum.} \tag{13}$$

Substitution of this expression for $u(r)$ into Eq. (7) gives

$$B'(T)/b_0=\sqrt{2}(\theta/T)^{\frac{1}{4}}[\Gamma(3/4)-\sum_{1}^{\infty}{}_n(2^{n-2}/n!)\Gamma[(2n-1)/4](\theta/T)^{n/2}] \tag{14}$$

where

$$b_0=2\pi N\sigma^3/3, \quad \theta=\epsilon/k. \tag{15}$$

Lennard-Jones proposed a graphical method for evaluating the parameters λ and μ, or b_0 and θ from experimental values of $B'(T)$. Tables of $B'(T)/b_0$ for various values of θ/T have been published.[5,6] Over the range of θ/T from 0.20 to 1.00 the function $(B'/b_0)/(\theta/T)^{\frac{1}{4}}$ is nearly a straight line which is represented fairly well by the equation,[7]

$$B'(T)/b_0=(\theta/T)^{\frac{1}{4}}[1.0591-3.5891\theta/T]. \tag{16}$$

The values of the second virial coefficient $B(T)$ of Table II were divided by RT to reduce them to $B'(T)$, and $T^{\frac{1}{4}}B'(T)$ least squared against $1/T$. The resulting expression is

$$T^{\frac{1}{4}}B'(T)=0.3470\bar{5}-264.06/T. \tag{17}$$

Comparison of this expression with Eq. (16) gives for xenon

$$\theta=224.5°\text{K}, \quad b_0=0.08465 \text{ liter per mole.} \tag{18}$$

In Table III are given the observed values of $T^{\frac{1}{4}}B'(T)$ and the deviations of the values computed by Eq. (17)

[5] Giving B'/b_0 to four decimal places for $0.20\leqq\theta/T\leqq1.00$ by W. H. Stockmayer and J. A. Beattie, J. Chem. Phys. **10**, 476 (1942).

[6] Giving B'/b_0 to seven decimal places also its first three temperature derivatives for $0.30\leqq T/\theta\leqq400$ by R. B. Bird and E. L. Spotz, *The Virial Equation of State*, University of Wisconsin CM-599, Project NOrd 9938 (10 May 1950).

[7] In reference 5 the constants 1.064 and 3.602 were given for this equation. These were obtained by drawing the "best straight line" through the points. The constants of Eq. (16) which differ less than 0.5 percent from these were found by the method of least squares.

TABLE II. Second and third virial coefficients of xenon $pV=RT+B(T)/V+C(T)/V^2+D(T)/V^4$.

Temp. °C (Int.)	$B(T)$ liter²-atmos. per mole²	$C(T)$ liter⁵-atmos. per mole³	$D(T)\times10^5$ liter⁶-atmos. per mole⁵
16.65	−3.2765226	+0.15083535	− 1.817262
25	−3.1846537	+0.14848238	− 3.447987
50	−2.9326460	+0.14070243	− 3.094376
75	−2.6990261	+0.13239593	+ 1.039908
100	−2.4858155	+0.12601427	+ 6.170592
125	−2.2899181	+0.12216339	+10.419633
150	−2.1090881	+0.12045462	+14.017763
175	−1.9357341	+0.11916358	+18.034551
200	−1.7618491	+0.11768102	+22.027967
225	−1.5965856	+0.11727675	+25.317369
250	−1.4258023	+0.11532629	+30.788426
275	−1.2606137	+0.11362860	+35.645011
300	−1.1076072	+0.11399209	+41.397926

from the experimental values in percent, which is the same percentage miss in $B'(T)$ or in $B(T)$. The temperature range of the experiments corresponds to θ/T varying from 0.77 to 0.39. In this range Eq. (17) reproduces the experimental second virial coefficients as well or perhaps slightly better than Eq. (16) reproduces the theoretical values given by Eq. (14).

In Table IV are given the various parameters of the Lennard-Jones potential for xenon derived from our experimentally determined second virial coefficients. All are computed from $\theta=224.5$°K and $b_0=84.65$ cm³ per mole. Hirschfelder, Bird, and Spotz[8] have evaluated these constants for xenon from various measurements. They find $\theta=230$°K and $\sigma=4.051$A from viscosity data; $\theta=228$°K from boiling point, and 192°K from critical temperature; and $\sigma=4.04$A from the critical volume. From the expression[9] $\theta=0.75T_c$ and our experimentally determined critical temperature, 289.80°K, we would find $\theta=217$°K.

The expression for the third virial coefficient $C'(T)$ given by classical statistical mechanics has been evaluated for a gas whose potential satisfies the Lennard-Jones (6, 12) potential. Montroll and Mayer,[10] and de Boer and Michels[11] present the results in form of plots while Bird, Spotz, and Hirschfelder,[12] using punched-card methods, give a table listing $C'(T)/b_0^2$ to five decimal places and its first and second temperature derivatives for T/θ ranging from 0.70 to 400. These latter values are shown in Fig. 1 as the solid curve. The circles are $C'(T)/b_0^2$ derived from our third virial coefficients $C(T)$ listed in Table II. For b_0 and θ we employed the values derived from our second virial coefficients and given in Table IV. The disagreement for small T/θ is not caused by our use of Eq. (6) with three terms in the expansion nor by the fact that the experimental second virial coefficients given by the Lennard-Jones potential with the values of θ and b_0 selected deviate from the experimental values. If for the 16.65° isotherm we write

$$C(V,T)=[V(pV-RT)-B(T)_{\text{Eq.(17)}}]V, \quad (19)$$

and plot the expression on the right hand against $1/V$ we find on extrapolation graphically to zero density $C(T)=0.136$ liter²-atmos per mole². This gives $C'(T)/b_0^2=0.80$ as against 0.885 for the ordinate at $T/\theta=1.29$, which is very little improvement in the agreement with the value read from the curve. Bird, Spotz, and Hirschfelder[12] give a similar comparison for argon, methane, and nitrogen over the range 1.8 to 4.2 in T/θ (when all three gases are taken together). Our plot shows the same general trend as does their graph: perhaps the xenon values fall somewhat closer to the theoretical curve above $T/\theta=1.8$.

TABLE III. Representation of $T^{\frac{1}{2}}B'(T)$ by Eq. (17).

T °K	$T^{\frac{1}{2}}B'(T)$ (obs.) °K½-liter/mole	obs.-calc. (in percent)
289.804	−0.568503	−0.77
298.152	−0.540918	−0.43
323.150	−0.468926	+0.25
348.153	−0.408110	+0.81
373.160	−0.356817	+1.06
398.170	−0.313088	+0.98
423.183	−0.275484	+0.53
448.198	−0.242181	−0.03
473.214	−0.211628	−0.31
498.231	−0.184509	−0.84
523.248	−0.158828	−0.76
548.264	−0.135593	−0.74
573.278	−0.115215	−1.42

TABLE IV. Values of the parameters in the Lennard-Jones (6, 12) potential for xenon.

b_0 (cm³ per mole)	84.65
θ (°K)	224.5
$\epsilon\times10^{16}$ (erg)	309.9
σ (A)	4.064
r_0 (A)	4.561
$\mu\times10^{58}$ (erg-cm⁶)	5.583
$\lambda\times10^{102}$ (erg-cm¹²)	2.514
$\theta/T_{\text{critical}}$	0.775

THE SECOND VIRIAL COEFFICIENT FOR AN EXPONENTIAL REPULSIVE POTENTIAL

Slater[13] used the following potential for two neutral helium atoms:

$$u(r)=ae^{-r/\rho}-br^{-6}, \quad (20)$$

$$=\epsilon[f_1e^{-\alpha(s-1)}-f_2s^{-6}], \quad (21)$$

where

$$\alpha=r_0/\rho, \quad s=r/r_0, \quad f_1=6/(\alpha-6), \quad f_2=\alpha/(\alpha-6), \quad (22)$$

$$\epsilon=b/r_0^6f_2=(a/f_1)e^{-\alpha}, \quad r_0^6=(6b/\alpha a)e^{\alpha}. \quad (23)$$

As in the Lennard-Jones potential, r_0 is the separation

[8] Hirschfelder, Bird, and Spotz, Chem. Revs. **44**, 205 (1949).
[9] J. E. Lennard-Jones and A. F. Devonshire, Proc. Roy. Soc. (London) **A163**, 53 (1937); *ibid.*, **A165**, 1 (1938).
[10] E. Montroll and J. E. Mayer, J. Chem. Phys., **9**, 626 (1941).
[11] J. de Boer and A. Michels, Physica **6**, 97 (1939).
[12] Bird, Spotz, and Hirschfelder, J. Chem. Phys. **18**, 1395 (1950).
[13] J. C. Slater, Phys. Rev. **32**, 349 (1928).

of a pair of molecules at the minimum potential and ϵ is the depth of the potential well. The potential depends on the three parameters a, b, and ρ, or on r_0, ϵ, and α.

Kane[14] has evaluated the constants a and b of Eq. (20) from the lattice distances and heat of sublimation of solid xenon on the basis of two assumptions regarding the value of ρ; 0.345×10^{-8} cm from the results of Born and Mayer[15] on alkali halide crystals, and 0.2091 $\times10^{-8}$ cm from those of Bleick and Mayer[16] for two neon atoms. These parameters are listed in Table V together with the values of r_0, ϵ, and α computed from the relations (22) and (23). The deviations of these values of ϵ and r_0 from the ones found by the application of the Lennard-Jones potential to our second virial coefficients are considerably smaller for the larger value of ρ.

Buckingham and Corner[17] write for the mutual potential energy of two molecules

$$u(r)=\epsilon f(s), \tag{24}$$

TABLE V. Values of the parameters of Eqs. (20) and (21) for xenon given by Kane.

		Percentage deviation[a]		Percentage deviation[a]
ρ(A)	0.345[b]		0.2091[b]	
$(a/b)\times10^{-48}$ (cm^{-6})	24.6		52,000	
$b\times10^{60}$ (erg-cm^6)	477		354	
r_0(A)	4.4703	+2.0	4.3877	+ 3.8
$\epsilon\times10^{16}$ (erg)	320.9	−3.5	354.2	−14.3
θ(°K)$(=\epsilon/k)$	232.5		256.6	
$\alpha(=r_0/\rho)$	12.957		20.984	

[a] From the values of Table IV.
[b] Assumed.

$$\left.\begin{aligned} s\geq1 \quad & f(s)=f_1e^{-\alpha(s-1)}-f_2s^{-6}(1+\beta s^{-2}),\\ s<1 \quad & f(s)=f_1e^{-\alpha(s-1)}\\ & \quad -f_2s^{-6}(1+\beta s^{-2}) \quad \exp\{-4[(1/s-1)^3]\}\end{aligned}\right\}, \tag{25}$$

$$f_1=\frac{6+8\beta}{\alpha(1+\beta)-6-8\beta}, \quad f_2=\frac{\alpha}{\alpha(1+\beta)-6-8\beta}, \tag{26}$$

where α and s have the same significance as in Eq. (21) and the term in s^{-8} is the contribution of the dipole-quadrupole interaction to the potential energy. The potential energy thus depends on the four parameters r_0, ϵ, α, and β. Eq. (24) gives for the second virial coefficient

$$B'(T)=2\pi Nr_0^3[F_0(x)+(\lambda/r_0)^2F_1(x)], \tag{27}$$

$$x=\epsilon/kT, \quad \lambda^2=h^2/2\pi mkT, \tag{28}$$

[14] G. Kane, J. Chem. Phys. **7**, 603 (1939).
[15] M. Born and J. E. Mayer, Z. Physik **75**, 1 (1932).
[16] W. E. Bleick and J. E. Mayer, J. Chem. Phys. **2**, 252 (1934).
[17] R. A. Buckingham and J. Corner, Proc. Roy. Soc. (London) A189, 118 (1947).

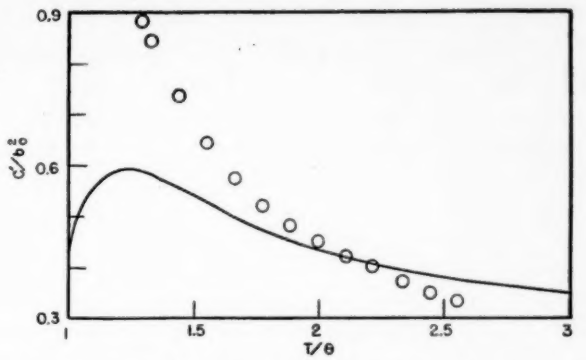

FIG. 1. Plot of C'/b_0^2 against θ/T for xenon. The circles are the observed values of C'/b_0^2, the curve gives the theoretical values for a Lennard-Jones (6, 12) potential.

where m is the weight of one molecule. The term $F_1(x)$ is the correction to the classical expression $F_0(x)$ for quantum effects. Both depend on the parameters α and β. For xenon $(\lambda/r_0)^2$ is about 4×10^{-4} at 300°K, the term $F_1(x)$ contributes less than 1×10^{-4} to $B'(T)$ in the temperature range here considered, and was neglected. Buckingham and Corner give two tables of $F_0(x)$ one for $\beta=0$ and one for $\beta=0.2$. In each table $F_0(x)$ is listed as a function of x for values of α ranging from 12 to 14 in steps of 0.5. Since Kane did not include the dipole-quadrupole contribution in his expression for $u(r)$ for xenon we are here concerned with the table for $\beta=0$. From Kane's value of r_0, α and $\epsilon/k(=\theta)$ corresponding to $\rho=0.345$A we computed from Buckingham and Corner's table for F_0 the second virial coefficients $B'(T)$ listed as "calculated" in Table VI. The values marked "observed" are our experimental results obtained from Table II. The α for Kane's value of $\rho=0.2091$A is too far outside the tabulated values of $F_0(x)$ to permit extrapolation within any certainty. The agreement of the theoretical value with that observed is not bad when we consider that the former were not obtained from the parameters derived from our observations but from ρ derived from alkali halide crystals and ϵ and r_0 from solid xenon.

TABLE VI. Comparison of the values of the second virial coefficients computed from Buckingham and Corner's table and Kane's values of r_0, α, and ϵ/k with the observed values.

T°K	$B'(T)$ (obs.) liter/mole	$B'(T)$ (calc.) liter/mole	Deviation liter/mole	Deviation percent
289.804	−0.1378	−0.1367	−0.0011	− 0.8
298.152	−0.1302	−0.1298	−0.0004	− 0.3
323.150	−0.1106	−0.1116	+0.0010	+ 0.9
348.153	−0.0945	−0.0966	+0.0021	+ 2.2
373.160	−0.0812	−0.0840	+0.0028	+ 3.4
398.170	−0.0701	−0.0733	+0.0032	+ 4.6
423.183	−0.0607	−0.0640	+0.0033	+ 5.4
448.198	−0.0526	−0.0560	+0.0034	+ 6.5
473.214	−0.0454	−0.0489	+0.0035	+ 7.7
498.231	−0.0391	−0.0427	+0.0036	+ 9.2
523.248	−0.0332	−0.0372	+0.0040	+12.0
548.264	−0.0280	−0.0322	+0.0042	+15.0
573.278	−0.0235	−0.0277	+0.0042	+17.9

ACKNOWLEDGMENT

This work was made possible by a grant-in-aid from the Linde Air Products Company. We are also grateful to the Company and to Dr. J. M. Gaines and Dr. R. J. Gillette for the gift of the xenon and for the painstaking analysis of the sample. We thank Professor I. Amdur and Professor W. H. Stockmayer for their continued interest in the work and valuable suggestions in regard to the application of various potential functions to our results.

THE JOURNAL OF CHEMICAL PHYSICS VOLUME 19, NUMBER 10 OCTOBER, 1951

Dielectric Constant of Benzene at 25°C by the Wyman Method*

A. S. BROWN, P. M. LEVIN,† AND E. W. ABRAHAMSON‡
McGregory Hall of Chemistry, Colgate University, Hamilton, New York
(Received July 2, 1951)

Apparatus and techniques are described for obtaining reliable absolute dielectric constants by the Wyman resonance cell method.

Calcium hydride has been shown to be a drying agent for benzene far more satisfactory than sodium wire, reducing drying time from the six-month period demonstrated in the literature to an interval approximating one day.

At 25°C the values for benzene's dielectric constant were 2.2747±0.0003, but the higher limit is presently preferred. These results fall within the range of the best recent values obtained in other laboratories. The reasons for the discrepancies appear explicable in view of the findings of this investigation.

IN initiating a program of dielectric constant measurements we selected the resonance cell method of Wyman,[1] its precision having been demonstrated by Geddes and Kraus.[2] A resonance cell comprising two concentric cylinders connected by a short loop is coupled to an oscillator delivering a signal of roughly constant strength over at least a small range of controllably variable frequencies. The resonance frequency of the cell is determined by varying the signal frequency to obtain maximum circulating current in the cell. The dielectric constant of the medium surrounding the cell is calculated as

$$C=C_r(f_r/f)^2,$$

in which C_r and f_r are the dielectric constant and cell resonance frequency in a reference medium while C and f are corresponding values for the medium under study. Using vacuum as reference an absolute value for the dielectric constant follows.

The chief problem in developing the Wyman method is that of isolating the resonance cell adequately to make its resonance frequency depend exclusively upon the surrounding medium.

APPARATUS

A Measurements Corporation Model 80 standard signal generator was modified by addition of a reduced speed dial drive on the capacitor. An output pad and coaxial cable with binding posts terminated in a single loop of copper wire formed to protrude slightly beyond these posts. The coil end of this cable was fixed in a glass tube axially movable along a wood holder to permit variable spacing of this generator coil with respect to the cell.

Resonance was detected through a similar coil placed at the opposite side of the cell from the generator coil. This detector coil was connected to a Millivac Instruments PT-2 probe coupled to a Millivac Model 18-B Millivoltmeter. Alternatively, this probe was connected to a Smith Industries VS-3 amplifier itself connected to the Model 18-B through a network tuned to the 400-cycle modulation of the signal generator. The latter detection scheme is much more sensitive and also facilitates minimization of 60-cycle background.

The signal frequency (without modulation) was measured with frequency meters manufactured by the Allen D. Cardwell Company bearing the Signal Corps designations TS-174/U and TS-173/U. Each meter has internal calibration against harmonics of a crystal whose fundamental (1 or 5 megacycles, respectively) had been adjusted with respect to the Bureau of Standards signals. The two meters agreed within the limits of reading their scales, i.e., about 0.001 percent.

All electronic equipment was operated from Sola constant-voltage transformers provided with harmonic filters.

The temperature was controlled by an air bath maintained at 25°C within about 0.05°C during the measurements. Benzene temperature was maintained within a tolerance of ±0.02°C as observed with a Beckman thermometer whose setting was compared with an NBS certified thermometer. This uncertainty corresponds to 0.00004 in the dielectric constant and is considered of small importance in the present results since it is largely removed in taking averages.

MATERIALS

Earlier measurements on benzene utilized thiophene-free material dried with calcium hydride with which the benzene was heated before being distilled through a 20 plate GLENLAB Oldershaw type column. Initial portions of distillate were rejected until the vapor temperature was constant within the uncertainty of reading the thermometer, graduated in 0.2°C.

* This work was sponsored by a Frederick Gardner Cottrell grant from the Research Corporation and by the ONR.

† Present address: E. I. DuPont de Nemours and Company, Wilmington, Delaware.

‡ Present address: Chemistry Department, Syracuse University, Syracuse, New York. Part of this work is a portion of the doctoral program of this author at Syracuse University.

[1] Wyman, Phys. Rev. **35**, 623 (1930).

[2] Geddes and Kraus, Trans. Faraday Soc. **32**, 585 (1936).

Final benzene measurements included treatment with concentrated sulfuric acid until fresh portions of acid remained uncolored, washing with sodium carbonate and water. Fractional crystallization was rejected as impractical with the quantities required to provide the two liters needed for a cell container filling. This appears justified by the observation that the acid treatment lowered the sample's dielectric constant by less than about 0.02 percent. Benzene was distilled directly into the cell container and could be maintained for days.

RESONANCE CELLS

Geddes and Kraus[2] indicate that the resonance cell method requires mechanical stability in the coil-cell system for reproducibility of resonance frequencies. This will be true if there is substantial coupling between circuit components. The more sensitive resonance detecting devices recently available led to the belief that this coupling could be reduced to such a degree that dielectric constants and perhaps the resonance frequencies themselves could be reasonably independent of coil size and proximity to the cell. The magnitude of this dependence may be considered a measure of the validity of the measurements.

All cells had a cylinder diameter approximating 1.6 inches, while cylinder spacing varied from 0.03 to 0.06 inches and lengths from 1 to 2.5 inches. The connecting loops, substantially rectangular, should be made as small as possible, a conclusion confirmed with cells having loop areas from about two square inches to less than half a square inch.

Cells were hung by loops of solvent-extracted glass threads from a stainless steel post vertically adjustable by sliding through a carefully ground joint in a plug seated in the central aperture of the standard cover for the 3-liter resin reaction kettle which served as cell container.

Of particular importance is the material of which the cell is constructed: to obtain sharp resonance peaks the high frequency resistance of the cell must be a minimum. Three materials of construction have been used:

A. Gold plated brass.
B. Plated platinum over gold on a brass base.
C. Solid platinum-15 percent iridium alloy.

The electrical characteristics of the gold plated cells were best, with the platinum plated cells being nearly as good. With these cells it was possible to obtain precise resonance settings with coils 3 inches or less in diameter without detector amplification. However, careful cleaning of the resonance cells is imperative to remove films which alter the effective dielectric constant of the medium between the cell cylinders. These cells usually appeared satisfactory in benzene but the vacuum resonance frequencies could never be reproduced after successive cell cleanings. These values would rise gradually as the cell was cleaned more thoroughly and would then change markedly, at which time surface failure was apparent to the eye. This was particularly true of the platinum plated cells due to the difficulty in obtaining satisfactory final plating after assembly of the cells. The excellent electrical characteristics of these cells resulted in an apparent achievement of the first objectives in that resonance frequencies were independent of the size and position of the generator and detector coils provided that the coil size did not exceed a maximum specific for each cell. Such cells were also used to show that the cell supporting apparatus, cell container and thermostating mechanism did not affect the cell's resonance frequency within the precision limits of the equipment, i.e., about 0.001 percent. However, the accuracy of the measurements was far less than this precision since repeated cleaning changed the cell's resonance frequency.

Two approaches to the minimization of this film effect were investigated. An increase in the spacing between the cylinders was first attempted. Since loop size is limited by coupling considerations, increased cylinder spacing raised the resonance frequency, increased the incidence of spurious line resonances, and caused some decrease in sensitively.

The second approach utilized cells of solid precious metal. Pure platinum is so soft that the requirement of cell rigidity would demand relatively thick metal sections. Trial of a platinum-10 percent iridium cell indicated that this alloy was too soft. The present cell of platinum-15 percent iridium is highly satisfactory mechanically and chemically. Unfortunately, this alloy's resistance limits the circulating current in the cell substantially, sensitivity being much lower than with the plated cells.

Various procedures have been tried in cleaning the resonance cells. The plated cells were treated with hot detergent solutions followed by water washes, then hot carbon tetrachloride and finally benzene. Subsequently, it was believed that an acid treatment would be needed to remove occluded cyanides and dilute acetic acid was used for this purpose. This initially raised the cell vacuum resonance frequency, indicating attainment of cleaner metal surfaces but probably was responsible for early failure of the plate mechanically, with tiny flakes of the plate raised from the metal surface. This was particularly true of the platinum plated cells, all of which showed this.

The Pt-Ir cell was cleaned by boiling in detergent (0.4 percent "Fab"), rinsing and boiling, successively, in water, carbon tetrachloride, and benzene for 30 minutes. The cell was mounted, pumped, and flushed with air which passed a 16-foot train of soda-lime, calcium chloride, and calcium hydride. Heating the cell with an "infrared" lamp did not produce any change in cell resonance frequency over that obtained after repeated dry air flushings.

Measurement of Resonance Frequency

The determination of cell resonance frequency requires setting of the signal generator's frequency to give maximum detector response, with subsequent measurement of this frequency. If the resonance peak is extremely sharp, the generator may simply be set to this peak response, a situation which has been encountered only rarely in this work. Many plated cells gave a small flat (0.01 to 0.04 megacycle) at the resonance peak. The edges of these flats could be used as setting points. Since the response was not entirely symmetrical, there arises a doubt as to the proper averaging of such frequencies; whether a simple mean or an average weighted for the different slopes of the response curve branches.

With detector response amplification these techniques gave poor precision as the maximum millivoltmeter response was too unsteady. A better technique comprised setting of the generator for a meter response a little less than maximum at both sides of maximum, with averaging of the corresponding frequencies. Comparison of averages taken from settings at different distances from maximum showed the response-frequency curve to be adequately symmetrical in this region, the averages agreeing within about 0.001 percent.

Results with Plated Cells

In Table I are summarized results of selected series of measurements using plated cells and benzene which

had *not* been treated with sulfuric acid, presented to show the magnitude of the effects previously discussed.

The listed resonance frequencies are averages of 8 to 15 determinations which differ in circuit elements and in signal intensity, each determination an average of 3 to 6 measurements. Exceptions to this are lines g through m, where each listed frequency averages 3 determinations differing in signal intensity. Frequencies are listed with one significant figure more than warranted for an individual measurement, the determinations included in each listed mean having an average deviation from that mean of 0.005 percent at most, all but four being within about 0.002 percent and half being within about 0.001 percent.

Cell A had a small loop connecting cylinders about 1.5 inches long and spaced about 0.06 inch. Cell B had a large loop (about 8 times the loop area of cell A) connecting 1-inch-long cylinders spaced 0.06 inch. Cell C had 2.5-inch cylinders, spaced 0.03 inch, connected by a loop clearing the cylinders by 0.5 inch.

Lines a and b show the reproducibility of these cell resonance frequencies if the cell is not disturbed, (2-day interval). Lines b and c show improvement in cleaning while lines e and f show damage by cleaning. Lines c and d show the reproducibility of preparing the benzene sample, as do lines n and o. Lines e and f also show that metal surface damage may affect vacuum and benzene frequencies differently while lines p and q show a case of damage shich gave the same change in both media, q results predating p results by ten days.

Lines g through l show the effect of coil size and spacing when a cell requires smaller coils and should be contrasted with line e whose listed frequencies have an average deviation of less than 4 parts per million for two coils whose areas differ by 40 percent, and for two coil spacings. The results for cell B also show that excessive coupling gives high dielectric constants with this apparatus. This was contrary to expectations and is currently believed to be a consequence of simultaneous inductive and capacitive coupling together with poor symmetry in the response curve. The effect of this asymmetry is shown by lines l and m. Line l contains simple means of the frequencies of the edges of the flat at the top of the curve's peak while line m gives averages obtained by extrapolating to intersection lines drawn between the edge-of-peak frequencies and those of one-half maximum response for each branch of the curve. For comparison, a similar treatment of the results whose means are given in line e (for balanced circuit conditions) leads to a dielectric constant value of 2.27367.

TABLE I. Plated cells.

	Cell Gold	Coil diam. in.	Coil to loop dist. in.	Resonance frequency Megacycles Vacuum	Benzene	Dielectric constant benzene
a.	*A*	3, 2.6	3, 3.5	182.9978		
b.				182.9984		
c.			3, 3.5, 4	183.0240	121.3390	2.27518
d.					121.3373	2.27524
e.	*B*	1.5, 1.9	3.1, 3.5	161.4986	107.1029	2.27371
f.				161.4791	107.1039	2.27312
g.		2.6	3	161.5459	107.1049	2.27496
h.			3.5	161.5336	107.1104	2.27438
i.			4	161.5195	107.1128	2.27388
j.		3	3	161.5587	107.0849	2.27617
k.			3.5	161.5355	107.1052	2.27465
l.			4	161.5235	107.0980	2.27462
m.				161.5187	107.1024	2.27430
n.	*C*–1	2.6, 3	3, 3.5	86.3928	57.2895	2.27408
o.					57.2904	2.27400
Platinum						
p.	*C*–2	3	3.1, 3.5	84.5679	56.0490	2.27654
q.		2.5, 3	3.1, 3.5	84.5857	56.0603	2.27658

The results with the platinum plated cell, lines p and q, are curious. The high dielectric constant values appear to confirm the 2.276 value preferred by Heston and Smyth,[3] especially when a correction of −0.01 to −0.02 percent is applied to the listed values because this benzene was not treated with acid. This is quite consistent with the view that more inert metal surfaces give more accurate vacuum frequencies. However even this cell, the best of this type, is known to have had progressively more flaking, which would be expected to lower resonance frequencies by shortening the dielectric path between the cylinders.

Results with Pt-Ir Cell

The Pt-Ir cell requires use of a coil size of at least 3 inches, even with amplification of detector response. Unfortunately, even a 3-inch coil is too large for high reproducibility of resonance frequencies in this cell, and the results obtained with it show some sensitivity to coil position with respect to the cell. However, since individual measurements of the dielectric constant of acid-treated benzene fall between the extremes of 2.27443 and 2.27504, some of this being due to temperature variations, the results appear comparable to the best reported in the literature.

That this cell is free from the surface deterioration found with plated cells is shown by the resonance frequency of this cell in vacuum being reproducible to about 0.002 percent after repeated cleanings. This variation is probably due largely to electrical variables since the higher vacuum values do not give higher benzene dielectric constants. Occasionally a vacuum frequency will be low, presumably because of faulty cleaning.

Table II summarizes the results obtained with the Pt-Ir cell on benzene which had been exhaustively treated with sulfuric acid.

Each entry in this table is a mean of five series of determinations, each of which comprises about 6 individual measurements of resonance frequency, usually with two settings of the coils. Each series represents a cleaning of the cell and a redistillation of the benzene after additional drying. The table entries in parentheses are for a single series as resonance can only infrequently be determined at this coil distance with benzene because of electrical background.

It will be noted that there is a distinct but small variation in dielectric constant with coil position, showing that coupling is still excessive. Probably 2-inch coils would correct this but these have not yet given adequate sensitivity. Comparison of the effect of coil position on this cell with cell B of Table I leads to the conclusion that the values of Table II must be very near to the correct value. Since coupling effects are expected to diminish with increasing separation, it is

[3] Heston and Smyth, J. Am. Chem. Soc. **72**, 99 (1950).

expected that the correct value is slightly higher than the values observed with this cell, i.e., about 2.2750. Such a value is quite consistent with those listed in Table I, allowing for known differences. The previously noted observation that measurements affected by coupling tend to be high lends a little merit to the selection of a value approximating 2.2744 but the evidence for this selection is less compelling.

There was no detectable variation in dielectric constant with extended drying of the benzene after an initial one day treatment followed by 8 hours of refluxing with calcium hydride. Table III lists dielectric constants obtained for a 3-inch coil spacing after repeated dryings and distillations.

Comparison with Previous Values

The importance of an accurate dielectric constant for a reference liquid has been recognized in the literature, benzene being the traditional selection. A summary of values obtained prior to 1928 is given by Hartshorn and Oliver[4] whose preferred value, converted to 25°C, is 2.2726 with an uncertainty stated as approximating

TABLE II. Platinum-iridium cell.

Coil to loop dist. in.	Coil diameter 3 inches Resonance frequency Megacycles Vacuum	Benzene	Dielectric constant
3	96.6997	64.1177	2.27454
3.25	96.6952	64.1120	2.27474
3.5	96.6890	64.1059	2.27488
3.75	96.6830	(64.1010)	(2.27494)

0.0005 units. These authors reported as the chief uncertainty the difficulty of filling the test condenser completely. They also considered water as the significant benzene contaminant and found drying over sodium wire to require several months, the value for 6-month drying being 0.0008 units lower than that for a 4-month drying period.

Van der Maesen[5] has recently measured benzene and confirmed the need of prolonged drying over sodium. His final selection, corrected to 25°C, is 2.2740 with an uncertainty of 0.0005 units. This is probably the best literature value. However, the six-month drying of the benzene over sodium wire is discouraging to wide use of this value.

TABLE III. Effect of extended drying with CaH_2.

Date	Benzene diel. const.
March 3, 1951	2.27458
March 9, 1951	2.27443
March 23, 1951	2.27457
March 28, 1951	2.27459
March 30, 1951	2.27454

Among other results pertinent to the present work are the 2.26800 value obtained by Geddes and Kraus[2] with the Wyman method using definite coupling between resonance cell and signal generator. Heston and Smyth[3] results, obtained at much higher frequencies, are absolute determinations. Their values, interpolated to 25°C, are 2.276, 2.275, and 2.274 at progressively higher frequencies, and they indicate that these agree within the limits of precision of the technique used. They used sodium drying but do not state its duration and their results may be somewhat high because of traces of moisture in the benzene.

The results of this investigation fit very well with the best literature values. Our selected value of 2.2750 is consistent with the 2.276 selection of Heston and Smyth, and Van der Maesen's value of 2.2740, this difference being probably related to metal surface cleanliness.

ACKNOWLEDGMENTS

We gratefully acknowledge our indebtedness to W. C. Fernelius of The Pennsylvania State College, A. J. King of Syracuse University, and T. Shedlovsky of the Rockefeller Institute for advice and assistance in initiating this work; to S. I. Reynolds and A. H. Sharbaugh of the General Electric Company for help in circuit problems; and to W. K. Volkers of Millivac Instruments, Inc., for his continued interest and aid in detector improvement. Unusual assistance was also tendered by G. B. Peckham of Hamilton and the Wagner and Bryant Company of Utica. This work was made possible only by the continued patience of the Office of Naval Research and the Research Corporation.

[4] Hartshorn and Oliver, Proc. Roy. Soc. (London) **123**, 664 (1929).

[5] Van der Maesen, Physica **XV**, 481 (1949).

UNIVERSITY OF MICHIGAN LIBRARIES

A Theory of Cooperative Phenomena. II. Equation of States for Classical Statistics

RYOICHI KIKUCHI*
Department of Physics, University of Tokyo, Tokyo, Japan
(Received April 24, 1951)

A method of obtaining the equation of state of a classical assembly through the solid, liquid, and gas phases based on the order-disorder concept is explained. At first, the method is illustrated on an imaginary two-dimensional model. Next, the general procedure to increase the number of interstitial sublattices to infinity is explained for a one-, two-, and three-dimensional lattice. In the one-dimensional case, the present method proves to be identical with Gürsey's rigorous solution. An approximate treatment for the solid state is added.

I. INTRODUCTION

VARIOUS ingenious methods have been devised to analyze the equation of state of matter and some of these are yielding fruitful results;[1–4] but it may be of some use to report a new approach which has some interesting features of its own. The present method is an application and a generalization of the theory on the cooperative phenomena reported recently by the author.[5] It can give the unified equation of state of the classical assembly through the solid, the liquid, and the gas phases with the same order of approximation. The superposition approximation[1,3] is not used. The ideas developed by Lennard-Jones-Devonshire[6] and by Cernuschi-Eyring[7] are combined together and extended.

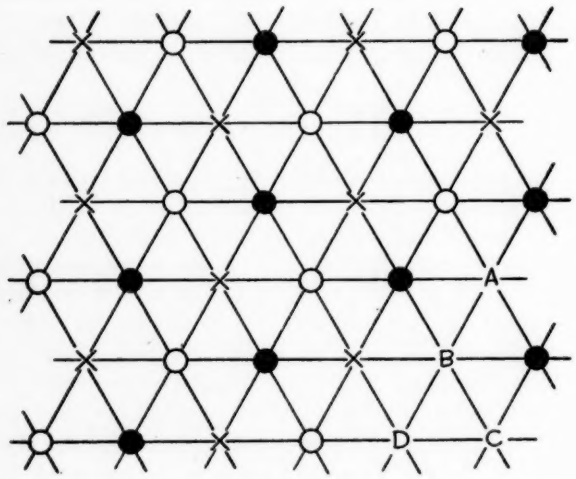

FIG. 1. Two-dimensional triangular lattice. ● sublattice I, ○ II, and × III.

II. PRELIMINARY ILLUSTRATION

As a preliminary illustration, an equation of state of an imaginary two-dimensional substance is derived as follows. Starting from Cernuschi and Eyring's theory of condensation,[7] let us take, as a particular example to summarize their ideas, a triangular lattice as shown by black circles in Fig. 1. They considered the assembly of atoms as an alloy of atoms and holes. It was assumed that an atom can occupy any lattice point and that two atoms on adjacent lattice points contribute a potential energy $-\epsilon$, while further removed pairs do not contribute. Applying Bethe's approximation of the order-disorder theory, the equation of state for the liquid and the gas phases was obtained, including the phase transition between them which was of the van der Waals type.

In reality, however, an atom can occupy any point in space, even in the solid state at least potentially. Therefore, an improvement that is possible is to insert additional interstitial points which an atom can occupy. The number of interstitial sublattices will be made infinite in the following sections, but for the present, let us consider the case in which the number of lattice points are three-fold. Hence, on the original lattice, two other sublattices are superposed as indicated with white circles and crosses in Fig. 1. It is assumed that if an atom exists on site A (Fig. 1), no atoms can lie at B, because of the high repulsive potential, and that an atomic pair $A-C$ has energy $-\epsilon_1$ and a pair $A-D$ has[8] energy $-\epsilon_2$.

Adding sublattices, the interpretation of the melting phenomenon by Lennard-Jones and Devonshire[6] can be applied directly. As already noticed by them and others,[9] the solid state is an ordered state and the liquid and the gas states are disordered, only the solid state having the long-range order. Therefore one expects that in the solid state, atoms exist chiefly on one of the three sublattices. Without loss of generality, one may choose this sublattice to be I, leaving II and III equivalent. In the fluid phases the probability of existence of an atom on each of the three sublattices is expected to be equal.

---

* Present address: Department of Physics, Massachusetts Institute of Technology, Cambridge, Massachusetts.

[1] J. G. Kirkwood, J. Chem. Phys. **3**, 300 (1935); J. G. Kirkwood and E. M. Boggs, J. Chem. Phys. **10**, 394 (1942); Kirkwood, Maun, and Alder, J. Chem. Phys. **18**, 1040 (1950).

[2] M. Born and H. S. Green, Proc. Roy. Soc. (London) **A188**, 10 (1946); **A189**, 103 (1947).

[3] J. E. Mayer, J. Chem. Phys. **15**, 187 (1947).

[4] J. E. Lennard-Jones and A. F. Devonshire, Proc. Roy. Soc. (London) **A163**, 53 (1937); **A165**, 1 (1938); Wentorf, Jr., Buehler, Hirschfelder, and Curtis, J. Chem. Phys. **18**, 1484 (1950).

[5] R. Kikuchi, Phys. Rev. **81**, 988 (1951). This paper will be cited by the abbreviation TCP I.

[6] J. E. Lennard-Jones and A. F. Devonshire, Proc. Roy. Soc. (London) **A169**, 317 (1939); **A170**, 464 (1939).

[7] F. Cernuschi and H. Eyring, J. Chem. Phys. **7**, 547 (1939).

[8] It is possible to reproduce the equation of state of the fluid states with only one potential energy, but, as shown in the discussion concerning the value of θ below, two kinds of energy are needed to make the solid melt easily.

[9] J. G. Kirkwood and E. Monroe, J. Chem. Phys. **9**, 514 (1941); G. H. Wannier, J. Chem. Phys. **7**, 810 (1939).

The smallest triangle in Fig. 1 is chosen as the *basic figure*[10] and the variables x_1, x_2, and x_3 are defined to be the probabilities of appearance of the configurations of the triangle as shown in Table I. α_i denotes the number of different configurations having the same probability. From Table I, one can derive Tables II and III. There also the variables y_i, z_i, u_i, and v_i are defined.

In order to get the formula for the energy, the assumptions shown in Table IV are made, following the ideas of Bragg and Williams.[11] These additional assumptions introduce more approximations and result in a transcendental equation troublesome to handle, but have the advantage of keeping the number of independent variables small.

Consider a system composed of $3M$ lattice points, each of the three sublattices containing M of them. Then the total energy E for the system becomes

$$E=-3M[(p_1+2p_2)\epsilon_1+(q_1+2q_2)\epsilon_2]. \quad (1)$$

TABLE I. Probabilities of appearance of configurations of a triangle. ●, ○, and × denote an atom on sublattice I, II, and III, respectively. Sublattices II and III are assumed to be equivalent without loss of generality. α_i denotes the number of different configurations having the same probability.

Triangle	Probability	α_i
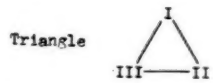	x_1	1
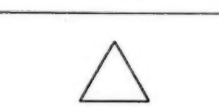	x_2	1
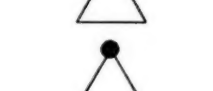	x_3	2

The formula of entropy of a system can be obtained following the method explained in TCP I, Sec. G. One constructs the whole lattice from one end adding a lattice point one by one. An intermediate stage is shown in Fig. 2. The number of ways G_I of adding a lattice point of sublattice I is approximated as follows:

$$G_I=\frac{\{\text{Bond II–III}\}_L}{\{\text{Triangle}\}_L}\times\left[\frac{\{\text{Bond III–II}\}_L}{\{\text{Triangle}\}_L}\div\frac{\{\text{Point III}\}_L}{\{\text{Bond III–I}\}_L}\right]=\frac{\{\text{Bond II–III}\}_L\{\text{Bond I–III}\}_L}{\{\text{Triangle}\}_L\{\text{Point III}\}_L}, \quad (2)$$

[10] The terminologies used in TCP I are taken over without explanation.

[11] W. L. Bragg and E. J. Williams, Proc. Roy. Soc. (London) **A145**, 699 (1934); Y. Takagi, Proc. Phys.-Math. Soc. (Japan) **23**, 44 (1941).

TABLE II. Probabilities of appearance of configurations of a bond. β_i and γ_i denote the number of different configurations having the same probability.

Bond I-II	Bond I-III	Probability	β_i
——	——	$y_1=x_1+x_3$	1
●——	●——	$y_2=x_2$	1
——○	——×	$y_3=x_3$	1

(a)

Bond II-III	Probability	γ_i
——	$z_1=x_1+x_2$	1
○—— ——×	$z_2=x_3$	2

(b)

where the bracket notations are defined by

$$X_L=\{\text{Triangle}\}_L=\prod_{i=1}^{3}(x_iL)!^{\alpha_i},$$

$$Y_L=\{\text{Bond I–II}\}_L=\{\text{Bond I–III}\}_L=\prod_{i=1}^{3}(y_iL)!^{\beta_i},$$

$$Z_L=\{\text{Bond II–III}\}_L=\prod_{i=1}^{2}(z_iL)!^{\gamma_i}, \quad (3)$$

$$U_L=\{\text{Point I}\}_L=\prod_{i=1}^{2}(u_iL)!,$$

$$V_L=\{\text{Point II}\}_L=\{\text{Point III}\}_L=\prod_{i=1}^{2}(v_iL)!.$$

TABLE III. Probabilities of appearance of configurations of a lattice point.

Point I	Probability
No atom	$u_1=x_1+2x_3$
●	$u_2=x_2$

(a)

Point II	Point III	Probability
No atom	No atom	$v_1=x_1+x_2+x_3$
○	×	$v_2=x_3$

(b)

UNIVERSITY OF MICHIGAN LIBRARIES

TABLE IV. Probabilities of appearance of configurations having the energy (a) $-\epsilon_1$, and (b) $-\epsilon_2$.

Configuration	Probability
	$p_1 \doteqdot \frac{x_2^2}{z_1}$
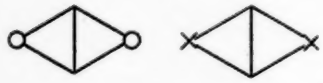	$p_2 \doteqdot \frac{x_3^2}{y_1}$

(a)

Configuration	Probability
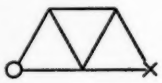	$q_1 \doteqdot \frac{x_1 x_3^2}{y_1^2}$
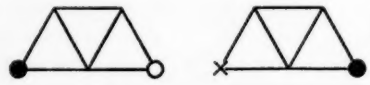	$q_2 \doteqdot \frac{x_1 x_2 x_3}{y_1 z_1}$

(b)

L systems having the same values for the probabilities are considered.[12]

Making the cyclic change of G_I and multiplying them together, one gets the number of ways G_L of adding three points I, II, and III:

$$G_L = G_I G_{II} G_{III} = (Y_L{}^6 Z_L{}^3)/(X_L{}^6 U_L V_L{}^2). \tag{4}$$

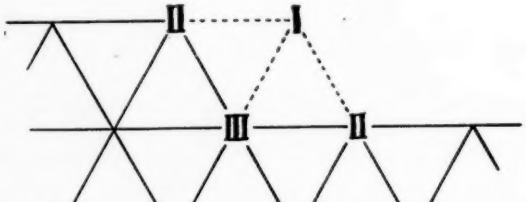

FIG. 2. An intermediate stage of constructing a two-dimensional triangular lattice.

[12] The totality of the L systems was called ensemble in TCP I, but this terminology is unsuitable. What are considered in Fig. 1, TCP I, are the systems having the same values for the probabilities y_i's and are only a part of the Gibbs' ensemble, in which there are other systems having different values for y_i's. Therefore, the word ensemble in TCP I should be replaced by *assembly*. The number L is used only to derive the formula of the entropy and plays a subsidiary role, being canceled out in the final expression of the free energy per system. Therefore, its value is quite arbitrary, provided it is large, and can be interpreted practically infinite.

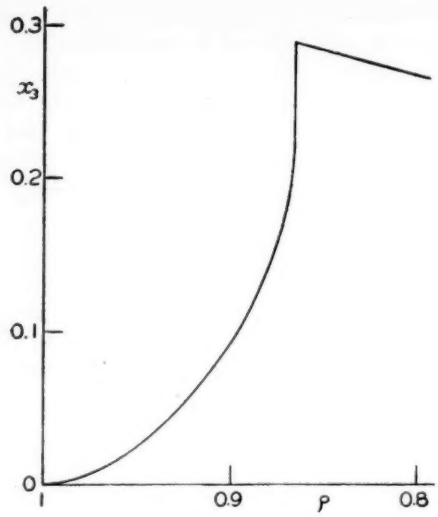

FIG. 3. x_3 *vs* ρ from Eq. (9) for values $\theta=2$ and $H_1=2.3$.

Hence the entropy S of a system becomes

$$S = k(M/L)\ln G_L$$

$$= kM[6\sum_{i=1}^{3}\beta_i y_i \ln y_i + 3\sum_{i=1}^{2}\gamma_i z_i \ln z_i - 6\sum_{i=1}^{3}\alpha_i x_i \ln x_i - \sum_{i=1}^{2} u_i \ln u_i - 2\sum_{i=1}^{2} v_i \ln v_i]. \tag{5}$$

The approximation contained in this formula is of the same degree as in TCP I, Sec. G.

From the normalization condition:

$$x_1 + x_2 + 2x_3 = 1, \tag{6}$$

and the definition of a parameter ρ related to the given density of atoms

$$\rho = x_2 + 2x_3, \tag{7}$$

one is able to choose x_3 as the independent variable. The total number of atoms N in a system is connected with ρ by $N=\rho M$. From the geometrical relationships shown in Tables II and III, other dependent variables can be expressed as linear combinations of x_3 as shown in Table V. x_3 is related to the long range order parameter ξ of the usual terminology by the following:

$$\xi = (x_2 - x_3)/\rho = (\rho - 3x_3)/\rho, \tag{8}$$

which becomes zero in the disordered state and unity in the perfectly ordered state as is shown in Table V.

Making the Helmholtz free energy minimum with respect to x_3, one obtains the fundamental equation:

$$\log\{[(\rho-2x_3)(1-x_3)(1-\rho+x_3)^3]/[x_3(1-\rho+2x_3)(1-2x_3)^3]\} = [3(1-\rho)^2(\rho-3x_3)\log H_1][(1-2x_3)^2(1-\rho+x_3)^3]^{-1} \times[(1-\rho)(2-\rho-\theta)-x_3(1-x_3)(2\theta-1)], \tag{9}$$

which determines x_3 as a function of $\theta \equiv \epsilon_2/\epsilon_1$, $H_1 \equiv \exp(\epsilon_1/kT)$, and ρ.

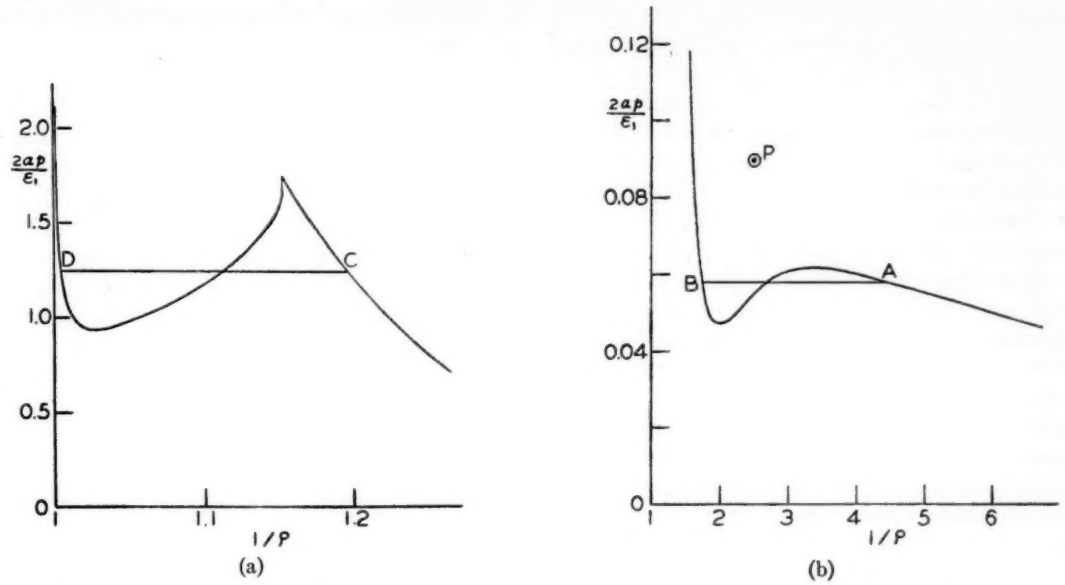

FIG. 4. p *vs* $1/\rho$ curve from Eq. (10) for $\theta=2$ and $H_1=2.3$. a is the area of a smallest triangle in Fig. 1, and is a constant. ⊙ indicates the critical point, for which $\epsilon_1/kT_c=0.77$.

Putting the area of a smallest triangle equal to a, the pressure p becomes

$$2ap/\epsilon_1=-P+Q\theta+R(3\log H_1)^{-1}, \tag{10}$$

where

$$P=[x_2(\rho+2x_3)/z_1]+2(x_3/y_1)^2(\rho-y_1),$$
$$Q=\{(\rho^2-2x_3)(2/z_1)+(x_3/y_1)-(x_3/y_1+x_2/z_1)(2x_1\rho/y_1)\}\{x_3/y_1\},$$
$$R=[2x_3\log x_2+6(1+x_3)\log y_1+3(1-2x_3)\log z_1]-[6\log x_1+2x_3\log x_3+(1+2x_3)\log u_1+2(1-x_3)\log v_1].$$

Equation (9) has a single root $x_3=\rho/3$ for values of ρ less than a certain critical number. These values of ρ pertain to the disordered state. Therefore numerical solutions of Eq. (9) are required only for the ordered state. The result is shown in Fig. 3 for values $\theta=2$, and $H_1=2.3$.

Inserting values of x_3 in Fig. 3 into Eq. (10), the pressure p *vs* $1/\rho$ curve is obtained, which is shown in Figs. 4 (a) and (b) .The positions of the phase transition lines in Fig. 4 have been determined by the crossing points of the curve of the chemical potential *vs* pressure.[13] In Fig. 4, the portion on the right of A is gas, that between B and C is liquid and that on the left of D is solid. AB and CD indicate two phase transition regions.[14]

It is necessary to add some remarks on the choice of the value θ. Since $-\epsilon_1$ is the interaction energy between two atoms belonging to the same sublattice, it has the effect of stabilizing the long range order, whereas $-\epsilon_2$, which is the interaction energy between two atoms belonging to different sublattices, serves to destroy the long range order. Therefore, the larger the ratio $\theta=\epsilon_2/\epsilon_1$ is, the less stable the solid state becomes. At first glance it is natural to assume that $-\epsilon_1$ corresponds to the minimum value of the potential energy between two atoms and hence θ is less than unity, so that the sublattice I is the stable solid structure. However, when one chooses $\theta\approx 1$, two phase transition regions AB and CD overlap and one cannot obtain the stable liquid phase. This fact must be due to the roughness of the model or the insufficiency of the number of sublattices. Therefore, recognizing this inadequacy of our model, we have chosen $\theta=2$ in order to realize the liquid phase, but this value of θ greater than unity can be justified to some extent by the following consideration. In reality, there are more interstitial sublattices, and all of them except sublattice I serve to destroy the long range order. Therefore, to increase the value of θ beyond the limit unity is equivalent to increasing the number of sublattices, so far as the melting phenomenon is concerned.

Another objection to this model is that the possible

TABLE V. Relations between the independent variable and the dependent ones. The meaning of this table is, for example, $y_1=1-\rho+x_3$.

	1	ρ	x_3
x_1	1	−1	
x_2		1	−2
y_1	1	−1	1
z_1	1		−2
u_1	1	−1	2
v_1	1		−1

[13] It should be noticed that in this method, the unstable portion of the $p-(1/\rho)$ curve where $dp/d(1/\rho)>0$ has not been used to determine the transition points, because the value of the chemical potential at a point (T, ρ) is known using the values of E, S, and p at that point without integrating $1/\rho$ with respect to p.

[14] The difference between the liquid and the gas phases are quantitative, both being disordered, and the one can be told from the other only by the criterion that the former lies on the lower temperature side of the van der Waals type transition region.

long range order shown in Fig. 5 has been neglected. The change from the long range order in Fig. 1 to that shown in Fig. 5 corresponds to the thermal expansion of the lattice constant; but for the purpose of showing the physical implication of the three phases of matter it might be permitted to disregard the long range order shown in Fig. 5, since, when it is taken into consideration, the liquid phase becomes metastable again. The thermal expansion of the lattice constant can be treated fully by the method of the following sections.

We do not want to emphasize the numerical results of this preliminary illustrative example, but the following numbers have some significance. Concerning the critical temperature of condensation, Kirkwood[15] criticized that Cernuschi-Eyring's theory gives too large a value of the critical temperature. For six nearest neighbors, they obtained $kT_c/\epsilon=1.23$. In comparison, assuming $\epsilon_2=0$, the present approximation gives $kT_c/\epsilon_1=0.92$, which is less than the former value. In order to improve their theory, Kirkwood[15] suggested taking the lattice vibrational factor into consideration, and it is our point of view that to increase the number of sublattices to infinity is equivalent to taking into account the lattice vibrational effect completely.

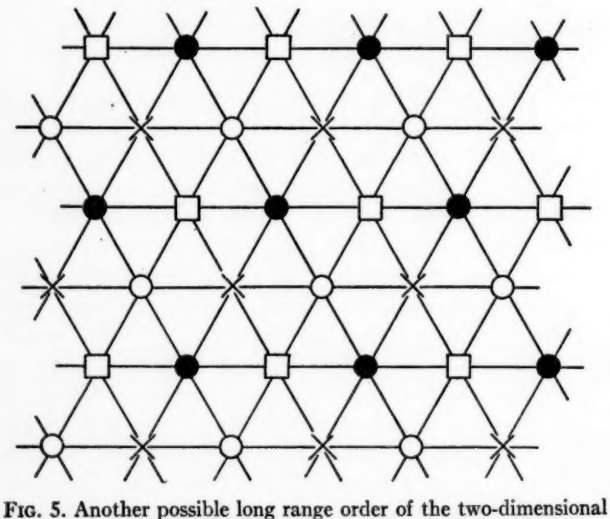

FIG. 5. Another possible long range order of the two-dimensional triangular lattice: ● sublattice I, ○ II, × III, and □ IV.

From the formula of pressure, it can be shown that there is no critical point for melting. This fact can be understood by a subsequent general consideration. By our interpretation, there is a qualitative difference between the fluid and the solid state, the former being disordered, and the latter ordered. Therefore, it is quite natural that the transition between them cannot occur continuously. The fact that there is a critical point for the transition between the liquid and the gas states is only made possible because the difference between these two states is quantitative.[14]

It should be pointed out that the present theory does not involve any difficulty concerning the communal entropy.[16]

[15] J. G. Kirkwood, J. Chem. Phys. 7, 908 (1939).

III. ONE-DIMENSIONAL CONTINUOUS LATTICE

In order to increase the number of interstitial sublattices to infinity, it seems desirable to begin with the one-dimensional case, which can be treated rigorously. Consider a linear lattice with the lattice constant u which is chosen much smaller than the distance of the nearest approach of two atoms. On each lattice point, an atom or a hole is put, with the restriction that two atoms cannot come closer to each other than the allowed nearest distance of approach. Consider as an auxiliary figure a line section having the length $(\kappa-1)u$. Putting an atom or a hole on each of the κ lattice points with the above restriction, various configurations of the line section are obtained. The probability of appearance of a configuration is denoted by $f_{\kappa;\,i}$ $(i=1, 2, \cdots)$, and for brevity's sake, let us put

$$\begin{aligned}\prod_i (f_{\kappa;\,i}L)!&\equiv\Phi_u(\kappa),\\ \sum_i f_{\kappa;\,i}\ln f_{\kappa;\,i}&=[\ln\Phi_u(\kappa)]/L-\ln L\\ &\equiv\Psi_u(\kappa),\end{aligned}\tag{11}$$

with the normalization

$$\sum_i f_{\kappa;\,i}=1,$$

where the product and the summations are carried over all allowed configurations, and L is a number of systems having the same values for the probabilities.[12]

Let us take a line section with $\kappa=m+1$ as a basic figure[10] and suppose that each system has Mm lattice points, where M is the quotient of the total length of a system divided by that of the basic figure mu. Following the method explained in TCP I, Sec. A, one constructs the system from an end adding lattice points one by one. Figure 6 shows an intermediate stage. The number of ways, G_L, of adding the lattice point A so that the portion from P to A has the right distribution[10] of probability and also provided that the part drawn with solid line has had the $r.d.$ is

$$G_L=\Phi_u(m)/\Phi_u(m+1),\tag{12}$$

giving the entropy $S(m)$ of a system:

$$\begin{aligned}S(m)&=k(Mm/L)\ln G_L\\ &=-kMm[\Psi_u(m+1)-\Psi_u(m)].\end{aligned}\tag{13}$$

It should be noted that this formula does not contain any approximation.

As a next step, let us make m infinite and u infinitesimal, keeping the length of the basic figure $l=mu$ constant. No confusion occurs when the dimensions of

[16] Hirschfelder, Stevenson, and Eyring, J. Chem. Phys. 5, 896 (1937); J. G. Kirkwood, J. Chem. Phys. 18, 380 (1950).

the arguments and the subscripts of Ψ are changed as

$$S\equiv\lim_{m\to\infty}S(m)$$

$$=-kMl\lim_{m\to\infty}\{[\Psi(l)_m-\Psi(l-l/m)_m]/[l/m]\}. \quad (14)$$

Here, the m's have two different meanings: those in the subscripts are used to label the functional form of Ψ and the other m's are related to the value of the variables. As shown in Appendix I, the former m's can be made to tend to infinity faster than the latter, so that

$$S=-kMl\lim_{m\to\infty}\lim_{n\to\infty}\{[\Psi(l)_{mn}-\Psi(l-l/m)_{mn}]/[l/m]\}. \quad (15)$$

Assuming that the limiting function

$$\Psi(a)_\infty\equiv\lim_{n\to\infty}\Psi(a)_n,$$

exists and that it is differentiable, Eq. (15) is transformed as follows

$$S=-kMl\lim_{u\to0}\{[\Psi(l)_\infty-\Psi(l-u)_\infty]/u\}$$

$$=-kMl[d\Psi(a)_\infty/da]_{a=l}. \quad (16)$$

At this point, it is perhaps well to say a word on l. As can be seen from the formula of the energy below, l should be chosen so that it covers the whole range where the interatomic potential is appreciably different from zero. Therefore, for inert gas atoms, for which the force is of the short range, l can be a little less than three times the distance of nearest approach r_0 of two atoms,[17] and hence in a basic figure there exist at most three atoms simultaneously. Such a case will be treated hereafter. For particles having the long range field of force, this method is hardly applicable at present.

Let us choose the one end O of the basic figure OA as the origin and place the coordinate as shown in Fig. 7. The portion OB of the length a is subsequently used and will be called an "a-section." The configuration of the line section is specified by the coordinates of the atoms in it, so that $f_a^{(n)}(x_1,\cdots,x_n)dx_1\cdots dx_n$ for $n=0$, 1, 2, and 3 denote the probability of appearance of a configuration of the a-section having n atoms within $dx_1\cdots dx_n$ neighborhood of points $(x_1,\cdots,x_n)$.[18] Then, following the method of generalization by Kirkwood[19] from the discrete to the continuous case, and considering

FIG. 6. An intermediate stage to construct a linear lattice.

the meaning of Eq. (11), $\Psi(a)_\infty$ can be written as[20,21]

$$\Psi(a)_\infty=\sum_{n=0}^{3}\frac{1}{n!}\int_0^a dx_1\cdots$$

$$\times\int_0^a dx_n f_a^{(n)}(x_1,\cdots,x_n)\ln f_a^{(n)}(x_1,\cdots,x_n). \quad (17)$$

$f_a^{(n)}$'s for the basic figure will be simply written as $f^{(n)}$'s omitting the subscript l. $f_a^{(n)}$'s can be expressed by them as follows, when a is larger than $l-r_0$,

$$f_a^{(n)}(x_1,\cdots,x_n)=f^{(n)}(x_1,\cdots,x_n)+\int_a^l dx_{n+1}f^{(n+1)}(x_1,\cdots,x_n,x_{n+1}), \quad (18)$$

where $n=0,\cdots,3$ and $f^{(4)}(x_1,\cdots,x_4)=0$. Using Eqs. (17) and (18), the entropy (16) can be written as[21]

$$S=-kMl\Big\{\sum_{n=1}^{3}\frac{1}{(n-1)!}\int_0^l dx_2\times\int_0^l dx_n f^{(n)}(l,x_2,x_n)\ln f^{(n)}(l,x_2,x_n)-\sum_{n=0}^{2}\frac{1}{n!}\int_0^l dx_1\cdots\int_0^l dx_n\times[1+f^{(n)}(x_1,\cdots,x_n)]f^{(n+1)}(x_1,\cdots,x_n,l)\Big\}. \quad (19)$$

The energy E of a system becomes

$$E=Ml\int_{r_0}^{l}\varphi(r)\rho^{(2)}(r)dr, \quad (20)$$

FIG. 7. The basic figure of the linear assembly with the coordinate system.

[17] See, for instance, R. H. Fowler and E. A. Guggenheim, *Statistical Thermodynamics* (Cambridge University Press, Cambridge, England, 1949), §716.

[18] It should be emphasized that, for instance, $f_a^{(2)}(x_1,x_2)$ does not give the probability density that at least two atoms exist in the a-section at x_1 and x_2, but that exactly two atoms exist in it at these points. The difference between these two probabilities is clearly shown in Eq. (21).

[19] J. G. Kirkwood, J. Chem. Phys. **8**, 205 (1940).

[20] The additional constant due to Planck's constant is omitted here as it plays no role in the present treatment.

[21] The following abbreviated notation is used throughout the rest of the paper

$$\Big[\int_0^a dx_{m+1}\cdots\int_0^a dx_n\psi^{(n)}(x_1,\cdots,x_m,\cdots x_n)\Big]_{n=m}=\psi^{(m)}(x_1,\cdots,x_m),$$

and

$$[\psi^{(n)}(x_1,\cdots,x_n)]_{n=0}=\psi^{(0)},$$

for any function ψ. Therefore in Eq. (17), the term for $n=0$ is $f_a^{(0)}\ln f_a^{(0)}$.

where $\varphi(r)$ is the potential energy between two atoms r apart, and $\rho^{(2)}(r)$ is derived as follows. The probability density of appearance of a configuration such that at least two particles exist in a basic figure at x_1 and x_2 is

$$\rho^{(2)}(x_1, x_2)=f^{(2)}(x_1, x_2)+\int_0^l dx_3 f^{(3)}(x_1, x_2, x_3). \quad (21)$$

This function should be invariant with regard to translations of the coordinate system, and on the other hand the space is understood to be homogeneous. Hence $\rho^{(2)}(x_1, x_2)$ depends only on $r=|x_1-x_2|$ and can be written as $\rho^{(2)}(r)$, which is used in Eq. (20).

Combining Eqs. (19) and (20), one obtains the Helmholtz free energy, and minimizing it under the following additional conditions the equilibrium state is solved as a function of the density ρ and the temperature T. One of the conditions is the normalization

$$\sum_{n=0}^{3} \frac{1}{n!} \int_0^l dx_1 \cdots \int_0^l dx_n f^{(n)}(x_1, \cdots, x_n)=1, \quad (22)$$

and another one is the constancy of the density

$$\rho=\sum_{n=1}^{3} \frac{1}{(n-1)!} \int_0^l dx_2 \cdots \times \int_0^l dx_n f^{(n)}(x, x_2, \cdots, x_n), \quad (23)$$

which has the meaning of the average number of particles per unit length for one system, and is a given quantity.

As an illustration, a little more specialized case will be solved in which l is assumed to be less than $2r_0$ so that one can put

$$f^{(3)}(x_1, x_2, x_3)=0. \quad (24)$$

Then Eq. (21) gives

$$\rho^{(2)}(r)=\rho^{(2)}(x_1, x_2)=f^{(2)}(x_1, x_2) \text{ with } r=|x_1-x_2|, \quad (25)$$

which can be written as $f^{(2)}(r)$, and this is the only unknown function in the formula of the Helmhotz free energy. The process to solve this problem is shown in Appendix II, and the result is

$$p/kT=\xi, \quad (26)$$

where ξ is a solution of

$$\Gamma_\infty(\xi, T)/\rho+\partial\Gamma_\infty(\xi, T)/\partial\xi=0, \quad (27)$$

with

$$\Gamma_l(\xi, T)=\int_{r_0}^{l} \exp[-\varphi(x)/kT-\xi x]dx. \quad (28)$$

This result is identical with what Gürsey[22] derived as the rigorous solution for the one-dimensional assembly. His only significant assumption is that the interaction of particles across other particles is neglected so that the total energy of the system E can be written as

$$E=\sum_{i=1}^{N-1} E_{i,\,i+1} \quad (29)$$

where $E_{i,\,i+1}$ is the potential energy between the i-th particle and its nearest neighbor, the $(i+1)$-th. The present treatment is different from his in the simplifying assumption,

$$\varphi(x)=0 \quad \text{for} \quad x>l \quad \text{and} \quad l<2r_0, \quad (30)$$

which subsequently results in the assumption (29).

This agreement of our results with Gürsey's justifies our method of generalization from the discrete lattice to the continuum. More precisely, our Eq. (16) for the entropy of the one dimensional continuous lattice has been proved to be rigorous.

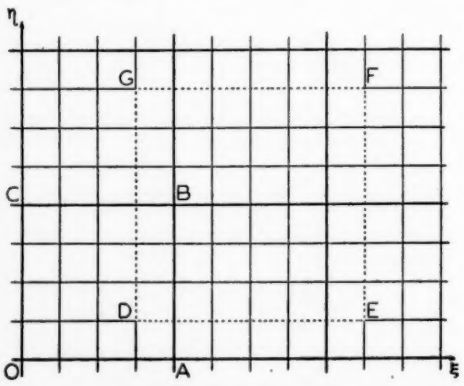

FIG. 8. Two-dimensional square lattice with long range order. $OA=hu$, $DE=mu$. $DEFG$ is a basic figure.

IV. TWO- AND THREE-DIMENSIONAL CONTINUOUS LATTICES

The essential difference of the two- or the three-dimensional assembly from the linear one is that the former has the possibility of becoming ordered whereas the latter has not. The method of treatment of the ordered state will be explained for the two-dimensional case, as it is easier to handle intuitively than the three-dimensional one.

It is assumed that the substance condenses in a square lattice, though the atoms are assumed to have a spherically symmetric field of force. To begin with, consider a square lattice with the lattice constant u which is chosen much smaller than the distance of the nearest approach of two atoms. When the lattice has long range order, its period is denoted by hu, and then the lattice points are divided into h^2 sublattices. One of the sublattices is taken as the standard and will be called the (0, 0)-sublattice, which is drawn in thick lines in Fig. 8. $OABC$ is one of the cells of this sublattice. The rectangular coordinate system (ξ, η) is placed with O as the origin as shown in Fig. 8. Then each of the points on this sublattice has the coordinate (0, 0) with (hu, hu) as the mode. Likewise, all the points having the coordi-

[22] F. Gürsey, Proc. Cambridge Phil. Soc. **46**, 182 (1950).

nates (pu, qu) with (hu, hu) as the mode lie on the same sublattice, and all the points of this sublattice have the coordinates of this type. Therefore one can name the sublattice with the coordinate of its point in the square $OABC$ or on the sides OA and OC. Hence the sublattices are named "(pu, qu)-sublattice" with $0 \leqq p, q \leqq h-1$.

A rectangle (or a square) having its left lower corner on the (pu, qu)-sublattice will be called a (pu, qu)-rectangle (or -square). The probability of appearance of a configuration of a (pu, qu)-rectangle having the width $(\lambda-1)u$ and the length $(\kappa-1)u$ is denoted by $f_{(p, q)\kappa, \lambda;\ i}$ and let us put

$$\prod_i [f_{(p, q)\kappa, \lambda;\ i} L]! \equiv \Phi_u(p, q; \kappa, \lambda), \tag{31}$$

where the product is carried over all allowed configurations and L is a number of systems having the same values for the probabilities.[12]

(pu, qu)-squares with $\kappa = \lambda = m+1$ are taken as the basic figure $(0 \leqq p, q \leqq h-1)$. m is taken larger than h. Following the method in TCP I, Sec. E, the number of ways, G, of constructing one whole lattice becomes

$$G = [\prod_{p=0}^{h-1} \prod_{q=0}^{h-1} G_{(p, q;\ m)}]^{(Mm^2)/(Lh^2)}, \tag{32}$$

where

$$G_{(p, q;\ m)} = [\Phi_u(p, q; m, m+1) \cdot \Phi_u(p, q; m+1, m)] \div [\Phi_u(p, q; m+1, m+1) \cdot \Phi_u(p, q; m, m)], \tag{33}$$

and M is the quotient of the total area of the system divided by that of the basic figure $(mu)^2$, so that the total number of lattice points in a system is Mm^2. The entropy of the system $S(m)$ becomes

$$S(m) = k \ln G = -kM(m^2/h^2) \sum_{p=0}^{h-1} \sum_{q=0}^{h-1} \times [\{\Psi_u(p, q; m+1, m+1) - \Psi_u(p, q; m+1, m)\} - \{\Psi_u(p, q; m, m+1) - \Psi_u(p, q; m, m)\}], \tag{34}$$

where,

$$\Psi_u(p, q; \kappa, \lambda) \equiv [\ln \Phi_u(p, q; \kappa, \lambda)]/L - \ln L = \sum_i f_{(p, q)\kappa, \lambda;\ i} \ln f_{(p, q)\kappa, \lambda;\ i}, \tag{35}$$

and

$$\sum_i f_{(p, q)\kappa, \lambda;\ i} = 1,$$

the summation being carried over all allowed configurations. It should be noted that Eq. (34) is an approximate formula as explained in TCP I, Sec. E, whereas Eq. (13) is rigorous.

Next, m and h are made infinite and u infinitesimal, keeping $l \equiv mu$ and $g \equiv hu$ constants, respectively. No confusion occurs when the dimensions of the arguments and the subscripts of Ψ are changed as

$$S \equiv \lim_{u \to 0} S(m) = -kM(l^2/g^2) \lim_{h \to 0} \sum_{p=0}^{h-1} \sum_{q=0}^{h-1} (g/h)^2 \times \lim_{m \to 0} \lim_{n \to 0} [\{\Psi(pu, qu; l, l)_{mn} - \Psi(pu, qu; l, l-l/m)_{mn}\} - \{\Psi(pu, qu; l-l/m, l)_{mn} - \Psi(pu, qu; l-l/m, l-l/m)_{mn}\}] \div (l/m)^2, \tag{36}$$

where n has been introduced by the same reasoning as in Eqs. (14) and (15), as explained in Appendix I, and again can be made to go to infinity faster than m. Moreover, in Eq. (36), m can be made to tend to infinity faster than h, too, as is shown in Appendix III, giving finally

$$S = -kM(l^2/g^2) \int_0^g d\xi \times \int_0^g d\eta [\partial^2 \Psi(\xi, \eta; a, b)_\infty / \partial a \partial b]_{a=b=l}, \tag{37}$$

where it is assumed as before that the limiting function

$$\Psi(\xi, \eta; a, b)_\infty \equiv \lim_{n \to \infty} \Psi(\xi, \eta; a, b)_n$$

exists and that it is differentiable.

In the linear case it is necessary and sufficient to choose l so that it covers the whole range of the interatomic potential, but for the two- and the three-dimensional assembly, the larger the l is, the better the approximation becomes, because the entropy formula is not rigorous. But to ease the mathematical difficulties, it is advisable to select l so that it just covers the range of interatomic potential of the short range force so that only several atoms can exist in the basic figure simultaneously. Because of the mathematical complexity, the present method is not applicable for the particle with long-range force.

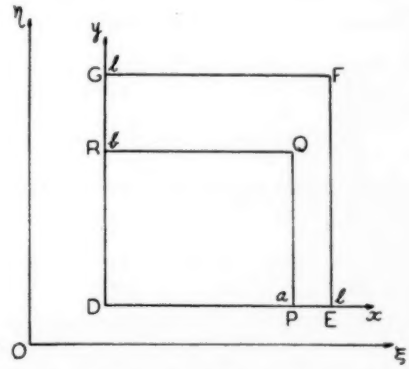

FIG. 9. The basic figure $DEFG$ and the coordinate system in the two-dimensional continuous lattice. $DPQR$ is a $(\xi, \eta; a, b)$-rectangle.

Choose the left lower corner D of the basic figure as the origin and place another rectangular coordinate system (x, y) as shown in Fig. 9. The coordinates of D are (ξ, η) with reference to the previous system. Rectangles in the basic figure having one corner at D, such as $DPQR$, are subsequently used, and when the length of the sides are a and b, it will be called a "$(\xi, \eta; a, b)$-rectangle.

A configuration of a $(\xi, \eta; a, b)$-rectangle is specified only by the coordinates of the atoms $(\mathbf{x}_1, \mathbf{x}_2, \cdots, \mathbf{x}_n)$ in it, since they are assumed to exert spherically symmetric field of force. $f_{(\xi,\eta)a,b}{}^{(n)}(\mathbf{x}_1, \mathbf{x}_2, \cdots, \mathbf{x}_n)d\mathbf{x}_1\cdots d\mathbf{x}_n$ denotes the probability of appearance of a configuration of the $(\xi, \eta; a, b)$-rectangle having n atoms within the $d\mathbf{x}_1\cdots d\mathbf{x}_n$ neighborhood of the points $(\mathbf{x}_1, \cdots, \mathbf{x}_n)$.[18] Following the method of Sec. III and considering the meaning of Eq. (35), $\Psi(\xi, \eta; a, b)_\infty$ can be written as follows,

$$\Psi(\xi,\eta;a,b)_\infty=\sum_{n=0}\frac{1}{n!}\int_{(a,b)}\cdots\int f_{(\xi,\eta)a,b}{}^{(n)}(\mathbf{x}_{1,\cdots,n}) \times\ln f_{(\xi,\eta)a,b}{}^{(n)}(\mathbf{x}_{1,\cdots,n})d\mathbf{x}_{1,\cdots,n}, \quad (38)$$

where the integration is carried over the $(\xi, \eta; a, b)$-rectangle for each variable and $(\mathbf{x}_{1,\cdots,n})$ and $d\mathbf{x}_{1,\cdots,n}$ stand for $(\mathbf{x}_1, \mathbf{x}_2, \cdots, \mathbf{x}_n)$ and $d\mathbf{x}_1 d\mathbf{x}_2\cdots d\mathbf{x}_n$, respectively.

$f_{(\xi,\eta)a,b}{}^{(n)}$'s can be expressed by $f_{(\xi,\eta)l,l}{}^{(n)}$'s, which will be written as $f_{(\xi,\eta)}{}^{(n)}$'s hereafter, as follows

$$f_{(\xi,\eta)a,b}{}^{(n)}(\mathbf{x}_{1,\cdots,n}) =f_{(\xi,\eta)}{}^{(n)}(\mathbf{x}_{1,\cdots,n})+\sum_{j=1}\frac{1}{j!}\mathbf{I}_{a,b}{}^{(n+1)}\mathbf{I}_{a,b}{}^{(n+2)}\cdots \times\mathbf{I}_{a,b}{}^{(n+j)}f_{(\xi,\eta)}{}^{(n+j)}(\mathbf{x}_{1,\cdots,n+j}), \quad (39)$$

where $\mathbf{I}_{a,b}{}^{(k)}$ is an integration operator:

$$\mathbf{I}_{a,b}{}^{(k)}=\int_0^l dx_k\int_0^l dy_k-\int_0^a dx_k\int_0^b dy_k.$$

Differentiating Eq. (38) and using the relation (39), the entropy S is obtained from Eq. (37), but the details are omitted. $f_{(\xi,\eta)a,b}{}^{(n)}$'s are normalized by

$$\sum_{n=0}\frac{1}{n!}\int_{(l,l)}\cdots\int f_{(\xi,\eta)}{}^{(n)}(\mathbf{x}_{1,\cdots,n})d\mathbf{x}_{1,\cdots,n}=1, \quad (40)$$

and the particle density at $\xi+\mathbf{x}$ (with the mode (g, g)) is given by

$$\rho^{(1)}(\xi+\mathbf{x})=\sum_{n=1}\frac{1}{(n-1)!} \times\int_{(l,l)}\cdots\int f_{(\xi,\eta)}{}^{(n)}(\mathbf{x}_{1,\cdots,n})d\mathbf{x}_{1,\cdots,n}, \quad (41)$$

which is not a constant for the ordered state, and is related to the given average density ρ by

$$\rho\equiv\frac{1}{g^2}\int_0^g d\xi\int_0^g d\eta\rho^{(1)}(\xi). \quad (42)$$

The probability density $\rho_{(\xi,\eta)}{}^{(2)}(\mathbf{x}, \mathbf{x}+\mathbf{r})$ that at least two atoms exist in the basic figure at $\mathbf{x}$ and $\mathbf{x}+\mathbf{r}$ becomes

$$\rho_{(\xi,\eta)}{}^{(2)}(\mathbf{x}, \mathbf{x}+\mathbf{r})=\sum_{n=2}\frac{1}{(n-2)!} \times\int_{(l,l)}\cdots\int f_{(\xi,\eta)}{}^{(n)}(\mathbf{x}, \mathbf{x}+\mathbf{r}, \mathbf{x}_{3,\cdots,n})d\mathbf{x}_{3,\cdots,n}, \quad (43)$$

which depends on $\xi+\mathbf{x}$ and $\mathbf{r}$. When the potential energy between two atoms $\varphi(r)$ is given, the total potential energy of the system becomes

$$E=(M/2)(l^2/g^2) \times\int_0^g d\xi\int_0^g d\eta\int\int_{(l,l)}\rho_{(\xi,\eta)}{}^{(2)}(0, \mathbf{r})\varphi(r)d\mathbf{r}. \quad (44)$$

Combining Eq. (44) and the entropy, the Helmholtz free energy can be constructed, which is made minimum, in order to obtain the equilibrium state, with respect to the functions $f_{(\xi,\eta)}{}^{(n)}$'s and at the same time with respect to g. The change of g with the temperature yields the thermal expansion of the lattice constant.

The equations for the two-dimensional case can easily be extended to the three-dimensional case. Only the results will be listed below without explanation. For the ordered state, the entropy S is

$$S=-kM(l^3/g^3)\int_0^g d\xi\int_0^g d\eta \times\int_0^g d\zeta[\partial^3\Psi(\xi;\mathbf{a})_\infty/\partial a\partial b\partial c]_{a=b=c=l}, \quad (45)$$

where $\boldsymbol{\xi}$ and $\mathbf{a}$ stand for (ξ, η, ζ) and (a, b, c), respectively, and

$$\Psi(\boldsymbol{\xi};\mathbf{a})_\infty=\sum_{n=0}\frac{1}{n!}\int_{(a,b,c)}\cdots\int f_{(\xi)\mathbf{a}}{}^{(n)}(\mathbf{x}_{1,\cdots,n}) \times\ln f_{(\xi)\mathbf{a}}{}^{(n)}(\mathbf{x}_{1,\cdots,n})d\mathbf{x}_{1,\cdots,n}. \quad (46)$$

The potential energy E is

$$E=(M/2)(l^3/g^3)\int_0^g d\xi\int_0^g d\eta \times\int_0^g d\zeta\int\int\int_{(l,l,l)}\rho_{(\xi)}{}^{(2)}(0, \mathbf{r})\varphi(r)d\mathbf{r}, \quad (47)$$

where

$$\rho_{(\xi)}{}^{(2)}(\mathbf{x}, \mathbf{x}+\mathbf{r}) = \rho^{(2)}(\xi+\mathbf{x}, \xi+\mathbf{x}+\mathbf{r}) = \sum_{n=2} \frac{1}{(n-2)!} \times \int_{(l,l,l)} \cdots \int f_{(\xi)}{}^{(n)}(\mathbf{x}, \mathbf{x}+\mathbf{r}, \mathbf{x}_{3,\ldots,n}) d\mathbf{x}_{3,\ldots,n}, \quad (48)$$

and

$$f_{(\xi)\mathfrak{a}}{}^{(n)}(\mathbf{x}_{1,\ldots,n}) = f_{(\xi)}{}^{(n)}(\mathbf{x}_{1,\ldots,n}) + \sum_{j=1} \frac{1}{j!} \mathbf{J}_{\mathfrak{a}}{}^{(n+1)} \cdots \mathbf{J}_{\mathfrak{a}}{}^{(n+j)} f_{(\xi)}{}^{(n+j)}(\mathbf{x}_{1,\ldots,n+j}), \quad (49)$$

with the integration operator

$$\mathbf{J}_{\mathfrak{a}}{}^{(k)} = \int_0^l dx_k \int_0^l dy_k \int_0^l dz_k - \int_0^a dx_k \int_0^b dy_k \int_0^c dz_k,$$

and $f_{(\xi)}{}^{(n)}(\mathbf{x}_{1,\ldots,n})$ stands for $f_{(\xi)l}{}^{(n)}(\mathbf{x}_{1,\ldots,n})$. With these relations, the Helmholtz free energy can be expressed as a function of $f_{(\xi)}{}^{(n)}$'s.

For both the two- and the three-dimensional cases, the formulas for the disordered states can be simplified when $f_{(\xi)}{}^{(n)}$'s are put independent of ξ; but no numerical calculations were made so far because the formulas are yet formidable to handle.

The present method seems hardly applicable to the triangular or to the hexagonal lattice, because the number of ways of constructing the lattice cannot be written in a form as simple as Eq. (33) when the basic figure has the hexagonal symmetry.

V. APPROXIMATION FOR SOLID

The solid state can be solved by the method in the previous section, but because of its long range order, the following short-cut method is more convenient. This method can be applied for any lattice type.

Consider some type of a lattice. The space can be divided into polyhedrons by bisecting planes of the lines connecting two nearest or next nearest neighbor lattice points. In the solid state, it can be assumed that each atom is attached to a lattice point and that the probability of finding an atom near the boundary of the polyhedron is small. This assumption leads to the following treatment of the solid phase. The approximation corresponding to Bethe's one will be explained.

The coordinate of each atom is measured from the corresponding lattice point. The lattice constant is denoted by u. Let $f_u{}^{(2)}(\mathbf{x}_1, \mathbf{x}_2) d\mathbf{x}_1 d\mathbf{x}_2$ denote[23] the probability of appearance of such a configuration of a particle pair that one particle exists in the $d\mathbf{x}_1$ neighborhood of point $\mathbf{x}_1$ and another particle exists in the $d\mathbf{x}_2$ neighborhood of point $\mathbf{x}_2$.

[23] In order to make the discussion simpler, no holes are assumed to exist. But the empty lattice points can be taken into account with slight modification.

$f_u{}^{(1)}(\mathbf{x})$ is defined by

$$f_u{}^{(1)}(\mathbf{x}) = \int f_u{}^{(2)}(\mathbf{x}, \mathbf{x}_2) d\mathbf{x}_2, \quad (50)$$

where the integration is carried over the space near the lattice point where $f_u{}^{(2)}(\mathbf{x}, \mathbf{x}_2)$ is significantly different from zero.

$f_u{}^{(2)}(\mathbf{x}_1, \mathbf{x}_2)$ and $f_u{}^{(1)}(\mathbf{x})$ are generalization of the probability variables y_i's and x_i's in Tables I and II in TCP I, Sec. A, and following Kirkwood,[19] Eq. (A.5) in that paper can be generalized to[20]

$$\begin{aligned} \ln X_L &= L \int f_u{}^{(1)}(\mathbf{x}) \ln f_u{}^{(1)}(\mathbf{x}) d\mathbf{x} + L \ln L, \\ \ln Y_L &= L \int d\mathbf{x}_1 \int d\mathbf{x}_2 f_u{}^{(2)}(\mathbf{x}_1, \mathbf{x}_2) \\ &\quad \times \ln f_u{}^{(2)}(\mathbf{x}_1, \mathbf{x}_2) + L \ln L. \end{aligned} \quad (51)$$

Then the last equation in Sec. B, TCP I gives

$$\begin{aligned} S_u &= k(M/L) \ln G_L \\ &= kM \Big[(2z'-1) \int f_u{}^{(1)}(\mathbf{x}) \ln f_u{}^{(1)}(\mathbf{x}) d\mathbf{x} \\ &\quad - z' \int d\mathbf{x}_1 \int d\mathbf{x}_2 f_u{}^{(2)}(\mathbf{x}_1, \mathbf{x}_2) \ln f_u{}^{(2)}(\mathbf{x}_1, \mathbf{x}_2) \Big], \end{aligned} \quad (52)$$

where $2z'$ is the coordination number. The potential energy E_u for a system becomes

$$E_u = z' M \int d\mathbf{x}_1 \int d\mathbf{x}_2 \varphi_u(\mathbf{x}_1, \mathbf{x}_2) f_u{}^{(2)}(\mathbf{x}_1, \mathbf{x}_2), \quad (53)$$

where $\varphi_u(\mathbf{x}_1, \mathbf{x}_2)$ is the potential energy between two particles.

The Helmholtz free energy F_u should be made minimum under the additional conditions (50) and the following three which are the requirements derived from the physical consideration,

$$\int d\mathbf{x}_1 \int d\mathbf{x}_2 f_u{}^{(2)}(\mathbf{x}_1, \mathbf{x}_2) = 1, \quad (54)$$

$$\begin{cases} f_u{}^{(1)}(\mathbf{x}) = f_u{}^{(1)}(-\mathbf{x}), \\ f_u{}^{(2)}(\mathbf{x}_1, \mathbf{x}_2) = f_u{}^{(2)}(-\mathbf{x}_2, -\mathbf{x}_1). \end{cases} \quad (55)$$

It must be noted that the potential function satisfies,

$$\varphi_u(\mathbf{x}_1, \mathbf{x}_2) = \varphi_u(-\mathbf{x}_2, -\mathbf{x}_1). \quad (56)$$

Using appropriate indeterminate multipliers, one ob-

tains the following relations:

$$f_u^{(1)}(\mathbf{x})=\exp\left[\frac{\lambda_2(\mathbf{x})+\lambda_2(-\mathbf{x})}{2(2z'-1)kT}-1\right],$$

$$f_u^{(2)}(\mathbf{x}_1,\ \mathbf{x}_2)=\exp\left[\frac{\lambda_2(\mathbf{x}_1)+\lambda_2(-\mathbf{x}_2)}{2z'kT}-\frac{\varphi_u(\mathbf{x}_1,\ \mathbf{x}_2)}{kT}-\frac{\lambda_1}{z'kT}-1\right], \tag{57}$$

and[24]

$$F_u/M=-\lambda_1+(z'-1)kT+K(T), \tag{58}$$

where λ_1 and $\lambda_2(\mathbf{x})$ are determined from Eqs. (50) and (54). The final equation for $\lambda_2(\mathbf{x})$ is

$$\exp\left[\frac{(1-z')\lambda_2(\mathbf{x})+z'\lambda_2(-\mathbf{x})}{2z'(2z'-1)kT}-1\right]$$

$$\times\int d\mathbf{x}_1\int d\mathbf{x}_2\exp\left[\frac{\lambda_2(\mathbf{x}_1)+\lambda_2(-\mathbf{x}_2)}{2z'kT}-\frac{\varphi_u(\mathbf{x}_1,\ \mathbf{x}_2)}{kT}\right]$$

$$=\int d\mathbf{x}_2\exp\left[\frac{\lambda_2(-\mathbf{x}_2)}{2z'kT}-\frac{\varphi_u(\mathbf{x},\ \mathbf{x}_2)}{kT}\right]. \tag{59}$$

When the potential energy is assumed as a function of the distance between two particles, Eq. (59) can be solved for each value of u, and the value of λ_1 is determined. The value of u which makes Eq. (58) minimum is the desired lattice constant.

Approximation better than Bethe's one can be formulated by taking larger basic figure[25] than the pair of particles and using the method explained in TCP I to approximate the entropy.

A remark may be added here concerning the problem of "rotational transformation." The method adopted in this section can be applied to that problem with slight modification to obtain Bethe's and better approximations. The Bethe's case is shown in Appendix IV.

VI. CONCLUSION

Ono and Murakami[26] showed the intimate relationships between the theory of (a) the discrete order-disorder system and (b) of the continuous aggregate system, deriving (a) from the Mayer-Born-Green-Kirkwood's method[1-3] for (b). In the present paper, the clear insight into the cooperative character of the aggregate states of matter has been shown deriving (b) from (a).

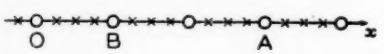

FIG. 10. The model of a linear lattice corresponding to Eq. (60). OA is the basic figure. $OA=l$ $OB=l/m$. O is the origin of the coordinate x. The case illustrated here is for $m=3$, and $n=4$. O and × denote the points in the first and the second group, respectively.

Before calculating with the present theory, various modifications to simplify the mathematical procedure seem necessary, but we are not in the position yet to report the further detail.

In conclusion the author wishes to thank Prof. T. Sakai of the University of Tokyo and Prof. John G. Kirkwood of the California Institute of Technology for their encouragement and advice.

APPENDIX I

In order to justify that Eq. (14) can be transformed into Eq. (15), one has to know what is meant by

$$-kMl[\Psi(l)_{mn}-\Psi(l-l/m)_{mn}]/[l/m]. \tag{60}$$

This is the entropy formula for the following model. The basic figure is a line section of length l, which is divided into mn parts, and has $(mn+1)$ lattice points. The probabilities of appearance of configurations of this basic figure are taken as variables. Introducing the coordinate system into the lattice as shown in Fig. 10, the lattice points can be divided into two groups. The points having the coordinates $x=pl/m$ with $p=0,\ \pm1,\ \pm2,\ \cdots$ are included into the first group as indicated by circles in Fig. 10, and other lattice points into the second as indicated by crosses.

Equation (60) gives the rigorous entropy for the case in which all the line sections of length l having their ends of the first group points have the right distribution[10] of probabilities, but other line sections with the length l having their ends on the second lattice points are not guaranteed to have the *r. d.* To change l/m in Eq. (60) into l/mn is to guarantee every line section of length l for the *r. d.*

APPENDIX II

When Eq. (24) is assumed, Eqs. (23) and (22) give

$$\begin{aligned}\rho&=f^{(1)}(x)+\int_{r_0}^{l-z}dxf^{(2)}(x), &&\text{for}\quad 0\leqq x\leqq l-r_0,\\ &=f^{(1)}(x), &&\text{for}\quad l-r_0\leqq x\leqq r_0,\\ &=f^{(1)}(x)+\int_{r_0}^{x}dxf^{(2)}(x), &&\text{for}\quad r_0\leqq x\leqq l,\end{aligned} \tag{61}$$

and

$$f^{(0)}+\rho l-\int_{r_0}^{l}dr(l-r)f^{(2)}(r)=1. \tag{62}$$

Combining Eqs. (19) and (20), modified by the assumption (24), and using indeterminate multipliers, ξ, $\eta(x)$, and ζ, for the additional conditions (61) and (62), the Helmholtz free energy per unit length F/Ml can be written as,[24]

$$\begin{aligned}F/Ml=&\int_{r_0}^{l}\varphi(r)f^{(2)}(r)dr\\ &+kT\Big\{-[1+\ln f^{(0)}]f^{(1)}(l)+f^{(1)}(l)\ln f^{(1)}(l)\\ &-\int_{r_0}^{l}dr[1+\ln f^{(1)}(r)]f^{(2)}(r)+\int_{r_0}^{l}drf^{(2)}(r)\ln f^{(2)}(r)\\ &+\xi\Big[f^{(0)}+\rho l-\int_{r_0}^{l}dr(l-r)f^{(2)}(r)-1\Big]\\ &+\int_{r_0}^{l}dx\eta(x)\Big[f^{(1)}(x)+\int_{r_0}^{x}drf^{(2)}(r)-\rho\Big]\\ &+\zeta\Big[f^{(1)}(l)+\int_{r_0}^{l}drf^{(2)}(r)-\rho\Big]\Big\}+K(T).\end{aligned} \tag{63}$$

Putting the variation of F/Ml equal to zero, one obtains the following simultaneous equations for the four unknown parame-

[24] $K(T)$ is the kinetic energy part and depends only on T.

[25] See reference 16 of TCP I.

[26] S. Ono and T. Murakami, Busseiron-Kenkyu (Japan) **28**, 39, 49 and 62 (1950); Memoirs of Faculty of Engineering, Kyushu University, Vol. 12, No. 3 (in press).

ters $f^{(0)}$, $f^{(1)}(l)$, ξ, ζ, and the three unknown functions $f^{(1)}(x)$, $f^{(2)}(r)$, $\eta(x)$,

$$f^{(1)}(l)=\xi f^{(0)}, \tag{64}$$

$$-\ln f^{(0)}+\ln f^{(1)}(l)+\zeta=0, \tag{65}$$

$$f^{(2)}(r)=\eta(r)f^{(1)}(r), \tag{66}$$

$$\varphi(r)/kT+\ln[f^{(2)}(r)/f^{(1)}(r)]-\xi(l-r)+\int_r^l \eta(x)dx+\zeta=0, \tag{67}$$

$$f^{(0)}+\rho l-\int_{r_0}^l dr(l-r)f^{(2)}(r)=1, \tag{68}$$

$$f^{(1)}(x)+\int_{r_0}^x drf^{(2)}(r)=\rho, \tag{69}$$

$$f^{(1)}(l)+\int_{r_0}^l drf^{(2)}(r)=\rho. \tag{70}$$

Eliminating ζ from Eqs. (65) and (67), and inserting Eqs. (64) and (66) into it, one obtains

$$\varphi(r)/kT+\ln\eta(r)-\xi(l-r)+\int_r^l \eta(x)dx-\ln\xi=0, \tag{71}$$

which can be solved for $\eta(r)$,

$$1/\eta(r)=\exp[\varphi(r)/kT+\xi r]\times\left\{\int_r^l \exp[-\varphi(r)/kT-\xi r]dr+e^{-\xi l}/\xi\right\}. \tag{72}$$

Next, from Eqs. (66) and (69),

$$f^{(2)}(r)/\eta(r)+\int_{r_0}^r dxf^{(2)}(x)=\rho, \tag{73}$$

which gives

$$f^{(2)}(r)=\rho\eta(r)\exp\left[-\int_{r_0}^r \eta(x)dx\right]. \tag{74}$$

Combining Eqs. (74), (71) and (72),

$$f^{(2)}(r)=\rho\xi[\xi\Gamma_l(\xi,T)+e^{-\xi l}]^{-1}\exp[-\varphi(r)/kT-\xi r], \tag{75}$$

where $\Gamma_l(\xi,T)$ is defined by Eq. (28).

Combining Eqs. (64), (68) and (69),

$$\left[\rho-\int_{r_0}^l drf^{(2)}(r)\right]\Big/\xi+\rho l-\int_{r_0}^l dr(l-r)f^{(2)}(r)=1. \tag{76}$$

Inserting Eq. (75) into this, one obtains:

$$\Gamma_l(\xi,T)/l+\partial\Gamma_l(\xi,T)/\partial\xi-(1+\xi l-\xi/\rho)e^{-\xi l}/\xi^2=0, \tag{77}$$

which can easily be transformed into Eq. (27) using the condition (30).

Equation (26) is derived as follows: the total length of the system is put $R\equiv Ml$ and the total number of particles $N\equiv\rho R$. The pressure p is then

$$p=-\partial F/\partial R=-\{\partial[FN/Ml\rho]/\partial\rho\}\cdot\{\partial\rho/\partial R\}=\rho[\partial(F/Ml)/\partial\rho]-[A/Ml]=\xi kT \tag{78}$$

from Eq. (63).

APPENDIX III

In order to justify the transformation of Eq. (36) into Eq. (37), it is sufficient to show what the approximation

$$-kM(l^2/g^2)\sum_{p=0}^{h-1}\sum_{q=0}^{h-1}(g/h)^2[\partial^2\Psi(pu,qu;a,b)_\infty/\partial a\partial b]_{a=b=l} \tag{79}$$

gives. This is the entropy formula in the following model. For (ξ,η)-square with

$$\begin{cases} pu\leqq\xi<(p+1)u, \\ qu\leqq\eta<(q+1)u, \end{cases}$$

the probabilities of appearance of a basic figure are assumed to have the same functional form with that corresponding to the (pu,qu)-square: $f_{(pu,qu)^{(n)}}(\mathbf{x}_1,\cdots,\mathbf{x}_n)$. This is a better approximation than

$$-kM(l^2/g^2)\sum_{p=0}^{h-1}\sum_{q=0}^{h-1}(g/h)^2\times[\{\Psi(pu,qu;l,l)_\infty-\Psi(pu,qu;l,l-l/m)_\infty\}-\{\Psi(pu,qu;l-l/m,l)_\infty-\Psi(pu,qu;l-l/m,l-l/m)_\infty\}]\div(l/m)^2, \tag{80}$$

because the right distribution of probabilities is guaranteed for every square in Eq. (79), whereas it is only for discrete squares in Eq. (80). To increase h to infinity in Eq. (79) corresponds to assign a probability density function for every point.

APPENDIX IV. ROTATIONAL TRANSFORMATION

On each lattice point, a polyatomic molecule is located which can take any direction ω. The potential energy between neighboring molecules is assumed to be a function of directions of the molecules, ω_1 and ω_2, and denoted by $\varphi(\omega_1,\omega_2)$. The case of two sublattices will be treated.

$g_{ab}^{(2)}(\omega_1,\omega_2)$ denotes the probability density of appearance of a configuration of a molecular pair such that a molecule on the a-sublattice has the direction ω_1 and the one on the adjacent b-sublattice has ω_2. The normalization condition is

$$\int d\omega_1\int d\omega_2 g_{ab}^{(2)}(\omega_1,\omega_2)=1. \tag{81}$$

$g_a^{(1)}(\omega)$ and $g_b^{(1)}(\omega)$ denote the probability density of appearance of a molecule having the direction ω on a- and b-sublattices respectively. These are connected with $g_{ab}^{(2)}(\omega_1,\omega_2)$ by

$$\begin{cases} g_a^{(1)}(\omega_1)=\int d\omega_2 g_{ab}^{(2)}(\omega_1,\omega_2), \\ g_b^{(1)}(\omega_2)=\int d\omega_1 g_{ab}^{(2)}(\omega_1,\omega_2). \end{cases} \tag{82}$$

The free energy per molecule is[24]

$$F/M=z'\int d\omega_1\int d\omega_2\varphi(\omega_1,\omega_2)g_{ab}^{(2)}(\omega_1,\omega_2)+kT\Big[z'\int d\omega_1\int d\omega_2 g_{ab}^{(2)}(\omega_1,\omega_2)\log g_{ab}^{(2)}(\omega_1,\omega_2)-\{(2z'-1)/2\}\int d\omega g_a^{(1)}(\omega)\log g_a^{(1)}(\omega)-\{(2z'-1)/2\}\int d\omega g_b^{(1)}(\omega)\log g_b^{(1)}(\omega)\Big]+K(T). \tag{83}$$

Minimizing F, under the conditions (81) and (82), one obtains

$$g_{ab}^{(2)}(\omega_1,\omega_2)\cdot\lambda=[g_a^{(1)}(\omega_1)\cdot g_b^{(1)}(\omega_2)]^{(2z'-1)/(2z')}\times\exp[-\varphi(\omega_1,\omega_2)/kT]. \tag{84}$$

Inserting this into Eqs. (81) and (82), three equations to determine λ, $g_a^{(1)}(\omega_1)$ and $g_b^{(1)}(\omega_2)$ are obtained. Equation (84) is identical with that obtained using a different method by T. Nakamura, who has solved the problem in his report.[27]

[27] T. Nakamura, Busseiron-Kenkyu (Japan) **29**, 44 (1950).

Self-Diffusion in CO_2 at Moderate Pressures*

K. D. TIMMERHAUS AND H. G. DRICKAMER
Department of Chemistry, University of Illinois, Urbana, Illinois

(Received June 14, 1951)

Diffusion data are presented for the system $CO_2-C^{14}O_2$ over a pressure range from 0.50 to 28.1 atmospheres. Within the accuracy of the data, agreement is obtained with the diffusion theory of Enskog and Chapman, using the Lennard-Jones model.

IN this paper diffusion data are presented for the system $C^{14}O_2$ at pressures from 0.50 to 28.1 atmospheres. These data are interesting in themselves, and essential for the calibration of a high pressure diffusion unit.

It has been shown[1,2] that at atmospheric pressure the diffusion theory of Enskog and Chapman[3] gives close agreement between theory and experiment provided the Lennard-Jones model for molecular interaction is used. This model assumes an attractive and repulsive potential of the form,

$$E=-4\epsilon[(r_0/r)^6-(r_0/r)^{12}], \tag{1}$$

r_0 = intermolecular distance when $E=0$; ϵ = energy difference between separated molecules and molecules in configuration of maximum attraction. The equation for the diffusion coefficient can then be written

$$D_{12}=\frac{3(kT)^{\frac{1}{2}}}{16(\pi)^{\frac{1}{2}}(\mu)^{\frac{1}{2}}r_0^2 n\cdot W^{(1)}{}_{(1)}\chi_{12}}, \tag{2}$$

where k = Boltzmann's constant; μ = reduced mass; $W_{12}{}^{(1)}{}_{(1)}$ = function of ϵ and T only; T = absolute temperature; n = number of molecules per unit volume; $\chi_{12}=1+5/12\pi nr_0^3$.

The $W_{12}{}^{(1)}{}_{(1)}$ integrals have been evaluated for the Lennard-Jones model by Hirschfelder *et al.*[4] Given r_0 and ϵ evaluated from *P-V-T* data or from viscosity it is then possible to calculate theoretical diffusion coefficients.

To obtain experimental diffusion coefficients it is necessary to solve the diffusion equation taking into consideration the geometry of the system. For the unit involved the following picture applies. Consider two cylindrical cells of equal length, one containing a certain uniform concentration of radioactive material, the other containing no radioactive material (this second cell is in contact with a scintillation crystal).

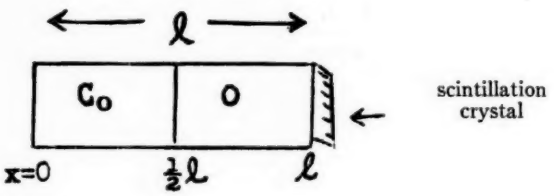

The diffusion equation is

$$\partial C/\partial t=-D\partial^2 C/\partial X^2. \tag{3}$$

The solution for the foregoing conditions is

$$C=C_0\tfrac{1}{2}+\frac{1}{\pi}\sum_{n=1}^{\infty}\frac{1}{n}[1-(-1)^n]\times\left(\cos n\frac{\pi X}{l}\right)\left[\exp-\left(\frac{n\pi}{l}\right)^2 Dt\right](-1)^{(n-1)/2}. \tag{4}$$

Now the crystal will count radiation at any point x with an efficiency (compared with the efficiency at l) depending on the strength of radiation. If the tracer element gives off only one kind of radiation the efficiency will be given by

$$F=\exp-(l-X/\lambda). \tag{5}$$

The total counts at any time t will be given by

$$I=\int_{-\infty}^{l}FCdX=C_0\lambda\left[\tfrac{1}{2}(1-e^{-l/\lambda})+\frac{1}{\pi}\sum_{n=1}^{\infty}\frac{1}{n}(1-(-1)^n)(-1)^{(n-1)/2}\times\exp-\left(\frac{n\pi}{l}\right)^2 Dt\frac{(-1)^{n+1}+e^{-l/\lambda}}{1+\left(\frac{\lambda n\pi}{l}\right)^2}\right]. \tag{6}$$

If we consider only weak beta-radiation (very small λ) the equation can be written

$$I=\frac{C_0\lambda}{2}+\frac{C_0\lambda}{\pi}\sum_{n=1}^{\infty}\frac{1}{n}(1-(-1)^n)(-1)^{(n-1)/2}\times\left(\exp-\left(\frac{n\pi}{l}\right)^2 Dt\right)(-1)^{n+1}. \tag{7a}$$

* This work was supported in part by the AEC.

[1] F. Hutchinson, J. Chem. Phys. **17**, 1081 (1949).

[2] Boyd, Stein, Steingrimsson, and Rumpel, J. Chem. Phys. **19**, (1951) (to be published).

[3] S. Chapman and T. C. Cowling, *Mathematical Theory of Non-Uniform Gas* (Cambridge University Press, London, 1939).

[4] Hirschfelder, Bird, and Spotz, J. Chem. Phys. **16**, 968 (1948).

TABLE I. Diffusion in the system $C^{14}O_2-CO_2$.

Run	Effective cell length (cm)	Pressure atm.	Temp. °K	D exp. cm²/sec	D theor. cm²/sec
1	33.75	1.243	296.2	0.0847	0.0847
2	33.75	2.49	296.9	0.0424	0.0422
3	33.75	2.77	296.1	0.0320	0.0380
4	33.75	6.38	296.6	0.0150	0.0164
5	33.75	9.33	296.4	0.0104	0.0111
6	33.75	18.49	296.5	0.0071	0.0055
7	21.35	6.34	295.7	0.0163	0.0165
8	21.35	9.24	296.2	0.0101	0.0112
9	21.35	18.59	296.5	0.00494	0.00546
10	21.35	21.4	296.0	0.00476	0.00460
11	21.35	28.1	296.0	0.00384	0.00328
12	60.05*	0.506	297.1	0.2060	0.2120
13	60.05*	0.98	296.0	0.1030	0.1090
14	60.05*	1.18	295.7	0.0910	0.0910
15	60.05*	2.18	295.9	0.0500	0.0490
16	60.05*	2.46	295.6	0.0437	0.0435

* 25.4 inches of fritted metal effective length = 2.04× measured length.

The final number of counts is then

$$I_f = C_0/2.$$

For long times Eq. (7a) reduces to

$$I = I_f - 2/\pi \exp -(n\pi/l)^2 Dt. \quad (7)$$

Then a plot of $\ln(I_f - I)$ *versus* t gives a line of slope $(\pi^2/l^2)D$. Where it is not convenient to run long enough to approach I_f one can use the entity δ where

$$\delta = (I_{t_1} - I_{t_2})/(I_{t_3} - I_{t_4}) \quad (8)$$

δ does not contain C_0 or I_f.

Generalized plots of $\gamma = (\pi^2/l^2)D$ *versus* δ have been prepared for various values of t_1, t_2, t_3, and t_4. Provided l is known, a diffusion coefficient can be calculated. Since the cells are packed with material to minimize convection, it is necessary to establish l experimentally. If it is presumed that D can be calculated from theory for self-diffusion near atmospheric pressure, then a run near atmospheric pressure permits one to establish l. The cell can then be run at higher pressures and values of D outside the theoretical range established. Because of the short path, it is not possible to run cells constructed for dense gases or liquids using a gas near atmospheric pressure. Therefore, this cell was built to operate from ½–30 atmospheres. The higher pressure cells can then be calibrated by overlapping the higher pressure end of the range of this cell.

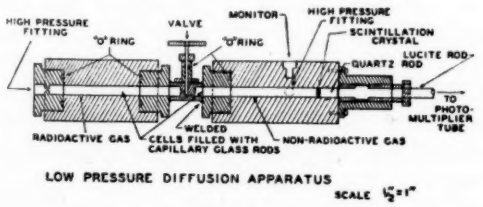

FIG. 1. Diffusion bomb.

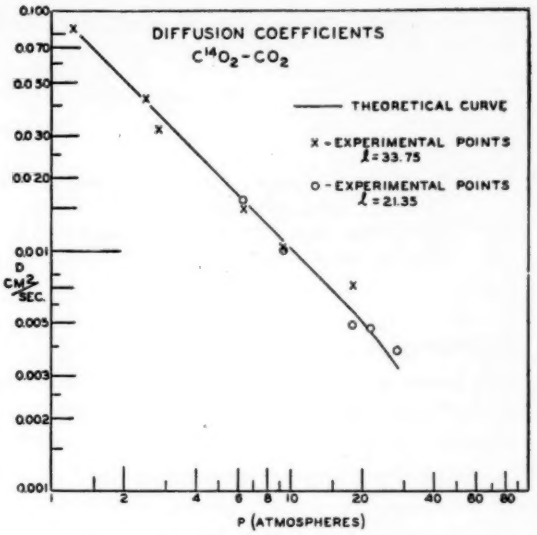

FIG. 2. Diffusion coefficients at moderate pressures comparison of theory and experiment.

The unit is shown in Fig. 1. The diagram is largely self-explanatory. The pressures on both sides of the valve were kept balanced by using a mercury pump to compress both sides simultaneously. The Lucite rod conducted the light to a photomultiplier tube. The pulses were amplified and counted on a scalar. The length of the cell could be varied by putting a blank in the left-hand cell and by using a longer quartz rod on the right.

Runs 1–11 were made with glass capillary tubing as packing. A theoretical diffusion coefficient was calculated at 1.243 atmospheres from Eq. 2 and the molecular constants of reference 4. This was used to establish the effective path length. If the effective length of the tubing was taken as equal to the apparent length, the effective length of the valve was calculated as 8.4 centimeters. This is a reasonable value considering the reduction in area at the valve. (Great care was taken to open the valve precisely the same distance each time.) Above 28 atmospheres turbulence on opening the valve became significant. For runs 7–11 the length of glass tubing on each side of the valve was reduced from 12.95 centimeters to 6.47 centimeters. Runs 12–16 were made using a packing of *F* porosity stainless steel fritted metal of 20 micron average pore diameter, as this material is being used in a high pressure diffusion unit. 12.7 centimeters of fritted metal were inserted on each side of the valve. The effective path length was determined as before by a theoretical calculation based on run 14. The effective path length in the fritted metal was 2.04 times the apparent length.

The results are shown in Table I and Fig. 2. The agreement with theory is very good, and indicates that even for a nonsymmetrical molecule such as CO_2, the dense gas theory applies at moderate pressure.

The Prediction of Isothermal Compressibilities by Light Scattering

L. G. Blosser and H. G. Drickamer
Department of Chemistry, University of Illinois, Urbana, Illinois
(Received June 14, 1951)

Light transmission measurements have been made on ethane, and on a mixture of methane and propane near the critical point, using the 4050, 4360, and 5460A lines from a mercury lamp. Isothermal compressibilities have been calculated. This appears to be a considerably more accurate method than the use of *p-v-t* data for the prediction of compressibilities near the critical point.

BECAUSE of the exceedingly rapid change of volume with pressure in the critical region, it is very difficult, if not impossible, to obtain sufficiently accurate *p-v-t* data for the prediction as isothermal compressibilities, thermal expansion coefficients, and thermal properties in general. In this paper, isothermal compressibilities are predicted from light transmission data.

The equation for the transmitted light as a fraction of the incident light can be written

$$I/I_0=\epsilon^{-\tau/l}, \tag{1}$$

where the turbidity τ depends on the mechanism assumed for the light scattering. Using the Smoluchowski-Einstein[1] approach, which is based on density fluctuations, the turbidity is

$$\tau=(8\pi^3(\mu^2-1)^2(\mu^2+2)^2kT\beta)/(27\lambda^4). \tag{2}$$

This equation shows infinite turbidity at the critical point. In the Ornstein-Zernike[2] equations, which assume a correlation coefficient between neighboring volumes, the turbidity becomes

$$\tau=\frac{8\pi^3}{27}(\mu^2-1)^2(\mu^2+2)^2kT\Big/\left(\frac{1}{\beta}\lambda^4+\left(\frac{2\pi\sigma}{\mu}\right)^2\lambda^2\right). \tag{3}$$

For this equation the wavelength dependence falls from λ^{-4} to λ^{-2} at the critical point. Solving Eq. (2) for the compressibility, one obtains

$$\beta=(\tau\lambda^4)/(Bl), \tag{4}$$

where

$$B=(8\pi^3)/27(\mu^2-1)^2(\mu^2+2)^2kT.$$

If one has transmission data at two wavelengths, Eq. (3) can be solved for the compressibility giving

$$1/\beta=B[1/\tau_1\lambda_1{}^2-1/\tau_2\lambda_2{}^2]1/(\lambda_1{}^2-\lambda_2{}^2). \tag{5}$$

Equation (4) may be used where the λ^{-4} law is valid, and Eq. (5) will be effective where the wavelength dependence falls off.

It must be understood that neither Eq. (2) nor Eq. (3) rest on entirely satisfactory theoretical grounds. The assumption of the application of the Lorentz-Lorenz law throws some doubt on the rigor of the Smoluchowski-Einstein approach. In addition the form of correlation coefficient assumed by Ornstein and Zernike is open to question.

Measurements were made on ethane, and on a binary mixture containing 30 mole percent methane-70 mole percent propane. The gases were Phillips Research Grade. The apparatus is shown in Fig. 1. The light source was a G.E. AH-4 lamp, with Corning filters to isolate the 5460, 4360, and 4050A, lines. By means of prisms, movable on tracks made from an optical bench, one could measure either the transmitted or the 90° scattered light with a cooled 1P21 photomultiplier tube. No satisfactory means was found to correct the scattered light for multiple scattering in regions of high attenuation, so that all calculations were based on transmitted light. The above considerations invalidate some wavelength dependences previously published.[3,4] At a temperature some 20–25° above the critical point the transmitted light did not change with temperature, and

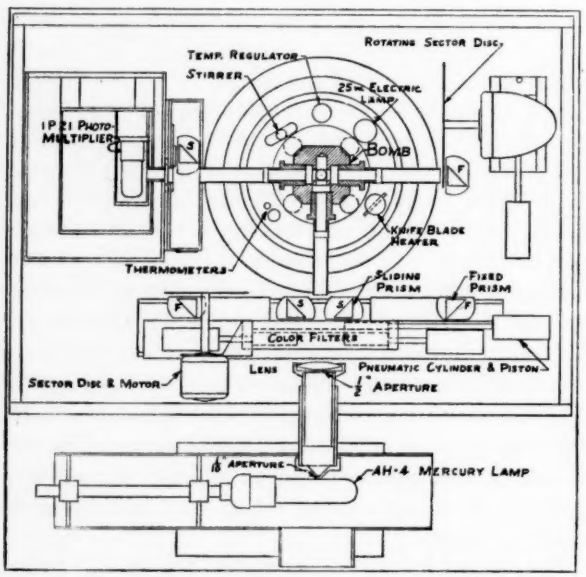

FIG. 1. Light scattering apparatus.

[1] A. Einstein, Ann. Physik **25**, 225 (1908).
[2] L. Ornstein and F. Zernike, Proc. Acad. Sci. Amsterdam **17**, 793 (1914).
[3] H. Cataldi and H. G. Drickamer, J. Chem. Phys. **18**, 650 (1950).
[4] A. L. Babb and H. G. Drickamer, J. Chem. Phys. **18**, 655 (1950).

TABLE I. Data for ethane.

Run 6 — 54.55 atmos at 37.78°C — Density: 0.2250 g/cc

Temp. °C	I/I_0, blue	I/I_0, green	Wavelength dependence λ^{-n} n	β, atmos^{-1} blue	β, atmos^{-1} green
33.60	0.877	0.930	2.60	0.65	0.88
33.30	0.850	0.916	2.70	0.81	1.07
33.00	0.796	0.885	2.7	1.13	1.48
32.70	0.685	0.855	3.8	1.87	1.90

Run 7 — 54.35 atmos at 37.78°C — Density: 0.2160 g/cc

33.50	0.775	0.903	4.0	1.38	1.36
33.20	0.709	0.867	3.8	1.86	1.91
33.00	0.598	0.815	4.0	2.79	2.74
32.90	0.483	0.753	4.1	3.94	3.79
32.85	0.403	0.704	4.1	4.92	4.68

Run 8 — 54.15 atmos at 37.78°C — Density: 0.2120 g/cc

33.60	0.772	0.897	4.0	1.47	1.52
33.35	0.700	0.868	4.0	2.02	1.98
33.15	0.578	0.801	3.9	3.10	3.09
33.00	0.390	0.670	3.7	5.33	5.56
32.97	0.325	0.630	3.9	6.35	6.42

Run 9 — 54.10 atmos at 37.78°C — Density: 0.2104 g/cc

33.60	0.769	0.886	3.4	1.52	1.72
33.30	0.666	0.841	3.7	2.34	2.46
33.10	0.509	0.747	3.7	3.90	4.15
32.95	0.263	0.562	3.7	7.73	8.19
32.92	0.193	0.501	3.8	9.50	9.81

Run 10 — 54.07 atmos at 37.78°C — Density: 0.2095 g/cc

33.55	0.740	0.876	3.6	1.75	1.89
33.25	0.588	0.800	3.8	3.09	3.20
33.05	0.320	0.656	4.2	6.65	6.05
32.96	0.170	0.490	4.0	10.3	10.2
32.94	0.120	0.411	3.8	12.4	12.7

Run 12 — 53.99 atmos at 37.78°C — Density: 0.2065 g/cc

Temp. °C	I/I_0, blue	I/I_0, green	Wavelength dependence λ^{-n} n	β, atmos^{-1} blue	β, atmos^{-1} green
33.55	0.670	0.855	4.1	2.41	2.33
33.30	0.525	0.770	3.9	3.88	3.87
33.10	0.237	0.556	3.9	8.66	8.70
33.03	0.072	0.340	3.9	15.8	16.0
33.00	0.0268	0.209	3.6	26.2	—

Run 13 — 53.93 atmos at 37.78°C — Density: 0.2045 g/cc

33.70	0.704	0.874	4.2	2.16	2.05
33.40	0.544	0.793	4.2	3.75	3.52
33.20	0.308	0.606	3.7	7.27	7.60
33.07	0.047	0.285	3.9	18.8	19.1
33.02	0.0083	0.120	3.6	38.1	—

Run 14 — 53.84 atmos at 37.78°C — Density: 0.2005 g/cc

33.75	0.685	0.859	4.0	2.44	2.41
33.40	0.440	0.720	4.0	5.30	5.22
33.20	0.139	0.460	4.0	12.7	12.3
33.10	0.010	0.140	3.7	29.7	31.3
33.076	0.00063	0.0316	3.3	75	—

Run 15 — 53.37 atmos at 37.78°C — Density: 0.181 g/cc

33.80	0.616	0.805	3.5	3.95	4.35
33.50	0.408	0.673	3.6	7.30	7.93
33.30	0.100	0.381	3.8	18.7	19.4

Run 17 — 53.15 atmos at 37.78°C — Density: 0.174 g/cc

33.80	0.704	0.872	4.1	3.12	3.00
33.50	0.541	0.783	4.0	5.45	5.37
33.28	0.275	0.590	3.9	11.5	11.6

there was no measurable scattering. At the beginning of each run a measurement was taken at this temperature and this was taken as "incident light" I_0. It was necessary to take several hours to cool down to the temperatures near the critical point, and usually one-half to one hour between readings in this region. The temperature was controlled to plus or minus 0.002°C and temperature fluctuations were not significant except possibly at the critical point.

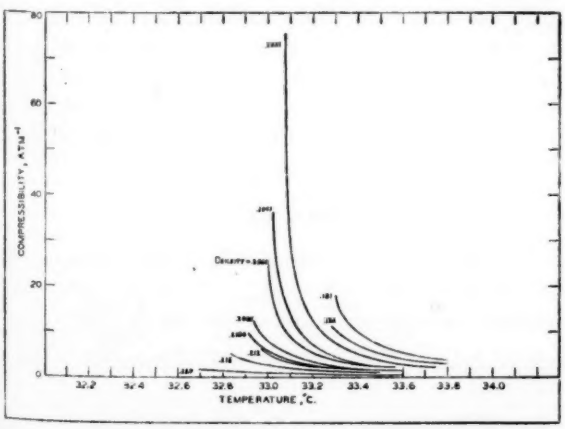

FIG. 2. Isothermal compressibilities—ethane.

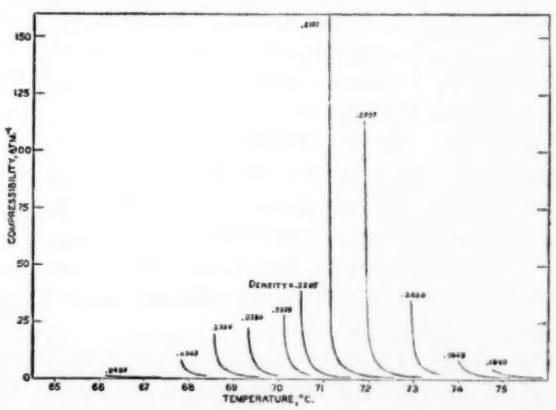

FIG. 3. Isothermal compressibilities—methane-propane mixture.

TABLE II. Data for methane-propane mixture.

Temp. °C	I/I_0, blue	I/I_0, green	Wavelength dependence λ^{-n} n	β, atmos^{-1} blue	β, atmos^{-1} green
Run 33 848.96 atmos at 77.86°C				Density: 0.2485 g/cc	
67.40	0.901	0.962	4.3	0.31	0.28
66.50	0.802	0.927	4.4	0.65	0.55
66.14	0.615	0.840	4.4	1.42	1.25
Run 34 849.03 atmos at 81.65°C				Density: 0.2365 g/cc	
69.40	0.847	0.933	3.9	0.54	0.56
68.50	0.680	0.857	4.0	1.26	1.24
68.00	0.375	0.678	4.0	3.21	3.13
67.84	0.120	0.450	4.1	7.92	6.43
Run 35 848.82 atmos at 82.82°C				Density: 0.2320 g/cc	
69.60	0.722	0.877	4.0	1.12	1.11
69.00	0.465	0.717	3.6	2.62	2.79
68.70	0.150	0.445	3.7	6.50	6.80
68.58	0.0103	0.133	3.6	19.9	—
Run 37 848.89 atmos at 84.24°C				Density: 0.2280 g/cc	
70.00	0.590	0.807	3.9	1.87	1.87
69.60	0.268	0.595	4.0	4.66	4.53
69.46	0.085	0.365	3.9	8.73	8.78
69.35	0.0081	0.116	3.5	22.8	—
Run 38 848.76 atmos at 85.74°C				Density: 0.2228 g/cc	
70.70	0.563	0.803	4.2	2.15	2.02
70.40	0.272	0.608	4.2	4.87	4.59
70.24	0.070	0.365	4.2	9.90	9.27
70.13	0.00572	0.0945	3.4	27.7	—
Run 39 848.76 atmos at 86.67°C				Density: 0.2205 g/cc	
71.60	0.721	0.880	4.1	1.25	1.21
71.00	0.467	0.743	4.1	2.91	2.82
70.66	0.075	0.385	4.2	9.90	9.00
70.51	0.00069	0.0381	3.5	37.6	—
Run 40 848.82 atmos at 88.30°C				Density: 0.2152 g/cc	
72.60	0.745	0.903	4.6	1.20	1.02
71.60	0.370	0.668	3.9	4.03	4.03
71.30	0.085	0.340	3.5	9.99	10.7
71.17	0.0031	0.110	4.1	23.4	22.0
71.10	8×10^{-7}	1.25×10^{-5}	—	—	—
Run 41 849.03 atmos at 90.37°C				Density: 0.2095 g/cc	
73.20	0.714	0.865	3.7	1.45	1.54
72.60	0.517	0.768	4.0	2.84	2.79
72.10	0.083	0.365	4.0	10.7	10.7
71.94	0.00069	0.0368	3.4	43.9	—
71.90	8.3×10^{-6}	0.00259	3.0	112	—
Run 42 848.96 atmos at 92.94°C				Density: 0.2020 g/cc	
73.60	0.562	0.786	3.8	2.70	2.78
73.30	0.362	0.657	3.8	4.77	4.85
73.06	0.100	0.375	3.7	10.8	11.3
72.94	0.0035	0.081	3.4	34.7	—
Run 43 849.03 atmos at 95.75°C				Density: 0.1948 g/cc	
75.40	0.813	0.918	3.8	1.06	1.07
74.60	0.666	0.846	3.9	2.07	2.10
74.20	0.475	0.700	3.2	3.79	4.48
74.03	0.248	0.550	3.7	7.11	7.52
Run 44 849.03 atmos at 99.94°C				Density: 0.1845 g/cc	
75.90	0.798	0.913	4.0	1.31	1.29
75.00	0.610	0.807	3.6	2.85	3.05
74.75	0.429	0.715	4.0	4.90	4.77

The results are shown in Tables I and II. The wavelength dependence was always between λ^{-4} and λ^{-2} within the accuracy of the data, indicating the probable applicability of the Ornstein-Zernike equations. The refractive indices were calculated using the Lorentz-Lorenz law. The path length was measured and was checked using a polymer solution of known turbidity. The maximum turbidity for ethane does not occur at the critical point. This is probably due to impurities, although the gas was 99.9 percent ethane and every effort was made to keep it pure. The methane-propane mixture has a large retrograde region. No unusual effects were noted in this region. The density range over which the turbidity was high is not significantly larger for the mixture than for pure ethane.

The compressibilities are shown in Figs. 2 and 3. They are of the same order of magnitude in both systems. The p-v-t data available on these systems are not nearly accurate enough to make check calculations.

It appears to the authors that this is a convenient means for obtaining accurate p-v-t information in a narrow region near the critical point. A recent paper by Wild[5] indicates a somewhat more elegant method of obtaining the same information by x-ray scattering. He did not obtain data sufficiently near the critical point to permit numerical comparison.

NOMENCLATURE

I = transmitted light; I_0 = incident light; k = Boltzmann's constant; l = path length; p = pressure; t = absolute temperature; v = volume; β = isothermal compressibility $= -\left(\frac{1}{v}\frac{\partial v}{\partial p}\right)$; λ = wavelength of light; μ = refractive index; σ = correlation coefficient; τ = turbidity.

[5] R. L. Wild, J. Chem. Phys. **18**, 1627 (1950).

Preparation and Reactions of Free Vinyl Radicals

A. W. TICKNER* AND D. J. LE ROY
Department of Chemistry, University of Toronto, Toronto, Canada
(Received July 9, 1951)

Ethylene, acetylene, and butadiene are the predominant gaseous products of the reaction of sodium vapor with vinyl iodide in the "diffusion flame." From the experimental evidence it is likely that these are formed by the disproportionation and recombination of vinyl radicals. In the presence of hydrogen, ethylene is also formed by the reaction $C_2H_3+H_2=C_2H_4+H$. More vinyl iodide than sodium is consumed in the reaction and a nonvolatile organic iodide is formed. This has an important bearing on the calculation of the rate constant of the primary process.

THE reactions of atomic sodium with a great variety of organic halides have been investigated by the "diffusion flame" method.[1,2] In most cases emphasis was placed on the kinetics of the primary process, $Na+RX=NaX+R$, rather than on the subsequent reactions of the radicals formed. That radicals are formed has been demonstrated by several workers, and in a number of cases the reactions of these with each other and with the carrier gas have been investigated. A review of this latter aspect of diffusion flame work has been given by Hodgins, Tickner, and Le Roy.[3] More recently Bawn and Tipper,[4] and Comstock and Rollefson[5] have studied the reactions of methyl and ethyl radicals produced in this way. In the present paper we wish to report the results obtained with vinyl radicals, formed by the action of atomic sodium on vinyl iodide.

EXPERIMENTAL

The apparatus was similar to that used by a number of workers to investigate the primary reaction (see, for example, reference 3), except that the temperature of the system in the vicinity of the flame was made independent of the temperature of the sodium saturator. Both hydrogen and helium were used as carrier gases, at pressures of approximately 3 mm. The flow rates were 10^{-5} mole sec^{-1} for hydrogen, 6.5×10^{-6} for helium. With flame diameters of approximately 2 cm, the partial pressure of halide was in the range 0.012 to 0.022 mm. The partial pressure of sodium in the carrier gas was controlled by the temperature of the saturator; for all of the experiments it was kept at approximately 5.5×10^{-3} mm.

The products of the reaction were removed from the circulating system in traps cooled with liquid air and then subjected to low temperature fractionation.[6] With the exception of a fraction having a vapor pressure of 0.33 mm at −40°C, which was too small to analyze, the only gaseous products formed were ethylene, acetylene and 1,3-butadiene. The first was analyzed by the hydroxy mercurial method,[7] the second by the mercuric cyanide method.[8] Butadiene was determined in the Blacet-Leighton apparatus by absorption with molten maleic anhydride; the reagent was held in a sintered glass bead maintained at 80°C with the micro furnace.

The deposit in the reaction chamber was found to contain both inorganic (NaI) and organic iodine. After its removal from the reaction chamber the iodine content was determined by the method of Gautier,[9] modified by carrying out the iodide-to-iodate oxidation with bromine water.[10] As shown in column nine of Table I, the deposit for experiments 1 and 2, and for 3 and 4 were analyzed together.

In Table I are given the results of four experiments with hydrogen and four with helium as the carrier gas. Variation of the temperature in the range 272° to 301°C had no significant effect. For better comparison, the sodium atom consumption and the formation of products are given relative to the vinyl iodide consumed. The ratio of iodide found in the cell to vinyl iodide consumed ($-\Delta C_2H_3I$) should be unity, since no other iodine-containing products were found; the deviation from unity of the values in column nine can probably be ascribed to errors in the analysis of the deposit. The term "polymer" has been given to the difference between the vinyl iodide consumed and the quantity (ethylene+acetylene+2×butadiene); it would include the small amount of unidentified product referred to previously, as well as the nonvolatile organic iodide deposited in the cell.

DISCUSSION

Despite the limitations in the accuracy of the method, a number of significant conclusions may be drawn from the data of Table I. The formation of ethylene, acetyl-

* Present address: Division of Chemistry, National Research Council, Ottawa, Canada.

[1] M. Polanyi, *Atomic Reactions* (Williams and Norgate, London 1932).

[2] C. E. H. Bawn, Ann. Reports Chem. Soc. **39**, 36 (1942).

[3] Hodgins, Tickner, and Le Roy, Can. J. Research **B26**, 619 (1948).

[4] C. E. H. Bawn and C. F. H. Tipper, Faraday Soc. Disc. **2**, 104 (1947).

[5] A. A. Comstock and G. K. Rollefson, J. Chem. Phys. **19**, 441 (1951).

[6] D. J. Le Roy, Can. J. Research **B28**, 492 (1950).

[7] Pyke, Kahn, and Le Roy, Ind. Eng. Chem. Anal. Ed. **19**, 65 (1947).

[8] Blacet, Sellers, and Blaedel, Ind. Eng. Chem. Anal. Ed. **12**, 356 (1940).

[9] J. A. Gautier, Bull. soc. chim. Belg, **4**, 219 (1937).

[10] F. P. Treadwell and W. T. Hall, *Analytical Chemistry*, Vol. II (John Wiley and Sons, Inc., New York, 1942).

TABLE I. Experimental data on reagents and products.

Expt.	Carrier	T°C	$C_2H_4/-\Delta C_2H_3I$	$C_2H_2/-\Delta C_2H_3I$	$C_4H_6\times 2/-\Delta C_2H_3I$	"Polymer"$/-\Delta C_2H_3I$	$-\Delta Na/-\Delta C_2H_3I$	I found$/-\Delta C_2H_3I$
1	H_2	282	0.59_2	0.120	0.074	0.21_2	0.66	0.98
2	H_2	272	0.47_0	0.086	0.059	0.38_3	0.74	
3	H_2	292	0.52_5	0.097	0.049	0.32_7	0.57	0.85
4	H_2	301	0.49_0	0.069	0.065	0.37_7	0.45	
5	He	301	0.27_5	0.087	0.102	0.53_2	0.79	0.92
6	He	291	0.24_4	0.065	0.059	0.63_9	0.55	...
7	He	274	0.104	0.099	0.075	0.73_2	0.64	0.86
8	He	292	0.075	0.074	0.070	0.78_0	0.62	...

ene, and butadiene has been definitely established. However, as shown in column seven, a considerable proportion of the vinyl iodide is consumed in the formation of nonvolatile products; this is especially marked when helium is used as the carrier gas.

Although considerably more ethylene than acetylene is formed in the presence of hydrogen, the amounts of these two products approach equality when helium is used as the carrier gas, particularly when extreme precautions are taken to remove all the hydrogen from the sodium (Expts. 7 and 8). There would seem to be little doubt that the larger values of $C_2H_4/-\Delta C_2H_3I$ in the case of experiments 1 to 4 are the result of the reaction

$$C_2H_3+H_2=C_2H_4+H. \quad (1)$$

If this is so, atomic hydrogen must be much less efficient than vinyl radicals in bringing about polymerization of vinyl iodide, since the formation of "polymer" is much greater in the absence of hydrogen, when (1) could not take place.

The equality between ethylene and acetylene in the absence of hydrogen could be taken as evidence for the disproportionation of vinyl radicals,

$$2C_2H_3=C_2H_4+C_2H_2. \quad (2)$$

The same products could, however, be produced by the sequence,

$$C_2H_3+C_2H_3I=C_2H_4+C_2H_2I \quad (3)$$

$$C_2H_2I=C_2H_2+I. \quad (4)$$

Butadiene undoubtedly arises by the reaction,

$$2C_2H_3=C_4H_6. \quad (5)$$

If acetylene is produced by (2), the ratio of acetylene to butadiene would be independent of the partial pressure of vinyl iodide; if by (4) then the quantity $(C_2H_2)/(C_4H_6)^{\frac{1}{2}}$ would be directly proportional to the vinyl iodide pressure. Unfortunately the nature of the diffusion flame reaction makes it difficult to change the iodide pressure over wide limits. The pressure of halide required to give a 2 cm diameter flame is much greater for vinyl bromide than vinyl iodide. Hence, if it could be assumed that the rate constant of (6),

$$C_2H_3+C_2H_3Br=C_2H_4+C_2H_2Br, \quad (6)$$

is not significantly different from that of (3), a comparison of the acetylene/butadiene ratio with the two different halides would settle the problem. However the vapor pressures of butadiene and vinyl bromide are almost the same and low temperature fractionation cannot be used to separate the butadiene from the large excess of vinyl bromide. For this reason Hodgins, Tickner, and LeRoy[3] were only able to detect ethylene and acetylene in the reaction of atomic sodium with vinyl bromide.

The experimental conditions using vinyl bromide[3] were almost identical with those reported here, except that the partial pressure of halide was ten times as great. From the kinetics of reactions (1) and (2) it follows that at any fixed point in the reaction zone at, say, a distance of r cm from the center of the flame, the rate of production of ethylene will be given by

$$\{d(C_2H_4)/dt\}_r=k_1(H_2)(C_2H_3)_r+k_2(C_2H_3)_r^2, \quad (a)$$

and the rate of production of acetylene by

$$\{d(C_2H_2)/dt\}_r=k_2(C_2H_3)_r^2. \quad (b)$$

Hence, for constant temperature and hydrogen pressure, the following relation will hold:

$$\varphi\equiv\frac{\{(C_2H_4-C_2H_2)/C_2H_2\}_I}{\{(C_2H_4-C_2H_2)/C_2H_2\}_{Br}}=\frac{\left\{\int_0^\infty (C_2H_3)_r dr\right\}_I\times\left\{\int_0^\infty (C_2H_3)_r^2 dr\right\}_{Br}}{\left\{\int_0^\infty (C_2H_3)_r dr\right\}_{Br}\times\left\{\int_0^\infty (C_2H_3)_r^2 dr\right\}_I} \quad (c)$$

in which the subscripts I and Br refer to experiments with vinyl iodide and vinyl bromide, respectively. For the same flame diameter the vinyl radical distribution would be approximately the same for the two halides, and the ratio φ would be close to unity, regardless of the greater partial pressure of the vinyl bromide. By using the actual values for ethylene and acetylene production in experiments 1 to 4 and the data given by Hodgins, Tickner, and Le Roy[3] for vinyl bromide the experimental value of φ was found to be 0.58.

If acetylene were formed by (4) φ would be equal to $\{k_6(C_2H_3Br)\}/\{k_3(C_2H_3I)\}$. It is unlikely that k_6 is less

than k_3, and the average concentration of iodide would be considerably less than 1/10 that of the bromide because of impoverishment in the flame. On the basis of reactions (3) and (4) the predicted value of φ would therefore be close to 20, compared to the experimental value of 0.58. It appears justified to conclude that acetylene is formed by the disproportionation of vinyl radicals.

The consumption of vinyl iodide by reactions other than $Na+C_2H_3I=C_2H_3+NaI$ is shown clearly in Table I. This has an important bearing on the validity of any calculation of the rate constant for the primary process. Hartel and Polanyi's treatment[11] is based on the simplifying assumption that the halide concentration is constant throughout the reaction zone. Polanyi[1] has estimated that this assumption is valid only for relatively slow reactions, with collision yields smaller than 1/10; Heller[12] reduced this limit to 1/50. The more elaborate treatment of Cvetanović and Le Roy[13] is free from the foregoing restriction, but is valid only for reactions in which the halide is consumed solely by the primary reaction with the alkali metal. In the case of vinyl iodide, particularly with helium as the carrier gas, a large proportion of the halide is consumed in other reactions.

Cvetanović and Le Roy[13] showed that the values of the rate constant calculated by the method of Hartel and Polanyi,[11] and based on experimental measurements with spherical diffusion flames, become progressively too small as the initial concentration of the halide approaches that of the sodium, and as the impoverishment of halide in the flame increases. They calculated that for ethyl chloride, with a collision yield of approximately 1/7000, the error in the rate constant calculated by the method of Hartel and Polanyi was of the order of 20 percent. A much larger error would be expected in the case of vinyl iodide, for which Evans and Walker[14] calculated a collision yield of 1/20, and this error would be accentuated by the additional impoverishment effect which we have shown to occur. We believe, therefore, that the activation energy of 3.2 kcal per mole calculated by Evans and Walker is considerably too large.

In carrying out diffusion flame measurements it is necessary to use halide concentrations which are approximately inversely proportional to the collision yields. Since the collision yields increase in the order chlorides, bromides, iodides, it is clear that a re-calculation of activation energies allowing for impoverishment would lower the values for iodides more than for bromides, and for bromides more than chlorides. This effect, together with the possibility of impoverishment by secondary reaction, so far shown only for vinyl iodide, suggests that any conclusions as to the relative "back co-ordinating power" of the various halides[14,15] must be accepted with caution.

The authors are pleased to acknowledge the financial assistance received from the Associate Committee on Scientific Research of the University of Toronto.

[11] H. v. Hartel and M. Polanyi, Z. physik. Chem. **B11**, 97 (1930).
[12] W. Heller, Trans. Faraday Soc. **33**, 1556 (1937).
[13] R. J. Cvetanović and D. J. Le Roy, Can. J. Chem. (formerly Can. J. Research, Section *B*) **29**, 597 (1951).
[14] A. G. Evans and H. Walker, Trans. Faraday Soc. **40**, 384 (1944).
[15] E. Warhurst, Quarterly Rev. Chem. Soc. **V**, 44 (1951).

The Photolysis of Acetic Anhydride*

RICHARD J. KANDEL AND H. AUSTIN TAYLOR
Department of Chemistry, New York University, New York, New York

(Received April 6, 1951)

The photolysis of acetic anhydride probably by 1849A radiation has been studied in the temperature range 80° to 300°C at pressures of 10–60 mm dibutyl phthalate. From 80° to 224°C the rate is first order during a run but the specific rate decreases with increasing pressure. The gaseous products are CO, CO_2 and C_2H_6 in approximately equivalent amounts. Biacetyl and methyl acetate have been identified among the liquid products. At 300°C the reaction is more complex, yields considerable amounts of H_2 and CH_4 and is not first order. Comparison with formic acid photolysis leads to an approximate quantum yield of 2. A mechanism is suggested which accounts qualitatively for the observations. Deactivation of activated reactant molecules by acetic anhydride and by the gaseous products accounts for the low quantum yield. Added C_2H_6 and CO_2 are shown to increase the rate of photolysis, the more so the lower the pressure of acetic anhydride. Preliminary experiments have shown that the reaction can also be mercury sensitized at a much faster rate at comparable temperatures but yielding the same products in similar amounts.

THE anhydrides are the only family of simple organic compounds that has not been subjected to extensive photochemical study. Berthelot and Gaudechon[1] report an analysis of the gaseous products from acetic anhydride upon irradiation with ultraviolet light for many hours, as follows: 36 percent CO, 22 percent CO_2, 23 percent C_2H_6, and 19 percent CH_4. No other report on the photolysis of an acid anhydride appears in the literature due undoubtedly to the lack of absorption of light above 2000A.[2] The absorption spectrum of acetic anhydride vapor in the region of strong absorption has not been determined. By using a mercury resonance lamp emitting some 1849A radiation built inside the reaction vessel, sufficient intensity of the light absorbed by acetic anhydride vapor was obtained to bring about a reasonably rapid photolysis permitting a general survey of the kinetics of the decomposition.

EXPERIMENTAL

The reaction vessel was modeled after the design of Steacie and Phillips.[3] It consisted of a quartz spiral of 10 mm outside diameter tubing connected through graded seals to Pyrex tubing of the same diameter carrying the electrodes which were standard neon sign coated electrodes, 8 mm in diameter and 3 cm long. The Pyrex reaction vessel of about one liter capacity was ring sealed to the Pyrex tubing near the electrode chambers and carried an inlet and outlet tubing, as also a thermocouple well. The quartz tube contained a drop of mercury and neon at a pressure of 10 mm. The lamp was operated from a 5000-volt, 25-ma transformer. The starting potential was 5000 volts though the normal operating potential was only 400 volts. The lamp furnished large amounts of 2537A and small amounts of 1849A radiation. At full intensity the reaction vessel maintained a temperature of 40°C. The temperature was measured using a chromel-alumel thermocouple.

A second reaction vessel similar to the foregoing but using larger electrodes, with 10-mm argon in place of neon and operated from a 5000-volt, 120-ma transformer was used in the later runs reported. The primary of the transformer was actuated by a Sorenson voltage regulator at 115 volts. Larger amounts of 1849A radiation were afforded by this lamp as judged by the more rapid reaction produced. The operating voltage was again 400 but the temperature of the reaction vessel was 80°C. This vessel was enclosed in a cylindrical oven which permitted the electrodes to protrude so that they would not be heated when the reaction vessel was heated to 300°C.

The reaction vessel was connected to a mercury diffusion and oil pump system, a McLeod gauge, a mercury manometer, a dibutyl phthalate manometer, and a Toepler pump leading to freeze-out traps and a Burrell gas analyzer.

Acetic anhydride was distilled through a column packed with carbon rings and a fraction boiling between 139 and 140°C was collected in a dry vessel open to the air through a drying tube containing anhydrous calcium sulfate. This vessel was connected to the manifold of the reaction system and the anhydride was distilled in vacuum into a storage bulb in dry ice. The solid was pumped out for several hours, allowed to warm to room temperature, refrozen, and pumped out again, the process being repeated until no bubbles appeared in the liquid on melting and no residual gas remained on freezing the liquid.

The formic acid used to determine quantum yields was dried over anhydrous calcium sulfate, introduced into the system and treated in a manner similar to that used for the anhydride. Both chemicals were stored under their own vapor pressures at room temperature.

Experiments were made using the first reaction vessel by both dynamic and static methods. The effect of the presence of mercury vapor was also studied. For this

* Abstract from a dissertation presented in partial fulfillment of the requirements for the degree of Doctor of Philosophy at New York University, February, 1950.

[1] Berthelot and Gaudechon, Compt. rend. **151**, 478 (1910); **153**, 383 (1911).

[2] Ley and Arends, Z. physik. Chem. **17B**, 177 (1932).

[3] Steacie and Phillips, Can. J. Research, **B16**, 219 (1938).

the acetic anhydride vapor was bubbled first through mercury at 100°C and then through mercury at 40°C, the temperature in the reaction system. In the flow runs the system was evacuated thoroughly, the lamp was turned on and allowed to warm up and acetic anhydride vapor was bled through the reaction vessel to a trap immersed in liquid nitrogen and a large gas reservoir connected to a Toepler pump. The undecomposed anhydride was caught in the cold trap along with any condensable products. The uncondensed gases filled the bulb and were periodically pumped off and stored over mercury for subsequent analysis. After a run the cold trap was warmed to room temperature and then immersed in dry ice. The remaining gases were pumped off and mixed with the uncondensed gases. For analysis the gases were passed through potassium hydroxide solution to remove carbon dioxide, bromine water for unsaturates and acid cuprous chloride for carbon monoxide. Hydrogen was estimated by combustion over copper oxide at 300°C and hydrocarbons by catalytic combustion in oxygen at 500°C.

In the static runs the lamp was warmed up and then shut off for the few seconds necessary to introduce the acetic anhydride vapor to the desired pressure and again turned on to start the reaction. Pressure changes were observed at periodic intervals. At the conclusion of the run the gases were pumped out and analyzed as in the dynamic runs. For runs made in the absence of mercury vapor the reaction vessel was isolated from mercury through gold-leaf traps. It was observed that in all runs, both static and dynamic, a brown deposit formed on the quartz of the lamp. It was never observed on any other part of the reaction vessel. The deposit was removed by filling the reaction vessel with oxygen and turning on the lamp. This was done after each run, the system being thoroughly evacuated and flushed with acetic anhydride vapor before a subsequent experiment.

For the runs made using the higher light intensity of the second reaction vessel, the mercury manometer was replaced with one containing dibutyl phthalate. The effect of temperature was studied by experiments at 80, 120, 140, 220, and 300°C. The effect of carbon dioxide and of ethane as diluents was studied at 80°C. To estimate the quantum yield a series of runs using formic acid was made at 80, 120, and 140°C. Finally, the undecomposed acetic anhydride and liquid products, collected from several runs, was distilled in a microrectification flask[4] and the first milliliter subjected to two tests. A part of this liquid was treated with an ammoniacal hydroxylamine solution and nickel sulfate added. A red precipitate of nickel dimethyl glyoxime showed the presence of biacetyl. The remainder of the liquid was heated with a large amount of salicylic acid and a few drops of concentrated sulfuric acid. The distinctive odor of wintergreen suggested the presence of methyl alcohol or methyl acetate in the distillate.

[4] Gettler and Siegel, Arch. Pathology **19**, 208 (1935).

TABLE I.

15-min runs		Initial pressure 50–60 mm			
		Percentages			
Temp. °C	CO_2	CO	C_2H_6	CH_4	H_2
40	28	37	30	0	2
80	29	36	31	0	4
120	30	35	30	1	4
140	28	36	30	1	5
224	25	41	28	0	6
300	22	44	18	6	10

RESULTS

Preliminary experiments using the first reaction vessel in both static and flow runs, unsensitized and mercury sensitized, showed analyses of products at variance with those mentioned earlier of Berthelot and Gaudechon most especially in the absence of methane at low temperature. The analysis of products appeared to be independent of the presence or absence of mercury vapor though the rate of decomposition was about fifty percent faster in the mercury sensitized runs. Reproducibility with this lamp was poor partly due to the weak intensity of the absorbable radiation and the second lamp, a stronger light source, was used in all the remaining work.

Table I contains the averages of analyses of gaseous products from runs at a series of temperatures. The average error of each value is between one and two percent. At low temperatures it is apparent that CO_2, CO, and C_2H_6 are the principal products. Considering the experimental difficulty of separation of the less volatile and more soluble carbon dioxide and ethane from undecomposed reactant it seemed possible that all three products were produced in equal amounts equivalent to the complete decomposition of a molecule of acetic anhydride. Analyses after five, ten, and fifteen minute runs at the lower temperatures showed reproducibility for the carbon dioxide and ethane with a tendency for the carbon monoxide to be higher the shorter the run again reflecting its higher volatility and lower solubility in acetic anhydride. At the highest temperature however the course of reaction is obviously different showing unmistakable amounts of hydrogen and methane accompanying the decrease in carbon dioxide and ethane and corresponding increase in carbon monoxide. A material balance on the gaseous products of runs up to 224°C, assuming all the oxygen is present therein, yields formulas very close to $C_4H_6O_3$ while at 300°C, the formula is $C_{3.5}H_5O_3$ suggesting a loss of $(CH_2)_n$.

Rate measurements in the absence of mercury vapor were made by following the pressure change on the dibutyl phthalate manometer during static experiments. Assuming acetic anhydride yields three products, the pressure of undecomposed anhydride could be calculated and plots of the logarithms of the anhydride pres-

TABLE II. Specific reaction rates and temperature.

Temp. °C	k (min^{-1})
80	0.22
120	0.23
140	0.22
224	0.26

sure as a function of time gave excellent straight lines indicating a first-order rate to about seventy percent completion of reaction. Beyond this point deviations from linearity were apparent. Specific reaction rates were calculated from the slopes of these plots. In Table II these rates are listed for several different temperatures.

The 300°C runs could not be treated in the same manner since the decomposition could no longer be considered to be a splitting into three fragments. It was apparent however from the rate of pressure change that the course of reaction was quite different and was not further investigated.

In order to check the first-order rate found during a run, the dependence of rate on initial pressure was studied at four different pressures, all at 80°C. The results are given in Table III. In view of the variation in rate observed with change in initial pressure the effects of carbon dioxide and ethane as diluents were investigated at three different initial pressures of acetic anhydride. The data are listed in Table IV. The percentage of diluent was not determined very accurately because of experimental difficulties. The rates given as k are those calculated from the slopes of the rate curves; k' is the calculated specific rate at the specified initial pressure of acetic anhydride in the absence of diluent. It is apparent that at low pressures of the anhydride both carbon dioxide and ethane increase the rate while at high pressures the diluent effect is negligible.

TABLE III. Specific reaction rates and pressure.

P_0 (mm)	k (min^{-1})
12.9	0.35
14.2	0.32
33.4	0.25
57.5	0.22

A series of runs was made on formic acid from 80° to 140°C in order to determine quantum yields. Formic acid exists as both monomer and dimer in the vapor phase and decomposes by two different mechanisms to give either carbon monoxide and water or carbon dioxide and hydrogen. The photolysis is first order and has a quantum yield of one over a wide range of temperature and pressure independent of the molecular weight of the starting material.[5] On the assumption that one molecule of the acid gives two molecules of product on photolysis, the rate of pressure change was plotted as logarithms of the undecomposed formic acid against time and the slope taken as the specific rate. At 80°, 120°, and 140° a constant specific rate of 0.10 min^{-1} was found, independent of the pressure. Neither acetic anhydride nor formic acid absorb radiation above 2000A. The spectrum of neither has been accurately determined but what evidence there is points to high absorption near 1849A. The output of the lamp used consists mostly of 2537A radiation and from five to fifteen percent of the total at 1849A. What decomposition occurs is consequently to be attributed to the 1849A radiation and it has therefore been assumed that this radiation is completely absorbed by both the formic acid and the acetic anhydride over the same range of pressure. At comparable pressures the ratio of the rates is therefore the ratio of quantum yields. A rough estimate of the quantum yield of acetic anhydride in the temperature range 80–140°C is thus two at the higher pressures studied, increasing somewhat as the pressure is decreased.

TABLE IV. Specific reaction rate and diluents.

Percentage diluent	P_0 (mm)	k (min^{-1})	k' (min^{-1})
0	57.5	0.22	0.22
40 CO_2	50.8	0.22	0.22
60 CO_2	55.4	0.22	0.22
55 CO_2	20.9	0.37	0.29
70 CO_2	20.0	0.34	0.29
55 C_2H_6	17.6	0.36	0.30
70 C_2H_6	19.7	0.30	0.29

DISCUSSION

Since the absorption in the 1849A region by acetic anhydride is high,[6] since the intensity in this region afforded by the lamp is low and since the rate of decomposition of the anhydride does not increase with increasing pressure, it is assumed that the radiation emitted by the lamp at 1849A is completely absorbed. On absorption of a quantum equivalent to about 150 kcal per mole, an excited molecule will be formed which may either decompose or be deactivated. The simplest mechanism consistent with the major observations is represented by the following reactions, in which I is the absorbed intensity,

$$(CH_3CO)_2O + h\nu \xrightarrow{I} (CH_3CO)_2O^{\pm} \quad (1)$$

$$(CH_3CO)_2O^{\pm} + M \xrightarrow{k_2} (CH_3CO)_2O + M \quad (2)$$

$$(CH_3CO)_2O^{\pm} \xrightarrow{k_3} 2CH_3 + CO + CO_2 \quad (3)$$

$$CH_3 + (CH_3CO)_2O \xrightarrow{k_4} C_2H_6 + CH_3 + CO + CO_2 \quad (4)$$

$$2CH_3 \xrightarrow{k_5} C_2H_6. \quad (5)$$

The usual steady-state treatment yields for the over-all decomposition,

$$-d[(CH_3CO)_2O]/dt = k_3[(CH_3CO)_2O^{\pm}] + k_4[CH_3][(CH_3CO)_2O],$$

[5] E. Gorin and H. S. Taylor, J. Am. Chem. Soc., **56**, 2042 (1934).
[6] Ley and Arends, Z. physik. Chem., **17B**, 177 (1932).

and assuming the rate of reaction 3 small in comparison with that of 4,

$$-d[(CH_3CO)_2O]/dt = k_4(4k_3I/k_5(k_2[M]+k_3))^{\frac{1}{2}}[(CH_3CO)_2O] = k[(CH_3CO)_2O],$$

if $[M]$ is constant, in agreement with the first-order rate observed and the approximate equivalence of the amounts of CO, CO_2 and C_2H_6. This picture is probably much over-simplified, since CO is found to be consistently higher than CO_2 with C_2H_6 intermediate but nearer that of CO_2 though the difference may be experimental. In addition the presence of biacetyl and methyl acetate has been demonstrated. Inspection of reactions (3) and (4) will show their improbability as single step reactions and the following seem reasonable alternative mechanistic steps:

$$(CH_3CO)_2O^{\ddagger} \xrightarrow{k_3'} CH_3$$

$$+CH_3COOCO^{\ddagger} \begin{cases} \xrightarrow{\alpha} CH_3COO+CO \\ \xrightarrow{1-\alpha} CH_3CO+CO_2 \end{cases} \quad (3')$$

$$CH_3+(CH_3CO)_2O \xrightarrow{k_4'} C_2H_6$$

$$+CH_3COOCO \rightarrow CH_3CO+CO_2 \quad (4')$$

$$2CH_3CO \rightarrow (CH_3CO)_2 \quad (6)$$

$$2CH_3COO \rightarrow C_2H_6+2CO_2 \quad (7)$$

$$CH_3+CH_3COO \rightarrow CH_3COOCH_3 \quad (8)$$

$$CH_3CO \rightarrow CH_3+CO. \quad (9)$$

In reaction (3′) the excited anhydride molecule has absorbed 150 kcal per mole. If 80 kcal are used in breaking C−C bonds, 70 kcal remain and the methyl radicals would be expected to take about 60 of these. Such methyl radicals would be expected to yield methane in quantity whereas no methane is observed. The radical CH_3COOCO must thus be electronically excited and could decompose in either of two ways. If it splits out CO_2, the energetic acetyl radical remaining would most probably break down into a methyl radical and CO_2 a reaction requiring 18 kcal energy of activation.[7] This sequence of reactions is equivalent to reaction (3).

An alternative possibility for the electronically excited CH_3COOCO radical would be to split out carbon monoxide producing an acetate radical. Judging from acetic acid photolysis the acetate radical is fairly stable and it has been estimated that 40 to 70 kcal are required to decompose it.[8] Reaction (7) is a step postulated in acetic acid photolysis and reaction (8) with a higher probability in the presence of methyl radicals accounts for the methyl acetate found.

[7] D. S. Herr and W. A. Noyes, J. Am. Chem. Soc. **62**, 2052 (1940).
[8] M. Burton, J. Am. Chem. Soc., **58**, 1655 (1936).

Reaction (4) similarly may be analyzed in terms of steps (4′) and (9), the CH_3COOCO radical not now being excited can probably only split out carbon dioxide, the residual acetyl radical not necessarily decomposing but being a potential source of the biacetyl observed.

From 80° to 224°C the specific reaction rate is constant suggesting that none of the major steps in the reaction has an appreciable activation energy. Since the excited acetic anhydride molecules have absorbed 150 kcal per mole, the fragments of the decomposition are energetic enough to break down without additional thermal activation. At 300°C the decomposition rate appears faster, methane is present in considerable amount and ten percent of the gaseous products are hydrogen. It is apparent that the mechanism is changed due no doubt to the possibility of thermal activation.

The rate of photolysis of acetic anhydride at 80°C increases as the initial pressure, a, decreases. The change is expressible by the empirical relation: $k_{obs} \cdot \log a = 0.38 \pm 0.01$. While no reason can be adduced for the logarithmic relation, an attempt can be made to explain the fact of a pressure dependence of the rate as well as the effect of added diluent. Comparison of the photolysis of acetic anhydride with that of formic acid under the assumptions previously noted shows that the quantum yield lies around 2–4, the highest value for the lowest initial pressure. The kinetic analysis shows reaction (4) more nearly rate-controlling and more important than (3). Reaction (2), the deactivation of excited acetic anhydride molecules must therefore be considerable to balance the chains of reaction (4). In addition since the reaction is first order, $[M]$ must be constant for a given run. As a deactivating molecule, acetic anhydride by its many modes of vibration should be very efficient, the most efficient of all molecules present. The product molecules ethane, carbon dioxide, and carbon monoxide having each approximately one-third the mass of acetic anhydride and correspondingly fewer vibrations would be less efficient as deactivating agents. If it is assumed tentatively that each is one-third as efficient, since per molecule decomposed approximately these three are produced, deactivation will remain constant throughout a run.

At high initial pressures of acetic anhydride, deactivation will be very efficient and further increase of pressure will have little effect on the rate. Had it been possible to carry the study to higher pressures than those used a rate constant independent of pressure might have been demonstrated. The low vapor pressure of the anhydride precluded this possibility in the apparatus used.

At low pressures of the anhydride the rate has been shown to increase. The concentration of excited molecules is given by the expression $I/(k_2[M]+k_3)$ and with the above assumptions $[M]$ may be replaced approximately by, a, the initial pressure. From this

$k_{obs}=k_4(4k_3I/k_5(k_2a+k_3)^{\frac{1}{2}}$ and is shown experimentally to be given by $0.38/\log a$, the rate increasing as the pressure is decreased. With added diluent, however, $[M]$ can no longer be replaced by a, but for example with carbon dioxide as diluent, $[M]$ becomes approximately $a+[CO_2]/3$. When a is large the effect of the added term on k_{obs} will be small but will become more effective the lower the initial pressure; collisions between excited anhydride molecules and diluent being only approximately one-third as effective cause an increase in rate. This is observed, in fact, the rate observed with a starting mixture of approximately three parts of ethane to one part of acetic anhydride is almost identical with the rate in the absence of diluent. Carbon dioxide, which would not be expected to be as efficient for deactivating as ethane, shows a higher rate than that in the absence of diluent.

The suggested mechanism accounts at least qualitatively for the experimental observations. The suggested steps have all been postulated previously in other studies. Many additional steps could conceivably be written and have been considered and rejected as incompatible either with the observed order of the rate or with the product analysis. Several consequences of the postulated mechanism are under further investigation and will be reported later. The possibility of a mercury sensitized reaction has not been overlooked as accounting particularly for the diluent effect observed. It is believed, however, that the precautions taken rendered the system free from mercury.

THE JOURNAL OF CHEMICAL PHYSICS VOLUME 19, NUMBER 10 OCTOBER, 1951

The Ionization Potentials of the Deuterated Methanes*

F. P. Lossing, A. W. Tickner,† and W. A. Bryce‡
Division of Chemistry, National Research Laboratories, Ottawa, Canada
(Received June 21, 1951)

The ionization potentials of methane, and of the four deuterated methanes, have been determined by electron impact using two 90° mass spectrometers with different types of sources. In addition, the ionization potentials of acetylene, deuterated acetylene, ethylene, and deuterated ethylene have been measured. A simple empirical method is used to obtain values which are reproducible to ±0.02 volt. For the methanes the ionization potential is found to increase with the number of deuterium atoms in the molecule, with a difference of 0.18 volt between the value for CH_4 and that for CD_4. Although this difference is found to be the same on each of the mass spectrometers, there is a difference of 0.11 volt between the absolute values of the ionization potential as determined for CH_4 on the two instruments. In order to explain the difference between the ionization potentials of CH_4 and CD_4 on the basis of zero point energy differences, it is estimated that the force constants in the ionic state would need to have only about ¼ of their value in the ground state. Since this seems unreasonably low, it is suggested that the difference between the ionization potentials of the methanes, as measured by electron impact, may be caused, in part, by excess energy required for a "vertical" transition.

INTRODUCTION

DURING the last few years deuterated compounds have been used often in kinetic studies. As a result, the analysis of the deuterated products, usually hydrocarbons, by means of a mass spectrometer has become important. A property of great interest in analyzing mixtures of deuterated hydrocarbons is the ionization potential.[1] Spectroscopic values are available for only a few simple molecules and, although considerable work has been done on the determination of ionization potentials by electron impact,[2–5] no data have been reported on the ionization potentials of a complete deuterium-substituted series. Honig[2] has reported values of 13.04 volts for CH_4 and 13.21 volts for CD_4. In this work the ionization potentials of the five hydrogen-deuterium isomers of methane have been determined by an electron impact method.

Various methods of obtaining the ionization potential from ionization efficiency curves have been employed. The extrapolation of the straight line portion of the curve, although used with some success by Vought[6] and by Koffel and Lad[3] seems in general to be the least preferred of the methods available. Stevenson and Hipple[5] have obtained consistent results by measuring the point of initial onset. More recently Honig,[2] and Mitchell and Coleman,[4] have used methods based on the shape of the initial portion of the curve. For comparing the ionization potentials of molecules as similar as those of the deuterated methanes, any of these methods would probably be satisfactory. The accurate determination of absolute values of the ionization

* Contribution No. 2514 from the Division of Chemistry, National Research Council, Ottawa, Canada.
† Holder of National Research Laboratories Postdoctorate Fellowship.
‡ Assistant Professor, Department of Chemistry, University of British Columbia, Vancouver, Canada.
[1] D. P. Stevenson and C. D. Wagner, J. Am. Chem. Soc. **72**, 5612 (1950).
[2] R. E. Honig, J. Chem. Phys. **16**, 105 (1948).
[3] M. B. Koffel and R. A. Lad, J. Chem. Phys. **16**, 420 (1948).
[4] J. J. Mitchell and F. F. Coleman, J. Chem. Phys. **17**, 44 (1949).
[5] D. P. Stevenson and J. A. Hipple, J. Am. Chem. Soc. **64**, 1588, 2766, 2769 (1942); **65**, 209 (1943).
[6] R. H. Vought, Phys. Rev. **71**, 93 (1947).

potential, by reference to gases for which the ionization potentials are known spectroscopically, is more difficult. Since ionization by electron impact represents a "vertical" transition, the impact values may be slightly higher than the spectroscopic, or adiabatic, values, as was found by Honig.[2]

Both Honig,[2] and Mitchell and Coleman,[4] have presented detailed discussions of the methods of interpreting the shape of the initial part of the ion efficiency curves, and have developed methods of obtaining ionization potentials from this part of the curve. The method employed in this work is empirical, but is based largely on their work.

EXPERIMENTAL

The CH_3D was made by the method of Childs and Jahn[7] and the CH_2D_2 was made by the procedure of MacWood and Urey.[8] The method of Urey and Price[9] was used to make the CD_4. A new method of preparation for CHD_3 was tried. A sample of deuterated acetic acid in which 97 percent of the hydrogen had been replaced by deuterium, was neutralized to give the sodium salt. About 1.5 g of the dried salt were intimately mixed with 20 g of soda-lime which had been heated to 800°C under vacuum for several hours. On heating the mixture to about 500°C, methane was evolved rapidly. The methanes formed consisted of about 50 percent CHD_3, the remainder being nearly equal amounts of CD_4 and CH_2D_2. Since the parent peak of CHD_3 was not interfered with by the other methanes a higher degree of purity was not required. Deuterium, which was formed in varying amounts in each of the above preparations, was removed by pumping the samples briefly at the temperature of liquid hydrogen.

Samples of C_2D_2 and C_2D_4, each having a purity greater than 95 percent, were kindly supplied by Dr. L. C. Leitch of the National Research Council.

The ionization potential measurements were made using two mass spectrometers of the 90° sector type, similar to that described by Thode,[10] but equipped with pen recording. Mass spectrometer *I* employed a source of the type described in the above paper, while mass spectrometer *II* used a source with drawing-out potentials, as described by Nier[11] instead of a pusher plate. Both instruments have permanent source magnets and employ magnetic scanning. The electron accelerating potential was measured on a Weston Type 622 microammeter (20 microamps full scale; internal resistance 2300 ohms) equipped with series resistors to read 0–100 volts and 0–20 volts full scale. This meter could be read to ±0.01 volt on the 0–20 volt range. The electron energy was varied by means of a double helical potentiometer, which permitted resetting to ±0.01 volt. Since the current required to operate the meter caused a small proportional change in the operating level of the filament emission regulator, a small manual adjustment of the electron beam current was required to maintain the emission constant at 200 microamps.

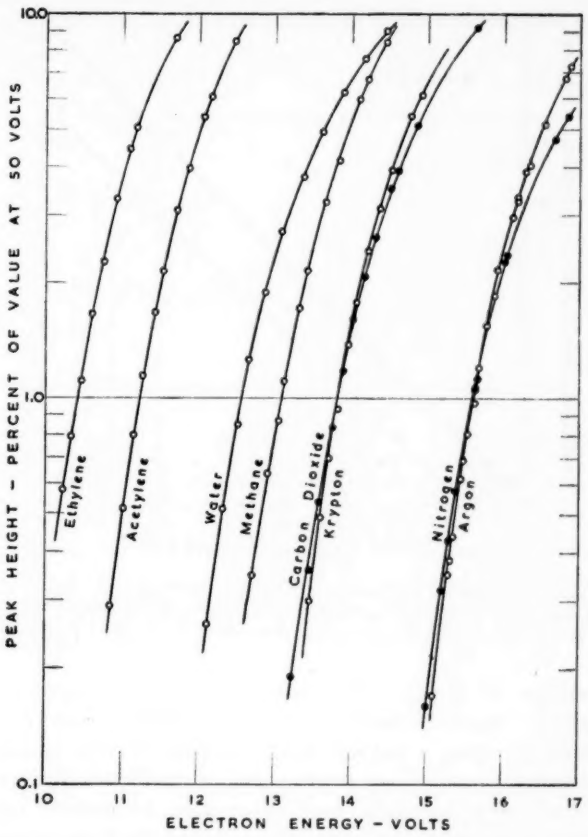

FIG. 1. Comparison of lower portions of ionization efficiency curves.

Both Honig,[2] and Mitchell and Coleman,[4] have devised methods for selecting unique points on the initial portions of the ion efficiency curves. Honig's method has a theoretical basis, while that of Mitchell and Coleman is largely empirical. The method adopted in this work was based on an examination of the shapes of the initial portions of the ion efficiency curves for a

TABLE I. Distances between curves in Fig. 1.

Peak ht.	Distance from argon curve in volts						
Percent of value at 50V	Nitrogen	Carbon dioxide	Krypton	Methane	Water	Acetylene	Ethylene
5.0	−0.24	1.64	1.78	2.56	2.84	4.46	5.30
4.0	−0.16	1.67	1.77	2.56	2.89	4.43	5.27
3.0	−0.10	1.71	1.77	2.55	2.94	4.41	5.25
2.0	−0.05	1.73	1.76	2.54	2.99	4.37	5.20
1.5	−0.01	1.76	1.77	2.55	3.00	4.36	5.18
1.0	+0.02	1.79	1.76	2.54	3.00	4.36	5.15
0.9	0.02	1.79	1.76	2.54	3.00	4.36	5.15
0.8	0.02	1.80	1.77	2.54	3.01	4.36	5.15
0.7	0.02	1.80	1.76	2.54	3.01	4.36	5.15
0.6	0.04	1.81	1.77	2.54	3.01	4.37	5.15
0.5	0.04	1.82	1.77	2.55	3.01	4.36	5.15
0.4	0.04	1.83	1.76	2.56	3.01	4.35	5.15

[7] W. H. J. Childs and H. A. Jahn, Proc. Roy. Soc. (London) A169, 428 (1939).
[8] G. E. MacWood and H. C. Urey, J. Chem. Phys. 4, 402 (1936).
[9] H. C. Urey and D. Price, J. Chem. Phys. 2, 300 (1934).
[10] Graham, Harkness, and Thode, J. Sci. Instr. 24, 119 (1947).
[11] A. O. Nier, Rev. Sci. Instr. 18, 398 (1947).

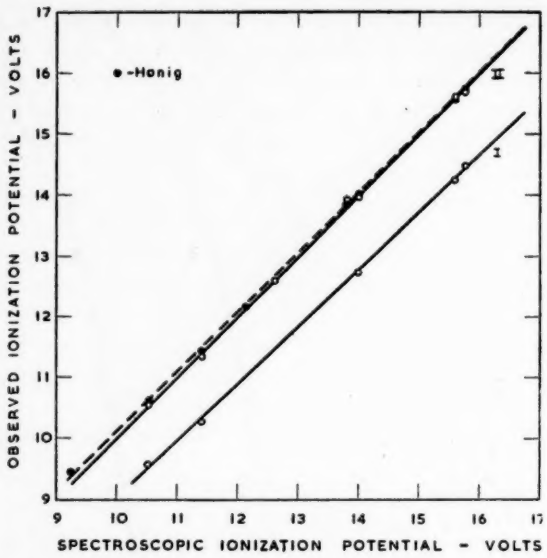

FIG. 2. Calibration curves obtained by plotting observed values of the ionization potential *versus* the spectroscopic values. The two mass spectrometers used have been designated I and II.

number of gases. The curves for argon, krypton, carbon dioxide, methane, and acetylene were determined using a mixture containing all of these gases. In order to avoid any overlapping of peaks, the curves for ethylene, nitrogen, and water were determined on separate mixtures of each gas with argon. The argon curve did not change appreciably from one experiment to another. The amounts of the gases were adjusted to give approximately the same peak heights at 50 volts, and the peak heights at various voltages were measured. In Fig. 1 these heights have been plotted on a logarithmic scale as a percentage of the peak height at 50 volts.

An examination of the curves shows that they are nearly parallel over the region plotted. The extent to which this is true can be shown by measuring the distance of a given curve from the argon curve along the voltage axis for different ordinates near 1 percent. These distances have been tabulated in Table I.

TABLE II. Corrected ionization potentials.

Compound	Ionization potentials (volts) *I*	*II*
CH_4	13.17 13.19	13.07 ···
CH_3D	13.21	13.12
CH_2D_2	13.25	13.14
CHD_3	13.32	13.18
CD_4	13.35 13.36	13.26 13.24
C_2H_2	···	11.40
C_2D_2	···	11.39
C_2H_4	···	10.60
C_2D_4	···	10.59

It can be seen that these curves, with the exception of carbon dioxide and, to a lesser extent, nitrogen, are parallel within the error of measurement for values of 1 percent or less. Since this is the case an intercalibration can be made at any ordinate below 1 percent. Thus it becomes apparent that the ionization potential of a gas can be measured by measuring the peak height at 50 volts and then measuring the electron energy at which the peak height is 1 percent of this value. In this way a value reproducible to ± 0.01 volt can be obtained without the necessity of measuring the whole ion efficiency curve point by point. This eliminates the need for corrections due to falling pressure during a determination.

The simplified procedure described above was used to determine the ionization potentials described in the remainder of this report. Values obtained in this manner must then be related to the spectroscopic values.

Most determinations of ionization potentials by electron impact have been carried out in the presence of a calibrating gas whose ionization potential has been determined spectroscopically. A simple additive constant is then applied to correct the measured value for the effects of contact potential and other instrumental factors. This implies that the relation between the observed ionization potentials and the spectroscopic values is a straight line with a slope of unity over the region between the unknown and the standard. Mitchell and Coleman[4] have pointed out that this procedure may not be accurate when the ionization potential to be measured is very different from that of the calibrating gas. This is confirmed by their results in which they obtained a calibration curve which was not a straight line. In this work, a number of gases having spectroscopically determined ionization potentials was used to construct calibration curves of the type shown in their paper. The observed or "uncorrected" ionization potentials obtained on both mass spectrometers have been plotted *versus* spectroscopic values in Fig. 2. It should be noted that the greatest deviation from the calibration curve is shown by carbon dioxide. By referring to Table I, it can be seen that the slope of the ion efficiency curve for carbon dioxide shows the greatest difference from that of argon. For this reason little weight was assigned to the value for carbon dioxide in drawing the calibration line. Since the ion efficiency curve for methane was parallel to those of the other standards, considerable confidence was placed in the values of the ionization potential of the methanes obtained from this calibration curve.

The ionization potentials of the five methanes were measured one at a time in mixtures with argon. Since fluctuations in the calibration curve were found to be mostly vertical displacements not involving a change in slope, small variations in the argon values were allowed for by means of an additive constant. In order to provide a basis for a comparison with other deuterated

series, the ionization potentials of C_2H_4, C_2D_4, C_2H_2, and C_2D_2 were determined by the same method.

RESULTS

The corrected ionization potentials obtained are given in Table II. These values have been obtained from the observed values by using the calibration curves described above.

DISCUSSION

It can be seen from the data in Table II that the same over-all difference in ionization potential between CH_4 and CD_4, namely, 0.18 volt, was found on each of the mass spectrometers. This difference is in good agreement with that of 0.17 volt reported by Honig.[2] The ionization potential for each of the methanes has been plotted as a function of its deuterium content in Fig. 3 and the straight lines were drawn between the values for CH_4 and CD_4. Values for the isomers of intermediate deuterium content appear to fall on this line within the experimental error of about ± 0.02 volt.

It is interesting to note that, although each set of results shows a high degree of internal consistency (about ± 0.02 volt), there is a difference in the absolute magnitude of the values of about 0.1 volt between the two instruments. As the summary in Table III shows, this is about the size of the difference between the values for the ionization potential of methane reported by various authors. It apparently represents a variation from instrument to instrument due to causes which are not properly allowed for by the calibration methods. Regardless of the uncertainty in the absolute values, the difference in ionization potential between the methanes, as measured by electron impact, appears to be fairly well established.

Within the experimental error, no difference in ionization potential between C_2H_2 and C_2D_2, or between C_2H_4 and C_2D_4 was found.

If Honig's data[2] are used to construct a calibration curve (see Fig. 2), a straight line is obtained with a slope of nearly unity. Since Honig used an additive correction based on a standard having an ionization potential close to that of the unknown gas, his results would be changed very little by a treatment of this type. His value for carbon dioxide, although slightly high, falls more nearly on the line than does the value obtained in this work. This can be explained on the basis of the shapes of the ion efficiency curves in Fig. 1. Since Honig's method involves finding a point on each curve to which a given slope is tangent, it leads to a point which for carbon dioxide is farther down the curve than for the other gases. Thus a relatively lower "observed" ionization potential potential is obtained for carbon dioxide.

It is possible to estimate the difference in ionization potential between CH_4 and CD_4 which might be expected on the basis of zero point energy differences.

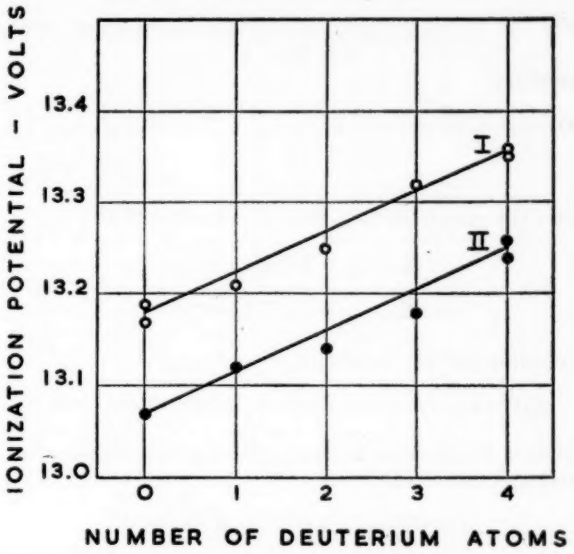

FIG. 3. The ionization potentials of the deuterated methanes as obtained on two mass spectrometers. Straight lines have been drawn joining the values found for CH_4 and CD_4 on each instrument.

This difference is given by

$$I_{CD_4} - I_{CH_4} = [G(0)_{CH_4} - G(0)_{CD_4}] - [G(0)_{CH_4^+} - G(0)_{CD_4^+}].$$

The zero point energy, $G(0)$, of a molecule can be written as

$$G(0) = \Sigma_i d_i(\omega_i/2)$$

where ω_i represents the vibration frequency in cm^{-1} of the ith fundamental, and d_i is the degeneracy of this fundamental. Then,

$$G(0)_{CH_4} - G(0)_{CD_4} = \tfrac{1}{2}[\Sigma_i d_i \omega_{i_{CH_4}} - \Sigma_i d_i \omega_{i_{CD_4}}].$$

To a very good approximation the frequency ω_i may be represented by a term $f_i(K_i/\mu_i)^{\frac{1}{2}}$, where f_i is independent of mass, so that

$$\Sigma_i d_i \omega_i \approx \Sigma_i d_i f_i (K_i/\mu_i)^{\frac{1}{2}} \approx (1/(m_H)^{\frac{1}{2}}) \Sigma_i d_i f_i (K_i)^{\frac{1}{2}}.$$

This follows since the reduced mass associated with any vibration is very nearly equal to the mass of the hydrogen atom, m_H. Then,

$$\Sigma_i d_i \omega_{i_{CD_4}} \approx (1/(2)^{\frac{1}{2}}) \Sigma_i d_i \omega_{i_{CH_4}},$$

TABLE III. Ionization potential of methane.

Reference	Ionization potential (volts)
Honig[a]	13.04±0.02
Mitchell and Coleman[b]	13.04±0.02
Smith[e]	13.18±0.4
Koffel and Lad[d]	13.02±0.2
McDowell and Warren[e]	13.12±0.02
This work	13.18±0.02
	13.07±0.02

[a] See reference 2.
[b] See reference 4.
[e] C. A. McDowell and J. W. Warren, Disc. Faraday Soc. (April, 1951).
[e] L. G. Smith, Phys. Rev. 51, 263 (1937).
[d] See reference 3.

since

$$m_H/m_D=\tfrac{1}{2}.$$

Therefore,

$$G(0)_{CH_4}-G(0)_{CD_4}\approx\tfrac{1}{2}[\Sigma_i d_i\omega_{i_{CH_4}}-(1/(2)^{\frac{1}{2}})\Sigma_i d_i\omega_{i_{CH_4}}]$$
$$\approx 0.15\Sigma_i d_i\omega_{i_{CH_4}}.$$

From the spectroscopic data it is known that[12]

$$\Sigma_i\omega_{i_{CH_4}}=19{,}994\ \text{cm}^{-1}$$

$$\Sigma_i\omega_{i_{CD_4}}=13{,}954\ \text{cm}^{-1}.$$

According to this argument,

$$G(0)_{CH_4}-G(0)_{CD_4}=0.15\times 19{,}994=3000\ \text{cm}^{-1},$$

which is in good agreement with the difference calculated spectroscopically of

$$(19{,}994-13{,}954)/2=3020\ \text{cm}^{-1}.$$

If the same assumptions are made for the zero point energy difference in the ionized state, it follows that

$$G(0)_{CH_4}{}^{+}-G(0)_{CD_4}{}^{+}=0.15\Sigma_i d_i\omega_{i_{CH_4}{}^{+}}.$$

Although it is not possible to calculate $\Sigma_i d_i\omega_{i_{CH_4}{}^{+}}$ from available spectroscopic data, its value can be estimated indirectly. Since we have seen that the approximation of $\omega_i\approx f_i(K_i/\mu_i)^{\frac{1}{2}}$ gives good agreement between the observed and calculated values for $G(0)_{CH_4}-G(0)_{CD_4}$ one may write

$$\omega_{i_{CH_4}{}^{+}}=f_i(K_i{}^{+}/\mu_i)^{\frac{1}{2}}$$

where $\omega_{i_{CH_4}{}^{+}}$ is the frequency of the ith fundamental in the ion and $K_i{}^{+}$ is the force constant in the ion. Then,

$$\omega_{i_{CH_4}{}^{+}}/\omega_{i_{CH_4}}\approx(K_i{}^{+}/K_i)^{\frac{1}{2}}$$

and

$$\Sigma_i d_i\omega_{i_{CH_4}{}^{+}}\approx(K^{+}/K)^{\frac{1}{2}}\Sigma_i d_i\omega_{i_{CH_4}}$$

if one assumes that the ratio of the force constants is the same for stretching and deformation vibrations.

In ionized methane one of the bonding electrons has been removed. Provided that the ion retains the tetrahedral symmetry of the molecule, it seems reasonable to assume that the carbon-hydrogen bonds in the ion are all approximately $\frac{1}{8}$ weaker than those in the neutral molecule. On this basis

$$(K^{+}/K)^{\frac{1}{2}}=(\tfrac{7}{8})^{\frac{1}{2}}$$

and

$$G(0)_{CH_4}{}^{+}-G(0)_{CD_4}{}^{+}=0.15\times(\tfrac{7}{8})^{\frac{1}{2}}\times 19{,}994=2740\ \text{cm}^{-1}.$$

Thus,

$$I_{CD_4}-I_{CH_4}=3000-2740=260\ \text{cm}^{-1},$$

or only about 0.03 volt. This difference appears reasonable when compared with the corresponding differences of 0.01 volt or less found for acetylene and ethylene. In order to obtain the observed difference of 0.18 volt on the basis of the above calculation, it would be necessary for the force constants in the ion to be reduced to only $\frac{1}{4}$ of those in the neutral molecule. This can be compared with the formation of the $H_2{}^{+}$ ion from the H_2 molecule. In this process half the bonding electrons are removed and the bond strength decreases to about $\frac{1}{2}$ of its value in the neutral molecule.[13] In the light of this, the reduction of the bond strength in $CH_4{}^{+}$ to $\frac{1}{4}$ of the value for CH_4 due to the loss of only one-eighth of the bonding electrons seems quite unreasonable. Thus if the assumptions made above are approximately correct, it would appear that the difference in ionization potential between CD_4 and CH_4 as determined by electron impact is at least 0.1 volt greater than can be explained on the basis of zero point energy differences.

Since the separation between the vibrational states in a given electronic level is smaller for the heavier isotope, it follows that the excess energy cannot be explained on the basis of excitation to equivalent vibrational states. If, for example, both CH_4 and CD_4 are raised to the $v=1$ level in the ionic state, this would tend to offset any difference due to the zero point energies. A change in the relative populations of the different vibrational levels might, however, account for the difference.

Regardless of the explanation, the fact that the $CD_4{}^{+}$ ion receives extra energy during its formation raises the question as to whether all electron impact values for the ionization potential of methane may not be too high by an amount larger than previously considered.

ACKNOWLEDGMENT

The authors wish to thank Dr. H. J. Bernstein of the National Research Council for helpful discussions throughout the course of this work.

[12] G. Herzberg, *Infrared and Raman Spectra of Polyatomic Molecules* (D. Van Nostrand Company, Inc., New York, 1950).

[13] G. Herzberg, *Molecular Spectra. I. Diatomic Molecules* (D. Van Nostrand Company, Inc., New York, 1950).

Nuclear Magnetic Shielding in Fluorine and Hydrogen Compounds*

H. S. GUTOWSKY AND C. J. HOFFMAN†
Noyes Chemical Laboratory,‡ University of Illinois, Urbana, Illinois
(Received June 29, 1951)

Measurements of the nuclear magnetic shielding of F^{19} and H^1 are reported for a number of their respective binary covalent compounds. The applied fields required for the F^{19} and H^1 nuclear magnetic resonances, at fixed frequency, vary in these compounds over a range of 3.98 and 0.122 gauss, respectively, at fields of about 6365 gauss. These ranges are of the same order of magnitude as the theoretical internal diamagnetic corrections for the unbound fluorine and hydrogen atoms. The dependence of nuclear magnetic shielding on the electronic structures of the molecules is discussed qualitatively and some general correlations indicated. One such correlation is that the magnetic shielding of the F^{19} nucleus decreases with increasing electronegativity of the atom to which the fluorine is bonded. This and other correlations differ in degree for the proton. The differences may arise from the relatively greater importance of the diamagnetic shielding term for the proton. Specific information regarding molecular and electronic structure is provided in several instances. The tetragonal pyramid structure for IF_5 is confirmed and a similar structure demonstrated for BrF_5. The appearance of double F^{19} resonance lines in PF_5, IF_5, and BrF_5 indicates nonequivalent electronic distributions in the structurally distinguishable bonds. The measurements were facilitated by a large permanent magnet, the design and field homogenization of which are described.

INTRODUCTION

THE magnetic field at the nucleus of an atom differs[1,2] to a small extent from that in the macroscopic sample. The external magnetic field interacts with the motions of the electrons about the nucleus, causing the electrons themselves to contribute a component to the net magnetic field at the nucleus. This component is opposite in direction to the external field and the effect is known as an internal atomic diamagnetism or nuclear magnetic shielding. The internal atomic diamagnetism exists in addition to the macroscopic or bulk magnetic susceptibility. The magnetic field induced in the macroscopic sample is called the external magnetic field, that is external to the atom. Lamb[1] related the internal diamagnetism of an atom to $v(0)$, the electrostatic potential at the nucleus produced by the electrons. The ratio of the induced shielding field, $H'(0)$, to the external field, H, is given as

$$H'(0)/H=(e^2/3\ mc^2)v(0). \quad (1)$$

If $v(0)$ is calculated by the Fermi-Thomas approximation,

$$H'(0)/H=-3.19\times10^{-5}Z^{4/3}. \quad (2)$$

An extension of this analysis has been given by Dickinson[2] who made more accurate estimates of $v(0)$, using the Hartree or Hartree-Fock electronic wave functions. The values obtained for $H'(0)/H$ range from -1.8×10^{-5} for $Z=1$ to -1.16×10^{-2} for $Z=92$.

Corrections of this sort for the neutral atom or simple ion have been applied regularly[3] to most experimental observations of nuclear magnetic moments. Recently, however, the inherently high resolution of nuclear magnetic resonance absorption and induction techniques[4] led to the discovery[5–7] that the nuclear magnetic resonance frequency of a particular nucleus in a given external field depends significantly on the chemical compound containing the nucleus. The resonance frequency ν is given by the Larmor equation,

$$\nu=g\beta H_0/h, \quad (3)$$

where β is the nuclear magneton. In principle the dependence of the resonance frequency on chemical compound might reflect the influence of molecular environment on either H_0, the magnetic field at the nucleus, or on g, the nuclear gyromagnetic ratio. In fact, there is some indication[8] that the apparent ratio of the quadrupole coupling constants of Cl^{35} and Cl^{37} varies slightly with molecular species. If this dependence is associated with an anisotropic polarization of the nuclei in the molecular fields, some exceedingly small differences might then occur in g itself. However, it has been reported[9] that the ratio of the resonance frequencies of the isotopic pairs $Cl^{35}-Cl^{37}$ and $N^{14}-N^{15}$ are the same in different compounds, supporting the non-nuclear nature of at least the major part of the chemical shift.

Ramsey has developed a general theory for nuclear magnetic shielding in molecules.[10] The total shielding is given as the sum of two terms. The first term is identical with Eq. 1 with the provision that $v(0)$ is determined by all the electrons in the molecule. The second term is a summation over the excited electronic states of the

* Reported in part at the Chicago meeting of the American Physical Society, November, 1950, Phys. Rev. 81, 305(A) (1951).
† Submitted in partial fulfillment of the requirements for the Ph.D. degree at the University of Illinois. Now at Los Alamos Scientific Laboratory, Los Alamos, New Mexico.
‡ Supported by the ONR.
[1] W. E. Lamb, Jr., Phys. Rev. 60, 817 (1941).
[2] W. C. Dickinson, Phys. Rev. 80, 563 (1950).
[3] J. E. Mack, Revs. Modern Phys. 22, 64 (1950).
[4] G. E. Pake, Am. J. Phys. 18, 438, 473 (1950), gives a general review and bibliography of most work prior to 1950.
[5] W. D. Knight, Phys. Rev. 76, 1259 (1949).
[6] W. C. Proctor and F. C. Yu, Phys. Rev. 77, 717 (1950).
[7] W. C. Dickinson, Phys. Rev. 77, 736 (1950).
[8] Gunther-Mohr, Geschwind, and Townes, Phys. Rev. 81, 289 (1951). See also R. Livingston, Phys. Rev. 82, 289 (1951).
[9] W. G. Proctor and F. C. Yu, Phys. Rev. 81, 20 (1951).
[10] N. F. Ramsey, Phys. Rev. 78, 699 (1950).

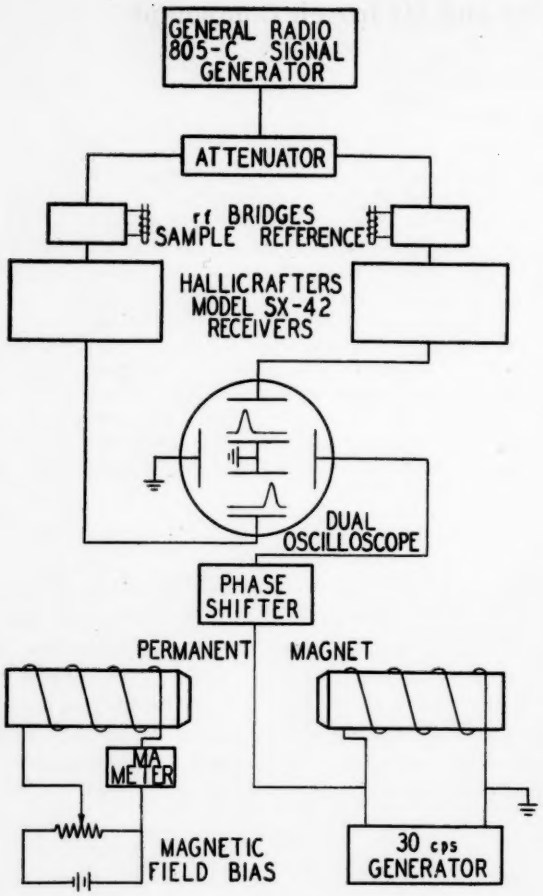

FIG. 1. Block diagram of dual nuclear magnetic resonance spectroscope.

molecule, and gives the effects of second-order paramagnetism. The difficulties inherent in evaluating the summation appear prohibitive for general application. However, in diatomic molecules, the second-order paramagnetism term can be obtained more simply.[10] Complete calculations have been made[10–12] only for H_2. The inapplicability in practice of the general theory recommended an experimental survey. Magnetic shielding data are potentially of basic interest in connection with molecular structure as well as in relation to the problem of obtaining unshielded values for nuclear magnetic moments. For a given nucleus, molecular differences in magnetic shielding should reflect differences in electronic structure associated with bond formation and should depend certainly on the electronic configuration of the other atoms in the molecule. It might be anticipated that the magnetic shielding of a nucleus should vary systematically with the electronic configuration, and nuclear charge of the atoms chemically bound to the observed nucleus. The existence of such trends in compounds[6,7] of B^{11}, N^{14}, F^{19} and P^{31} has been pointed out in a preliminary report[13] of magnetic shielding of the F^{19} nucleus. Herein we present experimental details and observations for the F^{19} and H^1 nuclear magnetic shielding in a variety of binary covalent fluorides and hydrides.

[11] E. Hylleraas and S. Skavlin, Phys. Rev. **79**, 117 (1950).
[12] G. F. Newell, Phys. Rev. **80**, 476 (1950).
[13] H. S. Gutowsky and C. J. Hoffman, Phys. Rev. **80**, 110 (1950).

EXPERIMENTAL

Procedure

Conventional[4,14] radio frequency bridge techniques were used for observing the nuclear magnetic resonance lines. In these experiments, instead of placing the different compounds in a given applied magnetic field and measuring the differences in resonance frequency, we found it preferable to keep the frequency constant and vary the applied magnetic field. The "unknown" and a reference compound were placed in a dual system shown schematically in Fig. 1. The resonance lines from the two samples were displayed either simultaneously on a dual oscilloscope, or alternately on a single beam oscilloscope by manual switching. In several cases, measurements were made by interchanging samples in a single probe system. The difference in magnetic shielding between the unknown and the reference was obtained by determining the change necessary in the applied magnetic field to center first one resonance line and then the other on the oscilloscope. Figure 2 is an oscilloscope picture of the F^{19} magnetic resonance lines in CF_3CO_2H and SF_6, at the top and bottom, respectively, of the figure. The F^{19} resonance occurred in CF_3CO_2H at an applied field 0.81 gauss lower than in SF_6 which implies that the F^{19} nuclei are magnetically shielded 0.81 gauss more in CF_3CO_2H than in SF_6. Small differences in the applied magnetic field at the probes containing the samples were canceled by interchanging

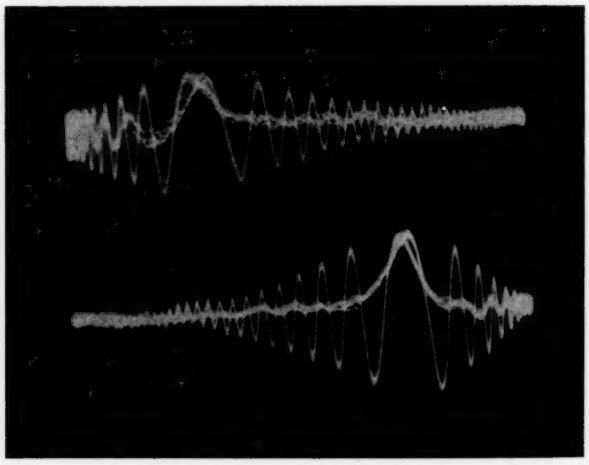

FIG. 2. The F^{19} magnetic resonance in CF_3CO_2H and SF_6, at top and bottom, respectively. The total modulation sweep is 1.9 gauss, with increasing field from left to right. The separation in resonance fields is 0.81 gauss with the F^{19} nuclei in CF_3CO_2H shielded more than in SF_6 by this amount.

[14] Bloembergen, Pound, and Purcell, Phys. Rev. **72**, 679 (1948).

samples or else were measured directly. A sharper setting point was obtained on a resonance line by adjusting the phase of the 30-cycle reference voltage on the oscilloscope to superpose the first relaxation wiggle[14] on the forward and reverse sweeps, rather than the resonance line itself. This is shown in Fig. 3, which is an oscilloscope picture of the proton resonance line in Nujol mineral oil.

The resolution of such an apparatus, and the accuracy of the measurements, is limited primarily by the line widths. In the liquid and gaseous samples used, the line widths are determined usually by inhomogeneities in the applied magnetic field,[14,15] so considerable pains were taken to obtain a highly homogeneous field. The limitations arising from field inhomogeneity and from the instability of electromagnets are met frequently in nuclear magnetic resonance research; therefore, the details of our permanent magnet design, construction and field homogeneization are given below.

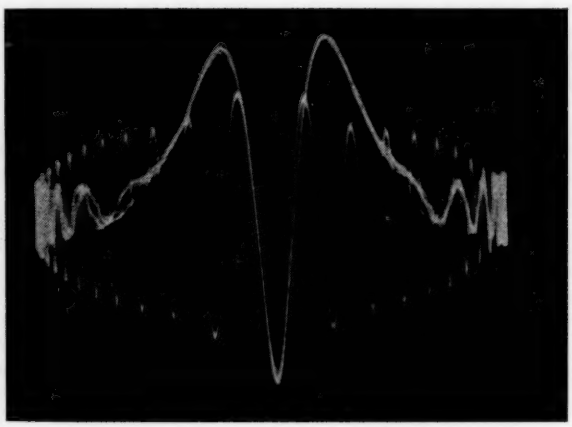

FIG. 3. The proton magnetic resonance in Nujol mineral oil. The phasing of the 30-cycle reference voltage on the horizontal plates of the oscilloscope is adjusted to superpose the first relaxation wiggle; the two maxima are the resonance line on forward and reverse sweeps. The total modulation sweep is about 0.8 gauss.

Permanent Magnet

The magnet used in this work is a large permanent magnet with a field strength of 6365 gauss in a 2-in. gap with 6-in.-diameter pole faces. It is similar in design to magnets constructed by Pake[16] and Pound.[17] The choice of a permanent rather than an electromagnet was dictated by the desire for a stable simple system with which detailed broad line shapes could be observed.[4] The 2-in. gap was considered desirable for low temperature experiments. A cut-a-way sketch of the magnet is given in Fig. 4. The Arnold Engineering Company, Marengo, Illinois, contributed materially to the design of the magnet, in addition to contracting for its construction. We are indebted particularly to their Chief Engineer, Mr. Charles Brand.

The Alnico V poles are 19 in. long, built up from circular castings about 2 in. thick. Each pole weighs approximately 300 pounds and has a straight cylindrical section $8\frac{7}{8}$ in. in diameter and 15.2 in. long followed by a section straight-tapered to 7.2 in. at the gap end to allow for flux leakage. A theoretical analysis[18] of the flux leakage as suggested by H. Bethe, leads to a curved taper towards the gap. However, the small saving in Alnico with the curved taper as compared to the straight taper is balanced by the added costs of designing and casting such a taper. The length/diameter ratio of the magnet should be chosen for the most efficient utilization of the Alnico.[19] The Alnico castings are cemented with shellac in a machined length of $8\frac{1}{2}$ in. i.d. and 10 in. o.d. phenolite tubing, National Vulcanized Fibre Company, grade X_M. Each phenolite tube has a turned down section which serves as a form for 2000 turns of B. and S. No. 20 copper magnet wire. A direct current passed through the coil about one pole permits variation of the field over a range of about ± 20 gauss; a 30-cycle current through the other coil is used to modulate the field.

The pole caps, or pole pieces, are the main items determining field homogeneity. Particularly critical are the magnetic homogeneity and dimensions of the pole caps themselves, and in the assembly, the parallelism and coaxiality of the pole faces. The pole caps were machined from cylindrical Armco Magnetic Ingot Iron forgings to a thickness of 1.540 in. with a 45° taper leading from the 7.2 in. o.d. to the 6-in.-diameter pole face. The pole face has a coaxial 5-in.-diameter counter bore 0.040 in. deep, providing a $\frac{1}{2}$-in.-wide Rose type shim[20] to correct for fringing effects at the edge of the gap. This shim design is derived for right-angled pole caps whereas the pole caps used have a 45° taper. Such a taper for unshimmed pole caps[21] is intermediate between the 30° value which leads to maximum field in the gap, and the 50° 46′ value which gives the most uniform field. The taper prevents saturation at the edge of the pole cap, provides a convenient means of assembly and does not appear to harm the usefulness of the Rose design shim. After the final machining, the pole caps were annealed in a hydrogen atmosphere, following the general instructions of G. H. Cole of Armco Steel Corporation, Middleton, Ohio. The annealing was at a temperature between 1450 and 1800°F. The heating and cooling rates above 800°F were not over 100°/hour, especially the cooling rate in the high temperature portion of the cycle. The temperature was held constant within ± 25°F during the soaking period of several hours. The annealing is desirable for high magnetic homogeneity.

The rectangular yoke is 3 in. thick, of low carbon iron, and is 43.08 in. by 21.5 in., inside dimensions, and 12 in. high. Each pole cap and pole assembly, as shown in Fig. 2, is held suspended in place by six stainless steel tie rods fastened to the yoke and to a stainless steel pole-cap ring, a bevel on which fits about the 45° taper on the pole caps. Also, each pole-cap ring is supported at the gap by a stainless steel rod bolted to the bottom of the yoke. A stainless steel shim 3 in. in diameter and 0.003 in. thick is mounted coaxially between each pole cap and the ground surface of the

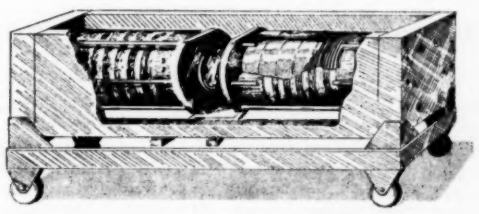

FIG. 4. Cut-a-way sketch of permanent magnet. The gap is 2″ and field strength is 6365 gauss.

[15] R. M. Brown, Phys. Rev. **78**, 530 (1950).
[16] G. E. Pake, J. Chem. Phys. **16**, 327 (1948).
[17] R. V. Pound, Phys. Rev. **79**, 685 (1950).
[18] J. D. Howe and I. Walerstein, Rev. Sci. Instr. **9**, 53 (1938).
[19] The main general aspects of permanent magnet design are discussed in two very useful pamphlets: R. L. Sanford, "Permanent magnets," Circular of the Natl. Bur. Standards, C448, U. S. G.P.O., Washington 25, D. C. (1944); "Indiana Permanent Magnet Manual No. 4," The Indiana Steel Products Company, Chicago 2, Illinois (1948).
[20] M. E. Rose, Phys. Rev. **53**, 715 (1938).
[21] L. F. Bates, *Modern Magnetism* (Cambridge University Press, Cambridge, 1948), second edition, p. 71.

TABLE I. Sources of fluorine compounds and experimental conditions under which they were observed.

Sample	Experimental conditions[a]	Source
AsF_3	sealed 10-mm o.d. test tube	synthesized
BF_3	glass-bulb probe, 500 ml, 150°K	Harshaw Chem.
BeF_2	10-mm o.d. test tube, aq. soln.	synthesized
BrF_3	sealed ¼-in. i.d. Kel-F polymer tube	Harshaw Chem.
BrF_5	sealed ¼-in. i.d. Kel-F polymer tube	Harshaw Chem.
CF_4	glass-bulb probe, 500 ml, 125°K	duPont Co.
ClF_3	sealed ¼-in. i.d. Kel-F polymer tube	Harshaw Chem.
F^-	10-mm o.d. test tube, aq. soln. KF	Baker & Adamson
F_2	gas, metal pressure probe, 25 atmos	Penn. Salt
GeF_4	sealed capillary, 3 mm i.d.	synthesized
HF	anhy., ¼-in. i.d. polystyrene tube	Harshaw Chem.
IF_5	sealed 10-mm o.d. test tube	Gen. Chem. Div.
IF_7	sealed ¼-in. i.d. Kel-F polymer tube[b]	Dr. W. C. Schumb
NF_3	glass-bulb probe, 500 ml, 125°K	Dr. A. B. Burg
PF_3	3-mm capillary pressure probe, 130°K	synthesized
PF_5	3-mm capillary pressure probe, 190°K	synthesized
SF_6	sealed capillary, 4 mm i.d.	Matheson Co.
SbF_3	10-mm o.d. test tube, aq. soln.	Harshaw Chem.
SbF_5	sealed 10-mm o.d. test tube	Gen. Chem. Div.
SeF_6	sealed capillary, 3 mm i.d.	synthesized
SiF_4	3-mm capillary pressure probe, 195°K	synthesized
TeF_6	sealed capillary, 3 mm i.d.	synthesized

[a] Unless otherwise specified the sample was liquid and measurements were made at room temperature.
[b] Line is broad; center located by plotting derivative of absorption line. (See reference 4.)

Alnico pole.[22] After assembly, the shim permits minor adjustments to be made in the parallelism of the pole faces by changing the tension on the appropriate tie rods.

The assembly was magnetized by passing approximately 275 amperes through a total of 1200 turns of B. and S. No. 7 square copper wire about the Alnico poles. This current was a considerable overload on the magnetizing coil but was permissible because of its short duration. The magnet was stabilized by reducing the field about 2.5 percent from the saturated value.

The variation of the field in the gap was measured by mechanically positioning a sample at various points in the gap and determining the field biasing current required, at a given frequency, to center a resonance line on the oscilloscope. After adjusting the tension of the tie rods several times to correct the parallelism of the pole faces, a meridian plot of the field was obtained in which the field gradually decreased from the center, with contours of 0.15, 0.45, and 1.50 gauss at diameters of about 1 in., 2 in., and 3 in., respectively. At larger diameters the field became too inhomogeneous to plot accurately, but appeared to increase again somewhat before falling off very rapidly at the edge of the gap. This would indicate a slight overcorrection, attributable perhaps to the 45° taper on the pole cap. However, the 1.50 gauss decrease at the 3 in. diameter compares favorably with the 0.1 percent decrease, or 6.4 gauss, predicted by the Rose equation[20] for the 4-in. diameter and suggests that the tapered pole cap may have some over-all advantages.

Initial attempts at improving the field homogeneity by hand polishing the centers of the pole faces with emery paper were only partially successful. A subsequent plot of the field with a dual probe in which two cylindrical samples ¾ in. long and ⅜ in. in diameter were located with their centers $\frac{5}{16}$ in. on either side of the meridian plane revealed inhomogeneities perpendicular to the pole faces. A check of alignment revealed that the pole faces were about $\frac{1}{16}$ in. from coaxiality in the horizontal line, while the bottom support rods at the gap maintained the vertical alignment. A brass jack was inserted between the yoke and pole-cap ring, the alignment corrected and parallelism readjusted. Thereafter, hand-polishing of the pole face centers reduced the total variation over the central 3-in. diameter by 1-in.-thick section to less than 0.4 gauss, and over the central 2-in. diameter section to 0.15 gauss. The variation in the meridian plane over the central 2-in. diameter was about 0.08 gauss. Further improvement appeared possible, but was not necessary for this work. No appreciable deterioration of the field homogeneity has been observed in ten months. It is to be noted, however, that the field is less homogeneous upon the application of large dc field biasing currents equivalent to ±15 gauss or more.

The magnetic field of 6365 gauss, after homogenization, was determined by measuring the proton resonance frequency against a secondary frequency standard set by reference to WWV. An approximate calibration of the dc field biasing current was made initially by using the increment dial on the General Radio 805 C signal generator and measuring the current equivalent to a 0.05 percent change in frequency. It was found later that the increment dial was ten percent lower.[23] A better method of calibration was developed using a low frequency standard at 10 kilocycles to amplitude modulate the signal generator. The biasing current was measured between the resonance lines from the carrier and the first two side bands. The calibration of the magnet is essentially linear, with one milliampere producing a change in field of 0.0315±0.0002 gauss. However, hysteresis of two to three tenths of a gauss results when large currents are applied first in one direction and then reversed. The modulation voltage was calibrated by measuring the field bias required to move a resonance line from one side of the modulation sweep to the other. It, too, is quite linear, with one volt giving a peak to peak modulation of 0.16 gauss.

TABLE II. Sources of hydrogen compounds and experimental conditions under which they were observed.

Sample	Experimental conditions*	Source
AsH_3	sealed capillary, 4 mm i.d.	synthesized
B_2H_6	glass-bulb probe, liter, 170°K	synthesized
CH_4	gas, metal pressure probe, 25 atmos	Matheson Co.
H_2	gas, metal pressure probe, 30 atmos	Matheson Co.
HBr	anhy., sealed capillary, 4 mm i.d.	Matheson Co.
HCl	anhy., glass-bulb probe, 500 ml, 175°K	Dow Chemical
HF	anhy., ¼-in. i.d. polystyrene tube	Harshaw Chem.
HI	sealed 10-mm o.d. test tube	synthesized
H_2O	10-mm o.d. test tube	conductivity H_2O
H_2S	sealed capillary, 4 mm i.d.	Matheson Co.
H_2Se	sealed capillary, 3 mm i.d.	synthesized
NH_3	sealed capillary, 4 mm i.d.	Matheson Co.
SiH_4	glass-bulb probe, 500 ml, 90°K	synthesized

* Unless otherwise specified the sample was liquid and measurements were made at room temperature.

Samples

Tables I and II summarize sources and experimental conditions for the fluorine and hydrogen compounds. The details of the various syntheses performed are given elsewhere.[24] Compounds liquid at room temperature were contained in thin-walled 10-mm o.d. Pyrex test tubes. Plastic tubes were used for compounds reacting with glass. The rf coil in which the tubes were placed was 0.75 in. long and 0.40-in. internal diameter, with 10½ turns of B. and S. No. 18 copper wire. Many of the substances investigated were gases at NTP and required compression or liquefaction to obtain a high enough concentration for observation. Hydrogen, methane, and fluorine gas were observed at pressures of about 25 atmospheres in the brass pressure probe described elsewhere.[25] A preamplifier was used with the gases and other samples giving relatively weak signals. The preamplifier utilizes a modified

[22] After a suggestion by R. V. Pound.

[23] Chemical shifts previously reported (see reference 13) for some fluorine compounds should be multiplied by 1.10.

[24] C. J. Hoffman, Ph.D. Thesis, Department of Chemistry, University of Illinois (1951). See also *Inorganic Syntheses* (McGraw-Hill Book Company, Inc., New York).

[25] H. S. Gutowsky and R. E. McClure, Phys. Rev. **81**, 276 (1951).

Wallman circuit, with a 6AK5 grounded cathode input tube, followed by a 6J6 grounded grid stage.

Liquefaction of gases was accomplished in several ways. Compounds with relatively high critical temperatures were condensed and sealed in capillary Pyrex tubing of 3- or 4-mm bore. Other samples were condensed to the liquid *in situ*. The cryostat employed is an all copper and brass analog of that described by Alpert,[26] with the exception that the rf coil is mounted in a copper block attached to a probe separate from the cooling well in which it is inserted. Compounds with widely separated melting and boiling points were placed in a 500-ml or liter bulb fitted with a long Pyrex tube which could be inserted into the rf coil in the cryostat. In other instances, where the solid sublimes at low pressures, a glass pressure probe was used to liquefy the solids which otherwise gave broad absorption lines.[4,14] The probe was a length of capillary tubing fitted with a heavy stopcock and standard ground joint. The sample was condensed to the solid in the evacuated probe with liquid nitrogen. Then the closed probe was inserted in the precooled cryostat, and the temperature gradually increased until a high enough pressure was developed to liquefy the solid. The small field differences between the cryostat and an external reference probe were measured directly using trifluoroacetic acid or hexane, and were applied to all apparent differences in magnetic shielding observed with the cryostat at the same temperature.

RESULTS

The positioning of the resonance absorption pattern on the oscilloscope introduces a statistical error by virtue of the finite width of the resonance line. Also, if the system is not tuned properly, or if the rf bridge does not have a pure amplitude balance,[14] the apparent maximum will not coincide with the actual center of the absorption line. However, when the balance and tuning are properly adjusted, a symmetrical oscilloscope pattern results. Even small deviations from symmetry are readily detectable visually. In Fig. 3 the resonance lines on the forward and reverse modulation sweeps are not quite the same amplitude, indicating that the tuning was very slightly out of adjustment. To minimize any systematic effects of tuning or of bridge balance, and also to reduce the statistical error, at least one set of ten measurements was made for each compound, with bridge balance and tuning readjusted periodically during the series to give a symmetrical oscilloscope pattern. The probable error of the magnetic field biasing currents in each set of readings was about ± 0.06 milliamperes, or ± 0.002 gauss, for most of the fluorides, and about half as great for the hydrogen compounds.

The main source of systematic error is the conversion of the field-biasing currents to magnetic field differences. The maximum calibration error, including hysteresis effects, over the range of biasing currents used, is ± 0.5 percent. The milliammeter accuracy is also ± 0.5 percent, so that the over-all maximum error of a systematic nature from these sources is ± 1.0 percent. The magnitude of the possible systematic error is directly proportional to the measured difference in applied magnetic fields and has a maximum of ± 0.04 gauss for the F^{19} data and ± 0.001 gauss for the proton.

[26] N. L. Alpert, Phys. Rev. **75**, 398 (1949). We are indebted to Dr. Alpert for a detailed drawing of his design.

TABLE III. Magnetic shielding of the F^{19} nucleus.[a]

Compound	H_r'	Statistical error[b]	H_r'/H_a
AsF_3	2.986 gauss[c]	± 0.001 gauss	4.691×10^{-4}
BF_3	3.536	0.002	5.555
BeF_2	3.813	0.003	5.991
BrF_3	2.935	0.001	4.611
BrF_5 (a)	1.849 s	0.005	2.905
(b)	0.973 w	0.010	1.529
CF_4	3.125	0.002	4.910
ClF_3	2.186	0.001	3.434
F^-	3.489	0.001	5.482
F_2	0.000	0.010	0.000
GeF_4	3.875	0.001	6.088
HF	3.978	0.002	6.250
IF_5 (a)	2.662 s	0.001	4.182
(b)	2.348 w	0.001	3.689
IF_7	1.664	0.050[d]	2.615
NF_3	1.814	0.001	2.850
PF_3 (a)	3.126 m	0.003	4.911
(b)	2.777 m	0.003	4.363
PF_5 (a)	3.312 m	0.003	5.203
(b)	3.080 s	0.003	4.839
SF_6	2.391	0.002	3.756
SbF_3	3.233	0.001	5.079
SbF_5	3.420	0.001	5.373
SeF_6	2.372	0.002	3.727
SiF_4	3.812	0.003	5.989
TeF_6	3.093	0.002	4.859

[a] Data are reduced to the F^{19} nucleus in F_2 as the zero of reference. H_r' the relative magnetic shielding, is the applied field for resonance in the compound less the applied field for resonance in F_2.
[b] The statistical error refers only to the internal consistency of the measurements for a given compound. In addition, there are systematic errors to a possible maximum of ± 1 percent of observed differences in shielding, as discussed in the text.
[c] The letters s, m, and w after components of complex lines refer to relative intensities as strong, medium, and weak.
[d] The line is broad, increasing the error of the measurement.

Another possible source of systematic error is the bulk diamagnetism, including differences in containers and sample shapes.[27] The magnetic field H in the bulk of the sample differs from the applied field H_a by an amount

$$H-H_a=(4\pi/3-\alpha)\kappa H\cong(4\pi/3-\alpha)\kappa H_a. \quad (4)$$

TABLE IV. Magnetic shielding of the proton.[a]

Compound	H'	Statistical error[b]	H'/H_a
AsH_3	0.191 gauss	± 0.001 gauss	3.00×10^{-5}
B_2H_6	0.220	0.001	3.46
CH_4	0.193	0.002	3.03
H_2[25]	0.169	0.002	2.66 ± 0.03[12]
HBr	0.219	0.001	3.44
HCl	0.198	0.001	3.11
HF	0.147	0.002	2.31
HI	0.269	0.001	4.23
H_2O	0.172	0.001	2.70
H_2S	0.195	0.001	3.06
H_2Se	0.215	0.001	3.38
NH_3	0.199	0.001	3.13
SiH_4	0.183	0.002	2.88

[a] Data are reduced to the unshielded proton as the zero of reference. The magnetic shielding H' is the applied field required for resonance of protons in the compound less the applied field that would be required for resonance of the unshielded proton.
[b] The statistical error refers only to the internal consistency of the measurements for the given compound. In addition, there are systematic errors to a possible maximum of ± 1 percent of observed differences in shielding, as discussed in the text.

[27] W. C. Dickinson, Phys. Rev. **81**, 717 (1951); we wish to thank Dr. Dickinson for sending us a draft of his article prior to publication.

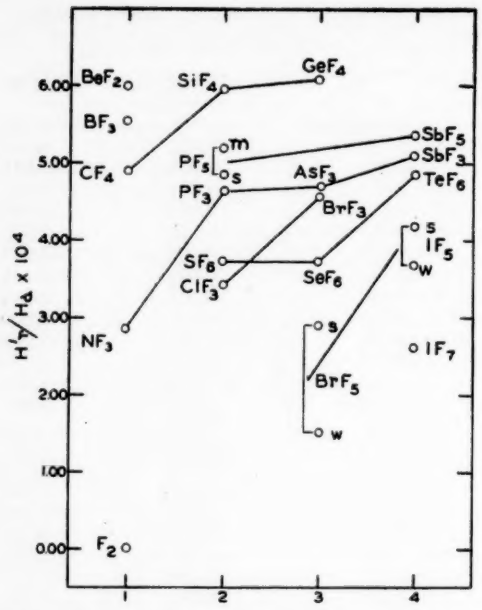

FIG. 5. The dependence of the magnetic shielding of the F^{19} nucleus upon the position in the periodic table of the other atomic species in binary covalent compounds.

κ is the volume susceptibility and α is the demagnetization factor; α is 2π for an infinite cylinder and $4\pi/3$ for a sphere. Most diamagnetic liquids differ in their volume susceptibilities over a range of about 0.2×10^{-6}, so with infinite cylinder samples at 6365 gauss, bulk diamagnetic differences of 0.002 to 0.003 gauss could result. In our samples, the length/diameter ratio was generally between 2 to 5, giving smaller[27] values of α and reducing the possible effects to 0.001 gauss. This correction is small in comparison to the differences observed in the magnetic shielding of the F^{19} nucleus, but is of some importance for the proton results. The bulk diamagnetic correction of a gas compared to a liquid is several times that between liquids. The correction for F_2 gas is small in comparison to the other errors, and was not made. The results for CH_4 and H_2 gas have been corrected in the manner previously[25] described. No other bulk diamagnetic corrections were attempted; however, identical sample containers and shapes were generally used to minimize the effects.

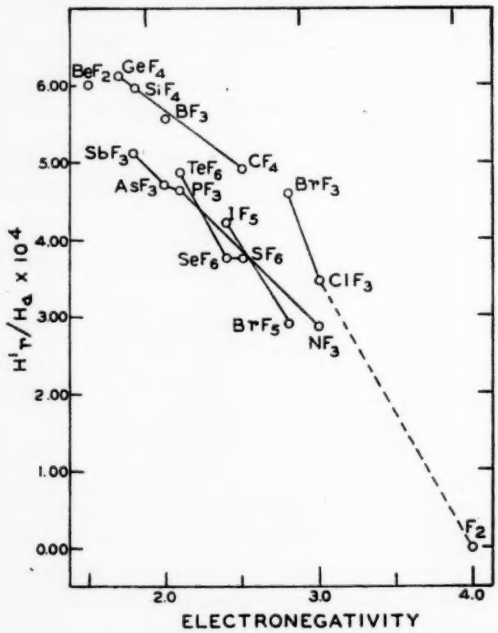

FIG. 6. The F^{19} nuclear magnetic shielding as related to the electronegativity of the other atomic species in binary covalent compounds.

The results for the fluorine and for the hydrogen compounds are tabulated in Tables III and IV, respectively. The shielding values are defined so that a larger, positive number corresponds to a smaller field at the nucleus. The H' column in the tables gives the observed values for the differences in the applied magnetic fields for the F^{19} resonance at 25.46 Mc, and for the proton resonance at 27.10 Mc. The second numerical column lists the statistical error of the data, *excluding* the possible systematic errors. The last column gives H'/H_a, the fractional difference in shielding. A value for H_a of 6365 gauss was used for all compounds; the differences in individual cases from this value were no more than +5 gauss, which may be neglected.

DISCUSSION

The data in Tables III and IV indicate that the total ranges in magnetic shielding of the F^{19} nucleus and of the proton, among different compounds, are of the same order of magnitude as the internal diamagnetic correction for the neutral atoms. For F^{19}, this correction has been computed by Dickinson[7] to be 4.64×10^{-4}. In Table III, the observed range of magnetic shielding is 6.25×10^{-4}. In the case of the proton, the correction for the neutral atom[7,11] is 1.8×10^{-5} while the observed range among the compounds in Table IV is 1.92×10^{-5}.

Absolute values for the magnetic shielding of the proton are given in Table IV on the basis of a theoretical shielding constant[10,12] for H_2 of 2.66×10^{-5}, used in conjunction with the measurements[26,28] on H_2 gas. For the hydrogen compounds, some conclusions can be drawn regarding the relative magnitudes of the two shielding terms obtained in Ramsey's theoretical analysis. In H_2, the computed electrostatic potential or diamagnetic term from the molecular electrons is 3.21×10^{-5} and the second order paramagnetic term[12] is -0.55×10^{-5}. The observed shielding values range from 2.31×10^{-5} in HF to 4.23×10^{-5} in HI, requiring that the maximum electrostatic potential term be at least the 4.23×10^{-5} in HI. No inferences can be made about the magnitudes of the individual terms in other compounds. However, since all observed proton shielding values are positive, it is apparent that the diamagnetic term is always larger than the second order paramagnetic term in these hydrogen compounds.

[28] H. A. Thomas, Phys. Rev. **80**, 801 (1950).

For F^{19}, there appears to be no means at present by which absolute shielding values can be derived unambiguously. The internal diamagnetic correction for the free fluoride ion may be calculated from data tabulated by Dickinson,[7] and a value of 4.72×10^{-4} is obtained. On this basis the absolute value of the shielding in F_2 would be -0.76×10^{-4}. Negative shielding appears to be possible on theoretical grounds.[10] However, the use of the F^- ion in solution to establish the absolute zero of the F^{19} magnetic shielding does not consider solvation effects. It seems preferable at this time to express the F^{19} shielding with respect to F_2 as an arbitrary zero of reference.

Fluorine Compounds

In Fig. 5, the shielding data are presented graphically for the fluorine compounds. The four columns correspond to the first four periods in the periodic table. As the nuclear charge of the atom bound to the fluorine increases in each period, the magnetic shielding of the F^{19} nucleus decreases. An exception to this trend is BrF_3; in it the F^{19} nucleus is shielded more than in SeF_6. Also, in Fig. 5, lines are drawn joining fluorides of elements in the same group in the periodic table. Different oxidation states of the element are indicated separately. For compounds with elements in the same group in the periodic table, in the same oxidation state, it is seen that the F^{19} magnetic shielding generally decreases with the nuclear charge. Compounds not following this trend include SF_6 in which the F^{19} shielding is greater than in SeF_6, and BrF_3 in which the shielding is greater than in IF_5. Different oxidation states are involved in the latter case.

From a qualitative standpoint at least, the general trends reflect the known properties of the electron distributions in the elements. In Fig. 6 the F^{19} magnetic shielding in the fluorine compounds is plotted *versus* the electronegativity of the atom to which the fluorine is bound. Points for elements in the same group and oxidation state are connected. The decrease in magnetic shielding with increasing electronegativity is seen to be quite systematic. This implies that the more tightly electrons are held by the atom bound to the fluorine, the less effective the electrons are in magnetically shielding the fluorine nucleus. The group and period trends with respect to nuclear charge may be interpreted in the same manner.

Complex F^{19} magnetic resonance absorption lines were observed in several compounds, including PF_5, IF_5, BrF_5, IF_7, and PF_3. Multiple F^{19} resonance lines have been reported in organic fluorides containing fluorine atoms in nonequivalent structural positions.[13,29] The simplest and most likely interpretation of these cases is that the magnetic shielding differs at the various structural positions in the compounds.

In PF_5 the F^{19} resonance line consisted of two components of unequal intensity, separated by 0.23 gauss, with the weaker component at the higher applied magnetic field. PF_5 has a trigonal bipyramid structure[30] with two sets of nonequivalent fluorine atoms, one set containing the two apex atoms and the other, the three atoms in the meridian plane of the bipyramid. The double resonance undoubtedly results from the existence of these two nonequivalent sets of F^{19} nuclei. The integrated line intensities are approximately in the ratio of 3:2, confirming the assignment. By analogy, SbF_5 should exhibit a double resonance. The resonance line in it was broader than field inhomogeneities, but structure was not observed under experimental conditions where resolution was about 0.05 gauss.

A structural interpretation similar to that of PF_5 can be given of the double F^{19} magnetic resonance in IF_5, an oscilloscope photograph of which is shown in Fig. 7. In this case the integrated resonance line intensities are in ratio of about 4:1, supporting the tetragonal pyramid

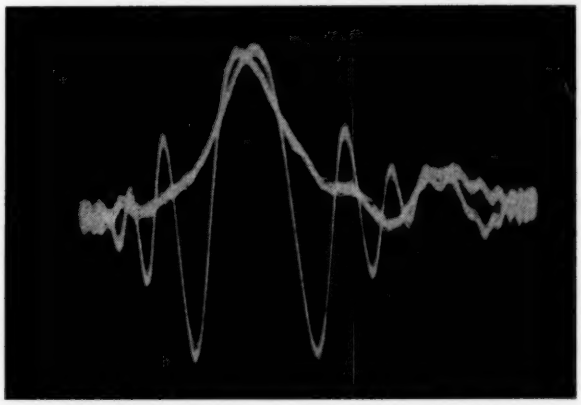

FIG. 7. The double F^{19} magnetic resonance in IF_5. The total modulation sweep is about 0.8 gauss, with increasing field from left to right. The separation of the components is 0.31 gauss.

structure proposed from spectroscopic evidence.[31] The F^{19} resonance in BrF_5 was like that observed in IF_5. There were two components with integrated line intensities in ratio of 4:1. The weaker line occurred at a lower applied field in both compounds. The separation of the components in BrF_5 was 0.89 gauss compared to 0.31 gauss in IF_5, a trend analogous to that implied for PF_5 and SbF_5. These factors indicate that BrF_5 has a tetragonal pyramid structure like IF_5. This proposal is supported by the appearance in the two main components of additional structure, the nature and source of which are discussed in more detail later.

In IF_7 the F^{19} magnetic resonance was also multiple. However, the individual lines overlap and no simple interpretation is evident other than the obvious conclusion that the seven fluorine nuclei are not equivalent. This eliminates the planar D_{7h} configuration and thereby

[29] E. L. Hahn, Phys. Rev. **80**, 580 (1950).

[30] P. W. Allen and L. E. Sutton, Acta Cryst. **3**, 46 (1950).

[31] Lord, Lynch, Schumb, and Slowinski, J. Am. Chem. Soc. **72**, 522 (1950).

supports the spectroscopic argument[31] for the D_{5h} pentagonal bipyramid structure. The line shape and magnetic shielding were determined by plotting the derivative[4] of the absorption line. The line is surprisingly broad for a liquid. The line width measured as the separation between the maximum and minimum on the derivative curve was 1.75 gauss; the shielding value listed corresponds to the midpoint.

PF_3 is a pyramid with equivalent fluorine atoms,[30] so structural factors cannot be the cause of the observed F^{19} doublet line. Multiplet lines have been reported for both the F^{19} and P^{31} resonances in several other phosphorus fluorides with structurally equivalent nuclei.[32] This variety of splitting results from a second order coupling of the nuclear magnetic dipoles via the nuclear magnetic shielding field.[33] The F^{19} resonance doublet in PF_3, with components of equal intensity, arises from interactions associated with the two P^{31} nuclear spin orientations with $m_I=\pm\frac{1}{2}$. Line splitting of the same general character was observed in BrF_5 and IF_5.

The stronger line in BrF_5 was a doublet with components of equal intensity, and the weaker line a quintuplet with relative intensities of 1:4:6:4:1. Adjacent components in the main lines were separated by about 0.018 gauss. This structure confirms the tetragonal pyramid model for BrF_5. The doublet structure of the stronger line is associated with the $m_I=\pm\frac{1}{2}$ nuclear spin orientations of the single fluorine atom at the apex of the pyramid. The quintuplet structure of the weaker line arises from the five possible values, $M_I=0, \pm1, \pm2$, of the total nuclear spin quantum number for the four equivalent F^{19} nuclei at the base of the pyramid and the corresponding interactions. The relative intensities of the various lines agree with the statistical weights of the associated m_I or M_I values. The two F^{19} resonance lines in IF_5 have similar fine structure. The transient effects associated with 30-cycle modulation interfere with the resolution of closely spaced resonance lines, and in such cases one observes only an amplitude modulation of the wiggles. The fine structure of the F^{19} resonances in BrF_5 and IF_5 were resolved by a low frequency modulation system similar to that reported by the group[34] at Stanford.

Dependence of the F^{19} magnetic shielding on oxidation state was observed in phosphorus and antimony tri- and penta-fluorides. Dickinson obtained similar results[27] for the P^{31} shielding. In the *V* oxidation state, *s* and *d* orbitals as well as *p* are required while in the *III* state only *p* orbitals are used. The higher energy *s* and *d* orbitals in the *V* oxidation state gave the greater magnetic shielding and the differences decreased with decreasing energy separation of the orbitals in the *III* and *V* states of the particular element. A related effect may be the greater F^{19} shielding in SF_6 compared to that in SeF_6. The bond orbitals in these compounds are[35] d^2sp^3. The energy separation of the $3d$ orbitals from the $3s$ and $3p$ is larger in sulfur than the separation of the $4d$ orbitals from the $4s$ and $4p$ in selenium. In the case of the halogen fluorides, the higher oxidation states were observed to have the *lower* F^{19} shielding, a reversal in trend for which no simple, likely interpretation has been developed.

The magnetic resonance lines that are complex because of differences in magnetic shielding demonstrate the nonequivalence of the electron distributions in the structurally distinguishable bonds. In PF_5, the double F^{19} magnetic resonance line was assigned to differences in the magnetic shielding of the two apex F^{19} nuclei compared to the three in the meridian plane. The weaker line from the apex nuclei had the greater magnetic shielding. The orbitals used in bond formation in PF_5 are $3p^3$, $3s$ and $4d$, which could give five equivalent bonding orbitals, in a bipyramid configuration, by dsp^3 hybridization. However, the larger magnetic shielding of the weaker line leads to the conclusion that the apex atoms have bonds with greater *d* character via an sp^2-dp partial dehybridization. In BrF_5, and IF_5 the hybridization for five equivalent bonds in a tetragonal pyramid is d^2p^3. The weak line from the apex F^{19} nucleus has considerably less magnetic shielding than the strong line from the four F^{19} nuclei at the pyramid base. Therefore, the apex bond is essentially *p* in character with the remaining set of four bonds primarily d^2p^2. The dp, sp^2, and d^2p^2 hybridization provide the linear, trigonal plane and tetragonal plane partial configurations found in PF_5 and in BrF_5 and IF_5.

Hydrogen Compounds

The magnetic shielding of the proton in the binary covalent hydrides is shown graphically in Fig. 8. Perhaps the most interesting aspect of this tabulation is the manner in which the systematic trends in shielding differ from those for the F^{19} nucleus. A plot of shielding of the proton against the electronegativity of the other atom exhibits similar differences. Figure 8 shows that, with the exception of CH_4 and NH_3 which are inverted, the proton shielding decreases with nuclear charge in the first period compounds, as does that of the fluorine nucleus. However, the trend is reversed in the other periods, in contrast to the fluorine results.

The variations in the proton magnetic shielding among compounds within a given group of the periodic table are likewise only in partial agreement with the results for fluorine. The shielding in group 7 hydrides increases with nuclear charge as it does at a slower rate in group 6 hydrides. However, in group 5 the shielding decreases with nuclear charge, and in group 4 the decrease is even more rapid. The fluorine compounds show somewhat similar differences in the dependence upon

[32] H. S. Gutowsky and D. W. McCall, Phys. Rev. **82**, 748 (1951).
[33] Slichter, Gutowsky, and McCall, Phys. Rev. (to be published).
[34] Arnold, Dharmatti, and Packard, J. Chem. Phys. **19**, 507 (1951).
[35] Eyring, Walter, and Kimball, *Quantum Chemistry* (John Wiley and Sons, Inc., New York, 1944), p. 231.

group of the rate of change of shielding with nuclear charge within the group. Thus the F^{19} shielding in group 4 fluorides increases with nuclear charge less rapidly than for group 5. In brief, the differences between H^1 and F^{19} nuclear magnetic shielding appear to be mainly of degree.

The separation of the shielding into diamagnetic and paramagnetic terms is rather artificial, but it is useful in suggesting a basis for the differences between H^1 and F^{19}. The fluorine atom has a $1s^2 2s^2$ core of electrons which is relatively unperturbed by bond formation. The electrostatic potential at the F^{19} nucleus and the diamagnetic shielding term are determined to a large extent[27] by this inner core of electrons. However, in hydrogen compounds, the diamagnetic term is determined primarily by the bonding electrons, and molecular differences will introduce a proportionately larger effect. In other words, the different trends in shielding in hydrogen as compared to fluorine compounds may be caused by greater variability in the diamagnetic term for the proton.

General Comments

Several specific aspects of chemical differences in nuclear magnetic shielding are of possible application. The magnetic shielding of a nucleus appears to be quite sensitive to the electronic distribution in a molecule and affords an experimental means of detecting such differences. As an example, the magnetic shielding of the F^{19} nucleus is measurably different in ortho-, meta-, and para-substituted mono-fluorobenzenes. The differences in shielding appear to be directly and simply related to the charge distributions[36] generally postulated for the ortho-, meta-, and para-positions in the nonfluorine-substituted compound. There is also the possibility of using differences in magnetic shielding in particular cases as a method of analysis, including qualitative, quantitative and structural. Fluorine compounds are sometimes not very amenable to ordinary analytical methods and the large differences in magnetic shielding among different fluorine compounds and the various factors leading to fine structure are suggestive.

While the discussion here has been descriptive in nature, it appears likely that a more or less rigorous quantum-mechanical analysis can be made, at least for some of the simpler compounds. Townes and Dailey[37] have been quite successful in obtaining approximate molecular electronic structures from nuclear electric quadrupole coupling constants, which depend on the *variation* of the electrostatic field at the nucleus. The magnetic shielding of a nucleus in a molecule depends on the electrostatic field itself at the nucleus and also on the electronic distribution in the molecule. The problem is more complex and difficult than that of the quadrupole coupling; however, an analogous treatment may be a means of obtaining additional insight into the electronic structures of molecules.

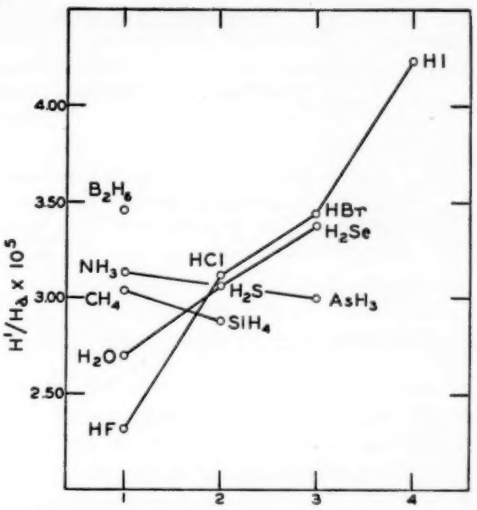

FIG. 8. The dependence of the magnetic shielding of the proton upon the position in the periodic table of the other atomic species in binary covalent compounds.

ACKNOWLEDGMENT

We wish to express our deep appreciation and thanks to Mr. R. E. McClure, our electronics research-assistant, for his very able assistance with the measurements, as well as for the design, construction, and maintenance of many of the electrical circuits. Equipment was provided mainly by a grant-in-aid from the Research Corporation. We are also indebted to Professor A. B. Burg of University of Southern California and Professor W. C. Schumb, of the Massachusetts Institute of Technology, who very kindly supplied the NH_3 and IF_7 samples.

[36] Gutowsky, McCall, McGarvey, and Meyer, J. Chem. Phys. **19**, 1328 (1951).

[37] C. H. Townes and B. P. Dailey, J. Chem. Phys. **17**, 782 (1949).

THE JOURNAL OF CHEMICAL PHYSICS VOLUME 19, NUMBER 10 OCTOBER, 1951

A Mobile Electron Model for Aromatic Molecules

KLAUS RÜDENBERG* AND ROBERT G. PARR
Department of Chemistry, Carnegie Institute of Technology, Pittsburgh, Pennsylvania
(Received June 22, 1951)

A three-dimensional mobile electron model for unsaturation electrons in aromatic molecules is described which allows leakage of electrons across rings and takes aromatic atoms explicitly into account. The model contains the free electron model as a limiting case. Applications to the spectra of cata-condensed hydrocarbons are discussed.

ONE-DIMENSIONAL FREE ELECTRON MODEL

IN the one-dimensional free electron for the unsaturation (π) electrons in an aromatic molecule such as benzene, the electrons, each of mass m, are assumed to move freely and independently on the circumference of a circle of radius R.[1,2] The energy eigenvalues for one of these electrons are given by the formula[1]

$$E_l=(h^2/8\pi^2mR^2)l^2,\ l=0,\pm1,\pm2,\cdots, \quad (1)$$
(free electron model)

where h is Planck's constant. This yields for the wave number of the $l\rightarrow l+1$ transition,

$$\omega_{l\rightarrow l+1}=(h/8\pi^2\,\mathrm{mc}R^2)(2l+1)$$
$$=30{,}736(2l+1)/R^2[\omega \text{ in cm}^{-1},\ R \text{ in } A], \quad (2)$$

where c is the velocity of light. For a molecule with $n=2+4N$ unsaturation electrons, since two electrons can go into each level, in the ground state the levels, $l=0,\ \pm1,\ \cdots,\ \pm N$, are filled; the lowest electronic excitation has $|l|$ changing from N to $N+1$.

In Table I are given, together with experimental values, first excitation frequencies of benzene and some higher cata-condensed hydrocarbons, computed employing two alternative assumptions regarding the radius R of the free electron circle:

(I) Area assumption: $\pi R^2=N(27/4)^{\frac{1}{2}}R_0^2$, N=number of rings, R_0=carbon-carbon distance in benzene=1.39A.

(II) Perimeter assumption: $2\pi R=nR_0$, n=number of electrons.[3]

Assumption I gives better agreement with experiment and seems physically more palatable;[4] accordingly we adopt it below as the reference point for calculations with a modified model.

THREE-DIMENSIONAL MOBILE ELECTRON MODEL

Let us now suppose that each of the unsaturation electrons in one of these molecules moves in three dimensions under the influence of a potential of the form,[5,6]

$$V(r,\phi,z)=V_r(r)+(1/r^2)V_\phi(\phi)+V_z(z), \quad (3)$$

where r, ϕ, and z are cylindrical coordinates with origin at the center of the molecule: z the coordinate perpendicular to the molecular plane $z=0$, ϕ the angular displacement in the molecular plane, and r the distance from the z axis. With k, α and V_0 as parameters to be determined, we take[7]

$$V_z(z)=(\tfrac{1}{2})kz^2, \quad (4)$$

$$V_r(r)=(h^2/8\pi^2m)(1/4R^2\alpha^2)[(R/r)^2+(r/R)^2-2], \quad (5)$$

and

$$V_\phi(\phi)=(h^2/8\pi^2m)2(R/R_0)^2(2\pi/n)V_0 \times\sum_{m=0}^{n-1}\delta(\phi-2\pi m/n), \quad (6)$$

where $\delta(\phi-\phi_0)$ is a Dirac delta function which is zero everywhere except at $\phi=\phi_0$, where it is infinite in such a way that

$$\int_0^{2\pi}\delta(\phi-\phi_0)d\phi=1. \quad (7)$$

V_z couples the electron to the molecular plane, V_r holds the electron near the radius R, and V_ϕ causes the ring nuclei to attract or repel the electron according as $V_0<0$ or $V_0>0$.

With V given by Eqs. (3)–(6), the Schroedinger equation for an unsaturation electron, namely,

$$\nabla^2\psi+(8\pi^2m/h^2)(E-V)\psi=0, \quad (8)$$

* Research Corporation Postdoctoral Fellow, Carnegie Institute of Technology, 1950; present address: Department of Physics, University of Chicago, Chicago, Illinois.

[1] W. T. Simpson, J. Chem. Phys. **16**, 1124 (1948).

[2] J. R. Platt, J. Chem. Phys. **17**, 484 (1949).

[3] This is the assumption made by Platt (reference 2).

[4] The actual "orbit" of a π electron in benzene is probably closer to a circle than to a hexagon. And the actual "orbits" in naphthalene and the higher cata-condensed hydrocarbons are probably fairly close to the area assumption circles—shorter than the zig-zag perimeters. For, an electron as it "travels" around one of these molecules would be expected to take frequent short cuts. R should not be considered fixed by geometry, however; the free electron formulation should not be said to contain no arbitrary constants.

[5] One might object to the multiplicative factor $(1/r^2)$ for the angular potential. The relative effect of this angular potential is still greatest for $r=R$, however, and the factor permits the separation of variables in the subsequent differential equation, Eq. (8).

[6] Interference of radial and angular motions distinguishes the case of the aromatic rings from that of the long chain polyenes, where justification of a one-dimensional approach is straightforward.

[7] It will be noted that $V_r(R)=0$ and $V_r(0)=\infty$. This last does not prevent the electron waves from propagating through the interior of the ring; indeed, the choice of Eq. (5) causes this "leakage phenomenon" to manifest itself in a particularly clear way.

TABLE I. Lowest excitation frequencies of cata-condensed hydrocarbons, cm^{-1}.

	Benzene	Naphthalene	3-Ring systems	4-Ring systems	5-Ring systems
Experimental[a, b]	43,400	39,400	34,750	32,300	29,600
Free electron model					
Perimeter assumption[c]	52,300	31,400	22,400	17,300	14,300
Area assumption[d]	57,700	48,100	44,900	43,300	42,300
Mobile electron model-Area assumption					
Radial potential only: $\alpha=0.0925$	55,400	43,500	37,550	33,250	29,600
Angular potential only: $V_0=-2.51$	43,400	41,900	41,600	41,250	40,950
Radial and angular potentials: $\alpha=0.13$, $V_0=-1.48$	53,950	45,250	39,050	33,350	28,750

[a] Values listed are weighted means of the several bands to which the first electronic excitation gives rise, as assigned by J. R. Platt and H. B. Klevens, J. Chem. Phys. 17, 470 (1949), or estimated by methods suggested by Platt (private communication).
[b] For the 3-, 4- and 5-ring systems, an average over-all possible non-substituted cata-condensed hydrocarbons of each type is given.
[c] Perimeter assumption: n = number of unsaturation electrons, R = radius of free electron circle, R_0 = carbon-carbon distance in benzene; $2\pi R=nR_0$.
[d] Area assumption: N = number of rings; $\pi R^2=N(27/4)^{\frac{1}{2}}R_0^2$.

may be solved by standard methods.[8] The allowed energies of an electron are found to be given by the formula,

$$E=E_z+E_r+E_\phi, \tag{9}$$

where [9]

$$E_z=[n_z+(\tfrac{1}{2})]h\nu_z,\ n_z=1, 3, 5, \cdots, \quad \nu_z=(1/2\pi)(k/m)^{\frac{1}{2}}, \tag{10}$$

$$E_r=[n_r+1]h\nu_r,\ n_r=0, 2, 4, \cdots, \quad \nu_r=(h/8\pi^2mR^2\alpha), \tag{11}$$

and

$$E_\phi=(h^2/8\pi^2mR^2)\lambda_l^2 f(\alpha^2\lambda_l^2),\ l=0, \pm1, \pm2, \cdots, \tag{12}$$

where [10]

$$1+2xf(x)=(1+4x)^{\frac{1}{2}}, \tag{13}$$

and λ_l is determined as a function of l from the equation,

$$\cos(2\pi l/n)=\cos(2\pi\lambda_l/n)+P[\sin(2\pi\lambda_l/n)/(2\pi\lambda_l/n)], \tag{14}$$

where

$$P=(2\pi R/nR_0)^2V_0. \tag{15}$$

The result embodied in Eqs. (9) to (15) may be given the following physical interpretation. The electron performs three kinds of motion: (1) oscillation perpendicular to the plane of the ring giving rise to the energy levels E_z, (2) oscillation across the ring giving rise to the energy levels E_r,[11] and (3) rotation about the z axis giving rise to the energy levels E_ϕ, motions (2) and (3) being interdependent.

Whereas the free electron formula, Eq. (1), contains only one parameter—the radius R, our final result, Eq. (9), has in it three additional parameters—the out-of-plane force constant k which enters E_z according to Eq. (10), the leakage parameter α which enters E_r and E_ϕ according to Eqs. (11) and (12), and the "Kronig-Penney"[8] parameter V_0 which enters E_ϕ through λ_l according to Eqs. (12), (14) and (15). We may immediately forget about k, since the selection rule even↔odd forbids all transitions between the (odd) levels of the out-of-plane motions.[9,12] We then have α and V_0 left to determine.

RESULTS

For $V_0=\alpha=0$, the potential of Eq. (3) becomes infinitely high everywhere in the plane $z=0$ except for an infinitely narrow gap down to $V=0$ for $r=R$, and Eq. (9) reduces in effect to the free electron formula, Eq. (1); Eq. (12) becomes identical with Eq. (1) and Eq. (11) yields radial excitation energies which are infinitely great.

For $V_0=0$, $\alpha\neq0$, we have, from Eq. (14)

$$\lambda_l=l \text{ (radial potential only)}, \tag{16}$$

and Eq. (12) reduces to

$$E_\phi=(h^2/8\pi^2mR^2)l^2f(\alpha^2l^2),\ l=0, \pm1, \pm2, \cdots \text{ (radial potential only)} \tag{17}$$

This is the free electron result, Eq. (1), except for the factor $f(\alpha^2l^2)$. This factor is tabulated in Table II and,

[8] One assumes $\psi(r,\phi,z)=F(r)\Phi(\phi)Z(z)$ and then obtains differential equations for F, Φ and Z. The equation for Z is that of a harmonic oscillator. The equation for F is essentially equivalent to one which is obtained when the three-dimensional isotropic harmonic oscillator is treated in cylindrical coordinates, the solution of which is outlined in Pauling and Wilson, *Introduction to Quantum Mechanics* (McGraw-Hill Book Company, New York, 1935), pp. 107–110. The equation for Φ is essentially equivalent to one met in the one-dimensional Kronig-Penney model of a metal: R. L. Kronig and W. G. Penney, Proc. Roy. Soc. (London) 130, 499 (1931); D. S. Saxon and R. A. Hutner, Philips Research Reports 4, 81 (1949).—See also reference 10.

[9] The quantum number n_z only assumes odd values because the π-electron wave functions must have nodes in the plane of the ring.

[10] The solution given by the Eqs. (11)–(13) is only valid if $1+4x\geq0$, i.e., in the case $\lambda^2\geq-(2\alpha)^{-2}$. This amounts to excluding too large negative values for the constant V_0 in (6) which determines λ^2 through Eqs. (14) and (15). The method of solution outlined in footnote 8 depends on the fact that $\mu=[\lambda^2+(2\alpha)^{-2}]^{\frac{1}{2}}$ is real. This quantity plays the same mathematical role as the (real) angular momentum m of the isotropic harmonic oscillator of footnote 8. In the case $\lambda^2<-(2\alpha)^{-2}$ our μ is imaginary and the polynomial method employed in footnote 8 no longer leads to Eqs. (11), (12), and (13).

[11] Since we have found the exact solution of our problem, the oscillatory levels of Eq. (11) cannot correspond to harmonic vibrations around the equilibrium distance R. Such vibrations result from parabolic approximation of the potential in the neighborhood of R, which yields a frequency twice that of Eq. (11). The latter corresponds to oscillation with the parabolic potential that is obtained by dropping the repulsive portion, $(R/r)^2-2$, from Eq. (5); that is, it corresponds to oscillation "across the ring."

[12] We assume $n_z=1$, giving the mobile electron wave functions a single nodal plane perpendicular to the z axis, in agreement with the nodal properties of $2p\pi$ atomic orbitals.

TABLE II. The correction factor for leakage, $f(x)$.[a]

x	$f(x)$	x	$f(x)$	x	$f(x)$
0.00	1.000	0.00	1.000	0.20	0.854
0.01	0.990	−0.01	1.010	0.25	0.828
0.02	0.981	−0.02	1.021	0.30	0.805
0.03	0.972	−0.03	1.032	0.35	0.785
0.04	0.963	−0.04	1.044	0.40	0.766
0.05	0.954	−0.05	1.056	0.45	0.748
0.06	0.946	−0.06	1.069	0.50	0.732
0.07	0.938	−0.07	1.082	0.55	0.717
0.08	0.931	−0.08	1.096	0.60	0.703
0.09	0.923	−0.09	1.111	0.65	0.690
0.10	0.916	−0.10	1.127	0.70	0.678
0.11	0.909	−0.11	1.144	0.75	0.667
0.12	0.902	−0.12	1.162	0.80	0.656
0.13	0.896	−0.13	1.181	0.85	0.646
0.14	0.889	−0.14	1.202	0.90	0.636
0.15	0.883	−0.15	1.225	0.95	0.627
0.16	0.877	−0.16	1.250	1.00	0.618
0.17	0.871	−0.17	1.277	1.05	0.610
0.18	0.865	−0.18	1.308	1.10	0.602
0.19	0.860	−0.19	1.342	1.15	0.594
0.20	0.854	−0.20	1.382	1.20	0.587

[a] See Eq. (12); $f(x)$, with $x=\alpha^2\lambda_l^2$, is merely the factor by which one must multiply a free electron level in order to obtain a level modified for the effect of leakage.

with $\alpha=0.0925$, leads to the excitation frequencies given in Table I in the row labeled "radial potential only."[13]

For $\alpha=0$, $V_0\neq 0$, Eq. (12) reduces to,

$$E_\phi=(h^2/8\pi^2mR^2)\lambda_l^2,\ l=0,\pm1,\pm2,\cdots, \quad (10)$$
(angular potential only)

where λ_l is to be determined from Eq. (14). This differs from the free electron result, Eq. (1), in the appearance of λ_l^2 in place of l^2. λ_l is tabulated in Table III for $n=6$, 10, 14, and 18, $l=N$ and $l=N+1$, and a range of values of P.[14] Computed excitation frequencies for the cata-condensed hydrocarbons for $V_0=-2.51$ are given in Table I in the row labeled "angular potential only."

Finally, for $\alpha\neq 0$, $V_0\neq 0$, with $\alpha=0.13$, $V_0=-1.48$, we find the excitation frequencies given in Table I in the row labeled "radial and angular potentials." To obtain these results, one assumes values of V_0 and α, determines the appropriate λ_l by solution of Eq. (14),

[13] We assume α small enough that the radial energies E_r are spaced much further apart than the angular energies E_ϕ. For purposes of computing the first excitation, E_ϕ may then be treated as if it were the total energy.

[14] As P varies from $+\infty$ to 0 to $-\infty$, the energy spectrum of Eq. (18) varies from the spectrum of an electron confined within one of n equivalent one-dimensional boxes of width $w=2\pi R/n$ to the spectrum of an electron free to move on a circle of perimeter $p=2\pi R$ to the spectrum of an electron moving under the influence of n equivalent holes spaced evenly on a circle of radius R. In the first case, $E_\phi=(h^2/8mw^2)q^2$, $q=1, 2, 3, \cdots$, each level n-fold degenerate; in the second case, $E_\phi=(h^2/2mp^2)l2$, $l=0,\pm1,\pm2,\cdots$, each level non-degenerate: in the third case, $E_\phi=(h^2/8mw^2)s^2$, $s=i\infty, 1, 2, 3, \cdots$, each level n-fold degenerate.

TABLE III. The correction factor for nuclear attractions, λ_l.[a]

	$n=6$[b]		$n=10$		$n=14$		$n=18$	
P	$l=1$	$l=2$	$l=2$	$l=3$	$l=3$	$l=4$	$l=4$	$l=5$
4.0	2.25	2.69	3.87	4.33	5.51	5.96	7.14	
2.0	1.91	2.51	3.35	3.96	4.80	5.42	6.26	6.87
1.0	1.59	2.33	2.87	3.61	4.16	4.90	5.44	6.20
0.0	1.00	2.00	2.00	3.00	3.00	4.00	4.00	5.00
−0.5	0.00	1.72	1.10	2.48	1.88	3.23	2.64	3.98
−1.0	1.10i	1.28	1.47i	1.61	1.76	1.89	2.03i	2.13
−1.5	1.63i	0.00	2.50i	1.34i	3.34i	2.22i	4.18i	3.06i
−2.0	2.09i	1.42i	3.34i	2.67i	4.57i	3.91i	5.79i	5.13i
−4.0	3.88i	3.74i	6.43i	6.29i	8.98i	8.82i	11.52i	

[a] See Eq. (12); λ_l is merely what one replaces l in a free electron formula by to obtain a formula modified for the effect of nuclear attractions.
[b] n is the number of attracting (or repelling) centers assumed equally spaced on the free electron circle. In the case of the cata-condensed hydrocarbons, this is equal to the number of unsaturation electrons.

computes the corresponding $f(\alpha^2\lambda_l^2)$ from Eq. (13), and then computes the appropriate E_ϕ from Eq. (12).[13]

DISCUSSION

As may be seen from Table I, the mobile electron model gives an improved fit of the experimental data on the cata-condensed hydrocarbons, but the improvement has been achieved only through the introduction of additional parameters.[15] The fact that improvement can be obtained by physically reasonable modifications of the free electron model is encouraging, however, and lends further confidence to that model as a semi-quantitative tool.

More important, our model may perhaps be adapted to describe the effect of aromatic substitution or correct the free electron circle approximation to higher cata-condensed hydrocarbons for the effect of the cross links. To do the former, one could introduce delta functions of different strengths at different nuclei;[16] to do the latter, one could introduce just two delta functions, opposite on the circle, providing in the three-dimensional formulation a channel across the ring through which electrons may flow.

ACKNOWLEDGMENT

We are very grateful to the Research Corporation for a grant which made this work possible. We also wish to thank Professor J. R. Platt for helpful discussions.

[15] Judicious choice of the radius R of the free electron circle would give a very good fit of the data with the introduction of no new parameters (see reference 4).

[16] As the simplest case, one could assign zero strength to the delta functions at the non-substituted carbons, non-zero strength to the delta function at a substituted carbon. For monosubstitution one then has the problem of one delta function only. This has been considered by Professor J. R. Platt (private communication), who indeed finds directing influence of the substituent neatly coming out of the theory.

LCAO Molecular Orbital Computation of Resonance Energies of Benzene and Butadiene, with General Analysis of Theoretical *Versus* Thermochemical Resonance Energies

ROBERT S. MULLIKEN, *Department of Physics, University of Chicago, Chicago, Illinois**

AND

ROBERT G. PARR, *Department of Chemistry, Carnegie Institute of Technology, Pittsburgh, Pennsylvania*

(Received June 22, 1951)

The decrease in π_z-electron energy for the change from a Kekulé to a proper benzene structure is computed purely theoretically by the method of antisymmetrized products of MO's (molecular orbitals), in LCAO approximation, using Slater $2p\pi_z$ AO's (atomic orbitals) of effective charge 3.18, and assuming a carbon-carbon distance of 1.39A. The result (73.1 kcal/mole) is a theoretical value for the gross (vertical) resonance energy of benzene taken for constant C—C distances of 1.39A. In order to make a comparison with the net or ordinary empirical resonance energy, several corrections to the latter are required. The principal one is for the "compression energy" required to compress the single and stretch the double bonds of the Kekulé structure from normal single and double-bond distances to 1.39A. The others (not hitherto clearly recognized) involve hyperconjugation and related effects. The corrections are discussed and their magnitudes estimated, but a reliable value can be obtained only for the compression energy. Allowing for this alone, the computed net resonance energy is 36.5 kcal. This agrees, within the uncertainties due to the omitted correction terms, with the value (41.8 kcal) of the "observed" resonance energy Δ based on thermochemical data.

Here Δ is the departure of the actual heat of formation ΔH_f^0 of benzene from the value given by a standard formula for nonresonating hydrocarbons. A new standard formula containing corrections for the mutual effects of neighboring carbon-carbon bonds is given; this is of interest also for itself, and its significance is briefly discussed.

The analysis given in the paper serves to clarify hitherto existing obscurities in what is meant by "resonance energy." An analysis of the nature and significance of "nonresonating" structures (like for example Kekulé benzene) is also included, using He_2, 1,3 butadiene, and benzene as examples. Repulsion terms in the LCAO MO theory occur for nonresonating structures, which appear to be the counterpart of exchange repulsions of the valence-bond theory. When resonance occurs, it more or less overcomes these repulsions.

The gross resonance energies of cis- and trans-1,3-butadiene are computed by the same method. For trans-butadiene, the computed value corrected for compression is 3.7 kcal/mole, while the "observed" thermochemical value Δ is 6.5.

1. INTRODUCTION

RECENT successful calculations of electronic excitation energies and vibrational force constants for the unsaturated organic molecules ethylene,[1–3] acetylene,[3,4] 1,3-butadiene,[5] allene,[6] and benzene[7–10] by the method of antisymmetrized products of MO's in LCAO approximation[11] have led us to hope that this method might be of value for computation of resonance energies. We have accordingly employed it to compute the resonance energies of benzene and 1,3-butadiene.

The concept of resonance energy has been used in both the LCAO MO and in the VB (valence-bond) methods. In the VB method, the resonance energy W_R of benzene is conceived as the difference between the energy W_K of a single Kekulé VB wave function ψ_K and the actual ground-state energy W_N,

$$W_R = W_K - W_N. \tag{1}$$

In the LCAO MO method, following Hückel, conjugation or resonance energy in olefinic or aromatic molecules may be conceived as the difference W_R between the energy W_K of a wave function in which the π_z electrons are assigned to two-center or "localized" LCAO MO's (like those in ethylene) and the energy W_N of one in which they are assigned to the best n-center LCAO MO's obtained by solving a secular equation (n=number of atoms carrying π_z electrons).[12,13] The computation of W_N for benzene is discussed in Sec. 2,

* This work was assisted in part by the ONR under Task Order IX of Contract N6ori-20 with the University of Chicago.

[1] R. S. Mulliken and C. C. J. Roothaan, Chem. Revs. **41**, 219 (1947).

[2] R. G. Parr and B. L. Crawford, Jr., J. Chem. Phys. **16**, 526 (1948).

[3] R. S. Mulliken, J. chim. phys. **46**, 497 (1949).

[4] G. R. Taylor, D.Sc. thesis, Carnegie Institute of Technology, 1951.

[5] R. G. Parr and R. S. Mulliken, J. Chem. Phys. **18**, 1338 (1950).

[6] R. G. Parr and G. R. Taylor, J. Chem. Phys. **19**, 497 (1951).

[7] B. L. Crawford, Jr., and R. G. Parr, J. Chem. Phys. **17**, 726 (1949).

[8] C. C. J. Roothaan and R. G. Parr, J. Chem. Phys. **17**, 1001 (1949).

[9] C. C. J. Roothaan, Revs. Modern Phys. **23**, 69 (1951).

[10] Parr, Craig, and Ross, J. Chem. Phys. **18**, 1561 (1950).

[11] M. Goeppert-Mayer and A. L. Sklar, J. Chem. Phys. **6**, 645 (1938).

[12] E. Hückel, Z. Physik **70**, 204 (1931), **76**, 628 (see table on p. 636). F. Hund, Z. Physik **73**, 1565 (1932)—introducing localized MO's for polyatomic molecules. J. E. Lennard-Jones and C. A. Coulson, Trans. Faraday Soc. **35**, 811 (1939) and references given there.

[13] Concerning π_z and π_y electrons, conjugation, and hyperconjugation, see Mulliken, Rieke, and Brown, J. Am. Chem. Soc. **63**, 41 (1941).

TABLE I. The vertical (or gross) resonance energy of benzene.[a]

Energy term	Ground state N	Kekulé structure K	Contribution to vertical resonance energy
I_0 or I_O	−40.26[b]	−40.26[b]	3.56
$I_1=I_{-1}$ or $I_I=I_{-I}$	−37.32[b]	−36.43[b]	
J_{00} or J_{OO}	8.63	8.63	+0.18
$J_{01}=J_{0-1}$ or $J_{OI}=J_{O-I}$	8.52	8.52	
$J_{11}=J_{-1-1}=J_{1-1}$ or $J_{II}=J_{-I-I}=J_{I-I}$	8.47	8.51	
$K_{01}=K_{0-1}$ or $K_{OI}=K_{O-I}$	2.58	2.37	−0.57
K_{1-1} or K_{I-I}	1.45	2.16	
$W_{N\pi}$[1.39] or $W_{K\pi}$[1.39]	−115.40[b]	−112.23[b]	3.17 (73.1 kcal/mole)

[a] Numerical values are taken or derived from reference 10. All are in ev.
[b] The energy zero for each π electron is taken as the energy of an electron in a $2p\pi$ orbital of a carbon atom in the tr$^3\pi$ tetravalent valence state (reference 3) (tr = trigonal hybrid orbital).

that of W_K and W_R in Sec. 3 and Sec. 4, in each case using antisymmetrized LCAO MO wave functions.

If a computed resonance energy is to be compared with a thermochemically determined one, considerable care must be exercised in defining the reference state K to be used in the computation. This phase of the benzene question is discussed in some detail in Sec. 3. Further, several corrections to the thermochemical resonance energy (Sec. 5) must be made (Sec. 6), particularly one for "compression energy" (Sec. 4).

The compression energy correction was evaluated some time ago, and used to obtain an empirical resonance energy corrected for compression.[13,14,15] A discussion along somewhat similar lines has recently been given by Hornig.[16] Van Dranen and Ketelaar[17] have recently proposed a method for theoretical calculation of the resonance energy of benzene (and other molecules) which is closely connected with ours. Their method is based on an inconsistent set of equations, however, and so cannot be regarded as purely theoretical.[18]

The results obtained for butadiene in the present work are given in Sec. 7.

2. THE NORMAL STATE OF BENZENE

The ground state of benzene in terms of the LCAO MO method has been discussed in detail elsewhere.[8–11,19] One assumes that W_N may to a reasonably good approximation be written as a sum of a core energy, $W_{N,\text{core}}$ and a π_z-electron energy, $W_{N\pi}$,

$$W_N=W_{N,\text{core}}+W_{N\pi}; \tag{2}$$

and that the wave function $\psi_{N\pi}$ for the six π_z electrons may be treated separately and written in normalized form as follows,

$$\psi_N\equiv\mathfrak{A}\phi_0^{(1)}\alpha^{(1)}\phi_0^{(2)}\beta^{(2)}\phi_1^{(3)} \times\alpha^{(3)}\phi_1^{(4)}\beta^{(4)}\phi_{-1}^{(5)}\alpha^{(5)}\phi_{-1}^{(6)}\beta^{(6)}. \tag{3}$$

Here the "antisymmetrizer" $\mathfrak{A}$ denotes $(6!)^{-\frac{1}{2}}\times\sum_P(-1)^{\sigma_P}P$, α and β are one-electron spin functions, and ϕ_0, ϕ_1, ϕ_{-1} are the π_z-electron MO's, formed as orthonormal linear combinations of $2p\pi_z$ AO's χ_1, $\chi_2\cdots\chi_6$ on the six carbon atoms:

$$\phi_j=\sum_p C_{jp}\chi_p.$$

For $W_{N\pi}$ one then finds

$$\left.\begin{aligned}W_{N\pi}=2I_0+2I_1+2I_{-1}+(4J_{01}-2K_{01})\\+(4J_{0-1}-2K_{0-1})+(4J_{1-1}-2K_{1-1})\\+J_{00}+J_{11}+J_{-1-1},\end{aligned}\right\} \tag{4}$$

where I_i is the energy of an electron in the MO ϕ_i in the field of the core, J_{ij} is the coulomb integral between the MO's ϕ_i and ϕ_j, and K_{ij} is the exchange integral between these MO's.

The coefficients C_{jp} are found by minimizing the energy $W_{N\pi}$ with respect to them, subject to orthonormalization of the ϕ_j.[20] The results for the ϕ_j are up to normalizing factors,

$$\phi_j\sim\sum_{p=1}^{6}\omega^{jp}\chi_p, \tag{5}$$

where $\omega=\exp(2\pi i/6)$.

Formulas and values for the various quantities which enter Eq. (4) when the ϕ_j are given by Eq. (5) have been given elsewhere[10]—the values are listed in Table I. These are for the normal 1.39A C−C distances and are based upon Slater $2p\pi$ AO's with effective charge $Z=3.18$.

[14] Reference 13, Sec. 13, especially footnote 28, and Table VI.

[15] The revised (unpublished) computations of Mulliken and Rieke (Abstract in Revs. Modern Phys. **14**, 259 (1942)) were based on force constant values $k_{C-C}=4.50\times10^5$ and $k_{C=C}=9.87\times10^5$ dynes/cm from analyses of the vibrational spectra of C_2H_6 and C_2H_4, values which were recommended by Professor B. L. Crawford, Jr., in 1942. However, since these k values were based on empirical frequencies uncorrected for the effect (due to zero-point vibration) of anharmonicity, Mulliken and Rieke first increased them by 5 percent to allow very roughly for this effect. They then set up Morse curve equations for C−C and for C=C, using these augmented k values and valence state dissociation energies D.

Valence state D's were used because it is to be expected that for not too large vibrations, the bonds should tend to dissociate into carbon atoms in their (tetravalent) valence states. The valence state D values later published in reference 3 (see reference 3, footnotes** to Tables V and VI) were used; two sets of values were tried, corresponding to the two conflicting current values of the heat of sublimation of graphite. Fortunately, the final value of C_K is so insensitive to the assumed D values, and to moderate variations (within the range of credibility) of the values of k used, that the probable uncertainty in C_K due to these causes is estimated as only about ±1 kcal. A more serious difficulty is discussed in Sec. 6.

[16] D. F. Hornig, J. Am. Chem. Soc. **72**, 5772 (1950).

[17] J. Van Dranen and J. A. A. Ketelaar, J. Chem. Phys. **17**, 1338 (1949); **18**, 151 (1950).

[18] R. G. Parr, J. Chem. Phys. **19**, 799 (1951). Eq. (5) of this reference should read $F=H_{\text{core}}+G$.

[19] R. S. Mulliken, J. chim. phys. **46**, 675 (1949).

[20] Actually computation is not necessary here, symmetry arguments giving the same result more simply. In the general case computation is necessary, however.

3. THE LCAO MO KEKULÉ STRUCTURE OF BENZENE

For benzene, the localized LCAO MO's (see Sec. 1) for a Kekulé structure can be chosen as follows,

$$\tau_1=N(\chi_1+\chi_2);\quad \tau_2=N(\chi_3+\chi_4);\quad \tau_3=N(\chi_5+\chi_6), \quad (6)$$

N being a normalizing factor. The Kekulé wave function $\psi_{K\pi}$ can be constructed by replacing the ϕ_j in Eq. (3) by the τ_j, and then placing an extra normalizing factor in front of the $\mathfrak{A}$ (this is needed because the τ_j, unlike the ϕ_j, are not mutually orthogonal). Instead of Eq. (6), one could equally well use $\tau_1'=N(\chi_2+\chi_3)$ and so on, corresponding to the other Kekulé structure.

In the earlier LCAO MO calculations of resonance or conjugation energy,[12,13] this was taken as the difference between sums $\sum\epsilon_j$ of one-electron energies for the π_z electrons assigned on the one hand to localized (2-center) LCAO's, on the other to the best n-center LCAO's. In this procedure, interelectronic interactions were not considered explicitly; instead, an average field governing the MO's was assumed.[12] The relation between the $\sum\epsilon_j$ method and the theoretically more obviously safe antisymmetrized-product method used here has been discussed,[19] but not adequately clarified; a recent note by one of the present authors contains some further analysis of this problem.[18]

In the antisymmetrized-product method, the total energy of the π_z electrons in the field of the core (nuclei plus non-π_z electrons) is computed from the relation $W_\pi=\int\psi_\pi^*H\psi_\pi dv$, where H is the hamiltonian in the form $V_{\text{core}}+H_\pi$, where V_{core} is an effective potential corresponding to the field of the core. This can be done first using $\psi_{N\pi}$ of Eq. (3), then using a similar expression for ψ_K described above, the difference being the π_z resonance energy. However, a relatively convenient expression for W_π in terms of I's, J's, and K's as in Eq. (4) is obtained only if the π_z LCAO MO's used form an orthonormal set. This is true of the ϕ_j's of $\psi_{N\pi}$ as given by Eq. (5), but not of the localized MO's τ_j of Eq. (6) used above for $\psi_{K\pi}$. The difficulty is overcome if the τ_j's are replaced by an equivalent orthonormal set of delocalized (n-center) LCAO's—which, however, it should be expressly noted, is not at all equivalent to the orthonormal set ϕ_j of best n-center LCAO's. Since the transformation from a localized to an equivalent delocalized set of MO's has implications of general interest for an understanding of the significance of "nonresonating" structures, it will be instructive at this point to consider two other examples before carrying out the transformation for benzene.[21]

The wave function for the ground state of two helium atoms close together, conceived of as an He_2 molecule, can be written in either of the following equivalent forms:

$$\psi_N=\mathfrak{N}\mathfrak{A}1s_a^{(1)}\alpha^{(1)}1s_a^{(2)}\beta^{(2)}1s_b^{(3)}\alpha^{(3)}1s_b^{(4)}\beta^{(4)}; \quad (7a)$$

$$\psi_N=\mathfrak{A}\phi_B^{(1)}\alpha^{(1)}\phi_B^{(2)}\beta^{(2)}\phi_A^{(3)}\alpha^{(3)}\phi_A^{(4)}\beta^{(4)}. \quad (7b)$$

The symbols $1s_a$ and $1s_b$ denote $1s$ AO's on the two atoms a and b, while ϕ_B and ϕ_A denote (respectively bonding and antibonding) LCAO MO's of the forms,

$$\left.\begin{aligned}\phi_B&=[2(1+S)]^{-\frac{1}{2}}(1s_a+1s_b),\\ \phi_A&=[2(1-S)]^{-\frac{1}{2}}(1s_a-1s_b),\end{aligned}\right\} \quad (8)$$

S being the non-orthogonality or overlap integral $\int 1s_a1s_b dv$. Because $1s_a$ and $1s_b$ are not mutually orthogonal, in contrast to ϕ_B and ϕ_A which are orthogonal, the extra normalizing factor $\mathfrak{N}$ is required in Eq. (7a). The complete identity of the functions described by Eqs. (7a) and (7b), if $\mathfrak{N}$ is taken as $1/(1-S^2)$, may be verified by putting both into determinant form.

Evaluation of the energy $\int\psi H\psi dv$ using Eq. (7a) leads to the familiar exchange repulsion of VB theory (plus multiple-exchange terms which are usually neglected in VB discussions) which always occurs between nonbonded electrons on two atoms. As will now be shown, a corresponding repulsion is obtained in the LCAO MO method using Eq. (7b), even in the simplified procedure[12] which uses the resonance terms contained in $\sum\epsilon_j$ as an approximation to the change in the total energy.[22] In the present example, $\sum\epsilon_j$ becomes $2\epsilon_B+2\epsilon_A$, with[23]

$$\left.\begin{aligned}\epsilon_B=\alpha+\beta/(1+S),\quad \epsilon_A=\alpha-\beta/(1-S),\\ \textstyle\sum\epsilon_j=4\alpha-4\beta S/(1-S^2)\end{aligned}\right\}. \quad (9)$$

Since $\beta<0$, the sum $-4\beta S/(1-S^2)$ of the resonance terms makes the total interaction energy positive, corresponding to a repulsion, if we assume (as seems justified by experience[23]) that the α's plus other necessary terms correspond approximately to the energy of the separate atoms.

Taking 1,3 butadiene $H_2C{=}CH{-}CH{=}CH_2$ as a second example, a $\psi_{K\pi}$ using localized bonding MO's

$$\tau_1=N(\chi_1+\chi_2),\quad \tau_2=N(\chi_3+\chi_4);\qquad N=[2(1+S_{12})]^{-\frac{1}{2}}, \quad (10)$$

can be constructed as follows,

$$\psi_{K\pi}=\mathfrak{N}\mathfrak{A}\tau_1^{(1)}\alpha^{(1)}\tau_1^{(2)}\beta^{(2)}\tau_2^{(3)}\alpha^{(3)}\tau_2^{(4)}\beta^{(4)}. \quad (11a)$$

Equation (11a) is formally analogous to Eq. (7a) for He_2, with the MO's τ_1 and τ_2 playing the same roles as the AO's $1s_a$ and $1s_b$ there. Equation (11a) is related to the following Eq. (11b) in exactly the same way as (7a) is to (7b):

$$\psi_{K\pi}=\mathfrak{A}\phi_{K1}^{(1)}\alpha^{(1)}\phi_{K1}^{(2)}\beta^{(2)}\phi_{K2}^{(3)}\alpha^{(3)}\phi_{K2}^{(4)}\beta^{(4)}, \quad (11b)$$

[21] See also C. A. Coulson, J. chim. phys. **46**, 5 (1949) for some instructive remarks on delocalization of localized MO's.

[22] This line of thought has been developed somewhat further in a recent paper: R. S. Mulliken, J. Am. Chem. Soc. **72**, 4493 (1950); and in J. Chem. Phys. **19**, 900 (1951).

[23] See reference 3, Secs. 7–8.

where the 4-center delocalized MO's ϕ_{Kj}, unlike τ_1 and τ_2, are mutually orthogonal; in normalized form, they are as follows (see Eq. (8)),

$$\phi_{K1}=[2(1+S_{23})]^{-\frac{1}{2}}(\tau_1+\tau_2),$$
$$\phi_{K2}=[2(1-S_{23})]^{-\frac{1}{2}}(\tau_1-\tau_2). \tag{12}$$

The energy of $\psi_{K\pi}$ must of course be identically the same whether computed from Eq. (11a) or Eq. (11b). However, comparing the discussion of Eqs. (7a) and (7b), Eq. (11a) will show an exchange repulsion between the electron-pairs in τ_1 and τ_2, while Eq. (11b) with the $\sum\epsilon_j$ method will show a corresponding repulsion expressed in the form $-4\beta_{23}S_{23}/(1-S_{23}^2)$. But if the ϕ_{Kj} in Eq (11b) are replaced by the best 4-center LCAO's, which are of the form:

$$\phi_{1,2}=(a_j\chi_1+b_j\chi_2)\pm(b_j\chi_3+a_j\chi_4), \tag{13}$$

with $b_1>a_1$ and the plus sign for ϕ_1, but $b_2<a_2$ and the minus sign[5] for ϕ_2, an attraction is superimposed on the repulsion just discussed. Nearly (see Sec. 6) the whole of this attraction corresponds to conjugation energy. The reason for it is easily understood ($b_1>a_1$ increases bonding in ϕ_1 and decreases antibonding in ϕ_2, as compared with Eq. (12) which is a special case of (13) with $a_j=b_j$), and it is easily computed by the $\sum\epsilon_j$ method.[13] The antisymmetrized MO-product method gives the conjugation energy in the form $W_{K\pi}-W_{N\pi}$, from $\psi_{K\pi}$ as in Eq. (11b), and $\psi_{N\pi}$ as in Eq. (11b) modified by substituting the ϕ_j's of Eq. (13).

The discussion of $\psi_{K\pi}$ of benzene now more or less parallels that of butadiene.[24] Using the three nonorthogonal 2-center LCAO MO's of Eqs. (6), a six-electron $\psi_{K\pi}$ analogous to that of Eq. (11a) could be constructed. But instead of the τ_j, an orthonormal set of three delocalized ϕ_j (analogous to those of Eqs. (12) for butadiene) can be formed as linear combinations of the τ_j, and these can be used to construct a $\psi_{K\pi}$ analogous to that of Eq. (11b). These delocalized ϕ_j, which we shall designate as ϕ_0, ϕ_I, and ϕ_{-I}, may be taken, up to normalizing factors, as

$$\phi_J\sim\sum_{p=1}^{3}\omega^{2Jp}\tau_p. \tag{14}$$

The π_x-electron energy corresponding to this choice of ϕ_J is now

$$W_{K\pi}=2I_0+2I_I+2I_{-I}+(4J_{0I}-2K_{0I})+(4J_{0-I}-2K_{0-1})+(4J_{I-I}-2K_{I-I})+J_{00}+J_{II}+J_{-I-I}. \tag{15}$$

Equation (15) is formally identical with Eq. (4), but differs because the set ϕ_0, ϕ_I, ϕ_{-I} is different from ϕ_0, ϕ_1, ϕ_{-1} (except that the MO ϕ_0 turns out to be the same in both).[25]

4. COMPRESSION ENERGY CORRECTIONS AND THE THEORETICAL LCAO RESONANCE ENERGY OF BENZENE

For any assumed values of the C−C distances, the quantities in Eq. (15) can be computed by the method used previously for Eq. (4). The difference $W_{K\pi}-W_{N\pi}$ can then be obtained. However, for a suitable theoretically computed resonance energy W_R to be compared with an empirical counterpart from thermochemical data (Sec. 5), we presumably should use a Kekulé structure in which the bonds have the lengths (1.54A and 1.34A) of normal single and double bonds alternately, whereas for normal benzene all the bonds are of length 1.39A. That is, we should take

$$W_R=W_K^{1.34,1.54}-W_N^{1.39}, \tag{16}$$

where superscripts denote bond lengths, and set out to compute this quantity. Direct approach through the formula,

$$W_R=(W_{K,\text{core}}^{1.34,1.54}-W_{N,\text{core}}^{1.39})+(W_{K\pi}^{1.34,1.54}-W_{N\pi}^{1.39}), \tag{17}$$

is unfortunately not practicable,—the variation of core energy with bond distances is too hard to handle.

We therefore adopt an alternative approach, by writing Eq. (16) in the form,

$$\left.\begin{aligned} &W_R=W_R^{1.39}-C_K,\\ &\text{with}\\ &W_R^{1.39}\equiv W_K^{1.39}-W_N^{1.39}\\ &\text{and}\\ &C_K\equiv W_K^{1.39}-W_K^{1.34,1.54}. \end{aligned}\right\} \tag{18}$$

[24] In the case of benzene (see reference 29), if α is the π_x exchange integral (negative in sign), the π_x bond energy of three isolated double bonds according to approximate VB theory (see end of Sec. 6) is -3α and the exchange repulsion is $+(3/2)\alpha$, giving a net π_x bond energy of $-(3/2)\alpha$ for the Kekulé structure; and the computed resonance energy $W_{K\pi}-W_{N\pi}$ is -1.11α, giving an over-all net computed π_x bond energy of -2.61α. (The signs here are confusing, but correspond to the usual definition of bond energies and resonance energies as intrinsically negative.) It seems anomalous here that even with strong resonance the π_x bond energy is less than for three isolated double bonds, but this is what the theory gives, and there is no reason to suppose that the LCAO MO theory would give a different result. The resolution of the anomaly must lie in the fact that bond energies in molecules with more than two electrons always include considerable exchange repulsions, so that the exchange repulsion term $+(3/2)\alpha$ mentioned above is not really added to the total energy, but is substituted for other exchange repulsion terms of the same order of magnitude which would have been present even if the double bonds had been associated only with single bonds, as for example in ethylene (C=C exchange repulsions with C−H bond electrons) or propylene or butylene (C=C exchange repulsions with C−C and C−H bond electrons). (See Syrkin and Dyatkina, reference 26, p. 242, for a survey of exchange repulsion and other terms included in the normal bond energies of the paraffins.)

[25] Equation (14) corresponds to a symmetry D_{3h} (all single bonds equivalent, all double bonds equivalent, with the single and double bonds possibly but not necessarily equal in length). Like ϕ_1 and ϕ_{-1} of Eq. (3), ϕ_I and ϕ_{-I} are degenerate, hence could be replaced by any mutually orthogonal pair of their linear combinations.

Further,

$$\left.\begin{aligned} W_R^{1.39} &= (W_{K,\text{core}}^{1.39} - W_{N,\text{core}}^{1.39}) \\ &\quad + (W_{K\pi}^{1.39} - W_{N\pi}^{1.39}) \\ &\approx W_{R\pi}^{1.39} \equiv (W_{K\pi}^{1.39} - W_{N\pi}^{1.39}), \end{aligned}\right\} \quad (19)$$

since the quantity $(W_{K,\text{core}}^{1.39} - W_{N,\text{core}}^{1.39})$ is doubtless so small that it can safely be neglected. In Eq. (18), C_K denotes "compression energy." $W_{K\pi}^{1.39} - W_{N\pi}^{1.39}$ can be computed from Eqs. (4) and (15), and C_K estimated rather precisely from empirical (primarily force constant) data if the Kekulé bonds are assumed to behave under compression or stretching like the single and double bonds in ethane and ethylene.

Results of the calculation of $W_{K\pi}^{1.39}$ are given in Table I. From these,

$$W_R^{1.39} \approx W_{K\pi}^{1.39} - W_{N\pi}^{1.39}$$
$$= 3.17 \text{ ev} = 73.1 \text{ kcal/mole}. \quad (20)$$

The quantity $W_R^{1.39}$ may be called the gross or 1.39A vertical resonance energy, the latter because it corresponds to a "vertical" process in the terminology used in applications of the Franck-Condon principle, that is, an electronic change with no accompanying change in internuclear distances. On the other hand, W_R is a net resonance energy.

For C_K, Mulliken, Rieke, and Brown[14] obtained 35.0 kcal, while in an improved computation, Mulliken and Rieke[15] obtained 36.6 kcal with an estimated uncertainty of ±1 kcal. Using the latter value, we find

$$W_R \text{ (theoretical)} = 36.5 \text{ kcal/mole}. \quad (21)$$

5. COMPARISON OF THERMOCHEMICAL AND THEORETICAL RESONANCE ENERGIES OF BENZENE

We now seek an empirical value of W_R which can properly be compared with the theoretical value obtained in Sec. 4. Since W_N is known empirically, the essential question is how to obtain a valid "empirical" W_K. Pauling answered this by setting up a standard bond energy formula of additive type designed to fit normal molecules believed to be "nonresonating." For any unsaturated hydrocarbon, this may be written

$$B = xN_{C-H} + yN_{C-C} + zN_{C=C} + \Delta, \quad (22)$$

B being the observed bond energy, and Δ any deviation from the standard energy, Δ if positive being interpreted as resonance energy. Similar formulas can be given for heats of combustion or hydrogenation, or for heats of formation ΔH_f^0, it being a matter of convenience which is used, since all if made equally accurate should give the same Δ.

However, when a formula such as Eq. (22) is used, small systematic deviations Δ occur, even in the paraffins, which cannot be attributed to the kind of π_x resonance with which we are now concerned. It is desirable to make some allowance for these before arriving at Δ. Following are suitable formulas for hydrocarbons, not containing triple bonds, in which no strong steric effects occur:[26,27]

$$\Delta H_f^0 = xN_{C-H} + yN_{C-C} + zN_{C=C} - \gamma_1 n_{C-C} - \gamma_2 n_{C=C} - \Delta \quad (23)$$

$$\Delta H_f^0(0°\text{K}) = -3.55N_{C-H} - 5.00N_{C-C} + 28.72N_{C=C} - 0.78n - \Delta. \quad (23a)$$

ΔH_f^0 here is in kcal/mole. In Eqs. (23), (23a), n_{C-C} is the sum, taken over all C−C single bonds, of the numbers of bonds going out from the two carbon atoms of the given bond to other carbon atoms; $n_{C=C}$ is a similar sum for C=C double bonds, and n is $n_{C-C} + n_{C=C}$. For example, $n=0$ for CH_4, C_2H_4, or C_2H_6; $n=2$ for propane; $n_{C-C}=2$ and $n_{C=C}=1$, so $n=3$, for propylene; and $n=12$ for neopentane ($C(CH_3)_4$). The term n is designed to take into account, as well as can be judged from data on aliphatic molecules, the mutual effect, exclusive of π_x resonance, of first-neighbor carbon-carbon bonds on ΔH_f^0. This type of correction is of obvious relevance for Kekulé benzene.[28]

For benzene, Eq. (23a) yields $\Delta = 41.82$ kcal/mole, differing little from the (25°C) value of 41 kcal/mole obtained by Pauling's method.[29] This value of Δ is in

[26] The basis and significance of Eqs. (23), (23a) may be discussed more fully in a later paper by R. S. Mulliken. Equation (23) is an improvement on a somewhat similar equation given in Sec. 12 and Eqs. (23) and (27) of reference 13. The coefficients in Eq. (23a) have been adjusted to fit the most recent ΔH_f^0 (0°K) data given in the A.P.I. tables.

The term $-0.78n$ is interpreted as arising from substitution-induced variations in second-order hyperconjugation and other second-order resonance effects, tempered by steric repulsions. Equation (23a) fits observed data well for most not too much branched hydrocarbons not containing triple bonds: $|\Delta| \leqq 0.5$ for acyclic aliphatic hydrocarbons of this category, except $\Delta = 1.8$ for methane (this is much better than by most formulas). For diamond, $\Delta = 0.06$. For cyclohexane ($n=12$), $\Delta = -1.95$, for cyclopentane ($n=10$) $\Delta = -7.62$; these negative Δ's may be attributed to ring strain. In molecules with first-order π_x hyperconjugation, Eq. (23a) yields small positive Δ's (e.g., 1.6 for propylene), and for molecules with π_x conjugation, larger positive Δ's (e.g. 6.48 for 1,3-butadiene).

See also J. R. Platt, J. Chem. Phys. **15**, 419 (1947); H. Wiener, J. Chem. Phys. **15**, 766 (1947); J. G. M. Bremner and G. D. Thomas, Trans. Faraday Soc. **44**, 338 (1948); and particularly Y. K. Syrkin and M. E. Dyatkina, *Structure of Molecules and the Chemical Bond*, translated and revised by M. A. Partridge and D. O. Jordan (Interscience Publishers, New York, 1950), pp. 243–4, for related considerations.

[27] Since our theoretical W_R is purely electronic, a 0°K equation like (23a) is preferable to the usual 25°C kind of equation. Still better would be an equation corrected for zero-point energy, but we doubt that this would make an important difference.

[28] Instead of using an equation like (23a), a common alternative procedure (see reference 29) is to take Δ as the difference between the heat of hydrogenation of one mole of benzene and that of three moles of cyclohexene. In our opinion, however, this involves more doubtful points than the use of Eq. (23). In particular, there seems to be no reason to expect ring strain in either actual or Kekulé benzene, with either normal single and double bond lengths or 1.39A bond lengths; in all these cases, a planar structure with 120° bond angles should be free from strain.

[29] See for example, G. W. Wheland, *The Theory of Resonance* (John Wiley and Sons, Inc., New York, 1944).

satisfactory agreement with the theoretical value 36.5 kcal obtained for W_R at the end of Sec. 4.

However, a more careful analysis shows that we should have made two corrections of some importance, the one to Δ, the other to C_K as given in Sec. 4, before comparing empirical and theoretical resonance energies. These will be considered in the next section.

6. THEORETICAL ANALYSIS OF MEANING OF THERMOCHEMICAL RESONANCE ENERGIES, WITH APPLICATION TO BENZENE

In order to make, so far as possible, a clean-cut comparison between theory and experiment, it will be useful now to write an equation relating the theoretical quantity $W_{R\pi}{}^{1.39}$ which we have actually computed to a sum of empirically based terms including C_K (cf. Eqs. (18)–(19)) and the other correction terms mentioned at the end of Sec. 5. It will prove useful first to introduce the concept of a "standard hydrocarbon," defined as one for which Eqs. (23), (23a) hold with $\Delta=0$. Here also we note that Eq. (23) should be valid not only for hydrocarbons with carbon-carbon bonds of the normal unconjugated equilibrium lengths 1.34A and 1.54A (in this case Eq. (23a) applies) but also, after suitable adjustments in the values of the coefficients, for hydrocarbons with the C=C and C−C bonds stretched or compressed to any values d and s, respectively. The values of the coefficients should then be functions of d and s. We shall denote the corresponding "standard energy" by $W_S{}^{d,s}$.

We next note that $W_S{}^{d,s}$, even though it corresponds to a "nonresonating" hydrocarbon (that is, one with no conspicuous π_x conjugation or resonance energy), must actually include a perhaps very appreciable amount of what may be called higher order resonance energy, corresponding to numerous minor contributions of miscellaneous VB structures present in the actual wave function. Part of this has been recognized under the name of second-order hyperconjugation energy, this in turn usually being described in terms of σ and π hyperconjugation energy, and the latter being divided into π_x and π_y hyperconjugation energy.[13]

The most important point in the present connection is that $W_S{}^{d,s}$ includes second-order π_x hyperconjugation energy. Further, if we write W_S as a sum of core and π_x energy, like W in Eq. (2), that is,

$$W_S{}^{d,s}=W_{S,\text{core}}{}^{d,s}-W_{S\pi}{}^{d,s}, \tag{24}$$

then this second-order π_x hyperconjugation energy is part of $W_{S\pi}$, the remainder and major portion of $W_{S\pi}$ being the ordinary nonresonant π_x energy of any double bonds which are present. The amount of second-order π_x hyperconjugation energy is believed to be approximately proportional to the number of C−C single bonds; the amount per single bond of length s (normal or compressed) has been called δ^s.[13]

The term $W_{S,\text{core}}$ in Eq. (24) contains (among other things) the remainder of the second-order resonance energy, including some σ and π_y hyperconjugation energy; for example, a fairly large amount of π_y hyperconjugation energy is believed to be associated with every C=C double bond.[13] In "resonating" unsaturated and aromatic molecules, the second-order π_x hyperconjugation energy in $W_{S\pi}$ is superseded by energy of first-order π_x resonance (that is, of first-order hyperconjugation as for example in propylene, or of conjugation as in butadiene, or of benzene-like resonance), it being this change from higher-order to first-order π_x resonance energy which corresponds to Δ; but $W_{S,\text{core}}$ should be affected only indirectly and very slightly.

We need now to examine carefully how $W_{K\pi}$ for a hypothetical "non-resonating" Kekulé-type structure is related to $W_{S\pi}$. Since by its definition, the Kekulé structure contains no π_x resonance energy whatever (see Sec. 3), while, as we have seen, the "standard" hydrocarbon contains an amount δ_s of π_x resonance energy per single bond of length s, we have

$$W_{K\pi}{}^{d,s}=W_{S\pi}{}^{d,s}+\delta^s N_{\text{C-C}}, \tag{25}$$

the (positive) energy being the greater for $W_{K\pi}{}^{d,s}$.

For benzene at its actual bond lengths, Eq. (25) becomes

$$W_{K\pi}{}^{1.39}=W_{S\pi}{}^{1.39}+3\delta^{1.39}=(W_S{}^{1.39}-W_{S,\text{core}}{}^{1.39})+3\delta^{1.39}.$$

Our theoretical resonance energy $W_{R\pi}{}^{1.39}$ is then

$$\begin{aligned}W_{R\pi}{}^{1.39}&=W_{K\pi}{}^{1.39}-W_{N\pi}{}^{1.39}\\&=W_{K\pi}{}^{1.39}-(W_N{}^{1.39}-W_{N,\text{core}}{}^{1.39})\\&=(W_S{}^{1.39}-W_N{}^{1.39})+3\delta^{1.39}+(W_{N,\text{core}}{}^{1.39}-W_{S,\text{core}}{}^{1.39}).\end{aligned}$$

Or, assuming the last term in parentheses to be negligible, like $W_{K,\text{core}}{}^{1.39}-W_{N,\text{core}}{}^{1.39}$ in Eqs. (19),

$$\begin{aligned}W_{R\pi}{}^{1.39}&=(W_S{}^{1.34,1.54}-W_N{}^{1.39})\\&\quad+(W_S{}^{1.39}-W_S{}^{1.34,1.54})+3\delta^{1.39}\\&=\Delta+C_S+3\delta^{1.39},\end{aligned} \tag{26}$$

since Δ is by definition (see Eq. (23)) equal to the first term in parentheses above, and where C_S denotes the energy required to stretch-compress a structure like a Kekulé structure but with *standard* single and double carbon-carbon bonds from $s=1.54$A, $d=1.34$A to $s=d=1.39$A.

From Eq. (23) with the values $N_{\text{C-C}}=N_{\text{C=C}}=3$, $n_{\text{C-C}}=12$, $n_{\text{C=C}}=6$, appropriate to benzene, C_S is

$$\left.\begin{aligned}&C_S=C_{S0}-\Delta\Gamma,\\&\text{where}\\&C_{S0}\equiv 3[(y^{1.39}-y^{1.54})+(z^{1.39}-z^{1.34})],\\&\Delta\Gamma\equiv 12(\gamma_1{}^{1.39}-\gamma_1{}^{1.54})+6(\gamma_2{}^{1.39}-\gamma_2{}^{1.34}).\end{aligned}\right\} \tag{27}$$

TABLE II. The vertical (or gross) resonance energy of 1,3-butadiene.[a]

Energy term	Ground state N		"Non-resonating" structure K		Contribution to vertical resonance energy	
	cis-	*trans-*	*cis-*	*trans-*	*cis-*	*trans-*
I_1 or I_I	−26.79[b]	−26.38[b]	−26.20[b]	−25.74[b]	0.72	0.73
I_2 or I_{II}	−23.45[b]	−22.91[b]	−23.67[b]	−23.18[b]		
J_{11} or J_{II}	10.10	9.99	9.68	9.56		
J_{22} or $J_{II\ II}$	9.55	9.36	9.58	9.42	0.15	0.08
J_{12} or $J_{I\ II}$	9.40	9.28	9.53	9.40		
K_{12} or $K_{I\ II}$	3.28	3.42	3.55	3.68	−0.54	−0.53
W_N or W_K	−49.78[b]	−48.93[b]	−49.44[b]	−48.65[b]	0.34 (7.8 kcal/mole)	0.28 (6.5 kcal/mole)

[a] Numerical values are taken or derived from reference 5. All are in ev.
[b] See Table I, footnote b.

The term C_{S0} represents the energy to compress three standard C−C single bonds, of type $n_{C-C}=0$ as in ethane, and to stretch three standard C=C double bonds, of type $n_{C=C}=0$ as in ethylene, to 1.39A. Since Eq. (23a) fits either ethane or ethylene with $\Delta=0$, C_{S0} may be set equal to the actual energy required to compress the carbon-carbon bonds in three ethane and stretch those in three ethylene molecules to 1.39A. A reliable empirical value (36.6±1 kcal) has been given for this quantity at the end of Sec. 4. Equation (26) now becomes

$$W_{R\pi}^{1.39}=\Delta+C_{S0}+(3\delta^{1.39}-\Delta\Gamma); \qquad (28)$$

or, introducing numerical values from Secs. 4 and 5,

$$73.1=41.8+36.6+(3\delta^{1.39}-\Delta\Gamma). \qquad (29)$$

Unfortunately, no reliable estimate is available for the correction term in parentheses. The sign of the hyperconjugation energy term $3\delta^{1.39}$ is surely positive. Empirically, $\gamma_1^{1.54}$ and $\gamma_2^{1.34}$ are positive (see Eq. (23a)). If the terms $\gamma_1 n_{C-C}$ and $\gamma_2 n_{C=C}$ have been interpreted correctly in Sec. 5 as enhancements of second-order resonance energy,[26] they would be expected to increase, and fairly fast, with decreasing s or d. This would make $\Delta\Gamma$ positive.

A quantitative value has been given for $\delta^{1.39}$ in reference 13, from which $3\delta^{1.39}=11.8$ kcal. This value cannot be accepted as accurate, although it is probably correct as to order of magnitude.[30] For $\Delta\Gamma$, a plausible guess would be that $\gamma_1^{1.39}=2\gamma_1^{1.54}$, hence $\gamma_1^{1.39}-\gamma_1^{1.54}=0.8$ (see Eq. (23a)), and $\Delta\Gamma$ about 8 kcal. Thus it is likely that $(3\delta^{1.39}-\Delta\Gamma)$ in Eq. (29) may be near zero, although possible that it may amount to ±10 kcal or even more. The agreement between the theoretical $W_{R\pi}^{1.39}$ on the left of Eq. (29) and the sum of the empirical or unknown quantities on the right is thus well within the uncertainties of the latter.

It seems worth pointing out here that Eq. (28) for $W_{R\pi}^{1.39}$ is equally as valid for calculations made by the VB as for those made by the LCAO MO method. However, existing calculations by the VB method appear to be confined to the early crude result $W_{R\pi}=1.11\alpha$, where α is the exchange integral for π_z electrons on adjacent carbon atoms.[24] These calculations took into account only Kekulé and Dewar structures, neglected higher exchange integrals, and involved no attempt to compute α itself theoretically. In the usual discussions,[29] α is determined empirically by setting $W_{R\pi}=1.11\alpha$ equal to Δ, ignoring the large correction term C_{S0} as well as the smaller ones which follow it in Eq. (28).

7. RESONANCE ENERGIES OF cis- AND trans-1,3-BUTADIENE

The vertical or gross resonance energies of cis- and trans-1,3-butadiene, for molecular dimensions equal to those in the actual ground states, can be computed from $W_{N\pi}-W_{K\pi}$ following the same general procedure as for benzene. We have

$$W_{N\pi}=2I_1+2I_2+J_{11}+4J_{12}-2K_{12} \qquad (30)$$

from Eq. (5) of reference 5 (corresponding to use of "best" LCAO MO's), while

$$W_{K\pi}=2I_{\rm I}+2I_{\rm II}+J_{\rm I\ I}+4J_{\rm I\ II}-2K_{\rm I\ II}, \qquad (31)$$

with the integrals I, J, K based on the delocalized but "non-resonating" butadiene MO's of Eq. (12) above. $W_{K\pi}$ is the π-electron energy corresponding to $\psi_{K\pi}$ of Eq. (11b) above. The basic integrals required may be found in reference 5. The results are given in Table II.

The computed gross or vertical resonance energies, after a correction[31] of −2.8 kcal for "compression energy" to obtain a theoretical value for the ordinary (net or nonvertical) resonance energy W_R, as was done for benzene in Sec. 4, may be compared with the thermochemical resonance energy of 6.5 kcal obtained[26]

[30] Reference 13, Table VII. However, since the computations were made by the $\Sigma\epsilon_j$ method with neglect of the overlap integral S, and involve also other assumptions, they cannot be accepted as accurate. Moreover, as has been found by one of the authors (RSM) they would be altered (though not changed as to order of magnitude) if revised to correct an error in one of the equations of key importance in reference 13, namely, Eq. (32), where δ^s and δ^d should be substituted for $\delta^{1.54}$ and $\delta^{1.33}$ (footnote 35 is incorrect).

[31] Reference 13, Table VI.

in the manner described in Sec. 5, using Eq. (23a). Since ordinary 1,3-butadiene is probably nearly all in the trans-form,[32] we use the trans-result from Table II, and obtain

$$\text{computed } W_R = 6.5 - 2.8 = 3.7; \qquad \text{observed } W_R = 6.5 \text{ kcal/mole}. \tag{32}$$

[32] Aston, Szasz, Woolley, and Brickwedde, J. Chem. Phys. **14**, 67 (1946).

Or more accurately, when additional small corrections of the type considered for benzene in Sec. 6 are included, we may write in analogy to Eq. (29) for benzene,

$$6.5 = 6.5 + 2.8 + [\delta^{1.46} - 4(\gamma_1^{1.46} - \gamma_1^{1.54}) - 2(\gamma_2^{1.35} - \gamma_2^{1.34})]. \tag{33}$$

The agreement between theory and experiment is not quite as good as that for benzene.

THE JOURNAL OF CHEMICAL PHYSICS VOLUME 19, NUMBER 10 OCTOBER, 1951

Isotope Effect in the Band Spectrum of HNO_2

GEORGE PORTER
Physical Chemistry Laboratory, University of Cambridge, Cambridge, England
(Received April 23, 1951)

The band system between 3100 and 3900A which has been attributed both to HNO_2 and enhanced NO_2 is shown to belong to the former molecule by means of the isotope effect. Measurements of the spectrum of DNO_2, and a partial interpretation of the band structure and isotope shift are given.

THERE has been considerable discussion about the identity of the molecule responsible for the system of bands in the region 3100 to 3900A observed by Melvin and Wulf[1] and by Bone, Newitt, and Outridge.[2] Melvin and Wulf discovered the system in the products of photochemical decomposition of N_2O and originally attributed it to N_2O_3; but they subsequently obtained the same spectrum in mixtures of NO, NO_2, and H_2O, found that all three molecules are necessary to produce the bands, and suggested HONO as the molecule responsible. They mentioned, however, that the bands agreed very closely in wavelength with some of the stronger bands of NO_2, suggesting the possibility that the system could be due to selective enhancement of certain bands of this molecule.

Newitt and Outridge pointed out that the measurements of Melvin and Wulf agreed with those obtained earlier by Bone and Newitt in self-absorption of explosions of $CO/NO/N_2O$ mixtures at high pressure. They repeated this work with very dry gases and also showed that the spectrum was present in CO/N_2O flames. In view of the fact that the intensity was not much diminished by intensive drying they challenged the interpretation of Melvin and Wulf and attributed the spectrum to selective enhancement of certain NO_2 bands. Thompson[3] points out the close similarity between these bands and those of the alkyl nitrates which supports the assignment to HNO_2, but suggests that the system of Newitt and Outridge may be different from that of Melvin and Wulf. Gaydon[4] concludes that there is little doubt that the two systems are identical but that they may be due either to HNO_2 or the carrier, $-NO_2$.

It would clearly be helpful if the origin of these bands could be settled, for the molecule must in any case be rather unstable and not easily studied by other methods. The main lack of agreement is as to whether or not hydrogen is necessary for their appearance, and it was thought possible that the isotopic molecular spectrum, obtained with deuterium in place of hydrogen would solve the problem unequivocably as well as assist in the interpretation of the bands. It will be seen that this is the case.

EXPERIMENTAL

Absorption spectra were taken of mixtures of NO, NO_2 and H_2O, or D_2O at various partial pressures. The nitric oxide was prepared from sodium nitrite and 10 percent sulfuric acid and the nitrogen dioxide by thermal decomposition of lead nitrate, both being fractionally distilled in vacuum before use. The heavy water was 99.7 percent D_2O supplied by the Norsk Hydro Company. The absorption cell was of quartz and 100 cm in length, the spectrograph was a quartz Littrow instrument with resolving power of 0.15A at 3000A and 0.6A at 4000A and the source of continuum was a xenon-filled flash discharge tube.[5] When using a substance with a high absorption coefficient, like NO_2, there is danger that in the process of recording its spectrum the absorbed light may initiate photochemical reactions which, especially if chains are possible, may produce sufficient product to be detected in the spectra. Nearly

[1] E. H. Melvin and O. R. Wulf, J. Chem. Phys. **3**, 755 (1935).
[2] D. M. Newitt and L. E. Outridge, J. Chem. Phys. **6**, 752 (1938).
[3] H. W. Thompson, J. Chem. Phys. **7**, 136 (1939).
[4] A. G. Gaydon, *Spectroscopy and Combustion Theory* (Chapman and Hall, Ltd., London, 1949); A. G. Gaydon and R. W. B. Pearse, *The Identification of Molecular Spectra* (Chapman and Hall, Ltd., London, 1950).
[5] G. Porter, Proc. Royal Soc. (London) **A284**, 200 (1950).

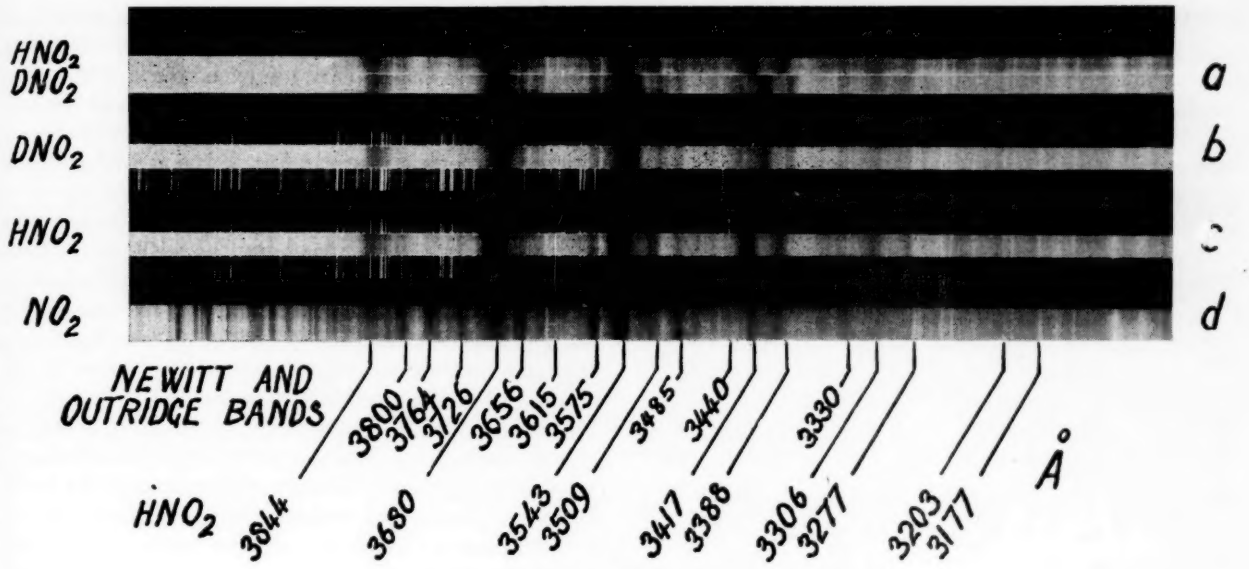

FIG. 1. Absorption spectra of HNO_2, DNO_2, and NO_2.

all such reactions are excluded by using the flash discharge, the duration of which is 5×10^{-5} sec, a time short enough to eliminate the possibility of three-body collisions or bimolecular reactions with activation energy greater than about 4 kcal at the pressures used and at room temperature. These considerations, and the fact that the results are unchanged when the flash source is used in place of the continuous one shows that the substance whose spectrum is being considered is formed in a thermal dark reaction.

Melvin and Wulf are careful to point out that in their experiments the gases were frozen out together between mixing and admission to the absorption cell. In these experiments this was not done, the gases being mixed in a 2-liter bulb and then admitted by excess pressure to the absorption cell.

RESULTS AND DISCUSSION

The results of Melvin and Wulf were confirmed, no trace of the bands being present in the absence of water vapor and at the higher dispersion there was still no resolved fine structure. Using a mixture of 300 mm NO, 3 mm NO_2, and 12 mm water vapor, the band system was photographed with H_2O and with D_2O, the results being shown in Fig. 1. Spectrum (a) shows the two band systems superposed by a Hartmann diaphragm, (b) and (c) were obtained with D_2O and H_2O, respectively, and have the iron arc superposed for wavelength comparison, and (d) is the spectrum of NO_2 alone at 2 mm pressure.

It is immediately apparent that although similar, the spectra obtained with H_2O and with D_2O show a pronounced isotopic shift. Furthermore, the bands obtained with D_2O no longer coincide with those of NO_2, showing that the correspondence in the case of H_2O is fortuitous. We may, therefore, conclude with certainty that the molecule responsible for the system does contain hydrogen and, this being so, there is no longer any reason to doubt the assignment of HNO_2. It is known that NO, NO_2, and water react to give nitrous acid and the equilibrium of this reaction has recently been studied.[6] No other molecule containing hydrogen is expected to be present, except perhaps HNO_3, which has a continuous spectrum. Further confirmation of the assignment is given by the similarity in position and separation between these bands and those of the alkyl nitrites.[7]

It remains to be decided whether the band system obtained in flames and explosions is the same as the above. The measurements of band maxima given in Table I for HNO_2 agree with those of Newitt and Outridge to within a few angstrom units, which is all that can be expected with such diffuse bands. Several of the bands are not symmetrical about the center and the choice of maxima is rather arbitrary. The published photograph provides a more accurate means of comparison for future reference. There remain, however, four weaker bands measured by Newitt and Outridge in high pressure explosions and five others in the low pressure explosions and flames which do not appear in Table I nor in the measurements of Melvin and Wulf. All these nine wavelengths have been marked on Fig. 1 and it will be seen that they correspond exactly to the remaining strong bands of NO_2. At room temperature it is not possible to obtain HNO_2 free from NO_2 owing to the dissociation equilibrium, so that these bands are always weakly present; but a comparison of the HNO_2 and DNO_2 spectra shows that these bands are not shifted and are therefore to be attributed to NO_2 alone. Their intensity does not lead to the necessity of any additional assumption about selective enhancement.

[6] L. G. Wayne and D. M. Yost, J. Chem. Phys. **19**, 41 (1951).
[7] C. H. Purkis and H. W. Thompson, Trans. Faraday Soc. **32**, 1466 (1936).

TABLE I. Position and relative intensities of band maxima in spectrum of HNO_2 and DNO_2.

	HNO_2			DNO_2	
λ (A)	*I*	ν(cm⁻¹)	λ (A)	*I*	ν(cm⁻¹)
3844	3	26008	3843	3	26015
3680	9	27167	3676	9	27196
3542.5	10	28221	3530	10	28321
3509	2	28490	3502.5	1	28543
			(3423	0	29206)
3417	7	29257	3401	6	29394
3387.5	4	29512	3378.5	3	29590
			(3305	0	30248)
3306	3	30239	3284	1	30441
3277	2	30506	3266	0	30609
3203	0	31211	...		...
3177	0	31466			

The system of Newitt and Outridge is, therefore, compounded of the HNO_2 spectrum and nine bands of the NO_2 molecule which occur in the same region. As the molecule HNO_2 is unstable at higher temperatures, it must have been formed, in their experiments, in the cooled gaseous products of combustion through which the light passed in both the flame and explosion investigations.

INTERPRETATION OF BAND STRUCTURE

Several different interpretations of this system have been put forward by the workers mentioned above, and it is necessary only to consider the new evidence given by the isotope effect. There are few known examples of isotopy in polyatomic band spectra and this system is, therefore, interesting from the point of view of the theory of molecular spectra as well as in connection with the structure of HNO_2. Unfortunately very little is known about this molecule, even in the ground state, so that any interpretation is rather speculative.

In view of the above interpretation of the bands of Newitt and Outridge their scheme must be discounted. The main feature of the HNO_2 spectrum is a strong band progression which, considering the independence of intensity on temperature, can safely be interpreted as arising from a constant level in the ground state, and may be called the $v_1''=0$ progression. The fact that the frequency is increased on substitution of deuterium

TABLE II. Assignment of frequency intervals in spectrum of HNO_2 and DNO_2.

					Δν (cm⁻¹)	
v_1'	v_3'		v_1'	v_3'	HONO	DONO
1	0	—	0	0	1159	1181
2	0	—	1	0	1054	1125
3	0	—	2	0	1036	1073
4	0	—	3	0	982	1047
5	0	—	4	0	972	...
2	1	—	2	0	269	222
3	1	—	3	0	255	196
4	1	—	4	0	267	158
5	1	—	5	0	255	...

shows that the frequency, ω_1, involved is not associated with the −O−H bond but with the −O−N−O group, which explains the similarity between this and the alkyl nitrite spectra. In view of the high intensity of the first band, and the complete absence of any others at a longer wavelength, the band at 3844A is probably the origin of the system.

The isotope shift which is observed in this progression, as it occurs to shorter wavelengths with the heavier molecule, must be due to a perturbation caused by interaction with another frequency ω_2 in one of the isotopic molecules and the frequency ω_2 must be closely associated with the motion of the hydrogen atom. In the absence of data on the HNO_2 molecule the frequencies of the molecules HNO_3 and DNO_3 in their ground state give a useful guide. The three frequencies which show a marked isotopic shift in these molecules are the O−H and O−D stretching and bending modes and the restricted rotation which are at 3386, 1680, and 480 cm⁻¹ in HNO_3 and at 2476, 1336, and 370 cm⁻¹ in DNO_3.[8] These frequencies will not be expected to be very different in the HNO_2 molecule but will probably be less in the excited state. The frequency ω_1 is about 1000 cm⁻¹, so only the bending mode of the −O−H or −O−D bond is of the right order to produce the perturbation, and of the two, the −O−D frequency seems more likely to have this frequency in the excited state. That the perturbation occurs in the DNO_2 molecule rather than in HNO_2 is confirmed by the later considerations of the second interval. The simplest explanation of the isotope effect is, therefore, that the intervals observed in the HNO_2 spectrum are the unperturbed frequencies of the progression; in DNO_2 this frequency is coupled with the −O−D bending frequency which in the upper state, and with no perturbation, would have a frequency of just under 1000 cm⁻¹. Resonance will therefore occur, and the perturbation will increase as the two frequencies, in zero-order perturbation approximation, approach each other, that is, as the quantum number increases and the frequency ω_1 is decreased by the anharmonicity term. The fact that the isotope splitting increases rather like that of a diatomic molecule, except for the reversed order, with zero splitting at the origin, is in accordance with the fact that the magnitude of the perturbation, for a given frequency separation, is dependent essentially on the anharmonic terms in the potential energy function.

The second band system, which is weaker and occurs to shorter wavelengths by about 250 cm⁻¹, can be interpreted in several ways; but the suggestion of Purkis and Thompson that it arises from the excitation of a second frequency of about 2250 cm⁻¹ can fairly certainly be discounted on the grounds that the only frequencies of this magnitude are those associated with −O−H and as the same bands occur in the DNO_2 molecule at a

[8] O. Redlich and L. E. Nielson, J. Am. Chem. Soc. 65, 654 (1943).

slightly higher frequency, they cannot be of this type. The constancy of the 250 cm^{-1} interval in HNO_2 supports their second suggestion that this interval corresponds to another frequency in the upper state, which we will call ω_3, and which is raised by only one quantum number. The decrease of this frequency in DNO_2 lends some support to this view, for a frequency as low as this must almost certainly be the restricted rotation which is expected to show a considerable frequency decrease on substituting the heavier isotope, as for example, in HNO_3 and DNO_3, where the corresponding frequencies are, respectively, 480 and 370 cm^{-1}. However, the perturbation makes the actual shift rather difficult to interpret and a second possibility, that the weaker system corresponds to another progression like the first, but involving a different mode of vibration of the $-O-N-O$ group of frequency about 1250 cm^{-1}, cannot be ruled out. The strongest evidence against this, and for the restricted rotation view, is the complete absence of this second interval in all the alkyl nitrites.

The intervals are given in Table II with quantum number assignments assuming the 250 cm^{-1} interval to be a fundamental. The apparent increased anharmonicity in DNO_2 is well explained in terms of the resonance already discussed; the perturbation of the stronger low frequency band will be relatively greater, with respect to the weaker band, at lower frequencies and higher quantum levels resulting in a closing together of the two bands, both of which are perturbed, owing to the greater perturbation of the low frequency one. This explanation is also applicable if the second system corresponds to a progression involving one quantum number only. The absence of the first two of the weaker bands is, possibly, simply a case of reduced intensity. The two additional weak bands reported in brackets for DNO_2, can be given many different assignments, the discussion of which serves little purpose until more information is available. It is hoped that there will be more study of infrared absorption of these molecules in order to extend the interpretation.

The author is indebted to Mr. G. Hall for a helpful discussion.

THE JOURNAL OF CHEMICAL PHYSICS VOLUME 19, NUMBER 10 OCTOBER, 1951

Second-Order Transitions and Critical Points

P. J. PRICE*
Royal Society Mond Laboratory, Cambridge, England
(Received May 28, 1951)

The thermodynamic formulas, of the Ehrenfest type, applicable to an isolated second-order point on a first-order equilibrium line (*e.g.*, a critical point) are discussed.

1. INTRODUCTION

SOME years ago there was a discussion, in the *Physical Review*,[1-3] of the applicability of Ehrenfest's equations[4] for a second-order equilibrium line

$$\left.\begin{aligned}\Delta C_p &= T(dp/dT)\Delta(\partial V/\partial T)_p \\ \Delta(\partial V/\partial T)_p &= -(dp/dT)\Delta(\partial V/\partial p)_T\end{aligned}\right\} \quad (1)$$

to the critical points, and to the lambda-point of liquid helium. Lype[1] proposed to modify the first of Eq. (1) by introducing a factor of 2 on the right-hand side, and concluded that the experimental data for the helium lambda-point supported this change. In this note the question is studied by introducing generalized Ehrenfest equations for a first-order transition and by considering their limiting form as one moves along the equilibrium line to a point at which the discontinuities in volume and entropy vanish.

It is concluded that, in the case of the vapor-liquid critical point, the original Ehrenfest equations are in fact formally correct; but like the Clausius-Clapeyron equation they become indeterminate, and more suitable "hybrid" equations are proposed. On the other hand, supposing the transformation of liquid helium II to liquid helium I to have a very small latent heat which vanishes at the lambda-point (i.e., on the vapor pressure line), it turns out that one cannot infer the correct relations for this point without fresh experimental data on the rate at which the various discontinuities tend to zero. However, the latest experimental results may confirm doubts as to the utility of the "discontinuity approach" to the transformation of liquid helium.

2. NOTATION AND BASIC EQUATIONS

Our variables are the internal energy, U, and—in the usual notation—p, V, S, and T. It is convenient to define

$$\sigma_x \equiv (\partial S/\partial T)_x, \quad \alpha_x \equiv (\partial V/\partial T)_x, \quad K_x \equiv (\partial V/\partial p)_x.$$

On an equilibrium line between two phases, $p=p(T)$,

---

*Now at Department of Chemistry, Duke University, Durham, North Carolina.

[1] E. F. Lype, Phys. Rev. **69**, 652 (1946).
[2] P. W. Bridgman, Phys. Rev. **70**, 425 (1946).
[3] R. Oldenburger, Phys. Rev. **70**, 433 (1946).
[4] P. Ehrenfest, Leiden. Comm. Suppl. 75b (1933).

put $\mu \equiv dp/dT$ and let $\sigma \equiv dS/dT$, $\alpha \equiv dV/dT$, etc., refer to differentiation along the line with, where relevant, σ_1 and σ_2, etc., referring to alternate sides of it. (When, for example, the entropy surface on the p, T plane has a "step," one may still, as in the Kirchhoff equation, give a meaning to the specific heats immediately on either side of the discontinuity.) Let $\Delta\omega \equiv \omega_2 - \omega_1$ for any variable ω.

For a first-order equilibrium, where p and T are continuous but not S and V, one has the Clausius-Clapeyron equation

$$\mu \Delta V = \Delta S.$$

We need the result of differentiating this equation:

$$\mu \Delta\alpha + (d\mu/dT)\Delta V = \Delta\sigma. \tag{2}$$

Also, from

$$\alpha = dV/dT = \alpha_p + \mu K_T,$$

we have

$$\Delta\alpha = \Delta\alpha_p + \mu \Delta K_T; \tag{3}$$

and from

$$\sigma = dS/dT = \sigma_p + \mu(\partial S/\partial p)_T = \sigma_p - \mu\alpha_p,$$

we have

$$\Delta\sigma = \Delta\sigma_p - \mu\Delta\alpha_p. \tag{4}$$

Equations (2), (3), and (4) are the generalized Ehrenfest equations: the formulas (1) for a second-order transition *line* (such as is thought to separate helium I and helium II in the phase diagram) result by putting ΔV and ΔS, and hence $\Delta\alpha$ and $\Delta\sigma$, equal to zero. As is well known, one can then show that, for any "x,"

$$\Delta\sigma_x = \mu\Delta\alpha_x. \tag{5}$$

Substituting Eqs. (3) and (4) in Eq. (2) gives a slight generalization of the equation introduced by Epstein:[5]

$$\mu^2 \Delta K_T + 2\mu\Delta\alpha_p + [(d\mu/dT)\Delta V - \Delta\sigma_p] = 0. \tag{6}$$

On a second-order line the term in $d\mu/dT$ vanishes, and the remaining quadratic in μ has equal roots. We shall see that this is also true of the critical point of the vapor-liquid equilibrium; but there seems to be no special significance in this vanishing of the discriminant, since Eq. (6) is merely a compatibility condition between Eqs. (2), (3), and (4), and both its roots need not satisfy these latter: we are concerned only with the one which does.

3. THE VAPOR-LIQUID CRITICAL POINT

The result sought is the degenerate form of Eqs. (1) to (4), when the various discontinuities tend to zero or infinity, as $T \to T_0$ along the equilibrium line. If $(T_0 - T)^{-n} \cdot f$ tends to a finite value, we write $f \sim t^n$, where $t = T_0 - T$. Now in the case of the vapor-liquid equilibrium, if T_0 is the critical temperature, it is known[6] that

$$\Delta V \sim t^{\frac{1}{2}}, \quad \Delta K_T \sim t^{-1}, \quad \mu \sim t^0. \tag{7}$$

From the first of Eq. (7), we have $\Delta\alpha \sim t^{-\frac{1}{2}}$ and hence from Eq. (2), $\Delta\sigma \sim t^{-\frac{1}{2}}$. Then Eq. (3) shows that $\Delta\alpha_p \sim t^{-1}$, and hence by Eq. (4), $\Delta\sigma_p \sim t^{-1}$. Thus, the terms which are negligible in Eqs. (2) to (4), in the limit, are just those which vanish on a second-order line; and hence we have

$$\left.\begin{aligned} \Delta\sigma_x &\to \mu\Delta\alpha_x \\ \Delta\alpha_p &\to -\mu\Delta K_T \end{aligned}\right\} \tag{8}$$

at the critical point. However, these expressions for μ are no more applicable than the Clausius-Clapeyron equation: the latter becoming the ratio of two zeros, the former of two infinities. By combining the two forms we obtain expressions in which the numerator and denominator remain finite. For example,

$$\left(\frac{dp}{dT}\right)^3 \to \frac{(\Delta S)^2 \Delta(\partial S/\partial T)_p}{(\Delta V)^2 \Delta(\partial V/\partial T)_p}, \quad \text{as} \quad T \to T_0. \tag{9}$$

As we have seen, there is no justification in this case for Lype's proposed alternative to Eqs. (8).

4. THE HELIUM LAMBDA-POINT

It is conceivable that the transition in liquid helium may be accompanied by a very small but finite latent heat and change in density (Ehrenfest's equations remaining approximately true along the line). We consider here the possibility that this is so, but that these discontinuities in entropy and volume vanish at the lambda-point, $T = T_0$, where the equilibrium line meets that of the vapor pressure.

That is, with μ remaining finite, we would have

$$\left.\begin{aligned} \Delta V &\sim t^n, \qquad \Delta S \sim t^n, \\ t &= T - T_0, \qquad n > 0. \end{aligned}\right\} \tag{10}$$

Then, whatever the value of n,

$$\Delta\sigma \to \mu\Delta\alpha. \tag{11}$$

Provided $\Delta\alpha_p$ and ΔK_T do not become infinite at T_0, from Eq. (3), $\Delta\alpha$ does not become infinite; and hence $n \geqslant 1$.[7] Then, from Eq. (10) $\Delta\sigma$, and hence from Eq. (4) $\Delta\sigma_p$ also, do not become infinite. Since this last conclusion is not obvious from the experimental results, it should be observed that it depends on $\mu = dp/dT$ not becoming infinite at T_0.

We have now to distinguish three possible cases:

(a) $n = 1$, and ΔK_T vanishes at T_0. Then Lype's equation $\Delta\sigma_p \to 2\mu\Delta\alpha_p$ holds.

[5] P. S. Epstein, *A Textbook of Thermodynamics* (John Wiley and Sons, Inc., New York, 1937), p. 131.

[6] L. Landau and E. Lifshitz, *Statistical Physics* (Oxford University Press, New York, 1938), p. 142.

[7] An analogous situation may occur, evidently, in the diagram of state of certain monolayers. D. G. Dervichian, J. Chem. Phys. 7, 931 (1939), Fig. 2.

(b) $n>1$, and any of $\Delta\alpha_p$, ΔK_T, $\Delta\sigma_p$ either does not vanish, or vanishes but not as fast as t^{n-1}. It then follows that all of $\Delta\alpha_p$, ΔK_T, and $\Delta\sigma_p$ vanish at the same rate, the left-hand sides of Eqs. (3) and (4) can be put equal to zero at T_0, and Eqs. (8) hold there.

(c) Whether $n>$ or $n=1$, in the limit the terms of Eqs. (3) and (4) remain all of the same order, in which case these equations are the simplest one has at the lambda-point.

The experimental evidence[8] indicates that, if "x" refers to the direction of the vapor-pressure curve, $\Delta\alpha_x\neq 0$ at T_0; and hence that not both of $\Delta\alpha_p$, ΔK_T are zero there. This evidence is from measurements of the density at intervals, in the neighborhood of the lambda-point, of 0.1 degree; and is not really sufficient to determine the behavior of the coefficients of expansion there. The variation of the specific heat[9] indicates that an important physical change occurs over a range of temperature within 0.1 degree of the lambda-point; and one might expect this change to be reflected in the density, and hence in sharp variations of the coefficients of expansion and the compressibility. The possibility is underlined by recent experiments,[10] which have revealed a sudden plung in the velocity of (first) sound in the liquid, in a somewhat smaller temperature interval.†

One naturally thinks of the possibility that the surfaces of V and S on the p, T plane actually form "stopping lines"‡ at the transition line (whether or not they are also discontinuous there) so that measurements of, say, K_T and α_p progressively closer to this line would lead to ever larger values, and formulas of the type considered above would not be applicable. This behavior is not, in fact, possible for the high temperature side of the transition line. For, from the equation preceding Eq. (3), since $\mu K_T>0$, $\alpha_p<\alpha$ and hence since α_p is positive on the high temperature side, it is *numerically* less than α there. Then α_p cannot become infinite along the transition line on this side (except at an isolated point, such as the lambda-point). This argument does not apply to the low temperature side, where $\alpha_p<0$; but there, again since α is finite, an infinite α_p implies an infinite K_T and would be expected to lead to "critical" opalescence. However, K_T and α_p might well become very much larger (numerically) over the last 0.1 degree, as the transition line is approached from below; so that it would not be practicable to apply equations relating the discontinuities, and in any case it would be equally relevant to the physical interpretation of the transition to treat it as extending over the critical temperature range, and investigate the relation between the continuous changes in the thermodynamic functions. Evidently, the present need is for more detailed experimental data on these changes: a closer examination of the variation in density of the liquid, along the vapor pressure line, seems especially desirable.

I am indebted to Mr. D. W. Sciama for introducing me to this problem and its literature, to Mr. H. N. V. Temperley for his critical reading of the manuscript, to Dr. K. R. Atkins and Mr. C. E. Chase for communicating their experimental results before publication, and to the D.S.I.R. for financial support.

[8] W. H. Keesom, *Helium* (Elsevier Publishing Company, Inc., New York, 1942), p. 207.

[9] Reference 8, p. 215.

[10] K. R. Atkins and C. E. Chase, private communication, Proc. Phys. Soc. (London), to be published.

† The relation of this change in velocity (at 14 megacycles) to that of $\rho^2 K_S$ may be complicated by relaxation effects, since the attenuation has simultaneously a sharp maximum. Also the data available (reference 10) at the time of writing might conceivably be wholly accounted for by variation of C_p in the formula

$$K_S=K_T+T\alpha_p^2/C_p,$$

with

$$\rho u_1^2=-V/K_S.$$

‡ The curve $y=-1/\ln x$, for example, has a stopping point (0, 0) where all the $d^n y/dx^n$ are infinite. Similarly, in three dimensions, the surface $z=-1/\ln f(x, y)$ has a stopping line $f(x, y)=0$.

The Coulomb Energy of Complex Crystals

EDWARD FISHER
Department of Physics, School of Mines and Metallurgy, University of Missouri, Rolla, Missouri
(Received May 14, 1951)

A method of computing Madelung constants is adapted to the problem of determining the electrostatic energy of complex ionic crystals.

INTRODUCTION

IN the application of chemical physics to theoretical problems in geology and ceramics a simple method is needed to estimate the cohesive energy of complex crystals. As an approximation these crystals are customarily assumed to be ionic. Then, by analogy with simple ionic crystals,[1] the principal contribution to the energy should come from coulomb forces.

A way of computing this coulomb energy is to use the method given by Slater[2] for obtaining successive approximations of the Madelung constants of simple crystals. In the application[2] to NaCl the first three approximations, for use with r_0, the cation-anion distance, are 1.457, 1.750, and 1.714, the correct value being 1.742. However, application of the same method to CsCl, still using a cubic cell, gives 1.155, 3.538, 0.508, and 3.594 as succesive approximations to the Madelung constant for use with the cube-edge length a_0.

In the present note an expression is derived for the error of each approximation. When only the first and third approximations for the energy of an ion in the field of its neighbors have been computed, this expression permits either a simple extrapolation to a better value for the energy if the error in the third approximation is not small, or an estimate of this error in case it is small.

THEORY

If the electrostatic energy W_i of each ion of charge Q_i in the field of all the other ions is known, then the coulomb energy of the crystal per unit cell is[1] $(1/2)\sum_i W_i$, where the sum is over all the ions of a unit cell. The energy W of an ion of charge Q in the field of its neighbors can be written

$$W/Q=\sum_j (Q_j/r_j) +\sum_n \sum_i Q_i\{1-[(x_i\partial/\partial x_0)+(y_i\partial/\partial y_0)+z_i\partial/\partial z_0] +(\ )^2/2!-(\ )^3/3!+(\ )^4/4!\cdots\}(1/r_n). \quad (1)$$

In forming Eq. (1) the neighborhood of Q is divided into two parts: a central cell with Q at its center, composed of one or more unit cells of the crystal, and all the rest of the crystal. The central cell gives the expression $\sum_j (Q_j/r_j)$ in Eq. (1), and the rest of the right hand side of (1) comes from all the other cells of the crystal by means of a multipole expansion.[3] That is, the sums $\sum_j$, $\sum_n$, and $\sum_i$ are taken over the ions of the central cell, excluding Q, the unit cells outside the central cell, and the ions of the nth unit cell, respectively. Q_j is the charge of the jth ion, multiplied by[2] 1, $\frac{1}{2}$, $\frac{1}{4}$, or $\frac{1}{8}$, according as the ion is inside, on a face, an edge, or a corner, respectively, of the central cell and likewise for Q_i and the nth unit cell. The faces of all the cells must be electrically neutral. The distances r_j and r_n are from Q to Q_j and from Q to center of nth cell, respectively. The coordinates x_i, y_i, z_i are those of Q_i with respect to the center of the nth cell, and x_0, y_0, z_0 are the coordinates of Q. The coordinate axes are parallel to the edges of the cells.

For the present purpose the crystal can be assumed similar in form to the central cell: then the terms $(\ )^{2k+1}/(2k+1)!$, $k=0, 1, 2, \cdots$, on the right side of Eq. (1) cancel out and $\sum_i Q_i=0$ for each unit cell.

Application of the multipole expansion[3] to the nth unit cell gives

$$\iiint_{(n)} (1/r)dv = \iiint_{(n)} \{1+(x\partial/\partial x)+(y\partial/\partial y)+(z\partial/\partial z) +(\ )^2/2!+(\ )^3/3!\cdots\}(1/r_n)dv$$
$$=\tau\{1+(1/6)[(a^2\partial^2/\partial x_0^2)+(b^2\partial^2/\partial y_0^2)+c^2\partial^2/\partial z_0^2] +\cdots\}(1/r_n). \quad (2)$$

In Eq. (2), (n) denotes integration over the nth unit cell. The coordinates x, y, and z of the element of volume dv are with respect to the center of the cell, and r is its distance from Q. The volume of a cell is τ, and its edges $2a$, $2b$, and $2c$.

By means of (2) Eq. (1) can be written

$$W/Q-\sum_j (Q_j/r_j) =(1/2\tau)\sum_i Q_i(x_i\partial/\partial x_0+y_i\partial/\partial y_0+z_i\partial/\partial z_0)^2 \times\{1-(1/6)(a^2\partial^2/\partial x_0^2+b^2\partial^2/\partial y_0^2+c^2\partial^2/\partial z_0^2) +(1/12)(x_i\partial/\partial x_0+y_i\partial/\partial y_0+z_i\partial/\partial z_0)^2 +4\text{th-and-higher derivatives}\}\iiint (1/r)dv. \quad (3)$$

[1] F. Seitz, *Modern Theory of Solids* (McGraw-Hill Book Company, Inc., New York, 1940), Chapter 2.
[2] J. C. Slater, *Introduction to Chemical Physics* (McGraw-Hill Book Company, Inc., New York, 1939), Chapter 23.
[3] J. A. Stratton, *Electromagnetic Theory* (McGraw-Hill Book Company, Inc., New York, 1941). Chap. 3.

The integration in Eq. (3) is over all the crystal outside the central cell.

By Gauss' theorem Eq. (3) is reduced to

$$(W/Q)-\sum_j (Q_j/r_j)$$
$$=(1/24\tau)\sum_i Q_i\{2[(x_i\partial/\partial x_0)+(y_i\partial/\partial y_0)+z_i\partial/\partial z_0]^2$$
$$\times[(a^2\partial^2/\partial x_0^2)+(b^2\partial^2/\partial y_0^2)+c^2\partial^2/\partial z_0^2]$$
$$-[(x_i\partial/\partial x_0)+(y_i\partial/\partial y_0)+z_i\partial/\partial z_0]^4$$
$$+\text{6th-and-higher derivatives}\}\int\int\int(1/r)dv. \quad (4)$$

The volume integral in Eq. (4) is over the central cell.

Now, in Eq. (4)

$$(1/\tau)\int\int\int(1/r)dv$$
$$=(1/8abc)\int_{-ka}^{ka}dx\int_{-kb}^{kb}dy\int_{-kc}^{kc}dz(1/r). \quad (5)$$

Here k is the order of the Slater approximation. For the first approximation $k=1$, and the central cell is a unit cell; for the second $k=2$, and the central cell has edges $4a$, $4b$, and $4c$, etc. If the fourth-order derivatives in Eq. (4) are assumed to be the dominant part of the expansion, then the right side of the equation is inversely proportional to k^2, the proportionality constant having one value for k even and another for k odd.

Hence, finally,

$$W/Q=\sum_k+\epsilon_k, \quad (6)$$

where $\sum_k$ is $\sum_j (Q_j/r_j)$ for the kth approximation, and $\epsilon_k \propto k^{-2}$, approximately, provided the fourth-order derivatives in Eq. (4) do not vanish. On the basis of Eq. (6) the following extrapolation is recommended: compute the first and third Slater approximations, skipping the second, which requires a different unit cell. Then

$$W/Q=\sum_3+(1/8)(\sum_3-\sum_1). \quad (7)$$

The foregoing application of multipole expansions could obviously be carried one step further so as to get directly the coulomb energy per unit cell, that is, $(1/2)\sum_i W_i$. However, the convergence of the series would be poorer, and therefore the extrapolation less accurate. Also, the sums $\sum_j(Q_j/r_j)$ would be more laborious, owing to the lack of symmetry, since the atoms Q would not now be at the center of the central cell.

Although the method is intended for complex triclinic crystals, it is instructive to test it on three simple lattices for which Madelung constants exist. For NaCl the fourth-order derivatives in Eq. (4) vanish. This accounts for the very good convergence found by Slater[2] for the successive approximations.

For CsCl the successive approximations, based on a cubic cell, do not converge because the cell faces are not electrically neutral. However, a unit cell can be found for which the cell faces are neutral, a rhombic dodecahedron bounded by the 110 planes. Then the first and third approximations to the Madelung constant are 1.30 and 1.81. And, from Eq. (7), $W/Q=1.87$. The correct value[1] is 2.035.

The third example is perovskite,[4] containing the ions A^+, B^{++}, and C^- according to the formula ABC_3. Applying Eq. (7) three times—for A, B, and C as cell-centers—leads to 12.56 for the Madelung constant for use with the cube-edge length a_0. The correct value[5] is 12.38. Using the third approximations directly without any extrapolation, one gets 12.25. From the details of the calculations it appears that this is due to the very symmetrical arrangement of the atoms. In such a case, where ϵ_3 is so small, the neglected terms in Eq. (4) are comparable with it, and there is no basis for the extrapolation. Then $W/Q\sim\sum_3$, and ϵ_3 serves to indicate the error in $\sum_3$.

[4] The author is indebted to Professor J. Rosenfeld for suggesting this example. Although very simple, it has interest in applications of chemical physics to geology.

[5] J. Sherman, Chem. Revs. **11**, 93 (1932).

Scintillations in the Diphenylpolyenes and Related Compounds*†

W. S. KOSKI AND C. O. THOMAS
Department of Chemistry, The Johns Hopkins University, Baltimore, Maryland
(Received July 25, 1951)

Scintillations in two series of structurally related organic compounds were investigated. One series was composed of the symmetrical diphenyl derivatives of ethane, ethylene, and acetylene. The other series consisted of the diphenyl polyenes from diphenyl to diphenyl octatetraene. In the first series it was found that the wavelength of the emission spectra ranged from 3550 to 4030A and the counting efficiency increased with the number of π-electrons in the system. In the second series the emission spectra wavelengths ranged from 3400A to 6000A and increased as one went up the series, whereas the counting efficiency went through a maximum at diphenyl butadiene. The results were interpreted in terms of the "metallic" model for conjugated compounds.

INTRODUCTION

NUMEROUS publications exist in the literature reporting the results of work done on organic crystals as nuclear radiation detectors. In the main, the various investigators have confined themselves to a study of such factors as efficiency, proportionality of pulse size and energy of the radiation, pulse duration, etc. None of these investigations were designed to make a systematic study of the influence of molecular structural factors on the performance of organic crystals as radiation detectors. We felt that such investigations might increase our understanding of nature of the fundamental processes involved when nuclear radiation interacts with such phosphors as well as giving us useful information as to the utility of these substances as detectors.

Published results in this field indicate that the nature of the binding in, and the dimensions of the molecules making up the phosphors are intimately connected with their performance as scintillators. For this reason we decided to investigate the performance of a series of structurally related organic compounds in which the dimensions and the binding could be varied more or less in a regular manner. Two series of organic phosphors immediately suggest themselves for such a study, (1) the diphenylpolyenes and (2) the fused ring compounds starting with benzene and going to naphthalene, anthracene, etc. Of these two series certain practical advantages such as ease of preparation, purification, and crystal growth favor the diphenylpolyenes. This investigation has been limited to a study of the structural factors mentioned above and the influence of such factors as impurities, crystal imperfections, etc., is not being considered at this time, and it is hoped that their effects have been eliminated or at least held constant by careful purification of the materials in question and the use of small selected crystals so that a high degree of crystal perfection might be attained.

EXPERIMENTAL METHOD

The diphenylpolyenes and related compounds used in this work were synthesized in this laboratory, and the crystals made from this source of raw material gave to within ± 4 percent the same counting rate as did corresponding crystals which were made from raw materials that had a different origin. The raw materials, with the exception of diphenyl octatetraene and diphenyl diacetylene were further purified by three recrystallizations from appropriate solvents and finally by a vacuum distillation. The octatetraene and diacetylene derivatives were subjected to a similar recrystallization procedure using ethyl acetate and methyl alcohol, respectively. The last traces of the solvent were removed by pumping; however, these materials were not vacuum distilled because of their tendency to decompose at temperatures appreciably above their melting points. All crystals were prepared by slow cooling of the appropriate melt in a nitrogen atmosphere. In the cases of the higher members of the series, care was taken not to heat the melts more than two degrees above the melting points, in order to keep thermal decomposition to a minimum. The diphenyl hexa and octatetraene crystals were clear and colored light yellow and golden yellow, respectively. The diphenyl butadiene crystals tended to be slightly cloudy. All the other crystals were clear and colorless. The crystals were cut and polished to the final dimensions of $1.5 \times 4.6 \times 6.5$ mm. All linear dimensions were held to within 3 percent of these figures.

Each of the crystals was then mounted in a reproducible geometry under a 5819 photomultiplier tube and its counting rate as a function of the discriminator bias was determined. Co^{60} was used as a γ-ray source. The potential divider and amplifier circuits used were similar to those used by Marshall, Coltman, and Bennett.[1] The discrimination of the pulses was made with a pulse height discriminator,[2] using a Schmitt trigger type circuit followed by a scale-of-1000 counter.

* This work was performed under the auspices of the AEC.
† Abstracted in part from a thesis to be submitted by Carl O. Thomas in partial fulfillment of the requirements for the degree of Doctor of Philosophy in The Johns Hopkins University.

[1] Marshall, Coltman, and Bennett, Rev. Sci. Instr. 19, 744 (1948).
[2] Higinbotham, Gallagher, and Sands, Rev. Sci. Instr. 18, 706 (1947).

The fluorescence spectra of these crystals were taken with a small Hilger quartz spectrograph using Eastman 103-O plates for all crystals except the diphenyl hexa and octatetraenes in which cases Eastman 103a-D plates were used. Copper x-rays were used as sources of excitation. In addition, the emission spectra of stilbene, anthracene, and diphenylacetylene were measured when Ra γ's, Poα's, and S^{35} β's were used as sources of excitation. The material to be studied was fastened directly over the slit of the spectrograph. The slit width was 0.1 mm. Exposures varied from a few minutes for the x-rays to several days with some of the other sources. The wavelengths were determined by comparison with a standard mercury spectrum.

DISCUSSION OF RESULTS

The counting rates *vs* discriminator bias curves for the various crystals studied are summarized in Fig. 1. For purposes of comparison, the curve for an anthracene crystal of the same geometry is included.

The spectroscopic data are summarized in Table 1 and in the densitometer tracings of Figs. 2 and 3. The positions of the emission bands in the spectrum are independent of the mode of excitation in the cases of stilbene, anthracene, and diphenylacetylene when Ra γ's Po α's, S^{35} β's, and x-rays were used. This is very probably true of all the crystals. This observation is in agreement with results previously reported by the authors[3] and by other investigators.[4]

The compounds that we are considering can be best discussed in terms of the following general structural formula for the diphenylpolyenes in which m is an integer running from zero for diphenyl to four for

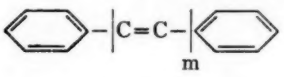

diphenyl octatetraene. It is convenient to divide the crystals into two series. The first series is composed of the diphenyl derivatives of ethane, ethylene, and acetylene. In this series we are increasing the number of electrons in the linkage between the two carbon atoms holding the phenyl rings. The over-all lengths of the three different molecules are about the same. Examination of Fig. 1 indicates that the counting efficiency increases as one goes in this series from the ethane to the ethylene and then to the acetylene derivative. Figure 3 indicates that the emission from these three crystals falls in approximately the same spectral region so the order of the counting efficiencies will be the same as the order of the emission intensities. This is further supported by a comparison of the densities of these emission bands on photographic plates which had been calibrated with a standard lamp enabling us to make corrections for the varying spectral sensitivity of the plates. These experimental results then indicate that if

[3] W. S. Koski and C. O. Thomas, Phys. Rev. **79**, 217 (1950).
[4] Louise Roth, Phys. Rev. **75**, 983 (1949).

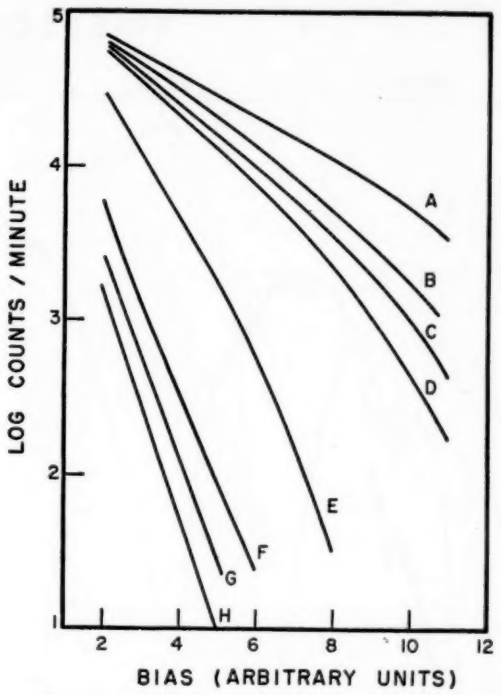

FIG. 1. Discriminator curves for some diphenylpolyenes and related compounds using Co^{60} as a γ-ray source. (A) anthracene, (B) diphenyl butadiene, (C) diphenyl acetylene, (D) stilbene, (E) diphenyl ethane, (F) diphenyl, (G) diphenyl hexatriene, and (H) diphenyl octatetraene.

one keeps the length of the molecule constant and increases the number of π-electrons in the system, that the scintillation intensity increases.

The second series of compounds is the one starting with diphenyl ($m=0$) and going in whole numbers to $m=4$ (diphenyl octatetraene). In this series one is varying the number of π-electrons between the rings and at the same time varying the over-all length of the system. Figure 1 indicates that in this case the counting efficiency using a 5819 increases and goes through a maximum at diphenyl butadiene and then decreases as one goes to higher members of the series. The diphenyl

TABLE I. Wavelengths of emission bands of some organic crystals. Source of excitation-copper x-rays.

Material	Wavelength (A)
Diphenyl	3420
Diphenyl ethane	3410 (weak)
	3550
	3730
	3910 (weak)
Stilbene	3800
	4030
Diphenyl acetylene	3620
	3760
	3980 (weak)
Diphenyl butadiene	4390
	4575
Diphenyl hexatriene	5220
	5915 (weak)
Diphenyl octatetraene	5480
	6000

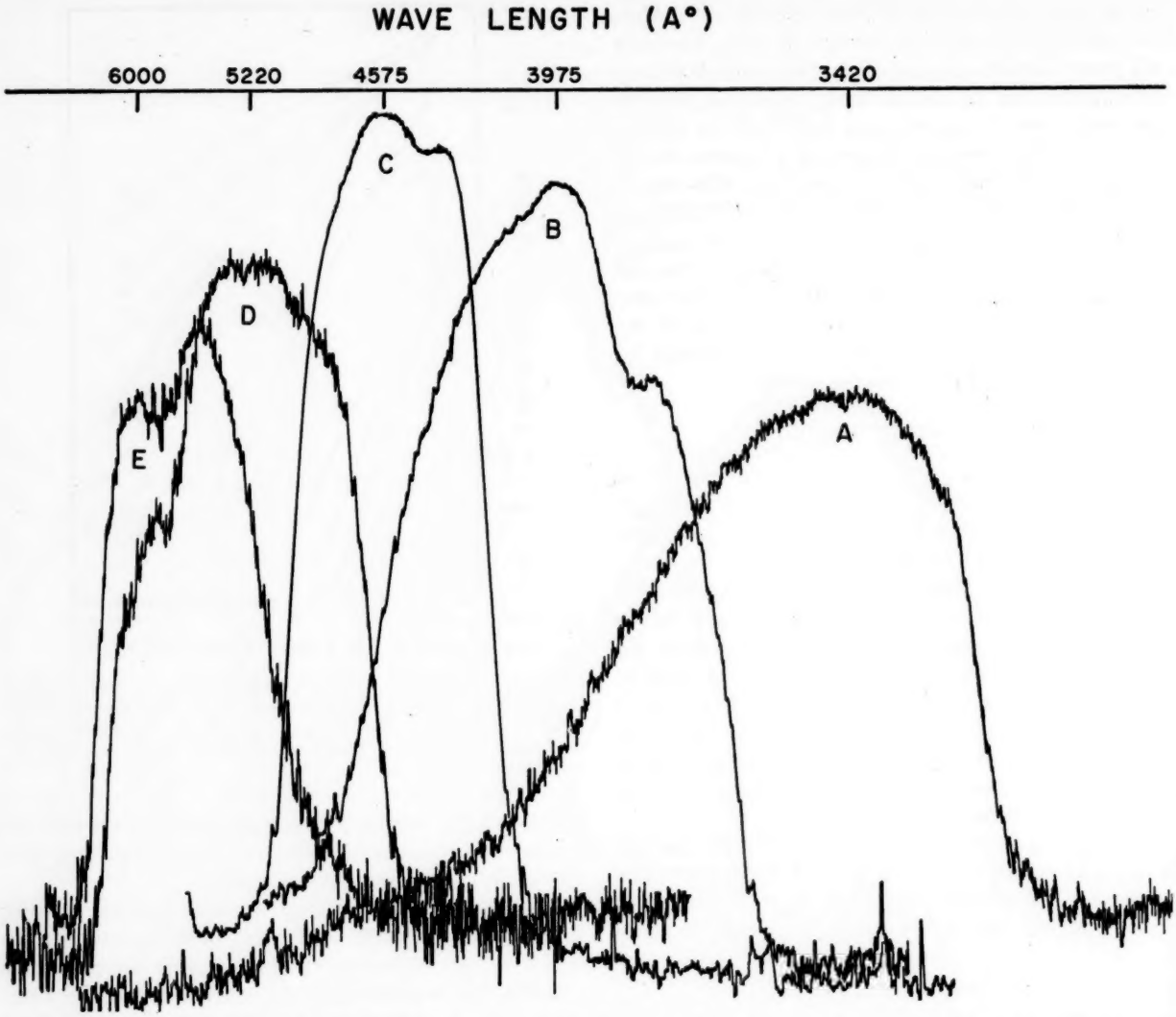

FIG. 2. Densitometer tracings of the emission spectrograms obtained with the following crystals. Copper x-rays were used as a source of excitation. (A) diphenyl, (B) stilbene, (C) diphenyl butadiene, (D) diphenyl hexatriene, and (E) diphenyl octatetraene.

octatetraene crystal gives a counting rate that is hardly distinguishable from background as far as the 5819 photomultiplier tube is concerned. One of the main reasons for this type of behavior is clear from the data in Table I and Fig. 2. As one proceeds up the series, the wavelengths of the emission bands shift toward the red. Since the peak sensitivity of the tube used in this work is in the region of 4500A and drops off fairly rapidly on each side (*S*-9 response), one would expect then to get a maximum in the counting rate as one proceeded from the lowest to the highest member of the series of diphenyl polyenes investigated in this work.

Another factor that contributes to the general behavior of the light emission of these crystals is determined by the relative role played by various competitive processes that lead to quenching of the fluorescence. Fluorescence and absorption in the diphenylpolyenes have been investigated in considerable detail by Hauser, *et al*,[5,6] and others and it has been found that the fluorescence yield becomes very low for $m>3$. This has been interpreted as due to the increasingly important role played by quenching processes as one goes to longer chain molecules.

Probably a better insight into the qualitative behavior of the variation of the intensity and wavelength of the emission bands reported here can be gained by application of the simplest form of the "metallic" model for conjugated molecules to the compounds studied in this work. This model, which assumes that the π-electron composing the conjugated double bonds have free mobility along the conjugated chain and that they behave as a one dimensional Fermi gas in a uniform potential energy, has been recently used to explain the absorption spectra of the diphenylpolyenes

[5] Hauser, Kuhn, and Kuhn, Z. physik. Chem. (B) **29**, 384 (1935).
[6] Hauser, Kuhn, and Smakula, Z. physik. Chem. (B) **29**, 417 (1935).

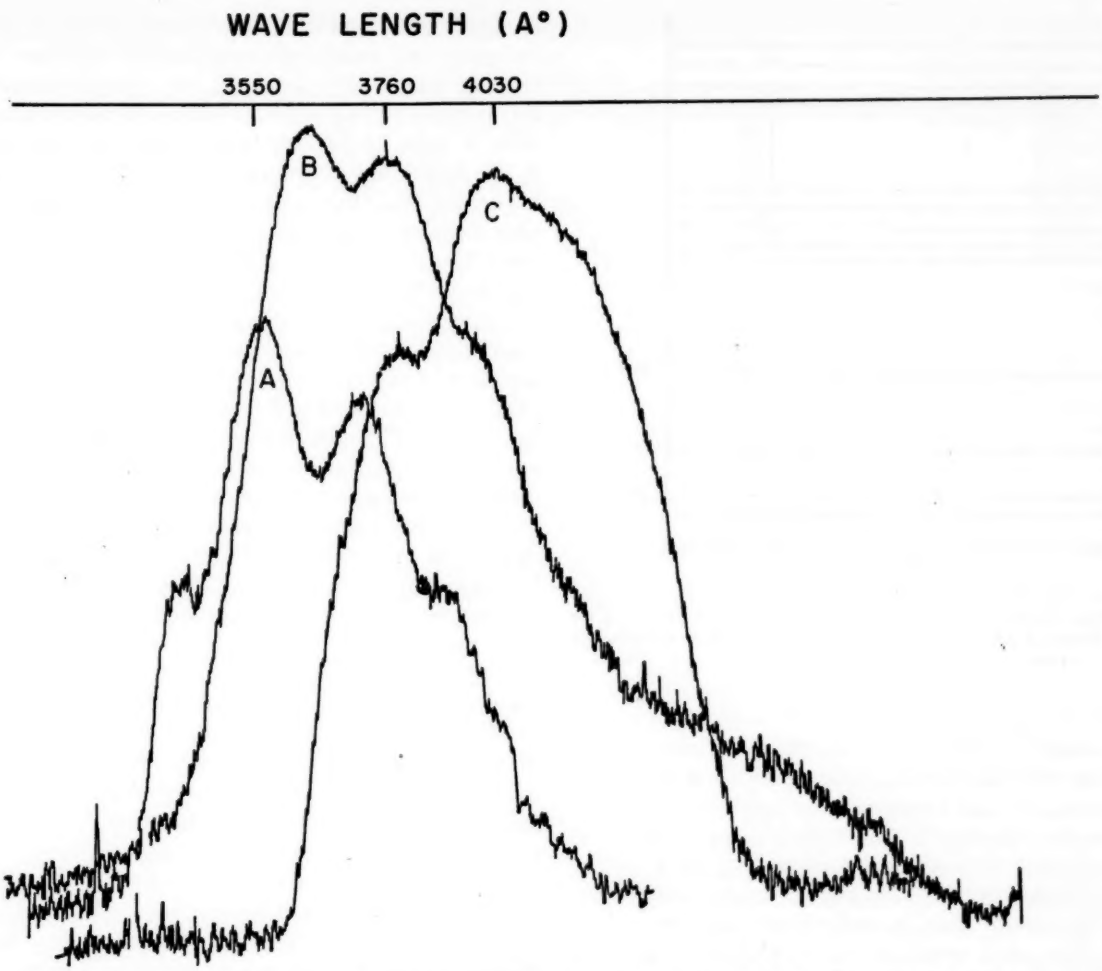

FIG. 3. Densitometer tracings of the emission spectrograms obtained with the following crystals. Copper x-rays used as a source of excitation. (A) diphenyl ethane, (B) diphenyl acetylene, and (C) stilbene.

and similar compounds.[7–9] A schematic representation of the model for a conjugated compound having eight π-electrons is given in Fig. 4. Some possible absorption transitions are indicated by dotted arrows and some fluorescence transitions by solid arrows. The vibrational structure for only two of the electronic levels is illustrated. Following the presentation of Bayliss the frequency of the most probable absorption is given by

$$\nu(N\rightarrow N+1)=(B/L)^2(2N+1),$$

and the intensity of this transition in terms of oscillator strength is given by

$$f\approx 0.134(2N+1),$$

where $2N$ is the number of π-electrons in the molecule and L is the effective length over which the π-electrons can migrate. In view of the fact that the absorption and fluorescence are generally assumed to involve transitions between the same electronic levels, the wavelength of the fluorescence bands would be expected to increase as one proceeds from the shorter to the longer members of the series just as the absorption wavelengths do and as is indicated by the first equation above.

The second equation, on the other hand, indicates that the absorption intensity increases with increase in number of π-electrons and a similar behavior would be expected of the fluorescence if competing (quenching) processes were absent, since in such a case all of the energy used to excite the molecule to the $N+1$ level could be re-emitted in the form of radiation. In our first series of compounds where the length was roughly constant the fluorescence appears to increase with increase in number of π-electrons. This does not imply the absence of quenching processes but merely that their effects are roughly the same in the three crystals. In the second series where the number of electrons and the length is varied the emission goes through a maximum, presumably because the quenching processes become more important for the longer molecules. Therefore, the counting efficiency of this series of

[7] N. S. Bayliss, J. Chem. Phys. **16**, 287 (1948).
[8] W. T. Simpson, J. Chem. Phys. **16**, 1124 (1948).
[9] H. Kuhn, J. Chem. Phys. **16**, 1198 (1949).

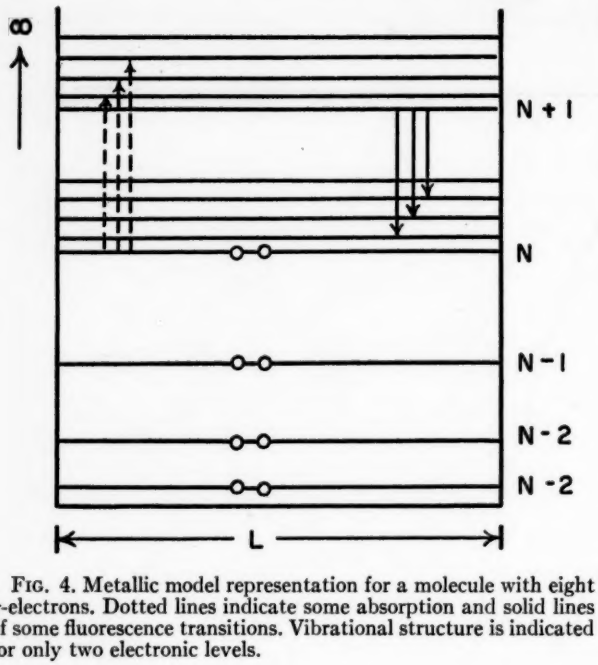

FIG. 4. Metallic model representation for a molecule with eight π-electrons. Dotted lines indicate some absorption and solid lines of some fluorescence transitions. Vibrational structure is indicated for only two electronic levels.

crystals is expected to go through a maximum, not only because of the narrow spectral response of the multiplier and the shifting in wavelength of the emission bands, but also because of the presence of competing processes inherent in the crystals themselves.

Our investigation of the corresponding series in the diphenyl polyacetylenes has not proceeded sufficiently far to give more than a preliminary statement. The peak in this series seems to come at diphenyl acetylene, since the only other member of this series that we have examined, i.e., diphenyl diacetylene is a poor scintillator, although the position of its emission spectra does not differ too greatly from diphenyl butadiene as far as wavelength is concerned. The higher members of the polyacetylene series have not been synthesized as yet.

There are several other compounds related to stilbene that we had occasion to examine, and although they are not good scintillators, a few comments concerning them might be of interest to investigators in the field. Some of the unsymmetrical phenyl derivatives of ethylene, such as triphenyl ethylene, were examined for their scintillation properties and they did not give promise as good counters, not only from the point that their scintillation efficiency was low, but also because such unsymmetrical compounds have strong tendencies to supercool, and consequently, are difficult to grow into crystals. The symmetrical derivatives of ethylene, on the other hand, are relatively easy to grow into crystals; and in addition to stilbene, which is in this category, we examined tetraphenyl ethylene. Good crystals were easily obtained, but the performance of this compound as a counter was much poorer than stilbene in spite of the fact that its emission spectra was in the 4500A region, matching the 5819 fairly well.

In comparing the counting efficiencies of our crystals with those of other investigators[10] we find general agreement in all cases except diphenyl acetylene. Sangster and Irvine have found that diphenyl acetylene is a less efficient counter than stilbene. Engelkemeir and Freedman[11] have obtained similar results. On the other hand, we observe that diphenyl acetylene is superior to stilbene as a counter and like results have been reported by others.[12] This disagreement may be due to the presence of small amounts of impurities in the diphenyl acetylene. In some preliminary experiments in which we added small amounts (less than 1 percent) of organic impurities to the diphenyl acetylene we found that if the impurity had a strong absorption band in the fluorescence region of the phosphor and at the same time the impurity did not fluoresce strongly itself, it could have a deleterious effect on the phosphor. Such a molecule is tetraphenyl ethylene. The poor fluorescence yield of this material is very likely due to steric effects of the four phenyl groups which twist the molecule out of the planar configuration. Addition of small amounts of this material to stilbene or diphenyl acetylene strongly affects the counting efficiency. Other methods of quenching the fluorescence exist, however, we mention this method since it is possible that during the synthesis of diphenyl acetylene from diphenyl ethane sterically hindered bromide derivatives might occur as impurities and hence be responsible for the discrepancies mentioned above.

ACKNOWLEDGMENT

The authors acknowledge their indebtedness to Professor J. D. H. Donnay for the use of his x-ray machine, to Professor E. B. Reid for supplying us with the raw material for several of the organic crystals used in this work and to Professor T. H. Berlin for some very informative discussions of the theoretical aspects of the problem. We are also indebted to Mr. R. C. Sangster and Professor John Irvine, Jr., of the Massachusetts Institute of Technology for supplying us with our initial samples of diphenyl hexatriene and diphenyl octatetraene and for a highly purified sample of stilbene.

[10] R. C. Sangster and J. W. Irvine, Jr. (private communication).
[11] D. W. Engelkemeir and M. S. Freedman (private communication).
[12] Ravilious, Elliot, and Liebson, Phys. Rev. **77**, 851 (1950).

Optical Absorption and Photoconductivity of Amorphous and Hexagonal Selenium*

M. A. GILLEO
Laboratory for Insulation Research, Massachusetts Institute of Technology, Cambridge, Massachusetts
(Received May 11, 1951)

In amorphous and hexagonal selenium optical absorption and photoconductivity were studied in their dependence on temperature. The absorption edge shifts for amorphous selenium toward shorter wavelengths with decreasing temperature. For a temperature change from 300° to 90°K and a layer thickness of 98μ, for example, a shift from 6600 to 6100A is observed at an optical density of 3; for higher densities (shorter wavelengths) the shift is smaller. It can be shown that this shift is related to the thermal excitation of vibrational levels. At higher temperatures the population of the higher vibration levels increases and the separation of these from the excited state diminishes.

At low temperature (*ca* 90°K) photoconductivity is observed only after the light quanta exceed 2.5 ev and the absorption coefficient has reached 10^5 cm^{-1}. Increase of temperature brings about a shift of the photoconductive threshold toward longer wavelengths, paralleling the absorption-edge shift. The absorption coefficient has been followed over the wavelength range 6900 to 2100A; its values at the end points of this range are 1.6×10^2 and 5.2×10^5 cm^{-1}, respectively; there is a slight maximum at 2600A where the absorption coefficient reaches 5.6×10^5 cm^{-1}.

The transformation of amorphous into hexagonal selenium by heat brings about an increase of the optical absorption in the 5000 to 7200A region and the appearance of a distinct hump in the absorption edge at 5200A. Decrease of temperature sharpens the hump and causes a decrease of absorption at all wavelengths in the 4000 to 7200A range except in the vicinity of the hump. In hexagonal selenium photoconductivity is observed at wavelengths as long as 7500A for films 0.5μ thick. A peak in the photoresponse is found where the optical density of these films reaches *ca* 1 (10 percent transmission). It can be shown that this behavior is to be expected for a bimolecular law of recombination of electrons and holes when their inhomogeneous distribution is taken into account. With decreasing temperature the peak response shifts consequently toward shorter wavelengths with the absorption edge.

INTRODUCTION

THE interrelation between chemical bonding, structure, and the electrical and optical properties of substances is one of the broad interests of this laboratory. These interrelations in group VI_b of the periodic system of elements have been discussed by von Hippel.[1] The case of selenium is of particular interest since its four polymorphic forms[2] show rather different optical absorption, conductivity, and photoconductivity. Two monoclinic forms (α and β), a hexagonal (metallic), and an amorphous (red) form are known. Se_8-ring molecules are the constituents of the α-monoclinic form;[3] Se_8 chains compose the β-modification.[4] The hexagonal form[5] consists of parallel chains of selenium atoms, while the amorphous form presumably is a random structure of chains[1,6] with perhaps a few ring molecules present.[7] Of these forms only the hexagonal shows much conductivity (5×10^{-5} mho cm^{-1} along the *c* axis and perhaps 100 times less perpendicular to the chain direction[8]) and may be classified as a semiconductor.

In hexagonal selenium each atom is connected by two covalent bonds to its two nearest neighbors in the chain. In addition, it is bonded to four selenium atoms located in three adjacent chains at bond distances which are shorter than the van der Waals distance. This situation and the resultant semiconductivity have been tentatively explained by von Hippel[1] on the basis that a third resonating *p* bond forms and the electronic charge projected out of the chain for this purpose leaves holes behind in the chain which are available for conduction.

The optical absorption and photoconductivity of selenium have been studied extensively, although often as independent phenomena. In the amorphous form it was observed that optical absorption begins at the wavelength of red light and rises steadily toward shorter wavelengths.[9] The absorption edge was found to be temperature-sensitive in that it moves toward shorter wavelengths with temperature decrease;[10] the cause of the shift has remained obscure.

Photoconductivity in the amorphous form was so small that it was frequently regarded as being absent.[11]

* Sponsored by the ONR, the Army Signal Corps, and the Air Force under ONR Contract N5ori-07801. In part from a thesis submitted in partial fulfillment of the requirements for the degree of Master of Science in Electrical Engineering at the Massachusetts Institute of Technology.

[1] A. von Hippel, J. Chem. Phys. **16**, 372 (1948).

[2] See, for example, G. P. Barnard, *The Selenium Cell* (Richard R. Smith, Inc., New York, 1930), and J. W. Mellor, *Inorganic and Theoretical Chemistry* (Longmans, Green and Co., New York, 1940).

[3] R. D. Burbank, Acta Cryst. **4**, 140 (1951).

[4] R. D. Burbank, Tech. Rept. 43, ONR Contract N5ori-07801, Laboratory of Insulation Research, Massachusetts Institute of Technology (April, 1951).

[5] A. J. Bradley, Phil. Mag. **48**, 477 (1924); M. K. Slattery, Phys. Rev. **25**, 333 (1925).

[6] See, for example, H. Hendus, Z. Physik **119**, 265 (1942).

[7] P. K. Weimer, Phys. Rev. **79**, 171 (1950).

[8] F. de Boer, Philips Research Rept. **2**, 352 (1947); a conductivity ratio for directions parallel and perpendicular to the *c* axis of 30 has been found by W. Sigrist, Progress Rept. III, ONR Contract N5ori-78, Laboratory for Insulation Research, Massachusetts Institute of Technology (May, 1948).

[9] See, for example, R. W. Wood, Phil. Mag. **3**, 607 (1902); A. Becker and I. Schaper, Z. Physik **122**, 49 (1944); K. Foersterling V. Fréedericksz, Ann. Physik **43**, 1227 (1914); G. P. Barnard, see reference 2.

[10] G. Mönch, Physik Z. **40**, 487 (1939); A. Becker and I. Schaper, see reference 9.

[11] See G. P. Barnard, reference 2; A. L. Hughes and L. A. DuBridge, *Photoelectric Phenomena* (McGraw-Hill Book Company, New York, 1932). B. Gudden and R. Pohl, Z. Physik **35**, 243 (1925), showed the red monoclinic form to be photoconductive in contradiction to prior claims.

Hexagonal selenium, on the other hand, has long been known for its prominent photoconductivity.[12] The maximum photoconductive response, located in the red region of the spectrum, shifts to shorter wavelengths with decrease of temperature.[13] The temperature dependence of the optical absorption of metallic selenium has received little attention; room temperature data[14] are not extensive, probably because of the difficulty of producing good, thin films.

The work to be reported here was undertaken in the hope that the origin of the temperature shift of the absorption edge in amorphous selenium might be understood, and that the nature of its photoconductivity might be more fully determined. In addition, we hoped to find a connection between optical absorption and photoconductivity in metallic selenium through the temperature dependence of both phenomena.

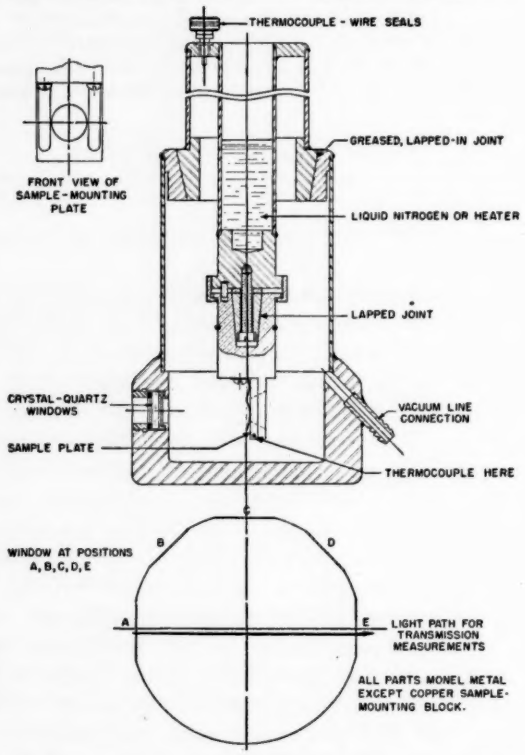

FIG. 1. Cross-sectional view of temperature controlled sample holder for optical absorption measurements.

I. EXPERIMENTAL PROCEDURE

A. Production of Selenium Films

All selenium films were prepared by vacuum deposition on glass, fused quartz, or rock-salt bases. High-purity selenium,† which showed only spectroscopic traces of sodium, potassium, magnesium, and copper, was employed; the latter two elements may have been present in the arc electrodes used in the analysis. Deposition took place at pressures between 3 and 10×10^{-5} mm Hg.

Film thickness determinations were carried out by weighing the slides on a microbalance before and after deposition. Since the thinnest film (0.03μ) weighed about 80μg, the weighing error of $\pm5\mu$g yielded a weighing accuracy always better than ±6 percent. The density of amorphous selenium was taken as 4.26.[2]

Hexagonal selenium films were obtained from amorphous selenium films by heat transformation at a temperature of 90° to 100°C in vacuum without excessive sublimation. Transformation after formation of nuclei is more rapid at temperatures greater than 90°C at which the nucleation rate reaches a maximum.[15] A semitransparent platinum film under the selenium was found to promote the transformation at room temperature so that the major portion was changed within a space of 2 years in one instance. In addition, holes do not develop as readily in thin layers during transformation when the selenium film is backed by platinum.

B. Optical Absorption

Optical-density *vs* wavelength curves were obtained for all specimens by means of a recording spectrophotometer‡ with a useful optical-density¶ range from 0 to 3.2 and a wavelength range from 2100 to 7000A. The optical density could be read with a precision of ±0.002; noise contributed fluctuations of ±1 percent. The quartz double monochromator in this instrument reduced stray light to a negligible amount; the spectral bandwidth between the half-intensity points ranged from <4A for $\lambda<5000$A to 30A at 7000A. The wavelength accuracy was ±5A for $2100\text{A}<\lambda<4000$A and ±10A for $4000\text{A}<\lambda<7000$A with reproducibility errors of about one fifth of the wavelength errors.

Optical absorption data for room temperature were obtained with the specimen in air. For other temperatures the specimen was mounted in an evacuated chamber and its temperature determined by that of a copper sample plate (Fig. 1) with which it was maintained in good thermal contact by low vapor pressure grease.§

[12] G. P. Barnard, see reference 2, A. L. Hughes and L. A. DuBridge, see reference 11; B. Gudden, *Lichtelektrische Erscheinungen* (Verlag. Julius Springer, Berlin, 1928).

[13] D. S. Elliott, Phys. Rev. **5**, 53 (1915) observed a shift of 600A of the peak of response toward short wavelengths for a temperature drop from room temperature to −190°C; E. O. Dieterich, Phys. Rev. **8**, 191 (1916), observed a shift of the peak toward long wavelengths with temperature rise above room temperature; A. Becker, Z. Physik **112**, 629 (1939) and **114**, 342 (1939) and B. Lange, Phys. Z. **32**, 850 (1931), among others, have made observations of temperature-dependent behavior of spectral response in barrier-layer-type selenium photocells. This type of cell behaves in quite a complicated manner which cannot be readily interpreted.

[14] A. H. Pfund, Phys. Rev. **28**, 324 (1909); A. Becker and I. Schaper (see reference 9); K. Foersterling and V. Fréedericksz, see reference 9 (reflection measurements).

† American Smelting and Refining Company, New York, N. Y.

[15] A. von Hippel and M. C. Bloom, J. Chem. Phys. **18**, 1243 (1950).

‡ Model 12M, Applied Physics Corporation, Pasadena, California.

¶ Optical density is defined as $(\log_{10}I_0/I)$ where I_0 is the intensity of the incident light and I the intensity of the transmitted light.

§ N. Apiezon, James G. Biddle Company, Philadelphia, Pennsylvania.

Some extraneous absorption was encountered at low temperature for wavelengths less than 3000A as a result of condensation of oil vapor on the specimen surface in spite of the inclusion of traps in the vacuum-pump lines.

Two procedures were employed in the determination of the value of the absorption coefficient $\alpha(\lambda)$. This coefficient is defined by

$$I/I_0 = \exp[-\alpha(\lambda)d],$$

where d is the thickness of the material and I_0 and I are the incident and transmitted light intensities, respectively, of wavelength λ. When several specimens were available of such thickness that each could provide a point suitably free from interference effects at the wavelength λ, $\alpha(\lambda)$ was determined from the slope of the density *vs* thickness plot. Above an optical density of *ca* 1.3 interference effects are negligible.

At long wavelengths, for which the absorption index is so small that its effect upon the reflection losses may be neglected, another procedure was used. Reflection losses were determined by observing the asymptote approached by the optical-density *vs* wavelength curve at long wavelengths. This density was then subtracted from the optical densities observed at shorter wavelengths. The remaining optical density was assumed to represent absorption only. In order to minimize the effect of a gradual increase of the index of refraction toward short wavelengths and the effects of multiple reflections, this method was applied only to density readings $>$ *ca* 1.3. The first method is probably the more accurate, but it requires that many specimens of different thickness be used in a region of rapidly varying optical density.

C. Photoconductivity

Selenium films for photoconductivity measurements were prepared by carrying out the vacuum deposition of selenium, as previously described, on a quartz surface upon which an interlocking gridwork had been drawn in Aquadag|| and baked on.

Conductivity changes produced by steady irradiation were measured in terms of current changes for a constant potential difference between the Aquadag grids. When modulated radiation was employed, interrupted for half-cycle intervals at a rate of 60 cps, the conductivity changes were observed by means of an electrometer tetrode.** It amplified the voltage fluctuations across a 10^8-ohm resistor in series with the photoconductor and a battery. The auxiliary amplification system had a bandwidth for noise of about 5 cps so that current fluctuations of less than 10^{-13} amp were detectable.

|| Acheson Colloids Corporation, Port Huron, Michigan.
** Type VX-41A, Victoreen Instrument Company, Cleveland, Ohio.

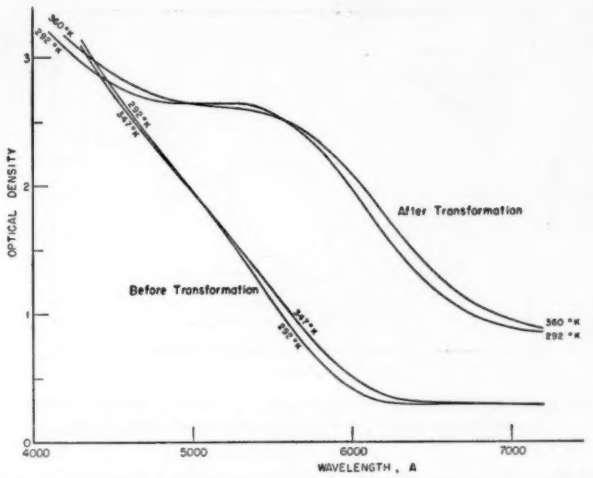

FIG. 2. Optical density *vs* wavelength curves for amorphous selenium film (*ca* $\frac{1}{4}\mu$ thick) over platinum film on glass before and after heat transformation.

II. EXPERIMENTAL RESULTS

A. Optical Absorption of Amorphous and Hexagonal Selenium

Amorphous selenium, a random structure of chains, transforms, upon heating, into the relatively well-conducting hexagonal modification. The optical effects

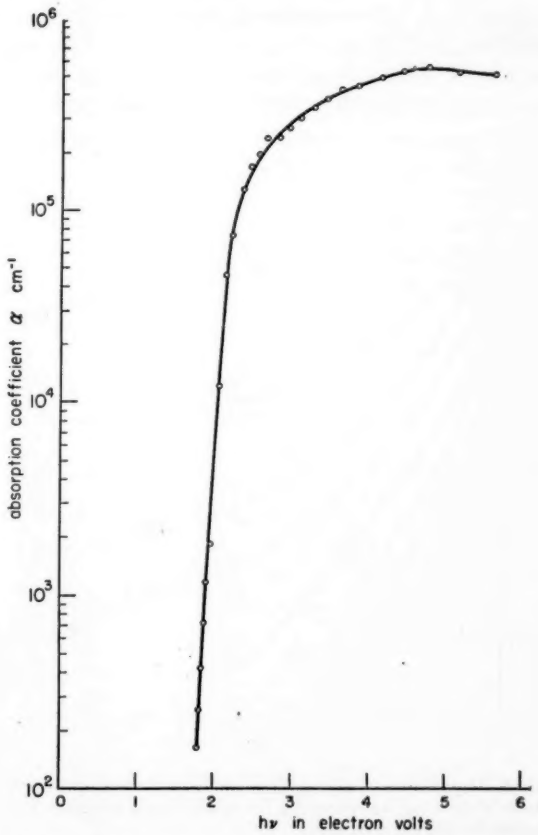

FIG. 3. Coefficient *vs* $h\nu$ for vacuum-deposited amorphous selenium at 295°K.

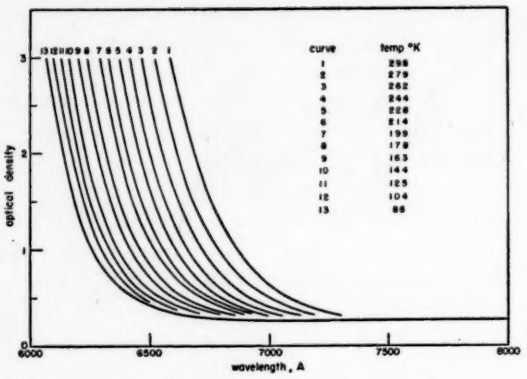

FIG. 4. Optical density *vs* wavelength at several temperatures of amorphous selenium film, 98μ thick, on NaCl base.

of the structure change are an increased absorption for wavelengths >4500A and the introduction of a distinct hump into the previously smoothly rising curve near 5000A (Fig. 2).

Only for amorphous selenium was it possible at the time of these experiments to obtain extremely thin films and thus to extend the measurements into the region of very high absorption at short wavelengths (Fig. 3). Films ranging in thickness from 0.03 to 98μ were employed. In Fig. 3, logα has been plotted as a function of $h\nu$ in ev in order to illustrate more clearly the existence of an "absorption edge." The position of this absorption edge corresponds roughly to the Se—Se bond strength 57.6 kg cal/mole[16] or 2.5 ev. The representation of α as a function of λ, used in general for convenience, makes this edge much less obvious.

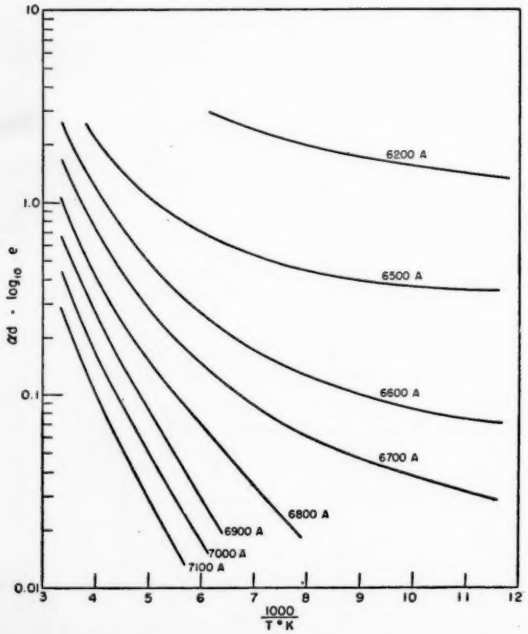

FIG. 5. Logarithm of absorption coefficient *vs* reciprocal temperature at several wavelengths for amorphous selenium film of thickness $d=98\mu$ on rock salt.

[16] L. C. Pauling, *The Nature of the Chemical Bond* (Cornell University Press, Ithaca, N. Y., 1940).

The agreement of these values with the results of previous observers is not very good. This may be partly a result of the fact that specimens prepared by sputtering or casting[17] might differ somewhat from those obtained by vacuum deposition.

In order to clarify mechanisms leading to optical absorption, its temperature dependence was studied for the amorphous and hexagonal forms. In both cases it was observed that decrease of temperature shifted the absorption edge toward shorter wavelengths. In amorphous selenium the temperature dependence was most pronounced in the wavelength region for which α was $<10^3$ cm^{-1} (Fig. 4); for $\lambda<3000$A, where α exceeds 10^5 cm^{-1}, little temperature dependence was noted.

The general features of this temperature dependence may be explained in terms of the effect of vibration upon the absorption spectra of the molecules composing the film. At short wavelengths the absorption takes place from the ground state. The ground state population is far greater than that of the vibrational levels at room temperature and below. Since the absorption is proportional to the number of absorbing molecules, absorption in this state is large and shows little temperature dependence. The vibrational level population is approximately governed by a Boltzmann factor so that absorption in these levels contains the factor $\exp(-nh\nu_0/kT)$. Here n is the vibrational quantum number for the vibration frequency ν_0. On the long wavelength tail the absorption of the temperature-dependent vibrational levels dominates since the transition probabilities are higher for them. Thus the temperature dependence for long wavelengths becomes more pronounced than for shorter. Moreover, for a given wavelength the rate of decrease of logα with increase of reciprocal temperature will be a steadily decreasing quantity because of the Boltzmann factors. The conclusions reached in this way are in agreement with the observations presented in Fig. 5. They will be rendered somewhat more precise in the discussion at the end of this paper.

In the case of hexagonal selenium, temperature dependence studies had to be limited at present to films in the thickness range $\frac{1}{4}$ to $\frac{1}{2}\mu$. In the 4000 to 7000A wavelength region investigated with this modification (Fig. 6), a similar displacement of the absorption edge toward shorter wavelengths with decreasing temperature is observed; in addition, there is a decided sharpening of the hump in the curve near 5000A.

In a crystalline solid the absorption edge has normally been treated as showing the transfer of an electron from a filled electron-energy band into an empty one. The energy required for such a transition is affected by temperature because the band separation may be changed

[17] R. W. Wood, see reference 9; and K. Foersterling and V. Fréedericksz, see reference 9, used cast and quenched Se; A. Becker and I. Schaper, see reference 9, used sputtered layers, etc.

by thermal expansion of the lattice,[18,19] and through the collision broadening of the electron-energy levels by lattice vibrations.[20] The effect of thermal expansion has been treated by Möglich and Rompe[18] on the basis of a one dimensional lattice.

Collision broadening has been treated by Radkowsky[20] who concludes that in a monatomic crystal there should be no noticeable effect of temperature on the absorption edge from this cause. According to Fan,[21] thermally excited lattice vibrations also contribute to a reduction of the energy gap with increasing temperature in such a way as to yield a shift of the absorption edge proportional to temperature. More extensive measurements have to be made on metallic selenium before accurate conclusions can be drawn. However, the explanation given above for the amorphous selenium may be more valid also in the case of hexagonal selenium than the other causes just cited.

The author feels that physical significance should not be given so much to the wavelength of the absorption edge, which cannot be precisely specified, as to the change of the absorption coefficient with temperature or pressure at a given wavelength near the edge.

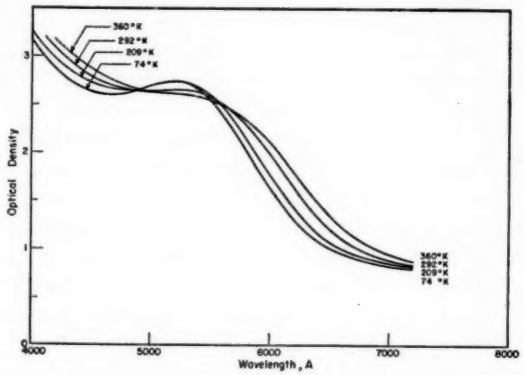

FIG. 6. Effect of temperature on optical absorption of hexagonal-selenium film *ca* $\frac{1}{4}\mu$ thick over semitransparent platinum film on glass.

B. Photoconductivity

The photoconductive effect in amorphous selenium was measured for light interrupted 60 times per second (Fig. 7), since this method provided greater sensitivity with the apparatus available. It was possible to obtain optical absorption data of Fig. 7 for this specimen. The oscillations of the density curves at low density are the result of interference effects. Photoconductivity sets in at 22°C at a wavelength of about 5600A which is almost completely absorbed.[7] Upon cooling the specimen to −172°C, the photoconductive threshold retreats to 5000A. This result is presumably a consequence of the depletion of vibrational levels, which becomes apparent also in the steepening of the absorption edge.

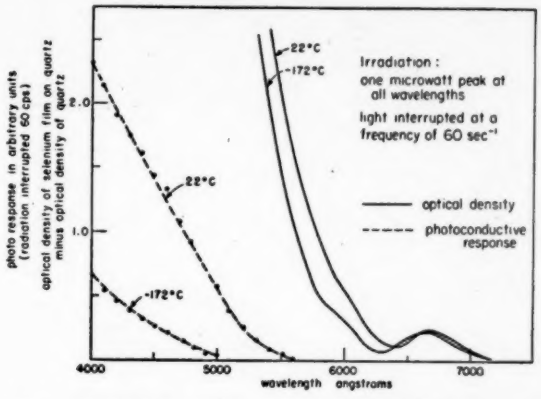

FIG. 7. Optical absorption and photoconductive response of an amorphous selenium photocell (~0.57μ thick).

The photoconductivity measurements may be extended on the same layer to hexagonal selenium by heat transformation. Unfortunately the present technique did not allow the retention of the platinum film which had facilitated the hole-free heat transformation to hexagonal selenium for absorption measurements. Consequently, the optical absorption measurements of Fig. 8 level off at high density due to the transmission of light through small holes. In contrast to amorphous selenium, the hexagonal form shows photoconductive sensitivity at wavelengths for which the optical absorption coefficient is still relatively small (Fig. 9). Furthermore, there is a peak in the photoconductive response at a wavelength for which the optical density is *ca* 1. This peak shifts toward shorter wavelengths with decreasing temperature in such a way that it remains at about the same value of optical density. In addition, irradiation of hexagonal selenium at low temperature (−170°C) leads to a more or less irreversible increase of the dark conductivity which may be removed by warming.

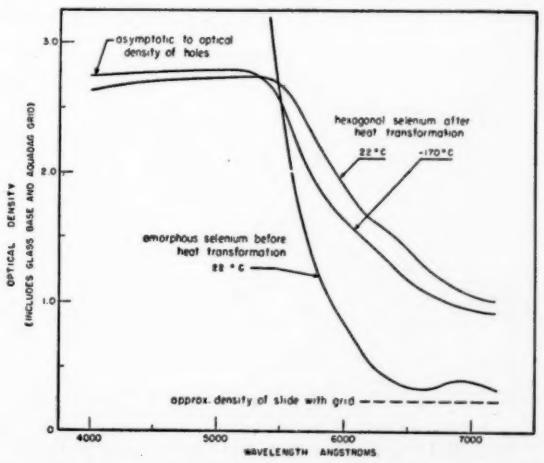

FIG. 8. Optical-density-*vs*-wavelength curve for amorphous selenium photocell on glass before and after heat transformation. (Thickness *ca* 0.65μ.)

[18] F. Möglich and R. Rompe, Z. Physik **119**, 472 (1942).
[19] J. Bardeen and W. Shockley, Phys. Rev. **80**, 72 (1950).
[20] A. Radkowsky, Phys. Rev. **73**, 749 (1948).
[21] H. Y. Fan, Phys. Rev. **78**, 808 (1950).

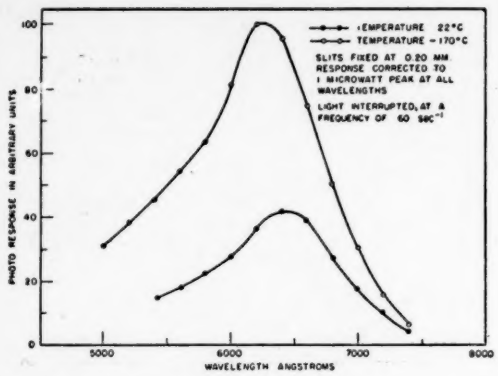

FIG. 9. Spectral response of hexagonal selenium photocell at 22° and −170°C. (Thickness, *ca* 0.65μ.)

Hole conduction is indicated by the observed direction of rectification of selenium rectifiers, and by the sign of the thermovoltage.[1] The relatively large dark conductivity at low temperature may be made possible by the space-charge-neutralizing effect of the electrons in excited states or traps.[22] If the recombination rate of holes and electrons in a chain is proportional to the product of the concentration of each, we have to deal with a bimolecular process.

The photoconductive phenomena observed for hexagonal selenium are in qualitative agreement with the effects expected from such a mechanism. The calculations show that a maximum response should occur for an optical density of *ca* 1, and that it consequently shifts with temperature as the absorption edge moves. For optical densities greater or less than *ca* 1 the response should decrease: for greater densities, because the penetration depth for light is so small that the charge-carrier concentration in a thin surface layer is limited by the high recombination rate; for smaller densities because the rate of charge-carrier release by light is reduced on account of the reduced absorption.

The relation between photoeffect and absorption coefficient is illustrated still more strikingly by Fig. 10. It shows that when the optical density exceeds the critical value near unity and the photocurrent is diminished on account of enhanced recombination, a fall of the absorption towards still shorter wavelengths leads again to a rise in photoresponse as would be expected. A more extensive discussion of the bimolecular recombination effect will be given elsewhere.

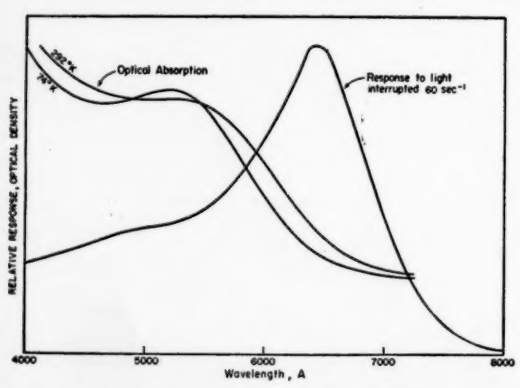

FIG. 10. Optical absorption and photoconductivity of hexagonal selenium.

[22] A. von Hippel and E. S. Rittner, J. Chem. Phys. 14, 370 (1946).

III. DISCUSSION

In order to support the previous conclusions regarding the origin of the temperature dependence of the optical absorption in amorphous selenium, the dependence of the molecular absorption coefficient upon the vibration quantum number must be discussed in more detail. We consider the case of a molecule for which the ground-state potential curve lies below a repulsive, upper-state curve as shown in Fig. 11.†† The transition probability between these states is proportional to $|I_n|^2$ where $I_n=\int\psi'\psi_n''dr$ is the overlap integral;[23] here ψ' is the repulsive-state wave function, ψ_n'' the wave function for the nth vibrational level of the ground state, and r a normal coordinate of nuclear displacement.

For large values of nuclear displacement the linear oscillator wave functions have the form $\psi_n''=$constant $[2^n n!]^{-\frac{1}{2}}(2x)^n \exp(-x^2/2)$; the displacement $(r-r_e)$ has been replaced by x times a constant containing the reduced mass and force constant. Thus there is a small, but finite, probability $|\psi_n''|^2dx$ of finding the nuclei with a separation between x and $x+dx$ outside of the limits of classical motion. This probability increases with n, accordingly with increase of the energy and amplitude of vibration. Hence, we expect that a small probability exists for inducing transitions from the vibrational levels of the ground state even when the available energy $h\nu_i$ is so small that they may take place only for large r.

Examination of I_n bears out this expectation. The upper-state wave function ψ' is oscillatory to the right of the turning point where it smoothly joins an exponential function decreasing toward the left approximately as

$$\exp\left(-\frac{1}{\hbar}\int_r^{r_1}[2m(V'-E')]^{\frac{1}{2}}dr\right), \quad r<r_1.$$

The decrease of ψ' is very rapid because of the steep rise of V' with decreasing r. Accordingly the integrand $\psi_n''\psi'$ is appreciable only for r in the neighborhood of the loop of ψ' adjacent to the turning point at r_1.

In comparison with $E'-E_n''=h\nu_i<2$ev, the *ca* 0.03

†† Evidence for the repulsive nature of the upper-state curve is taken from the energy proximity of the absorption edge and the threshold of the photoconductive effect to the Se−Se bond strength (see reference 16).

[23] For a discussion of this integral and its application see the valuable, original paper by Gibson, Rice, and Bayliss, Phys. Rev. 44, 193 (1933). Also see G. Herzberg, *Molecular Spectra and Molecular Structure, Volume I: Spectra of Diatomic Molecules*, (D. van Nostrand Company, Inc., New York, 1950), pp. 200 ff., 390 ff.

ev energy separation of the vibrational levels[24] is very small. With $h\nu_i$ held fixed, change of n will thus require only a very small shift of the intersection of E' with the upper-state curve. Consequently, the range of r which leads to the major contribution to I_n will be nearly the same for a small range of n. The transition probability between the states represented by ψ_n'' and ψ' (and accordingly the molecular absorption coefficients $\alpha_n(\lambda)$) is proportional to $\nu_i|I_n|^2$. We then see that $[\alpha_{n+1}(\lambda_i)/\alpha_n(\lambda_i)]>1$ and also that $[\alpha_{n+1}^2(\lambda_i)/\alpha_n(\lambda_i)\alpha_{n+2}(\lambda_i)]>1$ largely as a consequence of the dependence of ψ_n'' upon n. The total absorption coefficient for the nth vibrational level is $N_n\alpha_n(\lambda)$, where N_n is the vibrational level population. At temperatures for which the partition function times $\exp(h\nu/2kT)$ is nearly unity N_n is very nearly given by the product of the total number N of molecules present with the Boltzmann factor $\exp(-nh\nu/kT)$; for a given temperature N_n decreases rapidly with increasing n.

When $\log[N_n\alpha_n(\lambda_i)]$, λ_i constant, is plotted as a function of $(1/T)$, the condition $[\alpha_{n+1}(\lambda_i)/\alpha_n(\lambda_i)]>1$ determines that the resulting straight lines of slope $(-nh\nu/k)$ will intersect for $(1/T)=(k/h\nu)\ln[\alpha_{n+1}(\lambda_i)/\alpha_n(\lambda_i)]$. If in addition $[\alpha_{n+1}^2(\lambda_i)/\alpha_n(\lambda_i)\alpha_{n+2}(\lambda_i)]>1$ the intersections will be so ordered that the $(n+1)$th straight line will form, with the nth, the next intersection to the left of the intersection of the nth straight line with the $(n-1)$th. The curve of $\log\alpha=\log[\Sigma_n N_n\alpha_n(\lambda_i)]$ thus lies always above the straight line of greatest ordinate and steepest slope for any given value of $(1/T)$ on such a plot. Then $\log\alpha(\lambda_i)$ *vs* $(1/T)$ is a curve which shows increasingly negative slope with decrease of $(1/T)$. With increase of $\lambda_i=c/h\nu_i$ we see from Fig. 11 that r_1 also increases for transitions from a given vibrational level. As r_1 increases ψ_n'' decreases rapidly so that I_n and $\alpha_n(\lambda)$ also decrease. For longer wavelengths only those $\alpha_n(\lambda)$ with larger n will make an appreciable contribution to $\alpha(\lambda)$. This contribution will be strongly temperature dependent because the slope of the $\alpha_n(\lambda)$ lines is larger for larger n. Accordingly the slope of the $\log\alpha(\lambda)$ *vs* $(1/T)$ curve increases with increasing λ with $(1/T)$ constant; the magnitude of $\log\alpha(\lambda)$ decreases. In a group of $\log\alpha(\lambda_i)$ *vs* $(1/T)$ curves, plotted with λ_i as a parameter, the curves corresponding to larger λ_i will lie below and will be steeper than those for lesser λ_i. The curves of Fig. 5 show just the behavior postulated on the basis of the model assumed.

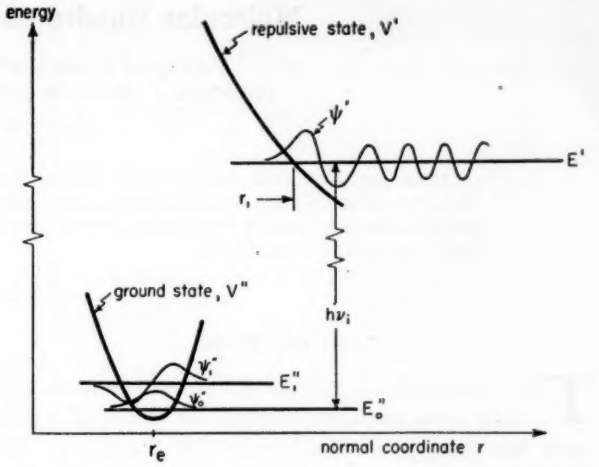

FIG. 11. Schematic representation of potential curves and wave functions for Se in chain molecules.

Thus far we have considered only one of the many possible frequencies ν_m of vibration. If we take all ν_m's into account we will have

$$\alpha=(1/Z)\sum_{m,n}\alpha_{mn}\exp(-h\nu_m/2kT)\exp(-nh\nu_m/kT),$$

where

$$Z=\prod_m \exp(-h\nu_m/2kT)[1-\exp(-h\nu_m/kT)]^{-1}$$

is the partition function.

ACKNOWLEDGMENT

The writer is deeply indebted to Professor A. von Hippel for his direction during the course of this work.

[24] H. Gerding and R. Westrik, Rec. trav. chim. **62**, 68 (1943), found lines of 269, 190, 164 cm^{-1} separation in the Raman spectrum for Se in CS_2. The 269 cm^{-1} frequency ($h\nu\simeq 0.033$ ev) presumably corresponds to the vibration of Se against Se in the chains and is assumed to be important to the temperature effects being discussed.

Molecular Quadrupole Moments of N_2 and O_2

CHARLES GREENHOW* AND WILLIAM V. SMITH†
Department of Physics, Duke University, Durham, North Carolina
(Received June 29, 1951)

Molecular orbital calculations of the quadrupole moments of N_2 and O_2 have been made. Models assuming 20 percent $s-p$ hybridization for N_2 and 5–10 percent $s-p$ hybridization for O_2 give calculated quadrupole moments agreeing with those deduced from microwave line broadening data ($0.27e\times10^{-16}$ esu for N_2 and $<0.09e\times10^{-16}$ esu for O_2).

INTRODUCTION

THE quadrupole moments of a number of molecules have been measured recently by means of microwave spectroscopy.[1,2] Quite generally the charge distribution of a molecule can be expanded in terms of its total charge, dipole moment, quadrupole moment, octupole moment, etc. In this expansion each successive term contributes successively shorter range terms to the potential field surrounding the molecule. For uncharged, nonpolar molecules the leading term in this expansion is thus the quadrupole moment Q.

For molecules possessing an axis of symmetry, Z, Q is defined as,‡

$$Q=\frac{1}{2}\int\int\int q_i\rho_i^2(3\cos^2\theta_i-1)d_\tau, \qquad (1)$$

where q_i is an element of charge (electron or nucleus), ρ_i is the distance from a chosen fixed point in the molecule, θ_i is the angle between the symmetry axis and ρ_i. In the symmetrical nonpolar molecules discussed in the present paper the origin for calculating Q is immaterial.§ It is convenient to choose the mass center of the molecule as the origin.

An examination of Eq. (1) reveals that Q may be either positive or negative. Indeed, the symmetry properties of atomic orbitals make Q zero for all spherically symmetric atomic S states. The symmetry conditions for most molecules do not require Q to be zero. It is, however, small and sensitive to the molecular orbital configuration. It is particularly sensitive to the amount of $s-p$ hybridization among the atomic orbitals chosen as a basis for the molecular orbitals.¶

Before considering a detailed molecular orbital analysis, it is instructive to examine the predictions of the extreme separated atom and united atom models for N_2 and O_2. The system of two $^4S_{\frac{3}{2}}$ N atoms possesses no quadrupole moment for large internuclear distances (no overlap of atomic orbitals) since the constituent atoms have no quadrupole moment. For very small separation of the N nuclei, however, the united atom with 14 electrons (silicon) is in a $^3P_0$ state,‖ giving rise to a negative quadrupole moment (cigar shaped distribution of electrons around the symmetry axis). In the case of oxygen, the separated $^3P_2$ atoms join with the extra two electrons (compared with N_2) in π-orbitals, giving a positive quadrupole moment. The united 16 electron atom (sulfur) is in a $^3P_2$ state, however, with about half the negative quadrupole moment of Si. Evidently at some intermediate interatomic distance the quadrupole moment of O_2 goes through zero. It is an experimental fact that the O_2 quadrupole moment is much smaller than that of N_2. Indeed, it is this observation that stimulated the present analysis.

QUANTUM-MECHANICAL FORMULATION

Equation (1) may be expanded to

$$Q=Q_N+Q_e$$

$$Q_N=\frac{e}{2}\sum Z_N\rho_N^2(3\cos^2\theta_N-1)=\text{nuclear contribution} \qquad (2)$$

$$Q_e=-\frac{e}{2}\langle\psi\sum\rho_e^2(3\cos^2\theta_e-1)\psi^*\rangle$$
$$=\text{electronic contribution},$$

where e is the magnitude of the electronic charge. The electronic wave function ψ is factored into molecular orbitals which are orthogonal in principle, but in practice are approximated by combinations of Slater atomic orbitals[3] (AO's) whose radial functions are slightly nonorthogonal. Of more importance, overlap integral contributions make the molecular orbitals (MO's) some-

* The research reported in this paper has been made possible through sponsorship extended by the Geophysical Research Directorate of Air Force Cambridge Research Laboratories under Contract No. W19–122-ac-35. It will be submitted by Charles Greenhow in partial fulfillment for the requirements of the Ph.D. degree.

† Now at the University of Delaware, Newark, Delaware.

[1] W. V. Smith and R. Howard, Phys. Rev. **79**, 132 (1950).

[2] R. M. Hill and W. V. Smith, Phys. Rev. **82**, 451 (1951).

‡ The definition for Q chosen here is consistent with general molecular usage, and differs from that employed in some of the references.

§ For unsymmetrical molecules the choice of origin for Q is important.

¶ We are indebted to Dr. W. O. Gordy for suggesting the importance of $s-p$ hybridization with particular reference to N_2.

‖ *Note added in proof:*—I am indebted to Professor R. S. Mulliken for pointing out to me that a more appropriate comparison could be made with the mixed ^1D_g and ^1S_g states of Si which have the same symmetry properties as the ground state of N_2. The contribution from the ^1D_g state would result in a non-zero quadrupole moment for the united atom so that the qualitative argument is unchanged.

[3] J. C. Slater, Phys. Rev. **36**, 57 (1930).

what nonorthogonal, even if the AO's are orthogonal.** This lack of orthogonality of the MO's is neglected. Thus the electronic contribution to the quadrupole moment becomes

$$Q_e=-\frac{e}{2}\sum_{MO}\langle\psi_{MO}\rho_e^2(3\cos^2\theta_e-1)\psi_{MO}^*\rangle, \quad (3)$$

a sum of contributions from each molecular orbital.

For the first row molecules N_2 and O_2, two electrons per atom are assumed to be in spherical $1s$ shells, completely cancelling two units of the nuclear quadrupole contribution. Thus the remaining nuclear quadrupole contribution Q_N' becomes

$$\begin{aligned}Q_N'(N_2)&=+10e(R_N/2)^2\\ Q_N'(O_2)&=+12e(R_O/2)^2,\end{aligned} \quad (4)$$

where R_N and R_O are the internuclear distances for N_2 and O_2, respectively.

Six of the remaining ten N_2 (12 O_2) electrons are assigned to σ orbitals having no angular momentum about the molecular axis. These σ orbitals are assumed to be obtained from hybrid $2s-2p\sigma$ AO's of the form:

$$\begin{aligned}\chi(\sigma)&=a\chi(2s)+(1-a^2)^{\frac{1}{2}}\chi(2p\sigma)\\ \chi(\sigma')&=(1-a^2)^{\frac{1}{2}}\chi(2s)-a\chi(2p\sigma).\end{aligned} \quad (5)$$

The remaining π-electrons are obtained from pure $\chi(2p\pi)$ AO's. The signs of the atomic orbitals are chosen to give positive overlap integrals $S=\int\chi_A\chi_B d\tau$ for the observed internuclear distance (i.e., if $R=0$, $S=-1$ for $2p\sigma$ orbitals).

Of the six σ electrons two are assigned to the bonding MO $\psi(\sigma_g)$

$$\psi(\sigma_g)=\frac{1}{[2(1+S_\sigma)]^{\frac{1}{2}}}[\chi_A(\sigma)+\chi_B(\sigma)]. \quad (6)$$

The remaining four σ electrons are assigned to the nonbonding pair of orbitals

$$\begin{aligned}\psi(\sigma_g)'&=\frac{1}{[2(1+S_\sigma')]^{\frac{1}{2}}}[\chi_A(\sigma)'+\chi_B(\sigma)']\\ \psi(\sigma_u)'&=\frac{1}{[2(1-S_\sigma')]^{\frac{1}{2}}}[\chi_A(\sigma)'-\chi_B(\sigma)'].\end{aligned} \quad (7)$$

The four π N_2 electrons, and four of the six π O_2 electrons are assigned to bonding π_u orbitals

$$\psi(\pi_u)=\frac{1}{[2(1+S_\pi)]^{\frac{1}{2}}}[\chi_A(2p\pi)+\chi_B(2p\pi)] \quad (8)$$

while the final two O_2 electrons are assigned to the antibonding π_g orbital

$$\psi(\pi_g)=\frac{1}{[2(1-S_\pi)]^{\frac{1}{2}}}[\chi_A(2p\pi)-\chi_B(2p\pi)]. \quad (9)$$

** *Note added in proof:*—For treatments of orthogonalized MO's, see W. Moffit, Proc. Roy. Soc. (London) **196A**, 510, 524 (1949); **202A**, 534, 548 (1950); and R. S. Mulliken, J. Chem. Phys. **19**, 912 (1951).

Substituting Eqs. (6) through (9) in Eq. (3), the electron contributions to the quadrupole moment are

$$\begin{aligned}Q(\sigma_g)&=2\frac{Q(p\sigma)+Q_e(p\sigma)}{1+S\sigma}\\ Q(\sigma)'=Q(\sigma_g)'+Q(\sigma_u)'&=4\frac{Q'(p\sigma)-S_\sigma'Q_e'(p\sigma)}{1-(S_\sigma')^2}\\ Q(\pi_u)&=4[Q(2p\pi)+Q_e(2p\pi)]/(1+S_\pi)\\ Q(\pi_g)&=2[Q(2p\pi)-Q_e(2p\pi)]/(1-S_\pi),\end{aligned} \quad (10)$$

where

$$\begin{aligned}Q(p\sigma)&=a^2Q(2s)+(1-a^2)Q(2p\sigma)\\ &\quad+2a(1-a^2)^{\frac{1}{2}}Q(2s2p\sigma),\\ Q'(p\sigma)&=(1-a^2)Q(2s)+a^2Q(2p\sigma)\\ &\quad-2a(1-a^2)^{\frac{1}{2}}Q(2s2p\sigma),\end{aligned} \quad (11)$$

with analogous equations for $Q_e(p\sigma)$, S_σ, $Q_e(p\sigma)'$, and

TABLE I. Molecular quadrupole moments of N_2 and O_2 as a function of the $s-p$ hybridization ratio a^2.

a^2	$S(N_2)$	$Q(N_2)/ea_H^2$	$S\sigma(O_2)$	$Q(O_2)/ea_H^2$
0	0.320	+1.455	0.307	+1.555
0.05	0.418	+0.287	0.442	+0.395
0.10	0.598	−0.163	0.491	−0.276
0.20	0.699	−1.040	0.549	−1.305
0.30	0.763	−1.806	0.583	−1.893

S_σ' and

$$\begin{aligned}Q(2s)&=-(1/2e)\int\chi_A(2s)\\ &\quad\times\rho_e^2(3\cos^2\theta_e-1)\chi_A(2s)d\tau,\\ Q_e(2s)&=-(1/2e)\int\chi_A(2s)\\ &\quad\times\rho_e^2(3\cos^2\theta_e-1)\chi_B(2s)d\tau,\\ Q(2s2p\sigma)&=-(1/2e)\int\chi_A(2s)\\ &\quad\times\rho_e^2(3\cos^2\theta_e-1)\chi_A(2p\sigma)d\tau,\end{aligned} \quad (12)$$

with analogous equations for $Q(2p\sigma)$, $Q_e(2p\sigma)$, S_{2s}, $S_{2p\sigma}$, and $S_{2s2p\sigma}$.

NUMERICAL EVALUATION

The overlap integrals S have been evaluated by Mulliken.[4] The quadrupole integrals have not previously been evaluated, and are listed in the appendix. It is to be noted that the exchange quadrupole contributions Q_e are generally quite small—and indeed they may be neglected without significantly affecting the over-all calculated quadrupole moments. They are, however, included in the present calculations.†† Table I lists calculated total Q values for O_2 and N_2 as a function of the $s-p$ hybridization ratio a^2. The units of Q

[4] R. S. Mulliken, J. Am. Chem. Soc. **72**, 4493 (1950). J. Chem. Phys. **19**, 900 (1951).

†† The unimportance of the exchange Q_e contrigutions justifies the neglect of the slight non-orthogonality of the MO's.

TABLE II. Overlap integrals and Q contributions for N_2 and O_2. Q is listed in units of eR^2.

	$S(2s)$	$S(2p\sigma)$	$S(2p\pi)$	$S(2s2p\sigma)$
N_2	0.449	0.320	0.281	0.441
O_2	0.276	0.307	0.145	0.311
	$Q(2s)$	$Q(2p\sigma)$	$Q(2p\pi)$	$Q(2s2p\sigma)$
N_2	−0.250	−0.434	−0.158	+0.357
O_2	−0.250	−0.366	−0.194	+0.277
	$Q_s(2s)$	$Q_s(2p\sigma)$	$Q_s(2p\pi)$	$Q_s(2s2p\sigma)$
N_2	−0.010	+0.097	+0.023	+0.012
O_2	−0.007	+0.033	+0.007	+0.002

are ea_H^2 where a_H is the Bohr atomic H radius (0.528×10^{-8} cm).

Examination of Table I reveals the marked dependence of Q on $s-p$ hybridization. This is essentially a result of the promotion of a fraction a^2 of a spherically symmetric s electron to a $p\sigma$ electron with a negative quadrupole contribution. The observed quadrupole moments are [1,5]

$$|Q(N_2)| = 0.27e\times10^{-16}\text{ esu} = 0.97ea_H^2,$$
$$|Q(O_2)| < 0.09e\times10^{-16}\text{ esu} = 0.32ea_H^2,$$

The signs of Q are not given by the experiment, and the magnitudes could be off as much as 50 percent as a result of some theoretical approximations in deriving quadrupole moments from the observed data of microwave line widths. The relative magnitudes of $Q(N_2)$ and $Q(O_2)$ are, however, certain. The observed quadrupole moments suggest the most reasonable $s-p$ hybridization values to be about 20 percent for N_2 and 5–10 percent for O_2.

DISCUSSION

The 20 percent $s-p$ hybridization ratio for N_2 deduced from molecular quadrupole moments may be compared with the values of 25 percent to 50 percent suggested by Townes and Dailey[6] for the similar C≡N group. Townes and Dailey's analysis is based on nuclear quadrupole coupling data (not to be confused with the molecular quadrupole moment). It is generally assumed that O_2 has no $s-p$ hybridization, owing to the large energy required to promote a $2s$ atomic electron to a $2p$ atomic electron. Mulliken,[4] however, has shown the importance of small amounts of $s-p$ hybridization in stabilizing orbitals—and indeed, it may be seen from Table I that the ratio of increase in $S\sigma$ overlap to fractional energy of promotion is greater for a 5 percent O_2 $s-p$ hybridization than for a 20 percent N_2 $s-p$ hybridization ratio, even assuming the promotional energy $2s-2p$ for O to be 50 percent greater than for N. Thus it is seen that the suggested $s-p$ hybridization ratios are reasonable.‡‡

[5] Anderson, Smith, and Gordy, Phys. Rev. **82**, 264 (1951).

[6] C. H. Townes and B. P. Dailey, J. Chem. Phys. **17**, 782 (1949).

‡‡ *Note added in proof:*—In the second paper of reference 4, Mulliken suggests hybridizations of 9 percent for O_2 and 22 percent for N_2, in excellent agreement with the values suggested here.

We wish to thank Professors E. Greuling, W. O. Gordy, and W. M. Nielsen for their interest and encouragement in this problem.

APPENDIX. THE EVALUATION OF ATOMIC AND EXCHANGE QUADRUPOLE MOMENTS FOR N_2 AND O_2

The Slater atomic orbitals used are [3,7]

$$\chi(2l\lambda) = R_2(r_a)Y_{2\lambda}(\theta_a,\varphi)$$
$$Y_{2s} = (1/4\pi)^{\frac{1}{2}};\quad Y_{2p\sigma} = (3/4\pi)^{\frac{1}{2}}\cos\theta_a;$$
$$Y_{2p\pi} = (3/4)^{\frac{1}{2}}\sin\theta_a\ (\cos\phi \text{ or } \sin\phi) \quad \text{(A-1)}$$
$$R_2(r_a) = (4\mu^5/3)^{\frac{1}{2}}r_a e^{-\mu r_a}.$$

The unit of length is the Bohr atomic H radius a_H. The quantity μ is a parameter having the values 1.95 and 2.275, respectively, for N and O.

The quadrupole operator $Q=-(e/2)\rho^2(3\cos^2\theta-1)$ where ρ and θ are measured from the mass center of the molecule. In terms of the internuclear distance R, r_a and θ_a, it becomes

$$Q=\frac{e}{2}[r_a^2-R^2/2+2Rr_a\cos\theta_a-3r_a^2\cos^2\theta_a]. \quad \text{(A-2)}$$

Substitution of (A-2) in (12), defining $t=uR$, yeilds

$$Q(2s) = -eR^2/4 \quad \text{(A-3)}$$
$$Q(2p) = -eR^2/4-3e/\mu^2 = -eR^2/4(1+12/t^2) \quad \text{(A-4)}$$
$$Q(2p\pi) = -eR^2/4+3/2e/\mu^2 = -eR^2/4(1-6/t^2) \quad \text{(A-5)}$$
$$Q(2s2p) = 5eR/2(3\mu)^{\frac{1}{2}} = 5eR^2/2(3t)^{\frac{1}{2}}. \quad \text{(A-6)}$$

The contributions (A-2) and (A-3) just cancel nuclear contribution $+eR^2/4$, giving a total zero quadrupole moment for neutral spherically symmetrical charge distributions. The exchange contributions to Q must be calculated in elliptical coordinates,[7] introducing the variables

$$p=r_a+r_b/R,\quad 1\leqq p\leqq\infty$$
$$s=r_a+r_b/R,\quad -1\leqq s\leqq 1. \quad \text{(A-7)}$$

The resulting integrals are closed power series in t

$$Q_s(2s) = -(eR^2/60)e^{-t}[1+t+10t^2/21+t^3/7+t^4/21] \quad \text{(A-8)}$$
$$Q_s(2p\sigma) = +(eR^2/4)(e^{-t}/t^2)[12+12t+615t^2/105+195t^3/105+39t^4/105+2t^5/105-t^6/105] \quad \text{(A-9)}$$
$$Q_s(2p\pi) = +(eR^2/4)(e^{-t}/t^2)[6+6t+255t^2/105+45t^3/105-t^5/105] \quad \text{(A-10)}$$
$$Q_s(2s2p\sigma) = +(eR^2/2(3)^{\frac{1}{2}})(e^{-t}/t)[1+t+171t^2/420+31t^3/240-(t^4+2t^5)/420]. \quad \text{(A-11)}$$

For N_2 $R=2.07a_H$, $t=4.04$ while for O_2 $R=2.28a_H$, $t=5.20$, yielding the Q values of Table II. S values are also tabulated for convenience.

[7] Mulliken, Rieke, Orloff, and Orloff, J. Chem. Phys. **17**, 1248 (1949).

The Ultraviolet Spectra of Benzene-Halogen Complexes and of Iodine in Solution*

J. S. HAM, J. R. PLATT, AND H. MCCONNELL†
Department of Physics, University of Chicago, Chicago, Illinois

(Received May 21, 1951)

The spectra of the 1:1 complexes between benzene and iodine and between benzene and bromine were examined in the wavelength range 2350–3500A using a 64-micron cell. In both cases a new absorption band was found at 2600A. This band is of considerable theoretical interest in connection with previous discussions of the spectra and structures of the benzene-halogen complexes. Also, the solution spectrum of iodine has been extended to 1820A and the f value compared with predictions.

I. INTRODUCTION

SOLUTIONS containing iodine or bromine in benzene exhibit an intense absorption band at *ca* 2900A. Pure liquid benzene and solutions of the halogens in an inert solvent such as carbon tetrachloride are comparatively transparent at this wavelength. Benesi and Hildebrand[1] and Andrews and Keefer[2] have shown that this optical absorption can be attributed to the 1:1 complexes represented in the equilibria,

$$Bz+X_2 \rightleftharpoons Bz\cdot X_2,$$

$$\frac{(Bz\cdot X_2)}{[Bz](X_2)}=K, \qquad (1)$$

where (X_2) and $(Bz\cdot X_2)$ denote the molar concentrations of free halogen and the complex. The mole fraction of benzene is $[Bz]$. We adopted the values of K given in the literature,[1,2] $K=1.15$ and 1.72 for $Bz\cdot I_2$ in n-heptane and in carbon tetrachloride, and $K=1.04$ for $Bz\cdot Br_2$ in carbon tetrachloride.[3]

In order to obtain a more complete description of the electronic states of these complexes, we have extended the previous spectrophotometric investigations to shorter wavelengths, ca 2350A. Also, the solution spectrum of iodine in n-heptane is extended to 1820A.

II. EXPERIMENTAL

The optical density of a solution containing the three molecular species of (1) as well as the solvent can be represented by

$$D=l[\epsilon_B(Bz)+\epsilon_X(X_2)+\epsilon_C(Bz\cdot X_2)+\epsilon_S(S)], \qquad (2)$$

where the ϵ's are the appropriate molar extinction coefficients and l is the light path. The molar concentration of the solvent is (S). The use of this equation to determine the spectra of the complexes is based on the assumption that the ϵ's are independent of the composition of the solution.

As solutions containing appreciable concentrations of the complex must also contain large concentrations of free benzene (*ca* 0.5 mole per liter) which absorbs in the wavelength range 2300–2700A, a short light path and large halogen concentrations (*ca* 0.1 mole per liter) were necessary to measure ϵ_C. The determination of ϵ_C at shorter wavelengths was prevented by the strong absorption of benzene ($\epsilon\sim 8000$) at 2000A.

The measurements were taken at room temperature, $22\pm 1°$, in the standard cell compartment of a model DU Beckman spectrophotometer. Our cells were specially constructed and consisted of a 64-micron lead spacer between two quartz plates in a holder.

Optical slit widths of 0.4 to 0.7 mm were employed corresponding to a nominal band width of about 10A in the 2300–2700A range. To maintain this slit width in the 2300–2400A range, it was found necessary to replace the usual 2000 megohm resistor of the phototube circuit with a 10^4 megohm resistor.

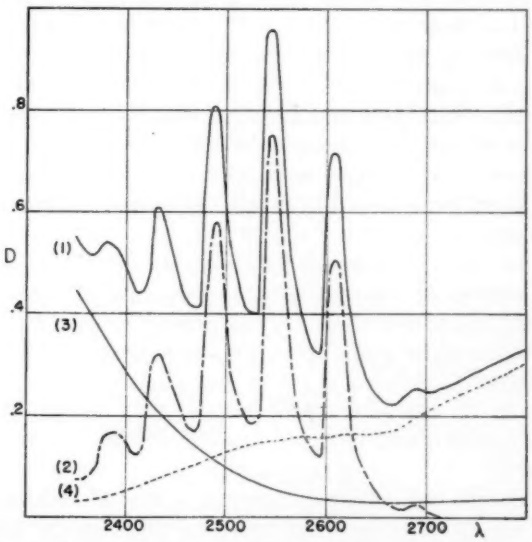

FIG. 1. Determination of the $Bz\cdot I_2$ spectrum. Calculated compositions: (1). ——— Mixture. $[Bz]=0.0839$ mole fraction, $(I_2)=2.90\times 10^{-2}$ mole per liter, $(Bz\cdot I_2)=2.80\times 10^{-3}$ mole per liter; (2). – – – – Benzene alone. $[Bz]=0.0839$ mole fraction; (3). ——— Iodine alone. $(I_2)=2.90\times 10^{-2}$ mole per liter; (4). – – – – – – Calculated complex absorption, difference between (1) and the sum of (2) and (3). $(Bz\cdot I_2)=2.80\times 10^{-3}$ mole per liter. The solvent, n-heptane, is used as the comparison blank.

* This work was assisted in part by the ONR under task order IX of contract N6ori-20 with the University of Chicago.

† National Research Council Postdoctoral Fellow.

[1] H. A. Benesi and J. H. Hildebrand, J. Am. Chem. Soc. **71**, 2703 (1949).

[2] L. J. Andrews and R. M. Keefer, J. Am. Chem. Soc. **72**, 4677 (1950).

[3] T. M. Cromwell and R. L. Scott, J. Am. Chem. Soc. **72**, 3825 (1950), used a method for calculating the equilibrium constants different from Benesi and Hildebrand's, and obtained slightly different values from those used here.

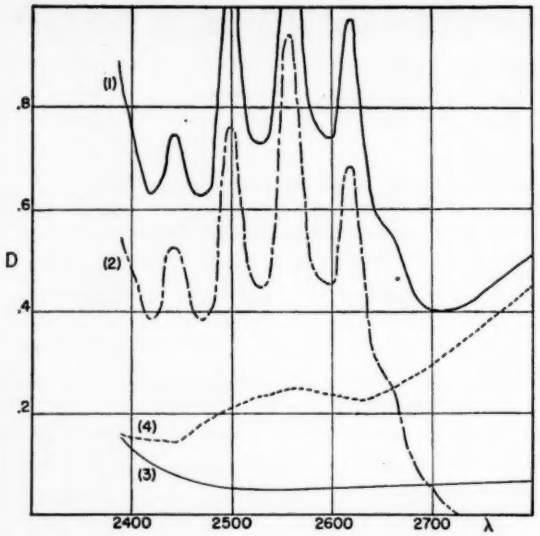

FIG. 2. Determination of the $Bz \cdot I_2$ spectrum. Calculated compositions: (1). ——— Mixture. $[Bz]=0.0630$ mole fraction, $(I_2)=5.17\times10^{-2}$ mole per liter, $(Bz \cdot I_2)=5.60\times10^{-3}$ mole per liter; (2). – – – – Benzene alone. $[Bz]=0.0630$ mole fraction; (3). ——— Iodine alone. $(I_2)=5.17\times10^{-2}$ moles per liter; (4). – – – – – – Calculated complex absorption, difference between (1) and the sum of (2) and (3). $(Bz \cdot I_2)=5.60\times10^{-3}$ mole per liter. The solvent, carbon tetrachloride, is used as the comparison blank.

III. SPECTRA

Figure 1 exhibits the data which have been used to calculate the absorption spectrum of the benzene-iodine complex in *n*-heptane. Curve 1 gives the absorption spectrum of a solution containing the benzene-iodine complex, together with free benzene and iodine in *n*-heptane solvent. Curves 2 and 3 give the absorptions by benzene and iodine respectively for concentrations equal to those calculated for the free molecules in curve 1. Curve 4, which is the difference between 1 and the sum of 2 and 3, gives the absorption by the $Bz \cdot I_2$ complex. In Figs. 2 and 3 similar data are given for the benzene-iodine and benzene-bromine complex in carbon tetrachloride. Similar data for the bromine complex could not be obtained in *n*-heptane because of chemical reactions.

The data are given in this form to facilitate future calculation of the absorption coefficients of the complexes in the event that the accepted values or interpretation of the equilibrium constants are changed.

Figure 4 exhibits the entire near ultraviolet spectra of the $Bz \cdot X_2$ complexes. Our values of ϵ_{max} near 2900A differ from those reported elsewhere[1,2] by less than 4 percent.

Benzene in heptane (but not in carbon tetrachloride) has molar extinction coefficients of 10–25 in the 2200–2400A range. These low extinction coefficients made it possible to determine the spectrum of the complex for relatively large benzene concentrations (*ca* 4 moles per liter) where 20–40 percent of the iodine is in the complexed form. The data are not included in Fig. 1 but the calculated spectrum of the complex in this range is included in Fig. 4. It is interesting to note that the $Bz \cdot I_2$ complex is transparent at about 2250A where free iodine in heptane has an extinction of about 5000 (see Fig. 5). The upturns at the short wavelength limits of the spectra in Fig. 4 are within the experimental error and so may not be real.

IV. EXPERIMENTAL ERRORS

If real, the shoulders and maxima near 2600A in the spectra of Fig. 4 are of considerable theoretical interest. For this reason, we have critically examined the question as to whether the apparent absorptions of the complexes at this wavelength could arise from the adventitious presence of impurities, experimental errors in the measurements of optical densities, or failures in the assumptions employed in the calculation of these spectra.

Since the solvent, the benzene, and the halogens were found to be spectroscopically pure in the 2200–3500A range, reaction products of benzene and the halogens are the only likely source of interfering substances. The most probable reaction products, phenyl bromide and iodide, have absorption maxima at 2650A and 2600A and, more significantly for the present purpose, absorb strongly at 2350A.[4] Judging from the absorptions of our solutions at 2350A, halogen substituted benzenes cannot have made an appreciable contribution to the observed absorption at 2600A.

The most important sources of experimental errors in the measurements of optical densities are thought to arise from uncertainties in the optical light path and in

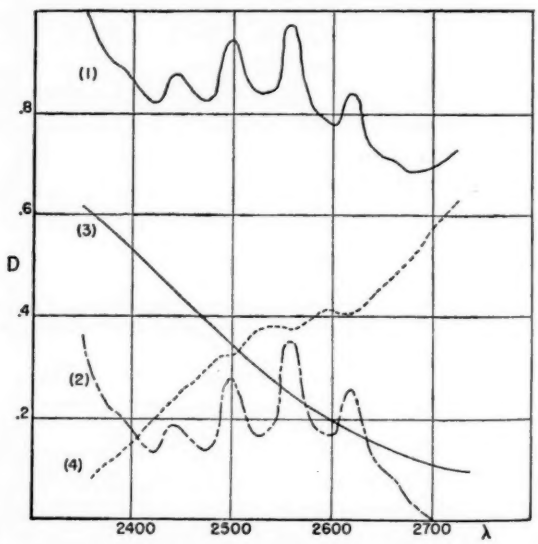

FIG. 3. Determination of the $Bz \cdot Br_2$ spectrum. Calculated compositions: (1). ——— Mixture. $[Bz]=0.0228$ mole fraction, $(Br_2)=0.387$ mole per liter, $(Bz \cdot Br_2)=9.17\times10^{-3}$ mole per liter; (2). – – – – Benzene alone. $[Bz]=0.0228$ mole fraction; (3). ——— Bromine alone. $(Br_2)=0.387$ mole per liter; (4). – – – – – – Calculated complex absorption, difference between (1) and the sum of (2) and (3), $(Bz \cdot Br_2)=9.17\times10^{-3}$ mole per liter. The solvent, carbon tetrachloride, is used as the comparison blank.

[4] American Petroleum Institute Catalog of Ultraviolet Spectrograms, Nos. 304 and 308 (Duke University).

the linearity in the response of the spectrophotometer. The light path, 64 microns, was determined from the optical densities of standard solutions and also by micrometer measurement of the thickness of the lead spacers. The cell could be dismantled and reassembled with less than 2 percent change in the optical light path. The linearity in the response of the instrument was checked by a study of the spectra of benzene-carbon tetrachloride solutions in *n*-heptane in the 2400–2700A range. The results show the intensity of scattered light at these wave lengths to be negligible. Also, deviations from linearity in the response of the spectrophotometer could account for only 5 percent error in the spectra of Fig. 4.

Although the magnitudes of the ϵ's in Fig. 4 are quite sensitive to the numerical values of the equilibrium constants, the calculated spectra of the complexes show maxima or pronounced shoulders near 2600A even when greatly different K values are assumed, $K=0.5$ to $K=2.0$.

In Figs. 1–3, the subtraction of curve 2 from curve 1 to account for the absorption of free benzene makes use of the assumption that the ϵ_B are independent of the halogen concentration. This is difficult to check. Failure of this assumption might account for the apparent "vibrational structure" of the $Bz\cdot Br_2$ spectrum at 2600A (see Fig. 4) because the free benzene spectrum, which is subtracted from the observed mixture absorption curve, might be smoothed out or otherwise different in the X_2-containing solutions from the observed free benzene spectrum in inert solvent which we actually used in the subtraction. This effect would be sufficient to account completely for the apparent vibrational structure and shoulders if the free benzene spectrum in X_2-containing solutions were 5–20 percent more intense and somewhat more smoothed out than in an inert solvent. On the other hand, such a marked change seems unlikely in, for example, Fig. 1, where the I_2 concentration is about 1/20 that of the free benzene. Also, it seems unlikely that the increase of intensity and the smoothing in the X_2-containing solutions would be so nicely balanced as to give the very smooth maxima and shoulders of Figs. 1 and 2; even in Fig. 3 the oscillations of intensity in the 2600A region are no greater than the experimental uncertainty.

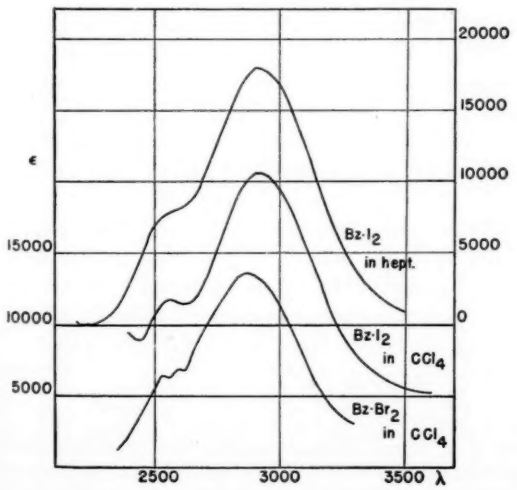

FIG. 4. Molar extinction coefficients, ϵ, of the benzene-halogen complexes. (1). $Bz\cdot I_2$ in heptane, right-hand scale; (2). $Bz\cdot I_2$ in carbon tetrachloride, right-hand scale plus 5000; (3). $Bz\cdot Br_2$ in carbon tetrachloride, left-hand scale.

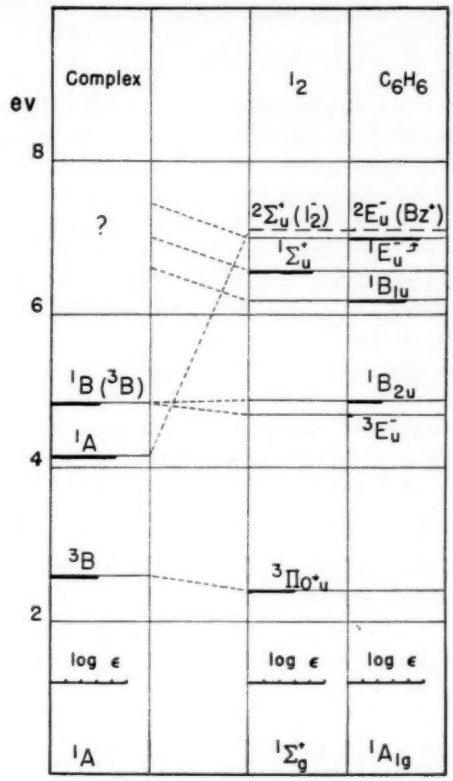

FIG. 5. Correlation diagram for the $Bz\cdot I_2$ complex. To the right are indicated the electronic energies of $Bz\cdot I_2$ at infinite intermolecular distance. The symmetries apply to the isolated molecules or to the molecular ions of the charge transfer state. Lengths of heavy lines indicate logϵ on scale of 0–5. Only the transitions with logϵ in solution >2.5 are included except to the $^2E_u^-$ state which has not been observed.

To the left are indicated the observed electronic states of the complex and their symmetries for the rotation group C_2.

We therefore conclude that the shoulders and maxima near 2600A may be real and characteristic of the $Bz\cdot X_2$ complexes themselves. The vibrational structure in Fig. 3 is probably due to imperfect correction for the benzene absorption.

V. DISCUSSION

The absorption by $Bz\cdot I_2$ and $Bz\cdot Br_2$ near 2600A, if real, represents in both cases an electronic transition of the benzene-halogen complex distinct from the intense absorption with maximum at 2900A. Mulliken[5] has attributed the 2900A band to an intermolecular charge-

[5] R. S. Mulliken, J. Am. Chem. Soc. **72**, 600 (1950); J. Chem. Phys. **19**, 514 (1951); and articles to be published elsewhere.

transfer type of transition, essentially,

$$(Bz\cdot X_2)\rightarrow(Bz^+-X_2^-),$$

between a $^1A_1$ ground state and a $^1A_1$ excited state. In this interpretation, the relevant excited electronic state of the complex is to be correlated at large intermolecular distances with Bz^+ and X_2^- in their ground states. The deduced[6] visible absorptions of $Bz\cdot I_2$ with peak at 5000A ($\epsilon\sim1300$) and $Bz\cdot Br_2$ with peak at 4300A ($\epsilon\sim220$) are quite similar to the visible spectra of the free halogens (I_2 at 5200A, $\epsilon\sim910$ and Br_2 at 4100A, $\epsilon\sim200$) in an inert solvent. Thus, these electronic states of the halogens are only slightly perturbed by complex formation with benzene. We may reasonably suppose that the electronic states of benzene should likewise be only slightly perturbed by complex formation with the halogens. It is then of interest to inquire whether the shoulders at 2600A in the spectrum of the complex might

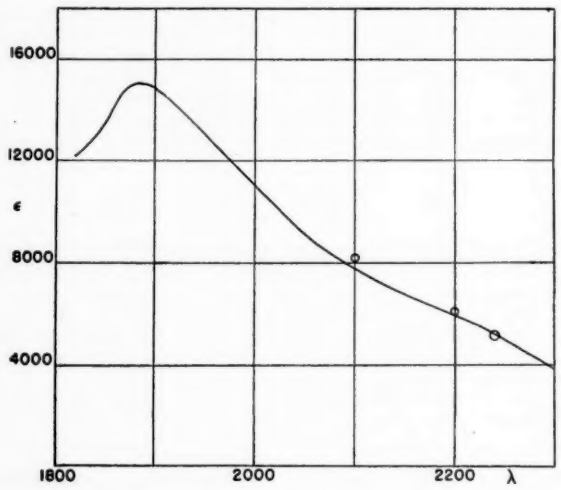

FIG. 6. Molar extinction coefficients, ϵ, of iodine in *n*-heptane. The circles represent points obtained with the Beckman spectrophotometer.

represent essentially a tenfold intensification of the 2600A benzene transition ($^1A_{1g}-^1B_{2u}$, $\epsilon\sim250$); that is, whether or not the excited electronic state of the complex corresponding to the 2600A shoulders is one which can be correlated, on disassociation, with the $^1\Sigma_g^+$ ground state of the halogen and the $^1B_{2u}$ excited state of benzene.

Mulliken[5] has suggested the most probable geometrical configuration for the benzene-halogen complex to be one in which the halogen molecule has its axis parallel to the plane of the benzene ring and its center on the sixfold symmetry axis of the benzene molecule (C_2 or C_{2v} total symmetry). A possible correlation between the electronic states of the pair, benzene and iodine, and the $Bz\cdot I_2$ complex is indicated in Fig. 5. For a geometrical structure with C_2 symmetry, the totally symmetrical charge transfer state (^1A of C_2) would not mix with any ^1B state of the complex. In particular, the ^1B state corresponding to a $^1\Sigma_g^+$ iodine combined with a $^1B_{2u}$ benzene state should not mix with the charge transfer state, and this makes plausible the absence of any large frequency displacement of the 2600A band of benzene. Similar considerations apply to C_{2v} symmetry and to the $Bz\cdot Br_2$ complex.

The possibility that a transition to the $^3E_u^-$ state of benzene (predicted to be at about 4.7 ev.[7]) makes a significant contribution to the spectra in the 2600A region has not been eliminated. The transition from the ground state of free benzene to this state is not orbitally forbidden as is the transition to the singlet, $^1B_{2u}$, but is only spin forbidden. Possibly the presence in $Bz\cdot I_2$ of the iodine atoms with their strong spin-orbit coupling, makes the $^1A_{1g}-^3E_u^-$ absorption in benzene as strong as that observed near 2600A in Fig. 4, yet affects the $^1A_{1g}-^1B_{2u}$ to a lesser degree. If this idea is correct, the $^1A_{1g}-^3E_u^-$ transition in the $Bz\cdot Br_2$ complex would be expected to be only half as strong as that in $Bz\cdot I_2$ because of the proportionally smaller spin-orbit coupling in the lighter bromine atoms. The appearance of the curves does not contradict this prediction, but of course the differences in the $Bz\cdot Br_2$ and $Bz\cdot I_2$ extinction coefficients at this wavelength are scarcely larger than the experimental error.

VI. SOLUTION SPECTRA OF IODINE

Figure 6 shows the absorption of iodine in *n*-heptane taken on the small fluorite spectrograph by methods described previously.[8] The peak molar extinction coefficient is 15,000±2000 at about 1880A. This is roughly sixteen times as large as the visible absorption of iodine at 5200A in *n*-heptane. This transition is probably largely the $^1\Sigma_g^+-^1\Sigma_u^+$ (V, N) transition although the broadness suggests that there are actually several transitions involved. Mulliken[9] has calculated theoretically using LCAO and AO methods that the f value of this (V, N) transition should be 1.21. By extrapolating our observed curve to shorter wavelengths and cutting off the long wavelength tail at 2400A (assuming that the still longer wavelength absorption is due to other transitions) we find the measured f to be 0.3±0.1. The difference between the predicted and observed f values is comparable to the difference found for the (V, N) transitions in dienes with LCAO approximation,[7] but is much larger than the difference found in the similar transition of O_2.

[6] The visible spectra of the complexes can be estimated from the equilibrium constants and spectra in references 1, 2 and Aikin, Bayliss, and Rees, Proc. Roy. Soc. (London) **A169**, 234 (1938), by methods similar to those used above for the ultraviolet portions of the spectra.

[7] C. C. J. Roothaan and R. S. Mulliken, J. Chem. Phys. **16**, 118 (1948). A. C. Pitts, J. Chem. Phys. **18**, 1416 (1950), has found evidence of a band at 2940A which, she seems to suggest, may be this triplet. If so, it is ten to a hundred times weaker than expected.

[8] L. E. Jacobs and J. R. Platt, J. Chem. Phys. **16**, 1137 (1948).

[9] R. S. Mulliken and C. A. Rieke, Rep. Prog. Phys. **8**, 231 (1941). For a recent summary of the iodine excited electronic states see Putcha Venkateswarlu, Phys. Rev. **81**, 821 (1951).

Studies of Ionization Efficiency. I. The Determination of Molecular Appearance Potentials Using the Mass Spectrometer

J. D. MORRISON
Chemical Physics Section, Commonwealth Scientific and Industrial Research Organization, Melbourne, Australia
(Received March 19, 1951)

The factors affecting the shape of ionization efficiency curves can be separated into two categories: those due to instrument design, and those depending on the molecular structure of the substance studied. By taking precautions to eliminate the former, details of individual fine structure can be detected and measured in the curves. The methods for the determination of appearance potentials in use at the present time are discussed, and the results for a number of substances measured by the principal methods are compared with spectroscopic ionization potentials. It is found that the critical slope method gives values in all cases within 0.3 volt of the spectroscopic figure, whereas the results of the other methods may be in error.

I. INTRODUCTION

IN the determination of appearance potentials using the mass spectrometer, the experimental data give the curve relating the number of ions of a given kind produced by electron impact to the energy of the ionizing electron beam. This is referred to as the ionization efficiency (I.E.) curve.

The general shape of I.E. curves is well established, consisting of a region of initial increase which is almost exactly exponential, a region of linear increase, and an upper region where the ion current reaches a maximum value, then decreases. There is, however, poor agreement between the I.E. curves published by different workers for the same substances, and it can only be concluded that the conditions of measurement contribute materially to the shape of the curves. Before an I.E. curve can be satisfactorily interpreted, it is necessary to identify the contributions made to its form by experimental factors, and by those depending on the nature of the collision process.

II. INSTRUMENTAL FACTORS

In the work described in this paper the instrument employed was the Consolidated Engineering Corporation 180°-type mass spectrometer model 21.102. For ionization efficiency measurements some changes were made in the connections to the ion chamber. The pusher electrodes, which for the measurement of mass spectra are maintained positive with respect to the ion chamber by proportions of the ion accelerating voltage, were joined together and given a fixed positive bias by means of a dry battery. Ionization efficiency curves were recorded using the automatic instrument described elsewhere.[1]

The instrumental conditions which were found to give the most reproducible results were:

Filament emission to electron trap $6\mu A$,
Electron accelerator potential $+40$ v,
Pusher electrodes $+3.0$ v with respect to ion chamber,
Electron trap $+210$ v.

The magnetic field was adjusted to bring the ions studied to focus at the collector with ion accelerating voltages between 1000 and 2000 volts. The time for the recording of a curve in no case exceeded five minutes, and the I.E. curve for argon or krypton was measured simultaneously, so that any changes in filament temperature, emission, conditions in the ion source or in the recording system could be detected and allowed for. The pressure of gas in the ion chamber was kept at 1.0×10^{-6} mm of Hg.

When high sensitivities were employed, ion current could still be detected at as much as ten volts below the ionization potential, and the I.E. curves appeared to be asymptotic to the voltage axis. This initial curvature did not appear to be affected by the potential on any of the electrodes surrounding the ion chamber, and its magnitude seemed to be mass dependent. Figure 1 shows the semilogarithmic I.E. curves for a number of gases. The mass dependence makes it possible that the curvature is due to the diffusion into the ion chamber of ions formed near the filament.

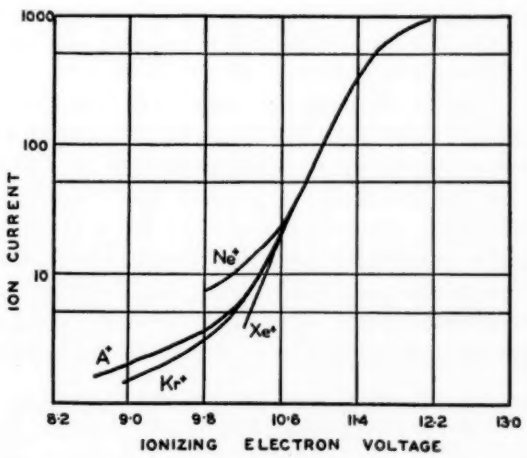

FIG. 1. Comparison of the initial parts of the ionization efficiency curves for the singly charged rare gas ions. The voltage scale is relative, the curves being drawn so that their upper parts are coincident.

[1] G. R. Hercus and J. D. Morrison, Rev. Sci. Instr. (to be published).

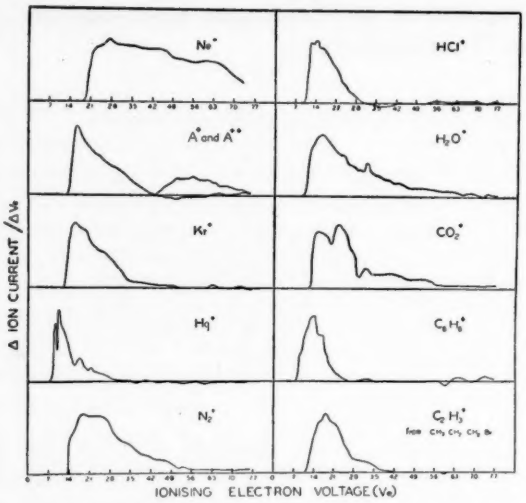

FIG. 2. Differential ionization efficiency curves for some common substances. The absolute voltage scale can be obtained from the curves for the rare gas ions.

III. STRUCTURAL FACTORS

The effect of the electron energy spread, which cannot be conveniently removed, will be to blur out fine details of the structure of the I.E. curves, but will not affect their general shape. To a certain extent allowance can be made for it. When all the instrumental effects except this have been eliminated, the shape of the curves obtained will presumably be due to the structural factors associated with the collision process.

The ionization probability for a given transition will depend on the probability of absorption of a given energy E_e by the molecule from an electron beam of energy E. The calculation of this probability theoretically presents considerable difficulty,[2] but experiments on the excitation of spectral lines by controlled electron impact[3] indicate that the ionization probability for a given process rises to a maximum value within about 0.1 volt above initial onset, and then decreases at a slower rate at higher energies. The nature of the transition affects this probability, the excitation for a triplet state having a much sharper maximum than that for a singlet.[4] In the mass spectrometric determination of ionization efficiencies, it has been assumed in the past that, for the first volt above initial onset, where presumably only one transition process is involved, the ionization probability is a linear function of the excess electron energy over the critical value.[5] Honig[6] finds experimentally that a better approximation is obtained taking the probability as proportional to the square of the excess energy. It is not possible to distinguish directly in the mass spectrometric I.E. curves between ions of a given kind which are produced by transitions to various excited electronic states. Therefore, the I.E. curves are the combination of the separate probabilities for all the possible transitions and it is also necessary to take into account the following structural factors:

(1) For monatomic and polyatomic fragments: (a) The number and position on the energy axis of the possible similarly ionized states. (b) The chance of there being more than one permissible electronic state near the ground state.

(2) For polyatomic molecules: (c) The value of the overlap integrals of the vibrational eigenfunctions between the ground and various possible ionized states, which will depend on their spatial distribution. (d) The distribution of molecules between the ground and higher vibrational levels at the temperature of measurement. (e) The blurring of vibrational levels, due to the rotational fine structure. The magnitude of this would be extremely small.

In view of the number of these factors contributing to the I.E. curve shape, it is surprising that the curves measured mass spectrometrically for a wide range of different ionic processes should show so little variation. When adequate instrumental precautions are taken in the measurements, however, it is possible to detect fine structure. This is shown up very well by the first differential of the I.E. curves with respect to the energy (Fig. 2).

A number of points call for comment. The initial increase in gradient of the I.E. curve is not the same for all the processes, indicating that the thermal energy spread of the ionizing electrons is not the only contributing factor to this curvature. Sudden upward changes in the gradient of the I.E. curve probably correspond to the onset of transitions to excited levels of the ion. These changes appear to be of three types, the first occurring over an energy range of 0.8 volt in the initial part of the mercury curve. It has been suggested by Nottingham[7] that in this case it is due to the differing shapes of the ionization probability curves for the excitation of the singlet and triplet states of the mercury ion. It could also be caused by the fact that excitation of an un-ionized level 0.9 volt above the first ionization potential is more probable than the transition involving ionization.

The second type occurs over a range of a few volts, as for example, in CO_2, H_2O, etc., and is probably due to the onset of additional ionization processes. A third, much more gradual type of change appears to be associated with the onset of an entirely different competing process, as occurs in argon, where the process $A \rightarrow A^{++}$ is sufficiently more probable than $A \rightarrow A^{+}$ at energies of 45 volts that the I.E. for the latter decreases. At higher

[2] N. F. Mott and H. S. W. Massey, *The Theory of Atomic Collisions* (Clarendon Press, Oxford, England, 1949), Chapter XI, p. 255.

[3] K. Larche, Z. Physik **67**, 440 (1931); W. C. Michels, Phys. Rev. **36**, 1362 (1930).

[4] W. G. Penney, Phys. Rev. **39**, 467 (1932).

[5] R. H. Vought, Phys. Rev. **71**, 93 (1947); also compare O. Oldenberg, J. Chem. Phys. **13**, 196 (1945).

[6] R. E. Honig, J. Chem. Phys. **16**, 105 (1948).

[7] W. B. Nottingham, Phys. Rev. **55**, 203 (1939).

energies the first process reaches its maximum efficiency, and the latter increases again.

It is obvious that the detailed interpretation of the relationship between the structural factors and the I.E. is somewhat complicated, and each case must be considered on its own merits in conjunction with its known spectroscopic data.

IV. THE DETERMINATION OF APPEARANCE POTENTIALS

For the numerous reasons discussed, one would expect that the determination of appearance potentials should present some difficulty, and that there should be some divergences in the published values. It appears probable, from the considerations mentioned in Sec. III, that if it were not for the electron energy spread, there would be a definite point of onset of the I.E. curve. This point would correspond to the ionization potential, except in a few extreme cases of molecules where the eigenfunctions for the ionized state are displaced so greatly from those of the ground state that the overlap integral corresponding to the least energetic transition is vanishingly small. In these cases, the value found would be higher than the minimum. The electron energy spread has the effect of removing the sharp point of initial onset.

The major difficulty lies in the interpretation of the initial curvature, and the methods in use at the present time which attempt to overcome this are:

(1) Linear extrapolation (L.E.).[8]

(2) Vanishing current: (a) Initial upward breaks.[9] (b) Extrapolated difference.[10] (c) Critical slope.[6]

In the initial breaks and extrapolated difference methods, the intensity scales of the I.E. curves are adjusted so that the linear portions are of the same slope. It is hard to justify this on theoretical grounds, and the differing curvatures shown by different substances at the foot of the curves which are illustrated in Figs. 1 and 2 make any extrapolation of doubtful value.

In the critical slope method, which is another modification of the vanishing current method, it is assumed that a major part, if not all, of the initial curvature of the I.E. curve is due to the energy spread of the ionizing electrons, that only one electronic transition is occurring, and that the probability of ionization by an electron of slightly higher than the critical energy is proportional to the square of the excess. If the logarithm of the ion current is plotted against the electron energy, the point at which the curve attains a certain critical value of slope corresponds to the appearance potential. From the present work it would appear that the point at which the semilogarithmic curve ceases to be a straight line also leads to a value for the appearance potential as good as that obtained with the critical gradient. This corresponds to the assumption that the ionization probability rises very abruptly above the critical energy. The fact that the straight line regions in the semilogarithmic I.E. curves of Fig. 1 can be made to coincide in all cases is a good argument in favor of the critical slope method.

In all these methods, the electron energy scale requires calibration. This is done by measuring the I.E. curve for a gas such as argon, where the ionization potential is known spectroscopically, and treating the data in a similar manner. The difference between the observed appearance potential and the spectroscopic ionization potential for the calibrating gas is then added to the observed appearance potential for the other, to bring it to the correct scale. This method of calibration has been questioned by Mitchell and Coleman,[11] who propose a calibration curve drawn up from the observed and spectroscopic ionization potentials for a number of gases.

To decide conclusively whether the critical slope method is capable of giving the correct values for molecular ionization potentials, and to compare it with the linear extrapolation method, almost all the molecules where the spectroscopic ionization potential is known accurately were measured in the mass spectrometer. The values found are listed in Table I. The curves for treatment by the L.E. method were measured at 0.35-volt intervals over a 10-volt range. Those

TABLE I.

Substance	Appearance potentials (mass spectrometric) Linear extrapolation method: No. of determinations	Linear extrapolation method: Mean value ev	Critical slope method: No. of determinations	Critical slope method: Mean value ev	Spectroscopic ionization potentials ev
A^+	Standard	15.77	Standard	15.77	15.77[a]
Kr^+	2	14.20±0.10	6	14.03±0.01	14.02[a]
Ne^+	2	21.57±0.13	2	21.53±0.02	21.58[a]
A^{++}	3	47.1 ±1.5	4	43.77±0.14	43.6[a]
Kr^{++}	2	41.84±1.0	2	38.49±0.2	38.6[a]
Hg^+	3	11.4 ±0.3	3	10.70±0.1	10.43[a]
N_2^+	19	15.57±0.17	6	15.66±0.03	15.58[b]
CO_2^+	15	13.78±0.12	3	13.88±0.03	13.79[c]
HCl^+	17	12.53±0.09	3	12.78±0.03	12.90[d]
H_2O^+	8	12.83±0.10	2	12.76±0.05	12.62[d]
CS_2^+	5	10.50±0.06	2	10.13±0.02	10.10[e]
H_2S^+	5	10.40±0.07	3	10.50±0.02	10.48[d]
$C_6H_6^+$	4	9.60±0.23	3	9.52±0.08	9.24[d]
$CH_3COCH_3^+$	2	9.76±0.02	2	9.92±0.01	10.21[d]
CH_3CHO^+	3	10.26±0.05	3	10.28±0.09	10.23[d]
cyclohexene$^+$	3	9.39±0.16	4	9.24±0.07	9.2[f]
CH_3Br^+	2	10.84±0.05	4	10.73±0.07	10.54[g]
$C_2H_5I^+$	4	9.62±0.09	3	9.47±0.06	9.34[g]
$HCOOH^+$	3	11.51±0.05	6	11.51±0.04	11.33[h]
furane$^+$	4	9.10±0.010	3	9.05±0.02	9.05[i]
isoprene$^+$	4	9.37±0.17	2	9.08±0.04	8.84[j]

[a] R. F. Bacher and S. Goudsmit, *Atomic Energy States* (McGraw-Hill Book Company, New York, New York, 1932).
[b] R. E. Worley and F. A. Jenkins, Phys. Rev. **54**, 305 (1938).
[c] W. C. Price and D. M. Simpson, Proc. Roy. Soc. (London) **A169**, 501 (1939).
[d] From a compilation by W. C. Price, Chem. Revs. **41**, 257 (1947).
[e] W. C. Price and D. M. Simpson, Proc. Roy. Soc. (London) **A165**, 272 (1938).
[f] W. C. Price and W. T. Tuttle, Proc. Roy. Soc. (London) **A174**, 207 (1940).
[g] W. C. Price, J. Chem. Phys. **4**, 539 (1936).
[h] W. C. Price and W. M. Evans, Nature **139**, 630 (1937).
[i] W. C. Price and A. D. Walsh, Proc. Roy. Soc. (London) **A179**, 201 (1941).
[j] W. C. Price and A. D. Walsh, Proc. Roy. Soc. (London) **A174**, 220 (1940).

[8] M. B. Koffel and R. A. Lad, J. Chem. Phys. **16**, 420 (1948).
[9] L. G. Smith, Phys. Rev. **51**, 263 (1937).
[10] J. W. Warren, Nature **165**, 810 (1950).
[11] J. J. Mitchell and F. F. Coleman, J. Chem. Phys. **17**, 44 (1949).

for the critical slope method were measured at 0.04-volt intervals over a 3- or 4-volt range at the foot of the curve, and interpreted using both values of slope referred to above. In all cases the curve for argon or krypton was measured simultaneously. Cross checks were made between other pairs of gases. Some of the L.E. values are very close to the spectroscopic figure, but in others the deviation is considerable. The critical slope values, on the other hand, are grouped much more closely around the spectroscopic figures. It is apparent that the L.E. value is much more dependent on the nature of the process under study. This is to be expected from the absence of plateaux in the differential I.E. curves of Fig. 2, which indicates that the straight line region of the I.E. curves is largely illusory.

In the results of neither method is there apparent any systematic relationship between deviation from the correct value of the appearance potential, and either the mass or the appearance potential. This indicates that the use of an additive constant from a single calibrating gas is satisfactory.

It is possible to obtain values from the differential I.E. curves for the onset of ionization to excited states of the ion under examination. These values, although approximate, may prove of assistance in the interpretation of far ultraviolet spectra.

V. SUMMARY

By taking care to have adequate control over the various instrumental factors affecting ionization efficiency curve shape, it is possible to detect fine structure in the curves, and measure the onset of electronic transitions involving energies above the ionization potential for any given ion fragment. The use of differential I.E. plots is of value in this respect. For the determination of appearance potentials, the region of linear increase has been found to have little significance and, in fact, only appears because the voltage scale on which the curves are drawn is compressed. The initial breaks method has been found impracticable, as at high sensitivities the ion current becomes asymptotic to the voltage axis, and has no point of definite onset. The values found for appearance potentials by the critical slope method are in all cases correct to within 0.3 volt, and in many much closer. This method does possess the disadvantage that high sensitivites are necessary in the ion-current measuring circuits, and the measurement of the appearance potentials of less abundant fragment ions is difficult. For a number of closely related processes, the L.E. values would probably be correct, and this will also be the case for the extrapolated difference method, but, in view of the complex nature of the structural factors affecting the I.E. curve shape, it is necessary to consider each case individually, taking into account the known spectroscopic data.

ACKNOWLEDGMENT

The author is indebted to Dr. A. L. G. Rees for helpful discussion of the subject.

Note on the Temperature-Independent Factors of Elementary Reactions

E. W. R. STEACIE, *Division of Chemistry, National Research Council, Ottawa, Canada*

AND

M. SZWARC, *Chemistry Department, University of Manchester, Manchester, England*

(Received December 11, 1950)

The "temperature-independent" factors of bimolecular and free radical reactions are discussed.

SOME confusion has arisen in recent discussions concerning the "temperature-independent" factors of bimolecular free radical reactions and the frequency factors in unimolecular decompositions. This note seeks to restate the position as seen by us from both the experimental and the theoretical points of view, and if possible to resolve some of the misunderstandings which have arisen from inconsistencies in the use of terms and from different treatments of experimental data.

(a) THE STERIC FACTORS IN BIMOLECULAR FREE RADICAL REACTIONS

The results of a kinetic investigation of a chemical reaction yield two *real experimental observables*, the energy of activation, E_1, and the temperature-independent factor, A. It has been common practice to interpret the results in terms of the collision theory or of the transition state theory of chemical kinetics. The collision theory provides a standard with which the experimental values of A may be compared by assuming a collision diameter which has reference to the kinetic sizes of the molecules involved. The "steric" or "P" factor was introduced to express the ratio between the value of A found and that predicted by the collision theory. Because the molecular sizes are uncertain, the calculated values of the steric factors are also uncertain; hence, this method of expressing results is not entirely satisfactory.

The calculation of the temperature-independent factor for a particular reaction is theoretically possible in terms of the transition state theory. It involves a knowledge of the structure and modes of motion of the reacting molecules and the activated complex. However, *a priori* and explicit calculations are very uncertain because they depend upon intelligent conjecture as to the structure of the activated complex. Nevertheless, the theory does enable one to understand the broad general trends which have been found.

In Table I the values of the $A=PZ$ factors for a number of reactions involving atoms, methyl radicals, and more complex radicals are given. Table I shows that in the best-established cases the temperature independent-factor diminishes with increasing complexity of the radicals involved. This general trend is no new feature and is similarly found in bimolecular reactions involving nonradical particles only. It has been related to the entropies of formation of the activated complexes, which can be evaluated only very approximately. The greatest uncertainty concerns the lack of information about the contribution of the internal rotations.

There is therefore a great need for accurate experimental determination of A for a large number of radical reactions. Such determinations have now been made for a considerable variety of reactions involving methyl radicals. The results provide information for the study of the effect of structure of the reacting molecule upon the magnitude of the A factor. Moreover, a knowledge of A factors for elementary reactions is of great importance for the estimation of the contributions of alternative reaction schemes devised to explain the over-all changes observed in kinetic and photochemical studies. It is evident that the magnitude of the contribution of two competing reactions cannot be estimated from a knowledge of their activation energies alone as has often been done in the past.

Some confusion has arisen in the use of terms. When steric factors are derived from the experimentally determined A factors, it is important that the explicit values used in the calculation of the collision frequency should be given. Similarly, discussion of A in terms of transition state theory should give details of the assumed activated complex. Some authors have used the

TABLE I.

Reaction	$A=PZ$	Reference
$H+H_2\rightarrow H_2+H$	3.5×10^{13}	a
$D+NH_3\rightarrow H+NH_2D$	2×10^{13}	b
$D+PH_3\rightarrow H+PH_2D$	1.5×10^{13}	b
$Br+CH_4\rightarrow HBr+CH_3$	1.5×10^{12}	c
$Br+H_2\rightarrow HBr+H$	1.1×10^{12}	d
$Br+CH_3Br\rightarrow HBr+CH_2Br$	1.3×10^{12}	c
$CH_3+CH_3COCH_3\rightarrow CH_4+CH_2COCH_3$	5×10^{11}	e
$CH_3+C_2H_6\rightarrow CH_4+C_2H_5$	2×10^{11}	e
$CH_3+n-C_4H_{10}\rightarrow CH_4+C_4H_9$	1×10^{11}	e
$CH_3+i-C_4H_{10}\rightarrow CH_4+C_4H_9$	1×10^{11}	e
CH_3+neo $C_5H_{12}\rightarrow CH_4+C_5H_{11}$	2×10^{11}	e
$(pC_6H_5\cdot C_6H_4)_3C+C_6H_5CH_3\rightarrow (pC_6H_5\cdot C_6H_4)_3CH+C_6H_5CH_2$	2×10^{10}	f
(p.t. $C_4H_9C_6H_4)_3C+C_6H_5CH_3\rightarrow$ (p.t. $C_4H_9\cdot C_6H_4)_3CH+C_6H_5CH_2$	5×10^{9}	f

[a] Farkas and Farkas, Proc. Roy. Soc. (London) **A155**, 124 (1935).
[b] Melville and Bolland, Proc. Roy. Soc. (London) **160**, 384 (1937).
[c] Kistiakowsky and van Artsdalen, J. Chem. Phys. **12**, 469 (1942).
[d] Jost, Z. physik. Chem. **B 3**, 118 (1929).
[e] Trotman-Dickenson and Steacie, J. Am. Chem. Soc. **72**, 2310 (1950) using Gomer's [J. Chem. Phys. **18**, 998 (1950)] value of 7×10^{13} cc/mole sec for the velocity constant for the combination of methyl radicals. The activation energy of this reaction is assumed to be zero.
[f] Dobres and Selwood, J. Am. Chem. Soc. **72**, 5731 (1950).

phrase "normal steric factor," meaning that the steric factor is practically unity. Other authors have used it to mean that the steric factor was roughly in accordance with that calculated from transition state theory. We feel that, in view of the above discussion, the use of the phrase "normal steric factor" is inadvisable.

(b) THE FREQUENCY FACTORS IN UNIMOLECULAR DISSOCIATION REACTIONS

In our opinion there are very few unimolecular reactions which are comparatively free from side reactions and have been subjected to a sufficient detailed experimental investigation to provide really definite values for A. Here we are particularly concerned with those reactions in which one bond is broken giving two radicals. The experimental material available at present seems to indicate that in cases of reactions which are apparently free from disturbing side processes, the frequency factors fall within the range 10^{12} to 10^{14} sec^{-1}, that is, within a factor of 10 of the value of 10^{13} sec^{-1} which was predicted on theoretical grounds by Polanyi and Wigner. This statement seems to be particularly valid for dissociation processes in which a single atom or a small radical is split off the decomposed molecule. There is, however, not a sufficiently large number of experimental determinations to generalize this finding in the form of a rule that the A factors for *all* unimolecular reactions involving single bond fission resulting in the release of an atom or small radical lie in the range $10^{12}-10^{14}$ sec^{-1}. The A factors of the unimolecular reactions about which our knowledge is less certain lie between 10^{11} and 10^{15} sec^{-1}.

Experimentally it is much easier to determine k than either E or A in the Arrhenius equation. So when E cannot be directly determined with sufficient accuracy, a suggestive interpretation of results may often be obtained by making the *assumption* that $A=10^{13}$ sec^{-1}. It must be realized that such an activation energy is quite likely to be in error by 2–3 kcal/mole and in extreme cases even by as much as 5 kcal.

The study of a series of related reactions, say the pyrolysis of a number of compounds $R'X$, $R''X$, $R'''X\cdots$, where X is a small radical or atom that is split off in the course of the reaction by breaking the same bond in each case, is of special interest in chemical kinetics. The recombination of the two radicals formed is believed to take place without any energy of activation, and hence the energy of activation of the decomposition may be used as a measure of bond strength. Then the principal interest lies in the variation of the energy of fission among the series. Frequently, the activation energies cannot be determined directly with sufficient accuracy to show clearly the differences between the various compounds, and it is often fruitful to *assume* that A is constant for the whole series so that the differences in activation energy may be calculated from the determination of the relative rate constants for the decomposition at one temperature. Errors in the differences are probably much smaller than the error involved in assuming any particular value of A for the calculation of an absolute energy of activation. The plausible assumption of constancy of A throughout a series of related reactions has not yet been shown to be valid, and it is justified solely by the interesting and reasonable variations in activation energies found by making use of it.

Letters to the Editor

THIS section will accept reports of new work, provided these are terse and contain few figures, and especially few half-tone cuts. The Editorial Board will not hold itself responsible for opinions expressed by the correspondents. Contributions to this section should not exceed 600 words in length and must reach the office of the Editor not later than the 15th of the second month preceding that of the issue in which the letter is to appear. No proof will be sent to the authors. A publication charge of $10.00 per Letter is made which, when honored, will entitle the Institution to 100 free reprints.

Direct Observation of the Rate of Recombination of Iodine Atoms*

NORMAN DAVIDSON, ROYAL MARSHALL, A. E. LARSH, JR., AND TUCKER CARRINGTON
Gates and Crellin Laboratories of Chemistry, California Institute of Technology, Pasadena, California
(Received July 19, 1951)

A SHORT, intense pulse of light from the flash lamp, FL (Fig. 1), dissociates some (*ca* 4 percent) of the iodine molecules in cell C. In the presence of an inert gas, M, the iodine atoms thus formed subsequently recombine by the homogeneous three body process:

$$I+I+M\rightarrow I_2+M, \quad d[I_2]/dt=k[I]^2[M]. \qquad (1)$$

The iodine molecule concentration as a function of time is measured photoelectrically with the aid of the constant light beam, L (wavelength selected by the filter, F), and displayed as the vertical coordinate on the screen of an oscilloscope. A single sweep (Fig. 1) shows a large spike due to scattered light from the flash lamp, and a subsequent slow return of the photocurrent to its steady value as reaction (1) occurs.

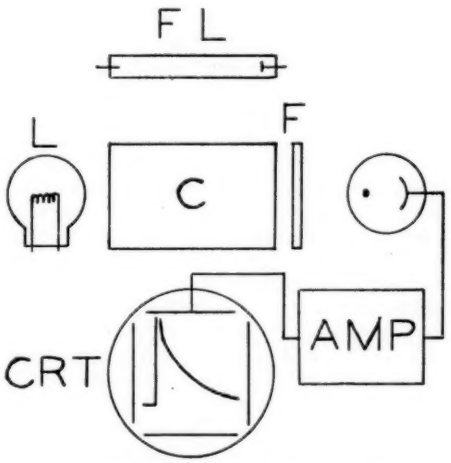

FIG. 1. Schematic diagram of the apparatus.

The flash tube is of quartz, 4 mm i.d., 15 cm long, and filled with xenon at *ca* 12-cm pressure; it is similar to the General Electric FT-127 tube. Fifty joules, stored in a 1-μf condenser at 10,000 volts, can be discharged through the tube in about 10 microseconds. Typically, the iodine pressure was 0.20 mm (1.1×10^{-6} mole liter^{-1}); the degree of dissociation was *ca* 4 percent, corresponding to the absorption of 5×10^{16} quanta (0.02 joule) in C. With argon at 1-atmos pressure as the third body, the half-time for recombination was about 0.004 sec.

The change in iodine molecule concentration from its equilibrium value, $\Delta(t)=[I_2]_\infty-[I_2]_t$, with time, t, after a flash satisfies the equation $[1/\Delta(t)-1/\Delta(0)]=k[M]t$, as predicted from (1). The values of k obtained in a series of experiments with argon as the third body (M) are:

p_A (mm)	206	380	627	703	740	1580
$k\times10^{-9}$ (mole^{-2} liter^2 sec^{-1})	4.7	4.4_5	4.5_5	4.1	4.3	3.9.

There is a hint that k decreases with increasing M; this is probably due to a systematic error not yet eliminated, rather than to the beginning of a transition from ter- to bimolecular recombination.

The average value of k (at 25°C) is 4.5×10^9. Rabinowitch and Wood[1] measured $k=6.5\times10^9$ for argon as a third body by the photostationary state technique.

With some improvements in instrumentation, the present technique can be used to measure the much faster rate of recombination of iodine atoms in solution, where the photostationary state method is not directly applicable because of uncertainty as to the quantum yield for photodissociation in solution.[2]

Further studies of the rate of recombination of iodine atoms in solution and in the gas phase are in progress. It may be recalled that Norrish and Porter[3] have independently introduced the use of flash lamps for the study of photochemical problems.

We are indebted to Haskell Shapiro and Dr. Alvin Tollestrup for helpful advice.

* Research supported by the ONR, under contract N-onr220 (01).

[1] E. Rabinowitch and W. C. Wood, J. Chem. Phys. **4**, 497 (1936).
[2] E. Rabinowitch and W. C. Wood, Trans. Faraday Soc. **32**, 547 (1936); see also, J. Zimmerman and R. M. Noyes, J. Chem. Phys. **18**, 658 (1950).
[3] R. G. W. Norrish and G. Porter, Nature, **164**, 658 (1949); G. Porter, Proc. Roy. Soc. (London) **A200**, 284 (1950).

Note on the Infrared Spectrum of Sulfur Hexafluoride

D. EDELSON AND K. B. MCAFEE
Bell Telephone Laboratories, Murray Hill, New Jersey
(Received June 20, 1951)

LAGEMANN and Jones[1] have recently reported a re-examination of the infrared spectrum of sulfur hexafluoride with a view toward improving the original work of Eucken and Ahrens.[2] We have also reinvestigated this spectrum, and, although our results agree in the main with those of Lagemann and Jones, a few differences are worth reporting.

The presence of other fluorides of sulfur in the sample of SF_6 is mentioned by Lagemann and Jones as a possible source of error, and they attribute some of the lines reported by Eucken and Ahrens to the presence of SF_4. One of us[3] has measured the infrared spectrum of disulfur decafluoride,[4] S_2F_{10}, and we have found that some of the bands reported in SF_6 which have not been satisfactorily explained may in reality be due to contamination with this fluoride. The main absorption peaks for S_2F_{10} occur at 544, 576, 683, 827, 890, 940, 1256, and 1497 cm^{-1}. The band reported by both previous workers at about 540 cm^{-1} has not been found by us in our sample of SF_6, nor have those reported by Lagemann and Jones at 693, 825, and 1502; it seems reasonable that these are due to S_2F_{10}. This resolves the difficulty of being forced to assign these frequencies to difference combinations of fundamentals where the corresponding sums do not appear.

The S_2F_{10} absorptions at 890 and 940 cm^{-1} occur in the same region as the strong absorptions in SF_6 and would be completely masked out. The peak at 1256 seems to have increased the intensity of the SF_6 peak at 1250 cm^{-1} (we find 1258 cm^{-1}) to about twice that of the neighboring peak at 1276 cm^{-1} (our value 1284 cm^{-1}) whereas we find it is only slightly higher in our sample. The absorption at 1276 cm^{-1} is left unassigned by Lagemann and Jones; we suggest the assignment $2\nu_3-\nu_4=1265$ cm^{-1}.

The very weak absorption at 1026 cm^{-1} has also been found by us; however, by subjecting the gas to electrical discharge this peak may be increased in intensity several hundred-fold, and we have concluded that it is most probably due to a decomposition product of SF_6 which has not yet been identified.

The value we obtain for the fundamental ν_3 is 947 cm^{-1} as compared to 940 reported by Lagemann and Jones; the discrepancy is probably within experimental error. The value 363 for the inactive fundamental ν_6 seems to be high by about 10–20 cm^{-1} in view of a consistent error in the calculated *vs* the observed frequencies. The agreement in the case of the peak at 925 cm^{-1} is probably fortuitous, and we doubt if the assignment $2\nu_2-\nu_6$ is proper for so strong a vibration.

The authors wish to acknowledge stimulating discussions with Mr. G. T. Kohman and the assistance of Mr. K. H. Storks and Miss D. M. Dodd in the spectrographic work.

[1] R. T. Lagemann and E. A. Jones, J. Chem. Phys. **19**, 534 (1951).
[2] A. Eucken and H. Ahrens, Z. physik Chem. **B26**, 297 (1934).
[3] D. Edelson (to be published).
[4] Obtained through the courtesy of the Pennsylvania Salt Manufacturing Company, Chestnut Hill, Philadelphia, Pennsylvania.

An Infrared Study of the Polymer Bands of Hydrogen Fluoride Vapor*

RUSSELL D. SHELTON AND ALVIN H. NIELSEN
Department of Physics, The University of Tennessee, Knoxville, Tennessee
(Received July 24, 1951)

THIS study was undertaken with a view to examining in greater detail the HF polymer bands reported by Bushwell, Maycock, and Rodebush.[1] They found that the polymer absorption consisted of two maxima with roughly the same separation as the *P* and *R* branches of the monomer absorption. An electron diffraction study by Bauer, Beach, and Simons[2] had predicted a fairly linear chainlike structure for the polymer with the hydrogen atoms not greatly out of line with the fluorine atoms. The polymers were supposed to exist as dimers, trimers, etc. Other models had also been suggested.

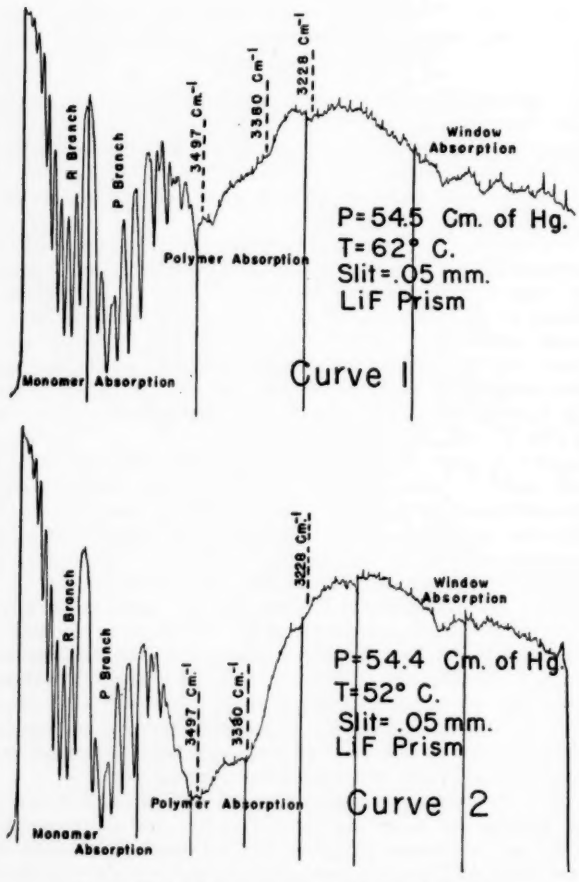

FIG. 1. Effect of temperature on polymer absorption.

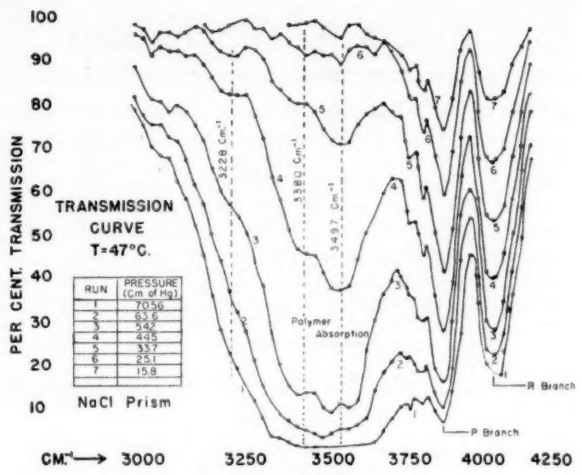

FIG. 2. Effect of pressure on polymer absorption.

The apparatus consisted of a 12.5-cm copper cell wrapped with a Nichrome heating coil and closed with fluorothene windows. A gas-handling system was arranged so that it could be conveniently mounted on a Perkin-Elmer model 12B spectrograph. Thermocouples were set in the cell for temperature measurements of the gas. Pressure measurements were made with a Booth-Kromer-type gauge. Spectral records were made at constant temperature for pressures which ranged from atmospheric to vacuum in steps of about 10 cm of mercury. The temperatures ranged from 32°C to 88°C in intervals of about 8°C. There should be no polymers at 85°C. Records were made with LiF, CaF_2, and NaCl prisms over the spectral interval, 3000 cm^{-1} to 4250 cm^{-1}.

Examples of the curves obtained are shown in Figs. 1 and 2. Figure 1 shows two records taken with the LiF prism at the same pressure but at different temperatures. In curve 1, at 62°C, the HF monomer is resolved into rotational structure. Three distinct bands ascribed to the polymer may be seen at 3228 cm^{-1}, 3380 cm^{-1}, and 3497 cm^{-1}. Curve 2, taken at 52°C, shows the monomer slightly less intense; but the three polymer bands are greatly enhanced, particularly the two high frequency ones. A fairly small temperature change has a large effect on the intensity of these bands. It appears from this that the polymers are comparatively few in number but that they are intense absorbers, for if they had contributed greatly to the total pressure, their disappearance at the higher temperature should have caused the monomer band to become much more intense. Figure 2 shows a series of percent transmission curves taken with the NaCl prism at 47°C, with the pressure varying from 15.8 cm to 70.56 cm. The three polymer bands may easily be seen, and in this figure it seems clear that the two high frequency polymer bands increase much more rapidly than the low frequency one.

If the chain model is assumed, it is possible to explain the three polymer bands on the basis of the perturbation of the HF frequency, depending on the position of the bond in the chain. Two positions of the HF bond might occur, an interior and an exterior. In one type of bond, the hydrogen lies between an external and an internal fluorine, in another type of bond, the hydrogen lies between internal fluorines, and in a third type of bond, the hydrogen is external. Because of the different associative fields, it seems reasonable to suggest that the HF frequency could have slightly different values for the three positions of the hydrogen and that there would thus be three bands.

An application of the Beer-Lambert law of absorption was made to the monomer band. A rough calculation of the monomer partial pressure demonstrated that the polymers were few in

number, even under the most favorable conditions for polymer formation—i.e., at low temperatures and high pressures. The absorption coefficient for the polymers was, however, much larger than for the monomer, which is consistent with the large dipole moment of the chain model, as was found by Oriani and Smyth.[3]

* Submitted to the Graduate School of the University of Tennessee in partial fulfillment of the requirements for the degree of Master of Science.

[1] Bushwell, Maycock, and Rodebush, J. Chem. Phys. **8**, 362 (1940).
[2] Bauer, Beach, and Simons, J. Am. Chem. Soc. **61**, 19 (1939).
[3] R. A. Oriani and C. P. Smyth, J. Am. Chem. Soc. **70**, 125 (1948).

Photoelectric Observation of the Rate of Dissociation of N_2O_4 by a Shock Wave

TUCKER CARRINGTON AND NORMAN DAVIDSON
Gates and Crellin Laboratories of Chemistry, California Institute of Technology, Pasadena, California
(Received August 13, 1951)

BESIDES being intrinsically of interest for chemical kinetics, the rates of the very fast reactions, $N_2O_4 \rightleftarrows 2NO_2$, have been of special interest in connection with the study of the dispersion of sound velocity in a dissociating gas.[1] The interpretation of the acoustic measurements is not certain because of the smallness of the observed effects, uncertainties as to the contribution of vibrational heat capacity lag, and other difficulties.[2,3] Brass and Tolman[4] measured the cooling of a gas mixture flowing from a set of orifices, and thus estimated the rate constant.

In view of the approximate nature of the results obtained so far, we are endeavoring to study the rate of the reaction by a more direct method. If an equilibrium NO_2, N_2O_4 mixture is rapidly compressed and heated, the subsequent dissociation of N_2O_4 can be followed by fast photoelectric techniques. Passage of a shock wave provides a rapid adiabatic (but not isentropic) compression. The weak uniform shocks required can be generated in a shock tube.[5,6]

The tube used was steel, 5 cm square in cross section, with a one-meter compression section separated from a two-meter expansion section by a Cellophane diaphragm. In a typical experiment, the compression chamber contained nitrogen at 25° and 2 atmos pressure; the expansion chamber, cooled to 4°, contained nitrogen at 1 atmos and NO_2 and N_2O_4 at 5.8 and 2.1 mm. When the membrane is burst, a shock wave travels down the expansion chamber. The shock pressure and temperature ratios are estimated as 1.40 and 1.08. Observations of the rate of dissociation of N_2O_4 in the shocked gas were made through quartz windows, flush with the tube walls, and 60 cm from the diaphragm. A light beam, defined by 1-mm slits, passes transversely through the tube and onto a photomultiplier tube. As the shock wave passes through the light beam, the photocurrent, displayed as an oscilloscope trace, shows a sharp negative spike followed immediately by a smaller positive one, altogether lasting about 4 microseconds. These are presumably schlieren effects and obscure the initial compression of the gas and the early stages of the reaction. When the observing light is $\lambda = 436$ mμ, absorbed by NO_2, the photocurrent subsequently falls, at a gradually decreasing rate, as the NO_2 concentration rises to its new equilibrium value. With $\lambda = 254$ mμ, absorbed principally by N_2O_4, the complementary decrease in N_2O_4 concentration is observed. The half-time of the reaction is about 5 microseconds.

Precise measurements of the shock velocity, and hence of the shock temperature and pressure, have not yet been made. These parameters have been estimated from the initial pressures in the compression and expansion chambers.[5] In spite of the low pressure of N_2O_4, the chemical contribution to the equilibrium heat capacity is significant (γ *ca* 1.3, instead of 1.4) in this estimation. The analysis of Bethe and Teller[7] is used to calculate the changes in pressure, temperature, and mass velocity as the gas immediately behind the shock front relaxes to chemical equilibrium. It is interesting that theory predicts that, for the weak shocks used, the gas warms up slightly (1–3°) as dissociation occurs.

Our preliminary experiments give a unimolecular rate constant for the dissociation of N_2O_4 of 1×10^5 sec^{-1}, at 25° and 1 atmos of N_2. A variation of rate with temperature of the expected magnitude is observed, but the measurements are not yet very accurate. Richards and Reid give 5×10^4 (25°, $P_{NO_2}+P_{N_2O_4}=250$ mm); Brass and Tolman estimate 6×10^4 (25°, $P_{NO_2}+P_{N_2O_4}=1$ atmos).

We are indebted to W. M. Cady and J. G. Kirkwood for advice and to the ONR for financial aid.

[1] A. Einstein, Sitzber. preuss. Akad. Wiss. 380 (1920).
[2] W. T. Richards and J. A. Reid, J. Chem. Phys. **1**, 114 (1933).
[3] H. O. Kneser and O. Gauler, Physik. Z. **37**, 677 (1936).
[4] P. D. Brass and R. C. Tolman, J. Am. Chem. Soc. **54**, 1003 (1932).
[5] W. Payman and W. C. F. Shepperd, Proc. Roy. Soc. (London) **A186**, 293 (1949).
[6] Bleakney, Weimer, and Fletcher, Rev. Sci. Instr. **20**, 807 (1949).
[7] H. A. Bethe and E. Teller, "Deviations from thermal equilibrium in shock waves," Aberdeen Proving Grounds Report No. X-117 (1940).

The Gas Imperfection Correction for the Entropy of Ethyl and Methyl Alcohol

KAZUO ITO
Department of Chemistry, Faculty of Science, Nagoya University, Nagoya, Japan
(Received August 13, 1951)

ON the entropy of ethylalcohol J. O. Halford[1] pointed out the important role of a gas imperfection correction. On the other hand, J. D. Rambert and his co-workers[2] found that the P–V–T relation of some organic vapors as acetaldehyde, aceton, acetnitrile, and methylalcohol which have some dipole moments indicate a rather large deviation from the Berthelot equation. It is very desirable, then, to find a simple and not so inaccurate method for a gas imperfection correction of entropy. The method of the correction now proposed is as follows. When the Berthelot type equation is assumed for the P–V–T relations of vapors, the gas imperfection correction of the entropy S^0-S and of the heat of vaporization L^0-L are

$$S^0-S=27RT^3cP/32T^3Pc, \quad (1)$$

$$L^0-L=-9RTcP(1-18T^2c/T^2)/128Pc=81RT^3cP/64T^2Pc, \quad (2)$$

where the constants Tc and Pc have no meaning as critical pressure and temperature without their dimensions. From (1) and (2)

$$S^0-S=2(L^0-L)/3T. \quad (3)$$

If the vapor pressure and heat of vaporization data, which are relatively accessible in many cases, are available, S^0-S can be calculated from L^0-L by (3). When this method is used, two-thirds of the error in the observed entropy of vaporization can be canceled, since $-2L/3T$ is in (3). Values obtained by the use of (3) for ethylalcohol[3,4] are given in Table I together with those by the Berthelot equation and by J. O. Halford.[1] Values obtained for methylalcohol[4] are given in Table II. About these correction values it is very notable that the hindering barriers of ethyl-[1] and methylalcohol[5–7] are not determined satisfactorily from thermal data. On the hindering barrier of methylalcohol, Crawford[5]

TABLE I.

	298.2	351.5	403.2°K	
Berthelot	0.01	0.08	0.32	e.u.
Halford	0.03∼0.05	0.22∼0.42	0.82∼1.61	
Ito	0.05	0.86	1.69	

TABLE II.

	298.2	337.9	383.2°K	
S^0-S	0.61	0.91	1.72	e.u.

pointed out that the hindering barrier, determined spectroscopically, gave the discrepancy of 0.6 e.u. between the observed and calculated entropy value at 298.2°K and Kimura[6] pointed out also that when the other molecular data are used, more discrepancy is possible at 298.2°K.

[1] J. O. Halford, J. Chem. Phys. **17**, 111 (1949).
[2] Lambert, Robert, Robinson, and Wilkinson, Proc. Roy. Soc. (London) **A196**, 113 (1949).
[3] Ransay and Yound, Trans. Roy. Soc. (London) **177**, 123 (1886).
[4] Fiock, Ginnings, and Holton, J. Research Natl. Bur. Standards **6**, 881 (1931).
[5] B. L. Crawford, J. Chem. Phys. **8**, 744 (1940).
[6] M. Kimura, J. Chem. Soc. Japan **71**, 19 (1950).
[7] F. A. French and R. S. Rasmussen, J. Chem. Phys. **14**, 394 (1946).

The Crystal Structure of Chromium (II) Chloride

L. L. Handy and N. W. Gregory
Department of Chemistry and Chemical Engineering, University of Washington, Seattle, Washington
(Received July 19, 1951)

In connection with studies pertaining to thermodynamic and structural properties of chromium halides, we have found it possible to index diffraction lines appearing on powder patterns of anhydrous $CrCl_2$ on the basis of an orthorhombic unit cell with lattice constants $a=6.65$, $b=5.99$, and $c=3.48$ A° with an estimated uncertainty of ±0.01 A°. Patterns were also obtained for $CrBr_2$ and CrI_2 but these have not been indexed. They do not appear to be hexagonal as would be predicted from consideration of radius ratio and comparison with the dihalides of other metals near chromium in the periodic table. The latter confirms the observations of Klemm and Grimm[1] who report that they were unable to index patterns observed for the chromium (II) halides. The hygroscopic character and low volatility of these substances make single crystal studies difficult.

Table I. Powder pattern data for chromous chloride.

h k l	Relative intensity	*d*(obs)	*d*(calc)
1 1 0	10	4.453	4.448
2 0 0	2	3.311	3.322
0 2 0	3	2.996	2.994
2 1 0	7	2.892	2.905
1 1 1	8	2.741	2.741
2 2 0	7	2.228	2.224
1 2 1	8	2.147	2.147
3 0 1	6	1.867	1.868
0 0 2	4	1.740	1.740
1 3 1	1	1.676	1.676
1 1 2	3	1.621	1.620
0 4 0	4	1.497	1.497
4 2 0	5	1.453	1.453
0 0 3			1.160
3 4 1	1	1.163	1.168
4 4 0	1	1.112	1.112
2 4 2	1	1.070	1.073

Some similarity between the diffraction pattern reported for $CaCl_2$[2] and that observed for $CrCl_2$ indicates that the latter may be related to the tetragonal rutile structure but with considerably more distortion. Assuming on this basis that the unit cell contains two molecules, the density of $CrCl_2$ calculated from the observed lattice constants is 2.95. This is in good agreement with the molar volume of 42 cc ($d=2.93$) estimated by Klemm and Grimm[1] and only slightly higher than the value 2.878 reported by Biltz and Birk.[3]

$CrCl_2$ was prepared by direct reaction of chromium metal with anhydrous HCl in a quartz vessel at 850°, and purified by sublimation under high vacuum. Samples were mounted in sealed thin-walled Pyrex tubes (approximately 0.6 mm diameter) and powder patterns taken with copper radiation filtered with nickel.

[1] W. Klemm and L. Grimm, Z. anorg. u. allgem. Chem. **249**, 198 (1942).
[2] W. Klemm and W. Doll, Z. anorg. u. allgem. Chem. **241**, 239 (1939).
[3] W. Biltz and E. Birk, Z. anorg. u. allgem. Chem. **134**, 125 (1924).

Rotation of *n*-Butylic Radical in Crystalline State

Tsutomu Oda, Kenzo Sakata, and Seiichi Kondo
Chemical Laboratory, Osaka Liberal Arts University, Osaka, Japan
(Received July 30, 1951)

Barium dicalcium *n*-butylate was first prepared by Fritz and Sansoni[1] who reported that it crystallizes in the cubic system, isomorphous with barium dicalcium propionate. The crystal structure of the latter had already been determined independently by Nitta and Watanabé[2] and by Biefeld and Harris.[3] According to their interpretation, the methyl group in the propionic radical is to be looked upon as rotating, partially or completely about the C−C bond. This point of view is in harmony with the recent thermometric investigation on this substance, in which a phase transition was found to occur at about −6°C.[4] We have undertaken an investigation to determine whether barium dicalcium *n*-butylate has the same type of structure as that of barium dicalcium propionate.

Single crystals of barium dicalcium *n*-butylate were grown from aqueous solutions containing barium and calcium *n*-butylate in roughly calculated proportions. The crystals obtained are confirmed to be optically isotropic, and the crystal density found to be 1.49 g/cm³ at 28°C. Laue, oscillation, and rotation photographs taken, using Cu−Kα and Mo−Kα radiations, show that the crystal conforms to a cubic face-centered lattice with a unit edge $a=18.6$A, containing eight formula units of $BaCa_2(CH_3CH_2CH_2COO)_6$. The space group is either O_h^7-Fd3m or O^4-F4_13. The structure factor calculations show that the crystal structure is isomorphous with the propionate. The β- and γ-carbon atoms possess no fixed positions, but either rotate or show orientational disorder about the C−C bond between the carboxyl and the α-carbon atoms, so as to fulfill the required diagonal symmetry (in the statistical sense) of the *n*-butylic radical. Thus, this structure affords another example of the $O-4_3$ type. It may be possible that the present crystal undergoes a phase transition at a lower temperature, analogously to barium dicalcium propionate.

The authors are deeply indebted to Professors Nitta, Watanabé, and Kikuchi and to Dr. Seki of the Osaka University for valuable suggestions and encouragements.

[1] A. Fritz and F. Sansoni, Ber. deut. chem. Ges. **13**, 1312 (1880); P. Groth, Chem. Krist. III. 245 (1910).
[2] I. Nitta and T. Watanabé, Sci. Papers Inst. Phys. Chem. Research, Tokyo **26**, 164 (1935).
[3] L. P. Biefeld and P. M. Harris, J. Am. Chem. Soc. **57**, 396 (1935).
[4] Seki, Momotani, and Nakatsu, J. Chem. Phys. (to be published).

Two New Absorption Bands of N_2O

J. H. Taylor
Department of Physics, Johns Hopkins University, Baltimore, Maryland
(Received August 15, 1951)

The purpose of this note is to report on the observation of the $0\ 1^1\ 0 \rightarrow 1\ 0\ 0$ and $0\ 2^0\ 0 \rightarrow 1\ 1^1\ 0$ bands of the nitrous oxide molecule.

A Perkin-Elmer Model 12-C infrared spectrometer was used with a one-meter absorption cell filled to atmospheric pressure. To guard against the possibility of an impurity both commercial N_2O obtained from the Mathieson Company (East Rutherford, New Jersey) as well as N_2O prepared for anaesthesia purposes

Table I. Calculated and observed wave numbers for two new absorption bands of gaseous N_2O.

Transition	ν (Calculated) cm^{-1}	ν (Observed) cm^{-1}
$0\ 1^1\ 0 \rightarrow 1\ 0\ 0$	696	696
$0\ 2^0\ 0 \rightarrow 1\ 1^1\ 0$	701	702

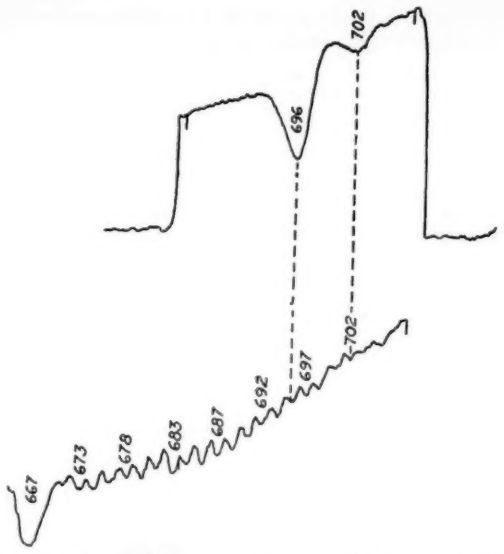

FIG. 1. (Upper curve.) The 0 1^1 0→1 0 0 and 0 2^0 0→1 1^1 0 bands of the nitrous oxide molecule using 0.30-mm slits. (Lower curve.) The 15-micron CO_2 band using 0.18-mm slits.

were examined. In addition, a sample of the medical grade gas was collected in a liquid nitrogen cold trap and subsequently distilled, the first and last thirds being discarded, and the middle third collected and passed into the absorption cell. In each case the two bands showed at the same relative intensity.

Figure 1 (upper curve) shows these two bands using 0.30-mm slits and a Globar source, and Table I gives the calculated and observed wave numbers for the two transitions. The calculated values for these two bands (to three places) have been determined from the data given by G. Herzberg.[1] In order to resolve the 15-micron CO_2 band more clearly for an accurate wavelength calibration in this spectral region, a carbon arc was set up as a source, giving the spectrum shown in Fig. 1 (lower curve). These spectra were all obtained with the gas at room temperature. The exact positions of these bands is somewhat difficult to determine, especially the weak 0 2^0 0→1 1^1 0 band, due to the unresolved background of CO_2.

[1] G. Herzberg, *Infrared and Raman Spectra* (D. Van Nostrand Company, Inc., New York), p. 278, Table 58.

The Configuration of Real Polymer Chains

T. B. GRIMLEY
Department of Inorganic and Physical Chemistry, University of Liverpool, Liverpool, England
(Received December 11, 1950)

IN a recent paper under this title, Flory[1] has attempted to discuss the volume effect in coiling long chain molecules. It is the purpose of this note to point out that the volume effect found by Flory is spurious, having its origin in inconsistencies in the mathematical treatment rather than in any real property of the polymer chain.

Flory considers a system containing N polymer molecules in a solution so dilute that interactions between polymer molecules may be disregarded and defines the state of the system in terms of the numbers N_i of molecules having their ends separated by the distance r_i. For ω_i, the number of configurations available to a chain molecule having the length r_i, Flory writes

$$\omega_i + f_i W_i \omega_0, \tag{1}$$

where ω_0 is the total number of configurations available to a random flight chain and W_i is the probability distribution of the r_i in such a chain. $\omega_0 W_i$ is the number of configurations available to a random flight chain of displacement length r_i, and f_i is the fraction of these which are acceptable to a real chain. For Ω, the total number of internal configurations of the system consistent with the distribution N_i, one thus has

$$\Omega = \Omega_0 N! \Pi_i [(f_i W_i)^{N_i}/N_i!], \tag{2}$$

where $\Omega_0 = \omega_0^N$ is the total number of internal configurations for a system of N random flight chains.

Now (N_i/N) is, by definition, the probability distribution of the r_i so that, using Eq. (1), we have

$$N_i/N = f_i W_i / \Sigma_i f_i W_i. \tag{3}$$

Taking logarithms in (2) and using (3) together with Stirling's approximation, the result may be written

$$\ln(\Omega/\Omega_0) = N \ln \bar{f}, \tag{4}$$

where the average value $\bar{f}$ is defined by

$$\bar{f} = \Sigma_i f_i W_i. \tag{5}$$

To the accuracy of Stirling's approximation, Eq. (4) is exact. It is not, however, the equation found by Flory. Flory's equation (Eq. (6) of his paper) may be put into the form,

$$\ln(\Omega/\Omega_0) = N \ln \bar{f} - \Sigma_i N_i \ln(f_i/f). \tag{6}$$

The quantity f is not defined explicitly in Flory's paper, but it is clear that f must be taken so that the second term on the right in (6) is zero. Flory takes f as the probability that the segments of a chain do not interfere when distribution of segments about the center of gravity has the form, $W'(s/\alpha)$. $W'(s)$ is the corresponding distribution in a random flight chain and α is a factor expressing the expansion of a real chain referred to a random flight chain. f is therefore a function of α. Flory also assumes that the probability distribution of the r_i in a real chain has the form $W(r_i/\alpha)$, where $W(r_i)$ is the corresponding distribution (W_i above) in a random flight chain. In this way he derives an equation for α by maximizing the expression (6) for $\ln(\Omega/\Omega_0)$. Since $\bar{f}$ involves only quantities defined in a random flight chain, the first term on the right in (6) is independent of α. Flory's choice of α (and, hence, of f) is therefore defined by

$$(\partial/\partial\alpha)\Sigma_i N_i \ln(f_i/f) = 0. \tag{7}$$

As already mentioned, the only choice of f is that for which the equation

$$\Sigma_i N_i \ln(f_i/f) = 0 \tag{8}$$

is satisfied. If we assume with Flory that the chain length distribution has the form, $W(f_i/\alpha)$, Eq. (8) leads to

$$\ln f = (3/2)(\alpha^2 - 1) - 3 \ln\alpha + \ln \bar{f}.$$

This is the definition of f in terms of the expansion factor α for which Eq. (6) is exact. The use of this definition reduces (7) to an identity and does not yield an equation for α. Of course, if we attribute to f the physical significance attributed to it by Flory than f is given approximately by Eq. (11) of reference 1, i.e., $\ln f = -cz^{\frac{1}{2}}/\alpha^3$, and Eq. (7) then gives

$$\alpha^5 - \alpha^3 = cz^{\frac{1}{2}}, \tag{9}$$

which is Flory's equation for α. It is obvious however that the value of α determined by (9) has nothing to do with the volume effect. The fact that we get an equation for α at all means only that f does not have the physical significance assumed.

[1] P. J. Flory, J. Chem. Phys. **17**, 303 (1949).

The Configuration of Real Polymer Chains

P. J. FLORY
Department of Chemistry, Cornell University, Ithaca, New York
(Received July 30, 1951)

EQUATION (6) in the foregoing letter is *not* equivalent to my Eq. (6),[1] which was written for any distribution of the N_i. Grimley's Eq. (6) is obtained from mine *only* for the special case of the most probable distribution $N_i = N f_i W_i / \Sigma f_i W_i = N f_i W_i / \bar{f}$.

Having already introduced the most probable distribution in this way, Grimley seeks to apply the operation of maximizing *his* $\ln(\Omega/\Omega_0)$, which is a constant! This unjustified step leads to his Eq. (7) and the identity resulting from its subsequent application, on the basis of which he condemns *my* procedure rather than his own! The fallacy involved is too obvious to warrant further comment. His criticisms are entirely unfounded.

Clarification of f and the derivation of the previous Eq. (6)[1] may be in order in view of the confusion which has arisen. Introducing Stirling's approximation into my Eq. (5)

$$\ln(\Omega/\Omega_0)=N\ln(fN)+\Sigma N_i\ln(W_i/N_i)+\Sigma N_i\ln(f_i/f), \quad (5')$$

where the quantity $N\ln f$ has been added to one term and subtracted from the other. Now in estimating the magnitude of the interference,[1] f has been treated as the average fraction of random flight configurations for the existing distribution (specified by the N_i) which are not rendered impossible by interference. Thus,

$$f=\Sigma N_i f_i/N$$

(not to be confused with Grimley's $\bar{f}$). With this definition of f, the last term in Eq. (5′) should be small. Neglecting it, we obtain my Eq. (6) as an approximate expression for $\ln(\Omega/\Omega_0)$ for any arbitrary distribution. We thus have Grimley's Eq. (8) as an approximate expression, according to the present definition of f, for *any arbitrary distribution.*

[1] P. J. Flory, J. Chem. Phys. **17**, 303 (1949).

External Oscillations and Specific Heat of Calcite

L. Giulotto and A. Loinger
Istituto di Fisica dell' Università di Pavia, Pavia, Italy
(Received May 18, 1951)

THE problem of the coupling between torsional and translational oscillations of a complex ion in a crystal lattice is here considered for calcite. The number and polarization of the lines in the low frequency Raman and infrared spectra of calcite have already been satisfactorily explained by consideration of the symmetry of the lattice forces.[1,2] By accepting certain external frequencies as data and by making certain simplifying assumptions we have evaluated the other external frequencies of calcite, and have then calculated the specific heat.

To illustrate the method of calculation the torsional and translational motions whose coupling gives rise to two Raman frequencies (chosen as an example) are shown in Fig. 1. The existence of such a coupling may be understood by consideration of the symmetry of the forces acting when the CO_3 ion leaves its equilibrium position in the lattice; see Fig. 2 where the position of a CO_3 group relative to the six nearest Ca ions is shown. The equations of motion of these oscillations are:

$$\begin{cases} -\dfrac{\partial^2 U_2}{\partial z^2}Z-\dfrac{\partial^2 U_2}{\partial y\partial z}Y=m\dfrac{d^2Z}{dt^2} \\ -\dfrac{\partial^2 U_1}{\partial y^2}+2\dfrac{\partial^2 U_2}{\partial y^2}Y-2\dfrac{\partial^2 U_2}{\partial y\partial z}Z=M\dfrac{d^2Y}{dt^2}, \end{cases} \quad (1)$$

where Z and Y are, respectively, torsional and translational coordinates and where m, M are respectively the masses of the oxygen atom and of the CO_3 ion and $U_1(x,y,z)$, $U_2(x,y,z)$ are the potential energies of the oxygen atoms, O_1 and O_2, relative to rigid motions of the CO_3 ion.

U_1 and U_2 are given by the following expressions, justified by reasons of symmetry:

$$U_1=c_1x^2+c_2y^2+c_3z^2+c_{13}xz;$$

$$U_2=[(c_1+3c_2)/4]x^2+[(3c_1+c_2)/4]y^2+c_3z^2 -[\sqrt{3}(c_1-c_2)/2]xy-(\tfrac{1}{2})c_{13}xz+(\sqrt{3}/2)c_{13}yz.$$

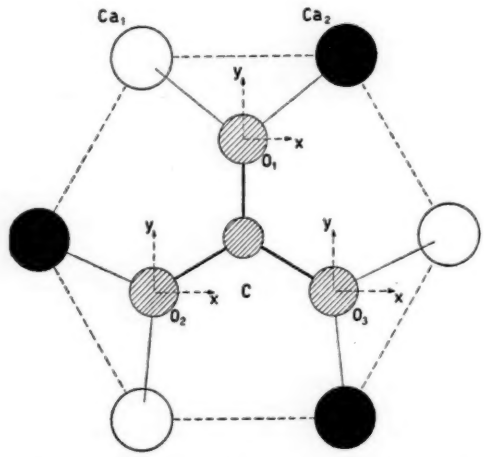

FIG. 2. Position of a CO ion with respect to the six nearest Ca ions. (See reference 3.) Black, grey, and white circles represent respectively atoms belonging to three successive lattice planes normal to the optical axis.

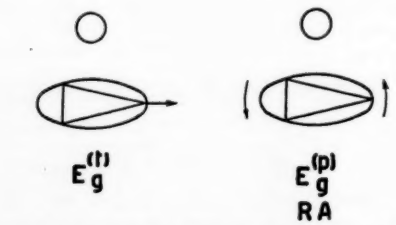

FIG. 1. Translational and torsional oscillations of the calcite unit cell whose coupling produces the two frequencies ν and ν_2. The curved arrows indicate motion into and out of the equilibrium plane.

The unit cell of a calcite lattice has, in all, ten distinct normal external frequencies; five of these are doubly degenerate. Hence ten equations of motion, analogous to (1), are obtained; from them certain relationships between the force constants c_1, c_2, c_3, c_{13}, c_{34}[3] and the frequencies can be easily deduced. By considering the ratio of the intensities of the two Raman lines, another equation containing the constants can be obtained.[4] If this ratio, the two Raman frequencies, and two of the infrared frequencies are taken from experimental data, it is possible to calculate the other external lattice frequencies, their values being reported in Table I (the values in ( ) are taken from experimental data).

The discrepancies between calculated and experimental values could be ascribed to the inaccuracy of the Reststrahlen data. In

TABLE I. Normal external frequencies of calcite (in cm^{-1}).

Exp	Calc
282	(282)
155	(155)
357	397
106	(106)
330	344
106	(106)
182(?)	260
...	269
...	99
...	295

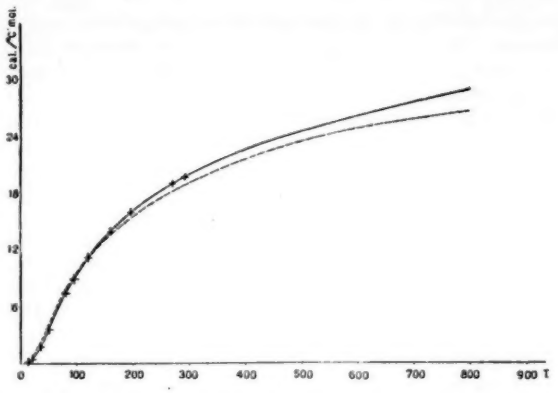

FIG. 3. Molal heat capacity of calcite as a function of the temperature. Full line: experimental C_p (from Landolt-Börnstein); dotted line: calculated C_v.

particular the experimental value of 182 cm^{-1} given by Liebisch and Rubens[5] must be considered as uncertain because the corresponding maximum is unresolved.

For the calculation of the specific heat the whole spectrum of crystal eigenfrequencies must be taken into consideration. A mole of calcite has $27(N/2)$ optical frequencies (of which $15(N/2)$ are external and $12(N/2)$ internal) and $3(N/2)$ acoustical frequencies. The contribution to the molal heat capacity, C_v, of the optical frequencies has been calculated by the use of Einstein functions and the contribution of the acoustical frequencies by Debye functions:

$$C_v=K(N/2)[\sum_{1j}^{15} E(\vartheta_j/T)+\sum_{1j}^{12} E(\vartheta_j'/T)+D(\Theta_e/T)+2D(\Theta_i/T)],$$

where ϑ_j, ϑ_j' are the Debye temperatures corresponding respectively to the external and internal eigenfrequencies,[6] Θ_e, and Θ_i are the Debye temperatures relative to the maximum acoustical longitudinal and transversal frequency of the "mean" crystal. From certain frequencies of the unit cell, with the aid of opportune approximations, Θ_e and Θ_i are evaluated. The values obtained are: $\Theta_e \simeq 203$ cm^{-1}; and $\Theta_i \simeq 149$ cm^{-1}.

In Fig. 3 the experimental molal heat capacity at constant pressure, C_p, and the computed molal heat capacity at constant volume, C_v, are compared. The agreement between them is good in the temperature range from 0 to ~150°K, in which the difference C_p-C_v is presumably negligible. Above 150°K a precise comparison with experiment cannot be made because the inadequacy of the experimental data on thermal expansion and compressibility coefficients make the determination of C_p from C_v impossible.

A more detailed paper will appear in the *Nuovo Cimento*.

[1] L. Giulotto and G. Olivelli, Nuovo cimento **5**, 52 (1948); J. Chem. Phys. **16**, 555 (1948).
[2] A. Kastler, Compt. rend. **227**, 1024 (1948); Proc. Indian Acad. Sci. **28**, 349 (1948); Z. Elektrochem. **54**, 101 (1950).
[3] c_{34} is a constant introduced to take into account the oscillations by which the Ca lattice is deformed.
[4] A. Loinger, Nuovo cimento **7**, 939 (1950).
[5] See for example, C. Schaefer and F. Matossi, *Das ultrarote Spektrum* (Berlin, 1930), p. 356.
[6] The distinct internal frequencies of the unit cell can be practically reduced to the distinct frequencies of the CO_3 ion, which are four in number.

Electrokinetic Potentials of Small Particles by the Sedimentation Method

G. A. H. ELTON
Chemistry Department, Battersea Polytechnic, London, England
(Received August 13, 1951)

IT has been shown theoretically and experimentally[1] that the rate of sedimentation of a suspension of fine particles in an ionic liquid is affected markedly by the electrokinetic potential at the particle/liquid interface due to the operation of an electroviscous resistance to the motion of each particle through its associated ionic double layer. For a dilute suspension of spherical particles of radius a in a uni-univalent electrolyte solution of ionic concentration n, the total apparent viscosity η_a at temperature T is given by[1]

$$\eta_a=\eta+\frac{16n\epsilon kTa^3N}{3\kappa}\sinh^2\left(\frac{e\zeta}{2kT}\right), \tag{1}$$

where η is the mechanical viscosity, ϵ the dielectric constant of the solution, k the Boltzmann constant, N the number of particles per cc, κ the specific conductivity of the suspension, e the charge on the electron, and ζ the electrokinetic potential of the particles. Observation of the rate of settling of particles in a given solution enables the calculation of the important quantity ζ from Eq. (1) only if the particles are spherical.[2,3] It is, however, possible, as shown below, to derive a corresponding equation for non-spherical particles, which should render fairly simple the determination of ζ for any powder,[3] provided that its surface area per gram is known or can be determined. The method of derivation given here closely follows that previously used.[1]

Consider a dilute suspension of uniform particles of any given shape, each of mass m and density ρ_2, sedimenting in an electrolyte solution of density ρ_1. If the particles carry a charge σ per unit area, a sedimentation potential gradient E is set up, given by

$$E=(AN\sigma u)/\kappa, \tag{2}$$

where A is the surface area of a single particle, and u is the velocity of sedimentation. As a given particle falls, it is subjected to a viscous resistance Fu, where F is a factor depending on the shape and size of the particle (equal to $6\pi\eta a$ for a sphere), and also to an electroviscous resistance $EA\sigma$, as the particle with charge $A\sigma$ moves against a potential gradient E. If the velocity of sedimentation in a concentrated electrolyte solution, where electroviscosity is negligible, is u_0, we have

$$Fu_0=m(1-\rho_1/\rho_2)g=Fu+EA\sigma. \tag{3}$$

Hence from Eqs. (2) and (3)

$$\sigma^2=\frac{F\kappa(u_0-u)}{A^2Nu}=\frac{mg\kappa(u_0-u)(\rho_2-\rho_1)}{A^2Nuu_0\rho_2}. \tag{4}$$

If M is the mass of particles per cc of suspension, and A_0 is the surface area per gram of powder, this reduces to

$$\sigma^2=\frac{g\kappa(u_0-u)(\rho_2-\rho_1)}{MA_0^2uu_0\rho_2}. \tag{5}$$

Thus the charge per unit area on the particles may be obtained from measurements of sedimentation velocity. The electrokinetic potential is then obtained from the expression given by Verwey and Overbeek[4]

$$\sigma=\left(\frac{2n\epsilon kT}{\pi}\right)^{\frac{1}{2}}\sinh\left(\frac{ze\zeta}{2kT}\right), \tag{6}$$

where z is the valency of the charge determining ion in the electrolyte.

A specimen of powder suitable for use in sedimentation experiments, and giving a sharp settling "meniscus" can generally be obtained fairly readily by fractional sedimentation. Calculations on the basis of Stokes' law would appear to indicate a very narrow permissible tolerance in particle size, but the electroviscous effect itself helps to sharpen the meniscus, since particles slightly larger than average carry a proportionately larger charge, and when settling in the field of the suspension experience a greater electroviscous retardation than average. They therefore show less tendency to fall away from the meniscus than would otherwise be the case. A similar effect operates with particles smaller than the average.

[1] G. A. H. Elton, Proc. Roy. Soc. (London) **A197**, 568 (1949).
[2] F. G. Hirschler, Ph.D. thesis, University of London (1951).
[3] Dulin, Elton, and Hirschler, to be published.
[4] E. J. W. Verwey and J. Th. G. Overbeek, *Theory of the Stability of Lyophobic Colloids* (Elsevier Publishing Company, Inc., London, 1948).

On the Propagation of Ultrasonic Waves in Acetic Acid

E. FREEDMAN
Department of Chemistry, Cornell University, Ithaca, New York
(Received August 13, 1951)

RECENTLY Lamb and Pinkerton[1] published extensive measurements on the velocity and absorption of ultrasonic waves in acetic acid which conclusively demonstrate the existence of velocity dispersion and the concomitant occurrence of a maximum in the absorption coefficient per wavelength near a sound frequency of one megacycle per second.[1] Acetic acid is the only liquid for which such phenomena have been observed at this low a frequency.[2]

It has been speculated[3] that this exceptional behavior is due to perturbation of the equilibrium that exists between monomeric and dimeric molecules in acetic acid. Attempts[4] have been made to work out a quasi-thermodynamic theory (similar to the one that has been given for absorption in non-associated liquids)[5] but they have not been successful. It would appear that this failure is primarily the result of the use of a first-order rate equation to describe the formation of the dimer, although the chemical equation

$$2\mathrm{HOAc} \underset{k_2}{\overset{k_1}{\rightleftarrows}} (\mathrm{HOAc})_2$$

(where k_1 and k_2 are rate constants) suggests that second-order equation be used instead. A calculation based on the use of a second-order equation has been carried through, the procedure used being otherwise quite similar to that employed by E. Bauer.[5] The principal result is the equation,

$$\mu(\nu)=\frac{\pi}{2}\frac{c^2}{c_0^2}\frac{C_P}{C_V}\frac{x(C_P-C_v)(\Delta H)^2K(\nu/\nu_1)}{RT^2\{(4K+1)C_P^2+(C_P'K\nu/\nu_1)^2\}},$$

where C_P, C_V = measured molar heat capacities at constant P and V, respectively, of one mole of the equilibrium mixture; ΔH = heat of reaction for the formation of one mole of dimer; K = mole fraction equilibrium constant for association; x = degree of association; $\nu_1=\frac{1}{2}\pi k_1$; c_0 = sound velocity in acetic acid at very low frequency; c = sound velocity in acetic acid at frequency ν; $\mu(\nu)$ = absorption coefficient per wavelength at frequency ν; C_P' = molar heat capacity at constant P of the components of the equilibrium mixture: $C_P'=C_P-x(1-x)(\Delta H/RT)^2$.

From this equation it is a simple matter to obtain expressions for the maximum absorption coefficient, μ_M; the frequency, ν_M, at which μ_M occurs; and the width at half-maximum, $\Delta\nu_{\frac{1}{2}}$, of the μ *vs* ν curve. These latter two quantities are simply related to α/ν^2 measured at very low frequencies, α being the absorption coefficient per centimeter. If ΔH and K were known for acetic acid, these equations could be checked at once; since they are not, a different procedure had to be used. By a graphical method, a set of values for ΔH and K were found which gave the observed values for μ_M at 293° and at 323°; these values were $\Delta H=-6215$ cal/mole, and $K=62.10$. These numbers were then used to complete the calculations for the remaining quantities at each temperature. The results of the computation are shown in Table I, where they are compared with Lamb and Pinkerton's[4] data, or with results obtainable directly therefrom.

TABLE I.

	$\mu_m\times10^2$		ν_m(mcps)		$\Delta\nu_{\frac{1}{2}}$		C_∞/C_0[b]		$\tau\times10^8$[c]
T°K[a]	obs	calc	obs	calc	obs	calc	obs	calc	sec
293	5.10	5.11	0.5560	0.5594	1.926	1.937	1.012	1.017	8.24
303	5.45	5.41	0.9150	0.9137	3.170	3.165	1.014	1.018	6.10
313	5.83	5.75	1.489	1.472	5.158	5.099	1.015	1.019	4.53
323	6.10	6.11	2.408	2.437	8.341	8.442	1.016	1.020	3.24
333	6.41	6.49	3.772	3.839	13.07	13.30	1.018	1.021	2.41

[a] These are the temperatures at which the calculations were made; the data are given at 20°, 30°, ···. The ratio $(c/c_0)^2$ was taken as 1 throughout, as the observed dispersion is small.

[b] The calculated values were obtained from the formula $\left[\frac{C_\infty}{c_0}\right]^2=\frac{C_p'C_v}{C_v'C_p}$.

[c] τ is the relaxation time, defined by $\tau=1/2\pi\nu_1$.

No account has been taken of the possibility of the existence of equilibria involving higher polymers. It may be that the second dispersion zone that is believed to exist near 67.5 megacycles per second[1] is due to such equilibria.

In the very near future it is proposed to study the absorption of ultrasonic waves in solutions of acetic acid in toluene, for which the requisite thermodynamic data are known. An apparatus for this work has been designed with the kind cooperation of Professor H. Sack, and Mr. Richard Aldrich, of the Cornell Physics Department, and is now being tested.

This research has been carried out under the direction of Professor S. H. Bauer, to whom I am indebted for many suggestions and discussions.

[1] These phenomena were first reported by P. Bazulin, Compt. rend. U.R.S.S. **3**, 285 (1935).
[2] For general surveys of the propagation of ultrasonic waves in liquids, see, e.g., L. Bergmann, *Der Ultraschall*, (Zurich), fifth edition; H. O. Kneser, Ergeb. exakt. Naturwiss. **22**, 121 (1949).
[3] B. G. Shpakovskii, Compt. rend. U.R.S.S. (N.S.) **18**, 169 (1938).
[4] J. Lamb and J. M. M. Pinkerton, Proc. Roy. Soc. (London) **199A**, 114 (1949).
[5] E. Bauer, Proc. Phys. Soc. (London) **62A**, 141 (1949). The propagation of sound in a reacting fluid was first treated by A. Einstein, Sitzber. preuss. Akad. Wiss. 380 (1920), but his considerations applied only to a perfect gas.

Luminescence of Zinc Tantalo-Niobate with Manganese Activator

SIMON LARACH
Radio Corporation of America, RCA Laboratories Division, Princeton, New Jersey
(Received July 30, 1951)

ALTHOUGH niobium, and to a lesser extent, tantalum, have been reported as activators for several phosphors,[1-4] compounds containing these elements have received little attention from the standpoint of use as host crystal constituents.

Within the *VA* group of elements, Weyl[5] has reported a yellow photoluminescence from zinc vanadate, while Bär[6] found a green gold photoluminescence from an electrolytically prepared thin layer of tantalum pentoxide.

The oxides of tantalum and niobium, as well as $ZnTa_2O_6$ and $ZnNb_2O_6$, with or without manganese activator, are nonluminescent. However, it was found that $Zn_2Nb_2Ta_2O_{12}$:Mn has a cathodoluminescence emission in the green region of the spectrum, with peak wavelength at 5250A, *practically identical* with that of rbhdl.-Zn_2SiO_4:Mn. The peak emission intensity of the tantalo-niobate is 10 percent that of the silicate.

The phosphors were prepared by mixing the required amounts of zinc oxide, tantalum pentoxide, niobium pentoxide, and manganese chloride to yield 0.5 percent Mn^{++} by weight. The mixture was then slurried with triple-distilled water, and dried in an oven at 150°C. Firings were carried out in platinum containers, in air, at 1100°C, for 30 minutes, at which point the containers were removed and cooled in air.

TABLE I. Band widths at various emission intensities for zinc tantalo-niobate:Mn and zinc orthosilicate:Mn.

% maximum emission intensity	Band width, A	
	Niobate	Silicate
3	950	1370
6	850	1200
12.5	720	880
19	610	730
25	560	630
50	440	430
75	250	270
88	170	180

Measurements of spectral distribution were made in a special demountable cathode-ray tube operating at 6 kv and 1 μa/cm^2, in conjunction with an automatic recording spectroradiometer.[7]

Differences between the emission spectra of niobate and silicate phosphors are very slight. For example, Table I lists the band widths at various emission intensities for the two phosphors.

Experiments to date indicate that zinc, niobium, tantalum, and manganese are all necessary for the green emission, and that optimum results are obtained when the ratio of weights of zinc niobate to zinc tantalate are between 0.2 and 2.0.

From the similarity of the emission spectra of zinc tantaloniobate: Mn and zinc orthosilicate: Mn, it can be assumed that in both cases, the emitting centers are associated with MnO_4 groups, with manganese in substitutional sites for zinc, and fourfold coordinated with oxygen, in conformity with the Linwood-Weyl theory.[8] The decrease in emission intensity can perhaps be attributed to a decrease in the efficiency of the energy transfer process from the point of energy absorption to a luminescence center.[9]

[1] F. E. Williams and H. Eyring, J. Chem. Phys. **15**, 289 (1947).
[2] E. A. Ab, Bull. acad. sci. U.R.S.S., Sér. phys. **9**, 467 (1945).
[3] M. Hueniger *et al.*, U. S. Pat. 2,302,626; December 29, 1942.
[4] Y. Uehara and U. Umekawa, J. Chem. Soc. Japan **61**, 907 (1940).
[5] W. A. Weyl, U.S. Pat. 2,322,265; June 22, 1943.
[6] W. Bär, Z. Physik **115**, 658 (1940).
[7] V. K. Zworykin *et al.*, J. Opt. Soc. Am. **29**, 84 (1939).
[8] S. H. Linwood and W. A. Weyl, J. Opt. Soc. Am. **32**, 443 (1942).
[9] S. Larach, J. Phys. and Colloid Chem. **54**, 469 (1950).

Paramagnetic Resonance Absorption in Organic Free Radicals

A. N. Holden, W. A. Yager, and F. R. Merritt
Bell Telephone Laboratories, Murray Hill, New Jersey
(Received August 2, 1951)

In view of the growing interest in the use of paramagnetic resonance absorption by organic free radicals[1] as a method for measuring magnetic fields, it seems worth while to summarize the results obtained on such materials in polycrystalline form in this laboratory, at frequencies near 24,000 mc/sec, splitting fields near 8600 oersted, and room temperature.[2-4]

Substance	Reference	Landé splitting factor	Line width at half-power
Banfield and Kenyon's radical	1	2.0057 ±0.0002	18.4 oersted
Di-*p*-anisyl nitric oxide	1	2.0063 ±0.0005	31.4 oersted
Diphenyl trinitrophenyl hydrazyl	1	2.0036 ±0.0002	2.70 oersted
Porphyrexide	2	2.0064 ±0.0002	17.0 oersted
Porphyrindine	2	2.0057 ±0.0002	25.2 oersted
Phenazinium chloride	3	2.0031 ±0.0002	weak line
Phenanthro-phenazinium chlorstannite	3	2.0033 ±0.0002	6.4 oersted
2-nitro-phenanthro-phenazinium chlorstannite	3	2.0032 ±0.0002	weak line
Diphenyl quinoxalinium chlorstannite	3	2.0036 ±0.0005	weak line
Wurster's Red (as bromide)	4	line possibly multiple	
Wurster's Blue (as ferricyanide)	4	2.0028 ±0.0002	3.7 oersted
Wurster's Blue (as picrate)	4	2.0033 ±0.0002	6.0 oersted

We are unable with the present sensitivity of our equipment to observe paramagnetic resonance absorption in the following compounds, although speculations that they contain free radical ions have been published: Bindschedler's Green,[5] thianthronium chloraluminate,[6] and murexide and the barium salt of alloxantin.[7] In agreement with the current view that the thermochromic spiropyranes[8] do not contain unpaired electrons, we observe no resonance absorption in di-β-naphthaspiropyrane adsorbed on activated alumina and on fullers' earth, nor in its bridged 3,3′-orthophenylene derivative[9] adsorbed on alumina; but we are not certain that adsorption provides a sufficient sample for a definitive measurement.

The tabulated measurements fall in two groups, in which (1) the Landé *g*-factor is close to the free electron value and the line is narrow, and (2) the *g*-factor is larger and the line is wider. In group (2) fall the compounds containing the atomic grouping >N−O. This suggests that here the odd electron is relatively more localized in the molecule, a possibility consistent with the stability of the simple odd-electron compounds NO and NO_2. Localization would tend to make the *g*-value depart from that of a free electron, and would reduce the exchange-narrowing by reducing the time-average proximity of odd electrons in adjacent molecules.

[1] Holden, Kittel, Merritt, and Yager, Phys. Rev. **75**, 1614 (1949); **77**, 147 (1950); C. H. Townes and J. Turkevich, Phys. Rev. **77**, 148 (1950).
[2] E. Muller and I. Muller-Rodloff, Ann. **521**, 81 (1936), for paramagnetic susceptibility measurements.
[3] L. Michaelis and E. S. Hill, J. Am. Chem. Soc. **55**, 1481 (1933), for potentiometric studies of semiquinone ions of the phenazinium type.
[4] L. Michaelis, J. Am. Chem. Soc. **53**, 2953 (1931) for potentiometric studies of Wurster's dyes in solution.
[5] G. Schwarzenbach and L. Michaelis, J. Am. Chem. Soc. **60**, 1667 (1938). Our result, applying to the solid zinc chloride double salt in Bindschedler's form, does not affect the conclusions of these authors regarding aqueous solutions in certain *p*H ranges.
[6] A. Hantzsch, Ber. deut. chem. Ges. **49**, 519 (1916).
[7] J. M. Retinger, J. Am. Chem. Soc. **39**, 1059 (1917).
[8] A. Schonberg and W. Asker, Science **113**, 56 (1951).
[9] Not the compound so described by Ruhemann and Levy, J. Chem. Soc. **103**, 563 (which is probably the corresponding pyrilium chloride) but the yellow product of its hydrolysis in hot aqueous sodium acetate and recrystallization from xylol. The xylol solutions of the bridged derivative are not thermochromic up to the boiling point but give a deep blue adsorption color on freshly activated alumina, and a bright red color on alumina which has been allowed to adsorb some moisture.

Ultraviolet Absorption Spectrum of Gaseous Hydrogen Fluoride

E. Safary
Laboratoire de physique (Enseignement) Sorbonne, Paris
(Received July 26, 1951)

Since our recent letter appeared in this Journal,[1] we have been informed that a correction had been published previously by Plumley himself,[2] concerning the observation of discrete bands in the ultraviolet resulting from the presence of SO_2 traces.

Thus, our work confirms the Plumley results concerning the transparency of gaseous hydrogen fluoride in the near ultraviolet, and moreover gives new data of absorption in the Schumann region.

[1] Safary, Romand, and Vodar, J. Chem. Phys. **19**, 379 (1951).
[2] H. J. Plumley, Phys. Rev. **49**, 405 (1936).

On the Structure of Gas Hydrates

M. v. Stackelberg and H. R. Müller
Institut fur Physikalische Chemie der Universitat Bonn, Bonn, Germany
(Received August 3, 1951)

A structure for gas hydrates was recently proposed by W. F. Claussen.[1] We have in the meantime found that gas hydrates exist in two distinct structures, both of which are cubic. One structure is for hydrates of small molecules (Cl_2, SO_2, CH_3SH, H_2S, CH_3Br, CH_3Cl, Br_2); the unit cell has 48 water molecules and 8 void spaces (Hohlräume) where hydrating molecules may be located. The cell constant is about 12A, the space group probably O_h^3—*Pm3n*. The structure for this class of hydrates has still not been completely elucidated. The structure earlier proposed[2] by us is questionable.

A second structure for hydrates has been found for larger hydrating molecules ($CHCl_3$, CH_2Cl_2, C_2H_5Cl). The elementary cell has been found to possess 136 water molecules, with a space group of O_h^7—*Fd3m* and a cell constant of 17.2A. The elementary cell contains water molecules at the following points:

000, $\frac{1}{2}\frac{1}{2}0$, $\frac{1}{2}0\frac{1}{2}$, $0\frac{1}{2}\frac{1}{2}$, +
8 H_2O I in (a): (000) $(\frac{1}{4}\frac{1}{4}\frac{1}{4})$
32 H_2O II in (e): (xxx) etc., with $x=-0.093$
96 H_2O III in (g): (xxz) etc., with $x=-0.057$, $z=-0.242$
8 large void spaces I in (b): $(\frac{1}{2}\frac{1}{2}\frac{1}{2})$ $(\frac{3}{4}\frac{3}{4}\frac{3}{4})$

16 small void spaces II

$$\text{in (c)}: \left(\tfrac{111}{888}\right)\left(\tfrac{331}{888}\right)\left(\tfrac{313}{888}\right)\left(\tfrac{133}{888}\right).$$

The above description corresponds to the structure which was proposed by W. F. Claussen, which proposal proved to be of substantial aid in this structure determination.

In hydrates of large molecules, only the large holes are filled with hydrating molecules. Thus, the formula for the hydrate is $8M.136H_2O = M.17H_2O$. Certain smaller molecules (O_2, N_2, H_2, CO_2, H_2S) might occupy the smaller void spaces II in the above structure when the large molecules form such a hydrate. Also, the double-hydrates have a structure as proposed by Claussen, wherein the H_2S molecules occupy the small void spaces. The formula for such a hydrate must probably be $8CHCl_3.16H_2S.136H_2O$, or $CHCl_3.2H_2S.17H_2O$.

[1] W. F. Claussen, J. Chem. Phys. **19**, 259, 632 (1951).
[2] M. v. Stackelberg, Naturwiss. **36**, 327, 359 (1949).

Remark on the Notion of the Thermodynamic Pressure

T. Nishiyama
Department of Physics, Osaka University, Osaka, Japan
(Received July 30, 1951)

THERE have been some controversies among several authors[1] concerning the notion of pressure in a canonical ensemble. Recently H. S. Green[2] made some comments on the paper of Riddell and Uhlenbeck[3] and pointed out the difference between their result and ours. This difference comes from the shape of the wall potential adopted. Here it will be shown that the traces of the commutators vanish identically so far as the macroscopic observation is concerned.

Assuming that the wall potential* $\Psi(x)$ acting on the particle system under consideration is a smooth, though nearly steplike, function near the boundary, becoming infinite at the infinite distance, the average value of the virial of the system excluding the wall is equal to minus the average value of that of the wall potential for discrete states. Let the wave functions be

$$\varphi(x)=\varphi(x_1, x_2, \cdots, x_n).$$

Then one gets

$$2(\varphi, K\varphi)+(\varphi, W_0\varphi)=\sum_i \int\cdots\int \varphi^*(x)x_i\frac{\partial\psi}{\partial x_i}\varphi(x)dx_1dx_2\cdots dx_n,$$

in which

$$K=-\frac{\hbar^2}{2m}\sum_{i=1}^{n}\Delta_i, \quad W_0=-\tfrac{1}{2}\sum_{ik}^{n} r_{ik}\frac{\partial U}{\partial r_{ik}}, \quad r_{ik}=x_k-x_i,$$

and U is the interaction energy.

Now we consider a system immersed in a large thermostat at the temperature T. It is assumed that the region confining the system should be so large that the energy level is almost continuous. Then the system attains the thermal equilibrium. The density matrix of the canonical ensemble is given in the coordinate representation:

$$\rho_c(x, x')=\langle x|\exp(-\beta H_W)|x'\rangle,$$

in which H_W involves the wall potential. It is required that the free energy is minimum against the uniform expansion of the scale of the coordinates:

$$\delta F=0, \quad x\to(1+\epsilon)x, \quad F=-\frac{1}{\beta}\log\int\rho_c(x, x)dx,$$

which leads to

$$\text{Tr.}\sum_{m=0}^{\infty}\frac{\beta^{m+1}}{(m+1)!}\mu_m\exp(-\beta H_W)$$
$$=\int\left\langle x\left|\sum_{m=0}^{\infty}\frac{\beta^{m+1}}{(m+1)!}\mu_m\exp(-\beta H_W)\right|x\right\rangle dx=0, \quad (1)$$

where

$$\mu_0=-2K-W_0+\sum_i x_i\frac{\partial\psi}{\partial x_i}, \quad \mu_m=[\mu_{m-1}, H_W].$$

Owing to the fact that the derivatives of wave functions, hence the surface integrals, vanish identically at the infinite distance, one obtains

$$\text{Tr.}\,[\mu_{m-1}, H_W]=0, \quad m\neq 0.$$

Finally it becomes

$$\text{Tr.}\,(\mu_0\exp(-\beta H_W))=0$$

$$\left\langle\sum_i x_i\frac{\partial\psi}{\partial x_i}\right\rangle_{Av}=3PV$$

and one finds

$$3PV=2\langle K\rangle_{Av}+\langle W_0\rangle_{Av},$$

in which $\langle\cdots\rangle_{Av}$ means an average over the canonical ensemble.

It is worth while to notice that Eq. (1) becomes

$$\text{Tr.}\left[x\cdot\frac{\partial}{\partial x}, \exp(-\beta H_W)\right]=0, \quad (2)$$

which proves the opinion of Riddell and Uhlenbeck to be correct for the operator $x\partial/\partial x=\Sigma ix_i\cdot\partial/\partial x_i$ for discrete states.

If the region confining particles is sufficiently small, the situation is changed. Although at sufficiently high temperatures the thermal motion of the system which is nearly isotropic is balanced with the hydrostatic pressure of the environment, as the temperature is lowered, the number of particles occupying the lowest energy level becomes larger and larger. Because of the sharp discreteness of the energy level and the non-isopropic distribution of phase points it becomes very probable that the balance becomes unstable.

It is necessary that the region have a suitable macroscopic dimension.

The author wishes to thank Professor Husimi for the valuable discussions.

The major part of this report was published about a year and a half ago.[4]

[1] J. de Boer, Physica **15**, 843 (1949); H. S. Green, Physica **15**, 882 (1949); P. J. Price, Phil. Mag. **41**, 948 (1950); R. Kubo, Busseiron Kenkyu **18**, 64 (1949).
[2] H. S. Green, J. Chem. Phys. **18**, 1123 (1950).
[3] R. J. Riddell, Jr., and G. E. Uhlenbeck, J. Chem. Phys. **18**, 1066 (1950).
* Riddell and Uhlenbeck applied the wall potential of the form $\Psi(x/L)$.
[4] T. Nishiyama, Busseiron Kenkyu **25**, 63 (1950).

Low Temperature Second Virial Coefficients for a 6–12 Potential*

Leo F. Epstein and Glenn M. Roe
General Electric Company, Knolls Atomic Power Laboratory, Schenectady, New York
(Received August 14, 1951)

THE second virial coefficient of a gas

$$B(T)=2\pi N\int_0^{\infty} r^2[1-\exp\{-U(r)/kT\}]dr \quad (1)$$

with a Lennard-Jones 6–12 potential

$$U(r)=\epsilon[(r_0/r)^{12}-2(r_0/r)^6] \quad (2)$$

may be written[1] as

$$B(T)=(2\pi Nr_0^3/3)G(\theta), \quad (3)$$

where

$$\theta=\epsilon/kT \quad (4)$$

and

$$G(\theta)=-\tfrac{1}{4}\theta^{\frac{1}{2}}\sum_{m=0}^{\infty}\frac{2^m}{m!}\left(\frac{2m-5}{4}\right)!\theta^{m/2}. \quad (5)$$

Stockmayer and Beattie[2] have tabulated $\sqrt{2}G(\theta)$ for the range $0.20<\theta(0.01)<1.00$.

TABLE I. Values of $G(\theta)$ for $\theta<8.0$.

θ	$-G(\theta)$	$-e^{-\theta}G(\theta)$
0.5	0.443 797	0.269 176
1.0	1.794 695	0.660 231
1.5	3.629 213	0.809 787
2.0	6.166 13	0.834 495
2.5	9.757 20	0.800 919
3.0	14.952 6	0.744 447
3.5	22.612 2	0.682 828
4.0	34.084 4	0.624 278
4.5	51.493 0	0.572 035
5.0	78.190 1	0.526 840
5.5	119.490 4	0.488 330
6.0	183.830 4	0.455 670
6.5	284.665 7	0.427 978
7.0	443.392	0.404 321
7.5	694.277	0.383 994
8.0	1 092.26	0.366 411

Hirschfelder, Bird, Curtiss, and Spotz[3] using punched-card techniques have extended the numerical work to cover the range $0.0025<\theta<3.33\cdots$. Values of $G(\theta)$ for larger θ's are difficult to obtain from Eq. (5) because of the poor convergence properties of the series.

By dividing the sum in Eq. (5) into two sums, one over odd, the other over even values of the index, and substituting the relation,[4]

$$(2z)!=z!(z-\tfrac{1}{2})!\frac{4^z}{(-\tfrac{1}{2})!} \tag{6}$$

the equation can be transformed to

$$G(\theta)=-\tfrac{1}{4}\theta^{\frac{1}{2}}\Big[\sum_{n=0}^{\infty}\frac{\theta^n}{n!}\frac{(n-\frac{1}{4}-1)!(-\frac{1}{2})!}{(n-\frac{1}{2})!} +2\theta^{\frac{1}{2}}\sum_{n=0}^{\infty}\frac{\theta^n}{n!}\frac{(n+\frac{1}{4}-1)!(-\frac{1}{2})!}{(n+\frac{1}{2})!}\Big]. \tag{7}$$

In terms of the confluent hypergeometric function,[5]

$$M(\alpha,\gamma,\theta)\equiv\sum_{n=0}^{\infty}\frac{\theta^n}{n!}\cdot\frac{(\alpha+n-1)!}{(\alpha-1)!}\cdot\frac{(\gamma-1)!}{(\gamma+n-1)!}, \tag{8}$$

$G(\theta)$ can be written as

$$G(\theta)=\theta^{\frac{1}{2}}[(-\tfrac{1}{4})!\,M(-\tfrac{1}{4},+\tfrac{1}{2},\theta)-2\theta^{\frac{1}{2}}(+\tfrac{1}{4})!\,M(+\tfrac{1}{4},+\tfrac{3}{2},\theta)]. \tag{9}$$

Inserting the relation,[6]

$$M(-\tfrac{1}{4},+\tfrac{1}{2},\theta)=M(+\tfrac{3}{4},+\tfrac{1}{2},\theta)-2\theta M(+\tfrac{3}{4},+\tfrac{3}{2},\theta) \tag{10}$$

and using McDonald's tables of the confluent hypergeometric function,[7] the values of $G(\theta)$ for $0.5<\theta(0.5)<8.0$ can readily be found. These are given in Table I, and are in excellent agreement with previous evaluations[2,3] where comparison is possible. The function $e^{-\theta}G(\theta)$ which is also tabulated is useful for interpolation.

TABLE II. $G(\theta)$ for large values of θ.[a]

θ	$(\pi/4\theta)^{\frac{1}{2}}e^{\theta}$	$-G(\theta)$	$-e^{-\theta}G(\theta)$
8	934.0	1093	0.366 ±0.001
9	2393.7	2735	0.3376±0.0005
10	6172.9	6929	0.3146±0.0002
15	7.480 257 ×10⁵	8.026 49 ×10⁵	0.245 532
20	9.614 342 ×10⁷	10.117 79 ×10⁷	0.208 543
25	1.276 254 ×10¹⁰	1.328 422 ×10¹⁰	0.184 490
30	1.729 095 ×10¹²	1.787 084 ×10¹²	0.167 229
35	2.375 843 ×10¹⁴	2.443 407 ×10¹⁴	0.154 060
40	3.298 331 ×10¹⁶	3.379 756 ×10¹⁶	0.143 584
45	4.615 198 ×10¹⁸	4.715 861 ×10¹⁸	0.134 992
50	6.498 065 ×10²⁰	6.625 012 ×10²⁰	0.127 780
60	1.306 587 ×10²⁵	1.327 708 ×10²⁵	0.116 261
70	2.664 463 ×10²⁹	2.701 197 ×10²⁹	0.107 385
80	5.489 825 ×10³³	5.555 804 ×10³³	0.100 274
90	1.140 058 ×10³⁸	1.152 202 ×10³⁸	0.094 4116
100	2.382 282 ×10⁴²	2.405 069 ×10⁴²	0.089 4704

[a] The error in $G(\theta)$ at $\theta=8$, 9, and 10 is ±4; at $\theta=15$, the error in $G(\theta)$ is ±0.00005 ×10⁵; at $\theta=20$, $G(\theta)$ is good to ±0.000 004 ×10⁷; and for higher values of θ, $G(\theta)$ should be good to the last figure quoted.

By substituting the asymptotic expression[8] for $M(\alpha,\gamma,\theta)$ in Eq. (9), it follows that

$$G(\theta)\sim-(\pi/4\theta)^{\frac{1}{2}}e^{\theta}\sum_{n=0}\beta_n/\theta^n, \tag{11}$$

where[8]

$$\beta_n=\frac{1}{n!}\frac{(n+\frac{1}{4})!(n-\frac{1}{4})!}{(+\frac{1}{4})!(-\frac{1}{4})!} \tag{12a}$$

$$=\frac{1}{n!}(1^2-1/16)(2^2-1/16)(3^2-1/16)\cdots(n^2-1/16) \tag{12b}$$

$$=\Big(u-\frac{1}{16n}\Big)\beta_{n-1}. \tag{12c}$$

Values of $G(\theta)$ for large θ, computed using Eq. (11), are given in Table II.

At very large values of θ (low temperatures), $G(\theta)$ as given by the foregoing equations must be modified by adding in the quantum-mechanical corrections.[9,10] These are, however, nearly proportional to (θ/Mer_0^2) or some power of this quantity, and, while important for light gases such as H_2, D_2, and He, will usually be of negligible magnitude for materials of high molecular weight M.

* The Knolls Atomic Power Laboratory is operated by the General Electric Company for the AEC. The work reported here was carried out under contract No. W-31-109 Eng-52.

[1] R. H. Fowler and E. A. Guggenheim, *Statistical Thermodynamics* (Cambridge University Press, London, 1939), p. 279 *et seq.*
[2] W. H. Stockmayer and J. A. Beattie, J. Chem. Phys. **10**, 476 (1942).
[3] (a) Hirschfelder, Curtiss, Bird, and Spotz, *The Properties of Gases* (to be published). (Individual chapters, prepared under Navy Bur. Ordnance contract, have been issued to a limited distribution list, prior to April, 1951.) (b) Hirschfelder, Bird, and Spotz, Trans. Am. Soc. Mech. Engrs. **71**, 921 (1949).
[4] E. Jahnke and F. Emde, *Tables of Functions* (Dover Publications, New York, 1945), fourth edition, p. 18.
[5] E. P. Adams, *Smithsonian Mathematical Formulae and Tables of Elliptic Functions* (Washington, D. C., 1947), p. 185.
[6] Reference 5, p. 186.
[7] A. D. MacDonald, *Properties of the Confluent Hypergeometric Function*. Technical Report No. 84, November 18, 1948. M.I.T. Research Laboratory of Electronics, Cambridge, Massachusetts.
[8] Reference 4, p. 12.
[9] B. Kahn, dissertation, Utrecht (1938).
[10] J. de Boer and A. Michels, Physica **5**, 945 (1938); also, 3a, chapter 7, p. 126 *et seq.*

The Theory of the Rotational Phase Transition in Anisotropic Molecular Crystal

TAKEHIKO OGUCHI
Tokyo Institute of Technology, Oh-okayama, Tokyo, Japan
(Received July 30, 1951)

THE rigid dipolar molecules are arranged on a simple cubic lattice. We take the cartesian coordinate coincident with the crystal axes. The potential energy between i molecule in orientation $\omega_i(\theta_i,\varphi_i)$—$(\theta,\varphi)$ are polar coordinates—and its nearest neighbor j molecule in orientation ω_j is either

$$V_z=V_y=J/4\cos(\omega_i,\omega_j)$$

or (1)

$$V_z=-J/2\cos(\omega_i,\omega_j),$$

according to whether the pair of these molecules is in the x, y, or z direction, where (ω_i,ω_j) is the angle between the axes of two molecules concerned, and $J(>0)$ is the constant. In formula (1) the equations are chosen as the approximate dipolar potential energies so as to facilitate the calculations.

As is shown in Fig. 1, the lattice is divided into eight sublattices. Let the probability that the molecular axis on ith sublattice is in orientation ω_i be denoted by $x_i(\omega_i)$, and the probability that the pair whose end molecular axes in orientations ω_i, ω_j, respectively, be denoted by $y_{ij}(\omega_i,\omega_j)$ and the probability that the eight molecular axes on the cube shown in Fig. 1 are in orientations $\omega_1,\omega_2,\cdots,\omega_8$, respectively, be denoted by $Z(\omega_1,\omega_2,\cdots,\omega_8)$. The

relations among x, y, and z are

$$\int\int y_{ij}(\omega_i, \omega_j)d\omega_i d\omega_j = \int x_i(\omega_i)d\omega_i = 1$$

$$\int\cdots\int Z(\omega_1, \cdots, \omega_8)d\Omega = 1, \quad d\Omega \equiv \prod_{i=1}^{8} d\Omega_i$$

$$x_i(\omega_i) = \int\cdots\int Z(\omega_1, \cdots, \omega_8)d(\Omega-\omega_i), \quad d(\Omega-\omega_i) \equiv \prod_{j\neq i} d\omega_j$$

$$y_{ij}(\omega_i, \omega_j) = \int\cdots\int Z(\omega_1, \cdots, \omega_8)d(\Omega-\omega_i-\omega_j),$$
$$d(\Omega-\omega_i-\omega_j) \equiv \prod_{k\neq i,j} d\omega_k. \quad (2)$$

The configurational entropy can be approximated using Kikuchi's method[1] corresponding to Bethe's first approximation, and thus the free energy F is,

$$\frac{8F}{NkT} = 2\sum_{(i,j)}\int\cdots\int\frac{1}{kT}V_{ij}(\omega_i, \omega_j)Zd\Omega$$
$$-5\sum_{i=1}^{8}\int\cdots\int Z\left\{\ln\int\cdots\int Zd(\Omega-\omega_i)\right\}d\Omega$$
$$+2\sum_{(i,j)}\int\cdots\int Z\left\{\ln\int\cdots\int Zd(\Omega-\omega_i-\omega_j)\right\}d\Omega, \quad (3)$$

$\Sigma_{(i,j)}$ shall mean that the sum is carried out over all pairs (i, j) which are direct neighbors in Fig. 1 and V_{ij} shall mean that it is taken as V_x, V_y, or V_z according to whether the pair (i, j) is in the x, y, or z direction. The usual method of indeterminate multiplier gives immediately the first-order variational equation. We put

$$x_{i+4}(\omega_{i+4}) = x_i(\omega_i), \quad (i=1, 2, 3, 4)$$
$$y_{i+4,j+4}(\omega_{i+4}, \omega_{j+4}) = y_{ij}(\omega_i, \omega_j), \quad (4)$$

because in order to describe completely our anisotropic system the necessary number of the sorts of sublattices is four.[2] Thus, we obtain

$$y_{13}(\omega_1, \omega_3)\cdot y_{24}(\omega_2, \omega_4)$$
$$= \lambda\frac{[x_1(\omega_1)\cdot x_2(\omega_2)\cdot x_3(\omega_3)\cdot x_4(\omega_4)]^{5/4}}{[y_{12}(\omega_1, \omega_2)\cdot y_{34}(\omega_3, \omega_4)]^{3}}$$
$$\times\exp[(K/2)\cos(\omega_1, \omega_2)+(K/2)\cos(\omega_3, \omega_4)$$
$$-(K/2)\cos(\omega_1, \omega_3)-(K/2)\cos(\omega_2, \omega_4)]. \quad (5)$$
$$K = J/2kT, \quad (6)$$

where λ is the multiplier. If we eliminate x using (2), (5) is regarded as the integral equation concerning y. Considering the symmetry of the interactions,

$$y_{34}(\omega_3, \omega_4) = y_{12}(\pi-\omega_3, \pi-\omega_4),$$
$$y_{24}(\omega_2, \omega_4) = y_{13}(\omega_2, \omega_4), \quad (7)$$

where $(\pi-\omega_i)$ means $(\pi-\theta_i, \pi+\varphi_i)$. As easily seen, Eq. (5) has the following solutions,

$$y_{12}(\omega_1, \omega_2) = \frac{1}{H(K)(4\pi)^2}\exp[K\cos(\omega_1, \omega_2)]$$

$$y_{13}(\omega_1, \omega_3) = \frac{1}{H(K/2)(4\pi)^2}\exp[-(K/2)\cos(\omega_1, \omega_3)], \quad (8)$$

where

$$H(K) = \sinh K/K. \quad (9)$$

This corresponds to the disordered state. In order to obtain the solution corresponding to the ordered state, we shall expand $y_{12}(\omega_1, \omega_2)$ in a most general form as follows:

$$y_{12}(\omega_1, \omega_2) = \frac{\mu_1}{(4\pi)^2}\exp[K\cos(\omega_1, \omega_2)]$$
$$\cdot[1+c_{10}\{P_1(\cos\theta_1)+P_1(\cos\theta_2)\}$$
$$+c_{20}\{P_2(\cos\theta_1)+P_2(\cos\theta_2)\}+c_{21}P_1(\cos\theta_1)P_1(\cos\theta_2)$$
$$+c_{22}P_1'(\cos\theta_1)P_1'(\cos\theta_2)\cos(\varphi_1-\varphi_2)\cdots] \quad (10)$$

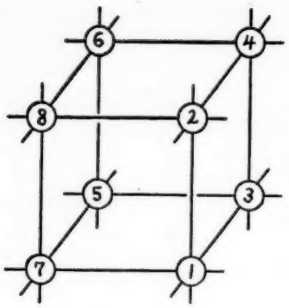

FIG. 1. Diagram of lattice.

where

$$\mu_1 \equiv \frac{1}{H(K)}[1-\tfrac{1}{3}c_{21}L(K)-\tfrac{2}{3}c_{22}L(K)\cdots] \quad (11)$$

$$L(K) = H'(K)/H(K) = \coth K - 1/K. \quad (12)$$

If we substitute (10) into (5) and integrate both sides with ω_3 and ω_4, and equate the coefficients of the corresponding spherical harmonics of both sides, we obtain the relations concerning the coefficients c's in (10). The transition temperature K_c is determined, as Chang[3] and Kubo[4] and Nakamura[5] had done, as the point at which the real root of c_{10} vanishes, so we obtain

$$1-L(K_c)-3L(K_c/2)-5L(K_c)L(K_c/2) = 0, \quad (13)$$
$$K_c = 0.949. \quad (14)$$

The amount of the specific heat discontinuity at the transition temperature is

$$\Delta C = \frac{8}{3}RK_c^2\left[\left\{\frac{H''(K_c)}{H(K_c)}-(L(K_c))^2\right\}\left(\frac{dc_{21}}{dK}\right)_{K=K_c}\right.$$
$$\left.+\frac{1}{16}\{3+5L(K_c)\}\left\{\frac{H''(K_c/2)}{H(K_c/2)}-(L(K_c/2))^2\right\}\left(\frac{dc_{10}^2}{dK}\right)_{K=K_c}\right]. \quad (15)$$

Both $[(dc_{21})/(dK)]_{K=K_c}$ and $[(dc_{10}^2)/(dK)]_{K=K_c}$ are calculated from the relations concerning the coefficients c's, and we obtain $\Delta C = 2.39R$.

A more detailed account will be published elsewhere.

[1] R. Kikuchi, Phys. Rev. **81**, 988 (1951).
[2] The same sublattices were discussed by Y. Takagi for the theory of rochelle salt, at the Meeting of the Phys. Soc., Japan, in 1947.
[3] T. S. Chang, Proc. Cambridge Phil. Soc. **33**, 524 (1937).
[4] R. Kubo and T. Hashimura, The Meeting of the Phys. Soc., Japan, in 1949.
[5] T. Nakamura, Busseiron-Kenkyu (Japanese) **29**, 44 (1950).

The Ionization Potential of Allyl Radical

M. G. EVANS AND M. SZWARC
Chemistry Department, University of Manchester, Manchester, England
(Received August 13, 1951)

THE determination of the ionization potentials of radicals is of a paramount importance for a better understanding of reactions involving ionic species. Such a determination is feasible if one combines data of the appearance potentials of the relevant ions with the respective bond dissociation energies. This procedure is illustrated by calculating the ionization potential of allyl radical.

The calculation of the ionization potential of allyl radical is based on the following data: 1. The appearance potential of $CH_2{:}CH.CH_2^+$ ions produced in the mass-spectrum of butene-1 is determined at 11.65 ± 0.1 ev/molecule (Stevenson[1]). 2. The $CH_2{:}CH.CH_2-CH_3$ bond dissociation energy is determined at 2.6 ev/molecule (pyrolysis of butene-1 by Sehon and Szwarc[2]). Assuming that the observed appearance potential of $C_3H_5^+$ ions is equal to the endothermicity of reaction (1)

$$CH_2{:}CH.CH_2CH_3 \rightarrow CH_2{:}CH.CH_2^+ + CH_3 \quad (1)$$

and knowing the endothermicity of reaction (2), i.e.,

$$CH_2{:}CH.CH_2CH_3 \rightarrow CH_2{:}CH.CH_2 + CH_3. \quad -2.6 \text{ ev/molecule} \quad (2)$$

one computes the ionization potential of allyl radical at

$$I^a(CH_2{:}CH.CH_2) = 11.65 - 2.6 = 9.05 \text{ ev/molecule.}$$

The above estimated value appears to be reasonable. The electronic structure of an allyl radical is represented schematically on Fig. 1, and the ionized electron comes from the 0-level. Thus,

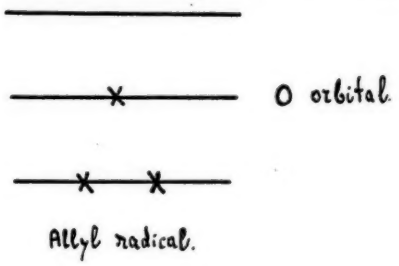

FIG. 1.

the ionization potential of allyl radical should be only slightly lower than that of methyl radical (the latter being estimated at 10.1 ev/molecule). The difference $I^a(CH_3) - I^a(CH_2{:}CH.CH_2)$ would measure the hyperconjugation effect which, of course, is much less pronounced in allyl radical than in ethyl radical.*

It is illuminating to compare the ionization potential of allyl radical with the ionization potential of propylene. In terms of equivalent orbitals[3] one might represent the allyl radical by Fig. 2(A), where each of the three equivalent orbitals is occupied by

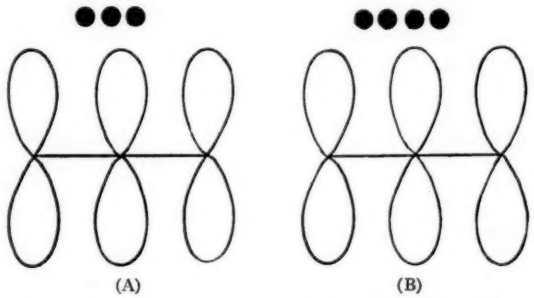

FIG. 2. 2A-allyl radical. 3 electrons in 3 equivalent π-orbitals. 2B-propylene. 4 electrons in 3 equivalent π-orbitals.

one electron. The representation of the propylene molecule is given by Fig. 2(B); there are the same three equivalent orbitals, one of them being occupied by two electrons, the remaining two by one electron each. This representation suggests that the ionization potential of propylene should be only slightly higher than that of the allyl radical. Indeed, the value of the former has been determined at 9.7 ev/molecule,[4] while our estimate for the latter is 9.05 ev/molecule.

Some points mentioned by Stevenson require clarification. In his paper,[1] describing the mass-spectrum of butene-1, Stevenson suggested that the recombination process

$$CH_2{:}CH.CH_2^+ + CH_3 \rightarrow CH_2{:}CH.CH_2.CH_3^+$$

requires an activation energy of at least 0.37 ev/molecule. This suggestion was deduced from consideration of the data on the appearance potential of $C_3H_5^+$ ions produced in the mass-spectra of proylene[4] and of butene-1 which, combined together, lead to the value of $D(CH_3-H)$ higher by 0.37 ev than expected. It seems, however, that this argument is not quite acceptable. Undoubtedly, the $C_3H_5^+$ ion produced in the spectrum of butene-1 has the structure $CH_2{:}CH.CH_2^+$ (i.e., *it is* an allyl$^+$ ion). On the other hand, it appears that the $C_3H_5^+$ ion produced in the mass-spectrum of propylene has the structure $CH_2{:}C^+.CH_3$. This conclusion is supported by the results obtained by considering the appearance potentials of $C_3H_5^+$ ions in the mass-spectra of propylene and of iso-butene.[4] These data lead to the correct value for $D(CH_3-H)$, thus indicating that *the same* $C_3H_5^+$ ion is produced from propylene and from iso-butene.

In the thermal dissociation of propylene the molecule splits into an allyl radical and a hydrogen atom. The $CH_2{:}CH.CH_2-H$ bond is the weakest one in the molecule of propylene. On the other hand the process

$$C_3H_6 \rightarrow C_3H_5^+ + H + e$$

apparently leads to the rupture of the middle C−H bond. The dissociation energy of the process

$$CH_2{:}CH.CH_3 \rightarrow CH_2.\dot{C}.CH_3 + H$$

is greater than $D(CH_2{:}CH.CH_2-H)$, but the ionization potential of the radical formed is much lower than that of the allyl radical. The $CH_2{:}\dot{C}.CH_3$ radical resembles the iso-propyl radical and one expects that its ionization potential would be of the same order as that of iso-propyl radical (the latter being 7.45 ev/molecule[5]). Hence, the gain in the ionization potential more than balances the loss in the dissociation energy, making the process

$$C_3H_6 \rightarrow CH_2.C^+.CH_3 + H + e$$

the most favorable energetically. There is no difficulty, therefore, in understanding the higher "stability" of $CH_2{:}C^+.CH_3$ ion-radical than the $CH_2{:}CH.CH_2^+$ ion-radical.

[1] D. P. Stevenson, J. Am. Chem. Soc. **65**, 209 (1943).
[2] A. H. Sehon and M. Szwarc, Proc. Roy. Soc. (London) **A202**, 263 (1950).
* See. A. G. Evans, Nature **157**, 438 (1946), for the consideration of hyperconjugation effects in hydrocarbon radical-ions.
[3] See, e.g., J. Lennard-Jones *et al.* in Disc. Faraday Soc. on hydrocarbons (1951).
[4] D. P. Stevenson and J. A. Hipple, J. Am. Chem. Soc. **64**, 2769 (1942).
[5] D. P. Stevenson, Disc. Faraday Soc. on hydrocarbons (1951).

Calculation of Electric Dipole Moments of Some Heterocyclics*

PER-OLOV LÖWDIN
Department of Physics, Duke University, Durham, North Carolina†
(Received July 30, 1951)

THE influence of a heteroatom in a conjugated system on the electronic orbitals and on the charge distribution can, according to Hückel[1] and to Wheland and Pauling,[2] be treated by introducing perturbation parameters δ in the coulomb integrals of the parent hydrocarbon. Here we will consider only compounds with six π-electrons having the character of perturbed benzene rings, and we will let $\delta_1, \delta_2, \ldots \delta_6$ denote the total perturbations in the different atomic positions. According to first-order perturbation theory, the charge distribution (in units of the electronic charge $e = 4.80 \times 10^{-10}$ esu) over these positions is then given by

$$q_1 = 1 + (43\delta_1 - 17\delta_2 + \delta_3 - 11\delta_4 + \delta_5 - 17\delta_6)/108,$$
$$q_2 = 1 + (43\delta_2 - 17\delta_3 + \delta_4 - 11\delta_5 + \delta_6 - 17\delta_1)/108, \qquad (1)$$
$$\ldots \text{ and cyclic.}$$

A special case of this formula was first given by Wheland and Pauling,[2] and the coefficients in general may be found in Coulson and Longuet-Higgins.[3] We note that this charge distribution is also independent of all additional perturbations, which may be introduced in the exchange integrals between different atoms.[4]

TABLE I. Dipole moments of some heterocyclics containing nitrogen in Debye units.

Compound	Calculated π-moment	Calculated σ-moment	Dipole moment calculated	Dipole moment observed[a]
Pyridine	1.51	0.85	2.36	2.22
Pyridazine	2.60	1.48	4.08	3.94
Pyrimidine	1.51	0.85	2.36	2.42
Pyrazine	0	0	0	0

[a] The observed data are taken from Wesson's compilation, L. G. Wesson, "Tables of electric dipole moments," Massachusetts Institute of Technology (1948).

Using a standard bond length[5] $a(=1.40\times10^{-8}$ cm), we find at once from (1) that each perturbation δ_k gives a vector contribution

$$ea\delta_k/3=2.24\delta_k \text{ Debye} \qquad (2)$$

to the dipole moment of the π-electrons. The total dipole moment of the compound is then found by adding also the contribution from the σ-electrons, calculated by vector addition from the bond moments. Each heteroatom A is generally assumed to give rise to

TABLE II. Dipole moments of some cyclic compounds containing methyl in Debye units.

Compound	Dipole moment calculated	Dipole moment observed[a]	Compound	Dipole moment calculated	Dipole moment observed[a]
			Toluene	0.25	0.37
α-picoline	2.49	1.72	o-xylene	0.44	0.52
β-picoline	2.25	2.30	m-xylene	0.25	0.37
γ-picoline	2.61	2.57	p-xylene	0	0

[a] See reference a, Table I.

a perturbation δ_A in its position and to smaller perturbations δ_A' in the adjacent positions, where δ_A' equals about $\delta_A/8$. This means, according to (2), that each heteroatom A gives a vector contribution of about $2.52\delta_A$ Debye to the π-moment.

On the whole, we have therefore theoretically found that the vector addition rule for calculating dipole moments holds even for the contribution from the *mobile* π-electrons in conjugated systems having the character of a perturbed benzene ring.

If, in pyridine, the value $\delta_N=2$, recommended by Wheland and Pauling is used, one finds from (2) the π-moment 5.04 D or from a more exact solution of the secular equation 4.48 D, which values both are much too high. Consequently, δ_N and then the whole δ-scale must be essentially reduced in value in order to give the correct dipole moments. We have found a value of $\delta_N=0.6$ more reasonable, and Table I gives the result for pyridine and the diazines. These results are supported by a recent paper by Orgel *et al.*,[6] where it is shown that a value of $\delta_N=1.0$ gives π-moments which are too high by a factor 1.6. We note that, in the region $\delta=0.6$, the perturbation theory is valid with sufficient accuracy.

If the influence of a methyl group is treated as only causing a perturbation δCH_3 on the ring (hyperconjugation neglected), and if the ratio between δCH_3 and δ_N is taken[7] to be $-\frac{1}{6}$, we find the results given in Table II. We note that a ratio of $-\frac{1}{4}$ would have given still better results for toluene and the xylenes.

In this investigation, two adjustable parameters give values of the dipole moments of eleven molecules in good agreement with experience. The values of the parameters δ have been used even in treating other properties of these molecules, and these results will be published elsewhere.

The author is greatly indebted to Professor H. Sponer, Duke University, for valuable and stimulating discussions.

* Work supported by the ONR under Contract N6ori-107, Task Order I, with Duke University.

† Permanent address: Institute of Mechanics and Mathematical Physics, University of Uppsala, Uppsala, Sweden.

[1] Hückel, Z. Physik **72**, 310 (1931).
[2] G. W. Wheland and L. Pauling, J. Am. Chem. Soc. **57**, 2086 (1935).
[3] C. A. Coulson and H. C. Longuet-Higgins, Proc. Roy. Soc. (London) **A192**, 16 (1947), p. 25; compare also Trans. Faraday Soc. **43**, 87 (1947).
[4] See reference 3, p. 23.
[5] V. Schomaker and L. Pauling, J. Am. Chem. Soc. **61**, 1769 (1939), and others.
[6] Orgel, Cottrell, Dick, and Sutton, Trans. Faraday Soc. **47**, 113 (1951).
[7] G. Nordheim and H. Sponer, to be published.

The Acid Decomposition of Sodium Thiosulfate

MILTON KERKER
Department of Chemistry, Clarkson College of Technology, Potsdam, New York
(Received August 13, 1951)

THE acid decomposition of thiosulfate leads to the formation of sulfite and sulfur which after an induction period precipitate as colloidal sulfur. The induction period, designated as t_B, is due to the time necessary for sulfur to exceed its critical supersaturation concentration.[1]

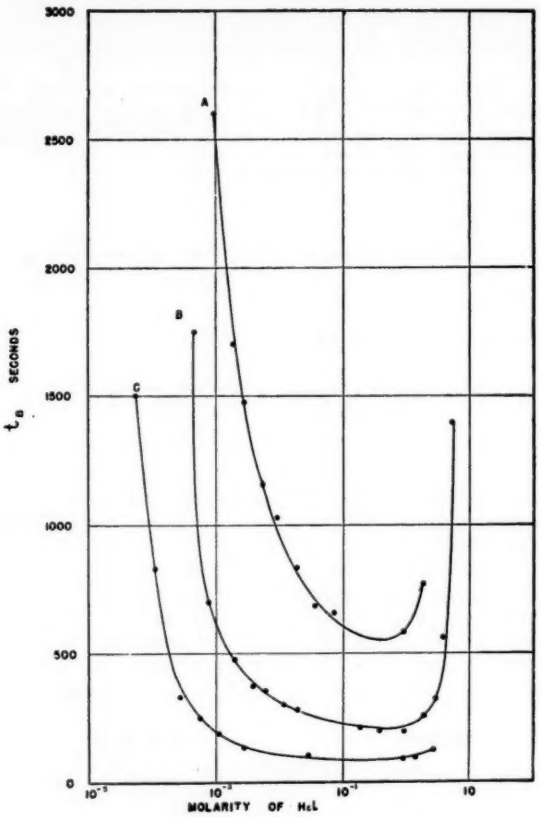

FIG. 1. Induction time *versus* acid concentration.
A. 0.00203 M $Na_2S_2O_3$. B. 0.00520 M $Na_2S_2O_3$. C. 0.0124 M $Na_2S_2O_3$.

t_B decreases with increasing thiosulfate concentration but goes through a minimum with respect to initial acid concentration. This leads to the interesting result that in concentrated hydrochloric acid, sodium thiosulfate does not produce a precipitate of colloidal sulfur even after several days. Basset and Durant[2] have determined t_B qualitatively for various thiosulfate and acid concentrations in both hydrochloric and phosphoric acids.

In order to obtain quantitative data upon which to formulate the kinetics of this reaction, the author has redetermined t_B as a function of initial concentrations. This was done by observing the increase in optical density of the reaction mixture at 3000A° as a function of time. The onset of turbidity at t_B is accompanied by a sharp increase in the slope of the optical density *versus* time curve. This technique has been used previously by La Mer, Kenyon, and Zaiser,[3,4] and we have confirmed its validity by light scattering measurements. The Beckmann Model DU quartz spectrophotometer with fused silica cells was used. The reaction was maintained at 25°C. The variation of t_B with concentration is shown in Fig. 1. The characteristic minimum was observed for each of the sodium thiosulfate concentrations used.

It was noted with great interest that the optical density of the solution at t_B varied with initial concentration. This is shown in Fig. 2. The optical densities are based on a 10-cm light path and vary almost 1000-fold over the range investigated.

Zaiser and La Mer[4] have previously reported that for the limited range of reactant concentrations employed in the preparation of mono-dispersed sulfur sols, the optical density at t_B is constant. They assumed that at 3000A° absorption is due only to molecularly dispersed sulfur, and they interpreted the constant optical density as a measure of the critical supersaturation concentration of molecular sulfur.

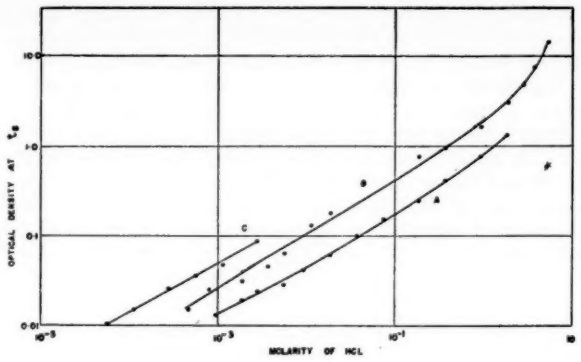

FIG. 2. Optical density at t_B *versus* HCl concentration.
A. 0.00203 *M* $Na_2S_2O_3$. B. 0.00520 *M* $Na_2S_2O_3$. C. 0.0124 *M* $Na_2S_2O_3$.

Our results indicate that even for the dilute range, the optical density at t_B is not constant. The variation could be interpreted as due to a change in the critical supersaturation concentration of sulfur with reactant concentration. However, it seems unlikely that this could account for the tremendous range of optical densities observed at t_B. It is more likely that molecular species other than sulfur which absorb at 3000A° are preferentially formed at the higher acid concentrations.

The polythionates have been identified among the acid decomposition products of thiosulfate.[5] Lorenzé and Samuel[6] have measured the absorption spectra of the polythionates. They give for the molar extinction coefficient of tetrathionate and pentathionate at 3000A°, 40, and 320, respectively. On the other hand, La Mer and Kenyon[3] found no appreciable absorption by tetrathionate at 3000A° and it was on the basis of this that they concluded that the transmission of their solutions during the homogeneous reaction was only a function of sulfur concentration. Messrs. Robert Penn and Carleton Hommel of this laboratory have redetermined the absorption spectra of tetrathionate and pentathionate and confirm the results of Lorenze and Samuel. This indicates that the optical density at 3000A° measures both polythionates and molecular sulfur.

This interpretation is consistent with the minimum in t_B. Both polythionates and sulfur are among the acid decomposition products of thiosulfate. The formation of polythionate is favored at higher acid concentrations so that although the rate of decomposition increases monotonically with acid concentration (as attested by the high optical densities atrained) the net rate of formation of sulfur becomes low, hence the large values of t_B.

[1] H. Reiss and V. K. La Mer, J. Chem. Phys. **18**, 1 (1950).
[2] Bassett and Durant, J. Chem. Soc. **129**, 1401 (1927).
[3] V. K. La Mer and A. S. Kenyon, J. Colloid Sci. **2**, 257 (1947).
[4] E. M. Zaiser and V. K. La Mer, J. Colloid Sci. **3**, 571 (1948).
[5] Janickis, Z. anorg. u. allgem. Chem. **234**, 193 (1937).
[6] Lorenze and Samuel, Z. physik. Chem. (B) **14**, 219 (1931).

The Polarization of Rayleigh Scattering As an Aid to the Determination of Molecular Orientation in Solids

E. G. Cox
Chemistry Department, University of Leeds, Leeds, England
(Received August 14, 1951)

ATTENTION[1] has been drawn by D. H. Rank to the value of the polarization of Rayleigh scattering ρ as an aid to the determination of molecular configuration in liquids. It may be of interest to point out that this constant can also be used to determine the approximate orientation of molecules in crystals. In the case of a non-associated molecule having two of its three principal polarizabilities equal or approximately so, the values of ρ and R, the molecular refraction, suffice to determine the numerical values of the polarizabilities; knowledge of the space-group, density, and refractive indices of the substance in the crystalline state then enables the approximate molecular orientation to be deduced. The results are not so accurate as those based on measurement of magnetic anisotropy, but the method is likely to be convenient for relatively simple substances of low melting point on which magnetic measurements are less easily made and for which the values of ρ are more likely to be available. A simple example is provided by benzene where it was found possible in this way to confirm the molecular orientation deduced by x-ray methods;[2] details of the calculation were not published at the time but are quoted by Hartshorne and Stuart.[3]

[1] D. H. Rank, J. Chem. Phys. **19**, 511 (1951).
[2] E. G. Cox, Proc. Roy. Soc. (London) **A135**, 491 (1932).
[3] *Crystals and the Polarizing Microscope* (Edward Arnold and Company, London, 1950), p. 151.

R-Branch Heads of Some CO_2 Infrared Bands in the $CO+O_2$ Flame Spectrum

W. S. BENEDICT
National Bureau of Standards, Washington, D. C.
AND
ROBERT C. HERMAN AND SHIRLEIGH SILVERMAN
Applied Physics Laboratory, The Johns Hopkins University, Silver Spring, Maryland*
(Received August 13, 1951)

SOME time ago the authors observed the presence of several small peaks on the short wavelength side of the CO_2 fundamental ν_3 in the emission spectrum of the $CO+O_2$ flame. These observations were made with a spectral slit width of ~ 8 cm^{-1}. Recently the spectrum was re-examined with a Perkin-Elmer spectrometer using a LiF prism, a sensitive Golay detector, and slit widths of 40 microns which give a resolving power of ~ 2.2 cm^{-1}. At this resolution these peaks were recognized as the *R*-branch heads of some of the vibration-rotation bands of the CO_2 molecule. The emission spectrum is shown in Fig. 1 together with the atmospheric transmission band of CO_2 at $\sim 4.2\mu$. A comparison of the observed and calculated positions of the *R*-branch heads found is given in Table I. The calculated values were obtained from well-known formulas[1,2] using a set of constants which were obtained in the course of a recent effort to fit all available data. These constants which differ slightly from previously published values[1] are given in cm^{-1} as follows: $\nu_1=1342.9$, $\nu_2=667.3$, $\nu_3=2349.3$, $X_{11}=3.06$, $X_{22}=0.67$, $X_{33}=22.5$, $X_{12}=-3.20$, $X_{13}=20.50$, $X_{23}=11.75$, $X_{ll}=-1.17$, $b^2=51.69(1-0.039\ V_3)$, $\alpha_1=0.00044$, $\alpha_2=-0.00072$, $\alpha_3=0.00307$, $B_0=0.3904$, and $D_0=1.8\times 10^{-7}$. The calculated value of the rotational quantum number at the *R*-branch heads of all the bands is $J(\text{head})=127$. The existence of moderately prominent heads is to be expected since in the $CO+O_2$ flame employed the rotational temperature has been determined from the CO overtone bands to be ~ 2700°K.[3]

TABLE I.[a]

Band	Transition	ν_0(cm^{-1})	ν (*R*-branch head) (cm^{-1}) Observed	Calculated
a	001 → 000	2349.3	2396.7	2397.1
b	01′1 → 01′0	2337.6	2385.3	2385.4
c	$\begin{Bmatrix}101\\02^01\end{Bmatrix} \rightarrow \begin{Bmatrix}100\\02^00\end{Bmatrix}$	2327.4	2377.1	2375.3
d		2326.3	2374.1	2373.9
	$02^21 \rightarrow 02^20$	2325.8	···	2373.6
e	002 → 001	2324.2	2372.4	2372.0

[a] Wave numbers are referred to vacuum (see Fig. 1).

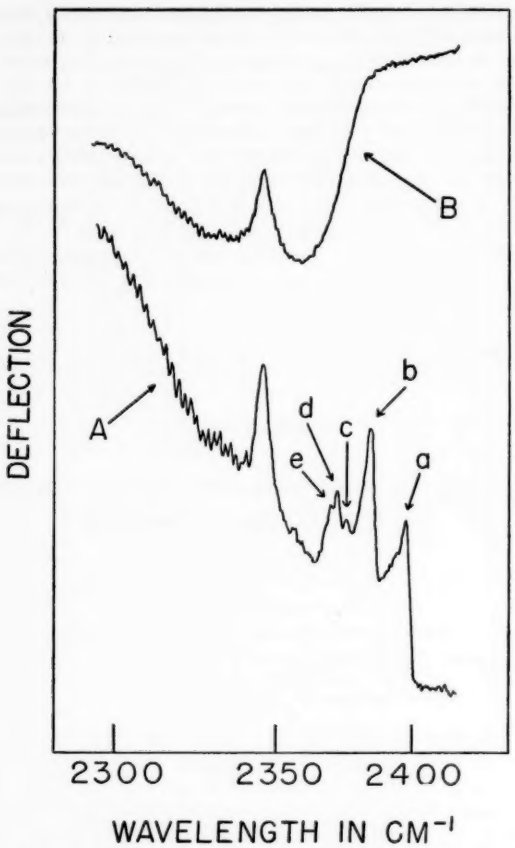

FIG. 1. (A) Infrared emission spectrum of the CO+O_2 flame showing the *R*-branch heads of several vibration-rotation bands of the CO_2 molecule. (B) The CO_2 atmospheric absorption band is shown for comparison.

It is clear that many additional bands from higher vibrational levels must appear in this spectral region. However, they are mostly at lower frequencies and overlap with each other as well as with the CO fundamental so that even high resolving power would be of little avail in unraveling these bands. It would be of interest to obtain the relative intensities of the bands reported in order to estimate a vibrational temperature. Unfortunately, the difficulties of overlap as well as atmospheric and self-absorption would seem to make this type of determination too inaccurate to be of much value.

* This work was supported in part by the U. S. Navy Bureau of Ordnance.
[1] D. M. Dennison, Revs. Modern Phys. 12, 175 (1940).
[2] G. Herzberg, *Infrared and Raman Spectra* (D. Van Nostrand Company, Inc., New York, 1945).
[3] Plyler, Benedict, and Silverman (submitted for publication).

Compressibilities of Concentrated Metal Ammonia Solutions*

ROBERT H. MAYBURY† AND LOWELL V. COULTER
Department of Chemistry, Boston University, Boston, Massachusetts
(Received August 14, 1951)

CONCENTRATED solutions of the alkali and alkaline earth metals in ammonia exhibit such characteristically metallic properties as high electrical conductivity,[1] reflectivity to light,[2] and degenerate paramagnetism.[3] In addition, these solutions, upon preparation, undergo an anomalous volume expansion with an accompanying decrease of density[4] indicating unusual orientation of the molecules and atoms in the solution. Further indication of this has been revealed by compressibility studies which are reported in part at this time.

Adiabatic compressibilities of concentrated sodium, lithium, calcium, and potassium iodide solutions have been determined between −33°C and −70°C from sound velocity measurements carried out by a modified electronic pulse technique.[5] Two *x*-cut quartz crystals were immersed face to face in the solution. The additional transit time of a sound signal sent from one crystal to the other upon increasing their separation by a measured amount was determined electronically. The Browning P-4 Synchroscope was used as the timing and presentation unit. Combination of the measured velocity with the corresponding density of the solution yields the adiabatic compressibility according to the expression:

$$\beta = 1/c^2\rho.$$

The results presented in Fig. 1 are striking in the case of the metal ammonia solutions in that the compressibility rapidly increases as the concentration increases. The generally observed behavior in the case of electrolyte solutions is a decreasing compressibility with increasing concentration, reflecting the operation of electrostrictive forces as is observed in the case of KI in ammonia. It appears that something other than electrolytic nature must be assigned to the metal ammonia solutions as a result of the observed compressibility behavior.

To account for the properties of the metal ammonia solutions, a model is proposed which regards these as an expanded metal[6] in

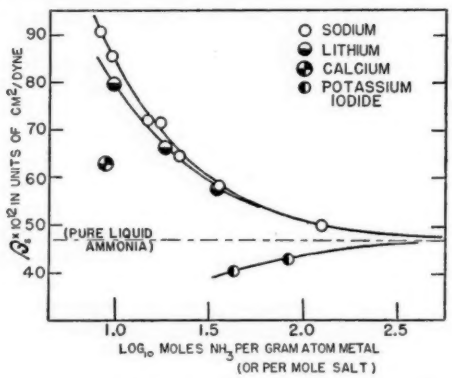

FIG. 1. Compressibilities of metal and KI ammonia solutions.

which the lattice unit is the cation solvated by six ammonia molecules having an outward orientation[3] of the hydrogens. This complex is reasonable in view of the strength of the ion-dipole bond as reflected in the existence of isolable solids as $Ca(NH_3)_6$ having metallic properties.[7] A degree of randomness, of course, exists in the lattice of the actual solution.

By analogy with metals the cohesive energy of the system arises from the binding together of the complexes by the metal valence electrons in the role of weak resonating covalent bonds.[8] That the metal electrons must be considered in such a role follows from the observed degenerate paramagnetism[3] implying Fermi statistical behavior and from the high electrical conductivity indicating broad conduction bands. The repulsive energy originates in the mutual electrostatic repulsion of the complexes since their exterior surfaces are composed of the hydrogen ends of ammonia dipoles.

The volume expansion observed suggests that a large equilibrium inter-complex distance is established in concentrated solutions by the mutual repulsion of the complexes; as a consequence, the magnitude of the attractive and repulsive forces at equilibrium is small. This conclusion provides a ready explanation of the observed high compressibility. The complexes are located in very shallow potential wells and as a result experience only small potential energy changes when the sound wave effects small displacements about the equilibrium position [i.e. $(\partial^2 V/\partial r^2)_{r=r_0}$ is very small and since $1/\beta \propto (\partial^2 V/\partial r^2)_{r=r_0}$, β is large as observed].

The individuality of the curves and the calcium point are accountable on the basis of the differences in the respective cohesive

energies of the pure metals which even in the greatly expanded lattices remain significant. In particular, the calcium-ammonia solution appears one-half as compressible as those of the alkalis, an expected result in view of the two valence electrons which increase the effective metallic binding.

The very low viscosities found by Kikuti[9] for these concentrated solutions may be understood by use of this model. As recently represented,[10] viscous flow involves the breaking of inter-complex bonds rather than the stronger intra-complex bonds. Thus in metal ammonia solutions the units of viscous flow are the complexes, the low viscosity indicating the weakness of the easily fractured inter-complex bonds which are the same weak bonds responsible for the high compressibility.

* Supported in part by a Frederick Cottrell Grant from the Research Corporation.
† Boston University Research Fellow supported by funds from the above grant.

[1] C. A. Kraus and W. W. Lucasse, J. Am. Chem. Soc. **43**, 2529 (1921); **44**, 1941 (1922).
[2] C. A. Kraus, J. Am. Chem. Soc. **29**, 1557 (1907).
[3] E. Huster, Ann. Physik **33**, 477 (1938).
[4] Kraus, Carney, and Johnson, J. Am. Chem. Soc. **49**, 2206 (1927).
[5] J. R. Pellam and J. K. Galt, J. Chem. Phys. **14**, 608 (1946).
[6] W. Hume-Rothery, *Atomic Theory for Students of Metallurgy* (The Institute of Metals, London, 1948), Chapter 26.
[7] C. A. Kraus, J. Am. Chem. Soc. **30**, 653 (1908).
[8] L. Pauling, *Nature of the Chemical Bond* (Cornell University Press, Ithaca, New York, 1945), second edition, Chapter 11.
[9] S. Kikuti, J. Soc. Chem. Ind. Japan **47**, 488 (1944).
[10] L. Grunberg and A. H. Nissan, Trans. Faraday Soc. **45**, 125 (1949).

Kinetics of the Exchange Reaction between Diborane and Deuterium

P. Calvin Maybury and W. S. Koski
Department of Chemistry, The Johns Hopkins University, Baltimore, Maryland

(Received August 20, 1951)

RECENT investigations on the kinetics of the pyrolysis of diborane[1,2] indicate that a BH_3 complex plays an important role in this reaction. These results have prompted us to make a brief report of some of our studies of the deuterium-diborane exchange which also appears to proceed through a complex involving BH_3.

The deuterium and diborane were mixed in glass bulbs which were rapidly raised to the reaction temperature. Bulbs were removed at various intervals of time and quenched in liquid nitrogen and the hydrogen-deuterium mixture was then removed and analyzed in a thermal-conductivity cell. The rate of appearance of hydrogen in the deuterium was used to follow the course of the reaction. The apparatus used was a modification of one described by Trenner.[3]

When the deuterium pressure was kept constant and the diborane pressure was varied from 4 cm to 40 cm, it was found that the order of the reaction was 1.6 with respect to diborane. On the other hand, when the diborane pressure was kept constant and the deuterium pressure was varied from 5 cm to 40 cm, the reaction appeared to show a zero-order dependence on deuterium. The course of the reaction can be satisfactorily represented by the usual reversible exchange equation[4] if the concentrations are in equivalents. The specific rate constant at 55°C was found to be 3.8×10^{-3} liter/equiv. sec.

The exchange was studied in a temperature range from 35°C to 75°C and from a plot of the log of the specific rate constants *versus* $1/T$, it was found that the experimental activation energy was approximately 18 kcal. To within our experimental error the plot was found to be linear, indicating that all of the hydrogens in diborane were exchanging at the same rate.

The reaction shows a relatively small surface effect. Changing the surface to volume ratio by 15 in Pyrex approximately doubled the rate. Using 5 g of glass wool in the reaction vessel had a similar effect on the rate. Pyrex reaction vessels covered with fluorocarbons or polystyrene or reaction vessels made of Tygon tubing failed to slow down the reaction measurably. We therefore conclude that the reaction is in the main homogeneous.

In some experiments the reaction was carried out in complete darkness, and the same rates were obtained indicating that the reaction was not appreciably affected by ordinary laboratory light.

The experimental results appear to be compatible with the following series of reactions representing the mechanism of the exchange. The first two reactions are considered to be rapid and the last reaction is the rate determing step.

$$B_2H_6 \rightleftarrows 2BH_3 \quad (1)$$

$$BH_3+D_2 \rightarrow BH_3D_2 \quad (2)$$

$$BH_3D_2+B_2H_6 \rightarrow B_2H_5D+BH_3+HD. \quad (3)$$

Equation (2) suggests that the presence of inert diatomic gases may influence the rate of the exchange and we are currently looking into this effect. We are also studying the rate of the exchange between normal diborane and completely deuterated diborane since this reaction may give us a better insight into the mechanism, especially the reaction represented by Eq. (1). These results and others will be reported in detail in the near future.

We are indebted to Dr. A. N. Webb of the University of California for some of the results of his unpublished experiments on this reaction.

[1] R. P. Clarke and R. N. Pease, J. Am. Chem. Soc. **73**, 2132 (1951).
[2] Bragg, McCarty, and Norton, J. Am. Chem. Soc. **73**, 2134 (1951).
[3] N. R. Trenner, J. Chem. Phys. **5**, 382 (1937).
[4] G. Friedlander and J. W. Kennedy, *Introduction to Radiochemistry* (John Wiley and Sons, Inc., New York, 1949), p. 285.

Errata: The Dielectric Constant of Water and the Saturation Effect

[J. Chem. Phys. **19**, 391–394 (1951)]

F. Booth
Department of Theoretical Physics, King's College, London, England

IN the above communication (referred to hereafter as I) the writer gave an analysis of the saturation effect in polar dielectrics. A general formula (Eq. (3.10)) was obtained for the dielectric constant ϵ, in terms of the applied field strength E, and certain mean moments $A[\mathbf{M}^{2n}]$, and $(\boldsymbol{\mu}\cdot A[\mathbf{M}^{2n+1}])$ defined in Eq. (3.8). The theory was applied to water using the Kirkwood model, in which it is assumed that ordering is complete for nearest neighbors but vanishes outside this region. To evaluate the mean moments Eqs. (3.14) were used. These relations enable ϵ to be expressed as a simple analytical function of E. In the text of I it was implied that they are exact. This is not so, however, except in the trivial cases of n equal to 1 or 0, respectively. Hence the use of Eqs. (3.14) constitutes an additional approximation; alternatively, they may be regarded as representing a modified form of the Kirkwood model.

It is not difficult, however, to obtain exact expressions for the mean moments in the case of the simple rough model we have assumed. For a given direction of a particular molecule there are three possible directions of each of the dipoles forming the four nearest neighbors.[1] Hence there are in all 81 possible distinct configurations of the group of 5 dipoles as a whole, each set of directions having the same probability as any other. The various possible values of the total moment of the group, together with the weights, are easily found by simple enumeration. From these the required average moments are found immediately, and we have

$$A[\mathbf{M}^{2n}]=\frac{\mu^{2n}}{81}[4+8.3^n+28.5^n+16.9^n+12.11^n+4.13^n+8.17^n+25^n], \quad (1)$$

$$(\boldsymbol{\mu}\cdot A[\mathbf{M}^{2n+1}])=\frac{\mu^{2n+2}}{81}[4+8.3^n+52.5^n+40.9^n+36.11^n+12.13^n+32.17^n+5.25^n]. \quad (2)$$

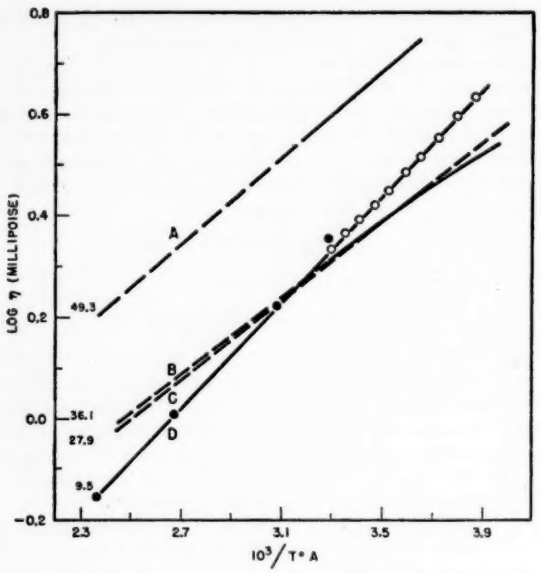

FIG. 1. The dielectric constant ϵ of water at 300°C, as a function of the field strength E (in 10^7 volts per cm). Curve 1, Eq. (3.15), paper I. Curve 2, from Eqs. (1) and (2).

Substituting Eqs. (1) and (2) in Eq. (3.10) of paper I gives the dielectric constant ϵ. The two series of Eq. (3.10) cannot be summed directly, and it is necessary to evaluate them numerically for each value of the field strength. For high field strengths they are both very cumbersome, since, owing to the slow convergence it is necessary to employ a large number of terms.

In Fig. 1 we have plotted ϵ as a function of E, using the old formula Eq. (3.16) of paper I, and the method just described. It will be seen that the new values give rather less saturation at low field strengths but approximate closely to the old for very high fields. Instead of Eq. (3.16) of I, we find for low field strengths

$$\epsilon = n^2 + \frac{14N_0\pi(n^2+2)^2\mu_v^2}{27kT}\left[1-\frac{49E^2\mu_v^2(n^2+2)^2}{540k^2T^2}\right]. \quad (3)$$

The second term in the bracket of Eq. (3.16) should be divided by 3; hence the saturation term at low fields is reduced by 33 percent in the new formulation.

For very intense fields the moments with n very large become the important terms in the series of Eq. (3.16) in paper I. For these we may take $\mathbf{M}=5\boldsymbol{\mu}$ and we then find approximately

$$\epsilon = n^2 + \frac{4\pi N_0\mu_v(n^2+2)}{3E}L\left(\frac{5[n^2+2]\mu_v E}{2kT}\right) \backsimeq n^2 + \frac{4\pi N_0\mu_v(n^2+2)}{3E}. \quad (4)$$

[1] H. Frohlich, *Theory of Dielectrics* (Oxford University Press, New York, 1949), 140, Fig. 40.

A Nuclear Magnetic Parameter Related to Electron Distribution in Molecules

H. S. GUTOWSKY, D. W. MCCALL, B. R. MCGARVEY, AND L. H. MEYER
Noyes Chemical Laboratory, University of Illinois, Urbana, Illinois*
(Received July 31, 1951)

OBSERVATIONS made on binary covalent fluorides have shown that molecular differences in the F^{19} nuclear magnetic shielding are proportional to the electronegativity of the atom to which the observed F^{19} nucleus is chemically bound.[1] The F^{19} magnetic shielding increases when the F^{19} nucleus is bound to less electronegative atoms. A higher applied magnetic field is required at a fixed resonance frequency for the more magnetically shielded nuclei. This note is a preliminary account of the determination of electron distribution in substituted benzenes by measuring the effect of the substituent group on the F^{19} magnetic shielding in the appropriate fluorobenzene.

Table I lists results obtained from several *o*-, *m*-, or *p*-, substituted fluorobenzenes. The nuclear magnetic shielding parameter δ is defined as $10^5\times(H_r-H_c)/H_r$. H_c is the applied magnetic field required for the F^{19} resonance in the substituted fluorobenzene, at a fixed resonance frequency of 25.5 megacycles/sec, and H_r is the magnetic field required for fluorobenzene. This definition of δ is such that it gives apparent relative electric charges, measured with respect to the phenyl group. Approximate magnitudes of differences in electron distribution are given by the observation for the binary covalent fluorides[1] that $dE_n/d\delta \cong 4\times10^{-2}$ where E_n is the electronegativity on the Pauling scale.[2] The apparent electronegativity of the substituted phenyl group to which the F^{19} is bound should be proportional to the experimental δ-value. On this basis, the range of δ in Table I corresponds to 0.1 electronegativity unit.

In Fig. 1, values[3] of Hammett's σ are plotted against δ-data from Table I. The two parameters are generally in good agreement; however, the σ-intercept is at about +0.20, indicating a systematic difference. The σ-values are determined by the effect of the substituent on reaction rates or ionization constants, assuming identical entropies of activation for all substituted compounds as well as for the unsubstituted reference.[3] To the extent that this assumption is invalid, σ is a composite term including not only the influence of the substituent on electronic distribution and thereby the activation energy, but also incorporating differences in entropy of activation. The magnetic shielding δ is a purely electronic phenomenon. It appears probable that the small differences in the two scales correspond to the effects of substitution on the entropy of activation. Values of δ from orthofluorobenzenes

TABLE I. F^{19} Nuclear magnetic shielding δ-values for several substituted benzenes.

Substituent	δ	Substituent	δ
o-NH_2	−2.20	*p*-Cl	−0.22
m-NH_2	+0.02	*p*-OCH_3	−1.12
p-NH_2	−1.42	*p*-CN	+0.97
o-Cl	−0.18	*p*-phenyl	−0.42
m-Cl	+0.18	*m*-CF_3	+0.18

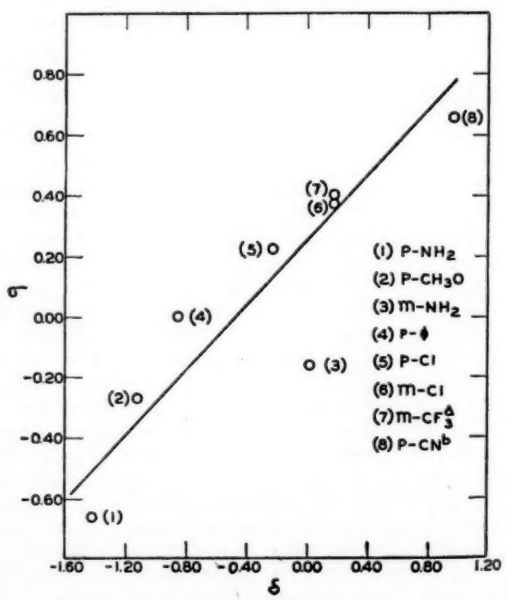

FIG. 1. A plot of Hammett's (reference 3) σ *versus* values of δ from Table I. [(a) Roberts *et al.*, J. Am. Chem. Soc. **72**, 408 (1950); (b) Roberts and McElhill, J. Am. Chem. Soc. **72**, 628 (1950).]

can be combined with kinetic data to evaluate the larger entropy or "steric" effects associated with ortho-substituents.

A detailed account of this and related work will be submitted for publication elsewhere.[4] Experiments in progress include observations on polysubstituted fluorobenzenes, napthalene derivatives, and other aromatic compounds, as well as selected aliphatic derivatives.

We wish to thank Dr. Glenn C. Finger, head of the Fluorospar Division of the Illinois State Geological Survey, who very generously gave us samples of many of the compounds used in this research. Equipment was furnished mainly by a grant-in-aid from Research Corporation.

* Supported in part by the ONR.

[1] H. S. Gutowsky and C. J. Hoffman, J. Chem. Phys. **19**, 1259 (1951). For a preliminary account, a bibliography, and a brief description of experimental details see Phys. Rev. **80**, 110 (1950).

[2] Linus Pauling, *The Nature of the Chemical Bond* (Cornell University Press, Ithaca, New York, 1940), second edition, p. 64.

[3] L. P. Hammett, *Physical Organic Chemistry* (McGraw-Hill Book Company, Inc., New York, 1940), p. 184.

[4] J. Am. Chem. Soc. (to be published).

Effect of Organic Substances on the γ-Ray Oxidation of Ferrous Sulfate

H. A. Dewhurst

Department of Natural Philosophy, University of Edinburgh, Edinburgh, Scotland

(Received August 23, 1951)

SMALL quantities of impurities have been known for some time to exert an important effect on the course of reactions induced by radiation in aqueous solution.[1] In systems where the buildup of hydrogen peroxide during irradiation is appreciable these traces of impurities are of considerable importance,[2] but even in cases where the steady-state concentration of hydrogen peroxide is presumably low they have been found to exert a significant influence. Thus Harker[3] reported that the oxidation of ferrous ions by γ-rays was accelerated or retarded by the addition of small amounts of various organic and inorganic substances, although the actual substances used were not specified. It is obvious, therefore, that effects of this sort must be carefully examined during any study of the kinetics of a radiation-induced reaction in aqueous solution, and particularly so when any such reaction is proposed as a basis for integral dosimetry.

The author has recently completed a series of experiments in which a number of aliphatic alcohols were added to solutions of ferrous sulfate in 0.8N sulfuric acid, and the effect of these on the initial oxidation yield for ferrous ions studied. The solutions were prepared with specially purified water and were saturated with air. The ferrous ammonium sulfate was of AR grade as were most of the alcohols which were used without further purification. 5 ml samples were irradiated with the γ-rays from a Co^{60} source of approximately two curies activity.

The initial oxidation yields are expressed in terms of $G_{Fe^{++}}$, the number of ferrous ions oxidized per 100 ev absorbed in the solution, and were obtained from plots of Fe^{++} ions oxidized against the energy absorbed in the solution. The amount of energy absorbed in the solutions was measured by the degree of oxidation of standard ferrous sulfate solutions using the oxidation yield which has been established by Miller.[4]

It was found that the aliphatic alcohols had a pronounced accelerating effect on the initial oxidation yield. In all cases the amount of oxidation was found to be a linear function of the energy absorbed, at least in the initial stages of the reaction. An interesting feature that emerged was that, in solutions of 5×10^{-4} M initial Fe^{++} ion concentration, the initial oxidation yield increased with the length of the carbon chain for a series of normal alcohols in equimolar concentration. Typical results are given in Table I. Similar behavior can be seen in the work of Fricke and Brownscombe[5] on the effect of a series of monobasic aliphatic acids on the reduction of dichromate solutions by x-rays. It was also observed by the author that branched chain alcohols were less effective, on an equimolar basis, than were the corresponding normal alcohols.

TABLE I. Effect of aliphatic alcohols on the initial oxidation yield for ferrous ions. Dose rate $=1.23\times10^{17}$ ev/hr/Ml.

Alcohol	(ROH) M×10⁵	$(Fe^{++})i$, M×10⁴	(NaCl) M×10²	$G_{Fe^{++}}$ ions oxid/100 ev
None	···	2	···	20.3
None	···	2	1	20.0
Ethanol	3.4	2	···	25.5
Ethanol	3.4	2	1	20.4
Ethanol	10	2	···	35.1
Ethanol	10	2	10	20.2
n-Propanol	10	5	···	34.2
iso-Propanol	10	5	···	27.2
n-Pentanol	10	4.7	···	39.0

The effect of the alcohols may be interpreted on the basis of a mechanism given below, parts of which are familiar from the studies of Kolthoff and Medalia[6] on the effect of organic compounds on the $Fe^{++}-H_2O_2$ reaction in the presence of oxygen.

The primary process of the absorption of γ-radiation in water is generally agreed to result in the formation of H atoms and OH free radicals.[7] An alcohol molecule will compete with ferrous ions for the OH radicals, thus:

$$RCH_2OH+OH\rightarrow RCHOH+H_2O. \quad (1)$$

The resulting organic free radical will react readily with dissolved oxygen to form an organic peroxide,

$$RCHOH+O_2\rightarrow RCHOH, \quad (2)$$
$$\qquad\qquad\quad O_2$$

which will ultimately lead to the further oxidation of two or more ferrous ions. Therefore, in this way it is possible to explain qualitatively the enhanced initial oxidation yields in the presence of alcohols.

The addition of sodium chloride in sufficient concentration to the ferrous-alcohol solutions was found to suppress the effect of the alcohol completely, the initial oxidation yield being restored to its value in the presumed absence of organic materials. Experiments under the same conditions but in the absence of alcohol have shown that the chloride ion had a negligible effect on the ferrous oxidation yield. (See Table I.) Any organic impurities in the water and other reagents used (acid and ferrous salt) were therefore in such low concentration as to have no detectable influence on the oxidation. These observations on the effect of the chloride ion are in accord with the recent work of Kolthoff and Medalia[6] and of Baxendale *et al.*[8] on the $Fe^{++}-H_2O_2$ reaction. According to Merz and Waters[9] the chloride ion acts by a radical transfer mechanism. Thus chlorine atoms produced by the reaction,

$$Cl^-+OH+H^+\rightarrow Cl+H_2O, \quad (3)$$

prefer to oxidize ferrous ions rather than undergo a reaction of type (1). As a result organic peroxides are not formed and the resultant acceleration is suppressed.

The bearing of this work on the application of the ferrous oxidation reaction as a mode of integral dosimetry is being studied in this laboratory.

The author wishes to express his gratitude to Dr. N. Miller for many valuable discussions, to the University of Edinburgh for the tenure of a research fellowship, and to I.C.I. Ltd. for a grant in aid of this work.

[1] See for example: W. Stenstrom and A. Lohmann, Radiology **16**, 322 (1931); G. L. Clark and W. S. Coe, J. Chem. Phys. **5**, 97 (1937); Fricke, Hart, and Smith, J. Chem. Phys. **6**, 229 (1938).

[2] A. O. Allen, J. Phys. Colloid Chem. **52**, 479 (1948).

[3] G. Harker, Nature **133**, 378 (1934).

[4] N. Miller, J. Chem. Phys. **18**, 79 (1950).

[5] H. Fricke and E. R. Brownscombe, J. Am. Chem. Soc. **55**, 2358 (1933).

[6] I. M. Kolthoff and A. I. Medalia, J. Am. Chem. Soc. **71**, 3784 (1949).

[7] See F. S. Dainton, Ann. Reports Chem. Soc. **45**, 15 (1949).

[8] Baxendale, Barb, George, and Hargrave, Trans. Faraday Soc. **47**, 462 (1951).

[9] J. H. Merz and W. A. Waters, J. Chem. Soc. S15 (1949).

Heats of Combustion and Formation of Some Organosilicon Compounds

TOSHIO TANAKA, UKIKO TAKAHASHI, ROKURO OKAWARA, AND TAKEO WATASE

Institute of Industrial Chemistry, Faculty of Engineering, Osaka University, Osaka, Japan

(Received July 30, 1951)

REGARDING the heats of combustion of organosilicon compounds no report has yet been obtainable in accordance with the calorimetric bomb procedure. We have recently measured the heats of combustion of five such substances (i.e., hexamethylcyclotrisiloxane, hexaphenylcyclotrisiloxane, diethylsilanediol, dimethyldiethoxysilane, and di-*n*-propyldiethoxysilane) using Berthelot-Mahler's bomb calorimeter. We have found the products of combustion to be carbon dioxide, water, and silica by chemical analysis.

Our measurements were made upon materials highly purified by means of fractional distillation and recrystallization. Because of their volatility, the liquid substances were sealed into the thin-walled ampoules of soft glass. We filled the ampoule with the liquid so that there might be no air left within it and that the ampoule might remain filled up at the temperature in the calorimeter. We performed its preliminary ignition by using a cotton string tied to an iron wire, the string being soaked with promoter which was kept touching on the ampoule. Under these conditions the glass fused quietly to allow a smooth combustion. For the same purpose Moore and his co-workers[1] employed specially formed glass capsules whose volumes were 0.5 to 0.8 ml and which weighed 0.065 to 0.085 g empty, while in our experiment the ampoules were of a single spherical form and the relation of weight and volume was similar to Moore's.

To determine the energy equivalent of the calorimeter at 20°C, we used Huffman's value of 6319.0 cal g^{-1} for the heat of combustion of the standard benzoic acid.[2] The resulting molar heats of combustion at 20°C and 1 atmos constant pressure, expressed in terms of the defined kilocalorie, and given under $-\Delta H_R$ in the sixth column of Table I. Each value represents the average of four to six combustion measurements and should not involve an overall uncertainty in excess of ±0.10 percent. The corresponding values for the heat of formation from the elements ($-\Delta H_f^0$) have been computed by use of −68.3174 kcal, −94.0518 kcal, and −203.34 kcal for the ΔH_f^0 of H_2O (1), CO_2 (*g*), and SiO_2 (*s*), respectively.[3]

Further, we calculated $-\Delta H_f^0$, calc in the eighth column of Table I, by using the following data in accordance with the presumptions below: data—heat of formation for the elements from monoatomic gas (85.0, 59.1, 51.7, and 124.3 kcal $mole^{-1}$, for the silicon, oxygen, hydrogen, and carbon);[4] bond energy (87.3, 57.6, 89.3, and 70.0 kcal $mole^{-1}$, for C−H, C−Si, Si−O and C−O);[4] resonance energy (39 kcal $mole^{-1}$, for benzene nucleus);[4] presumption—the heat of vaporization was presumed according to Clausius-Clapeyron's equation, and the heat of fusion was assumed to be one-tenth of that of vaporization.

TABLE I. Molar heat of combustion and formation at 20°C.

Substance	Formula	Melt. pt.	Boil. pt.	Mole wt.	$-\Delta H_R$ kcal $mole^{-1}$	$-\Delta H_f^\circ$, kcal $mole^{-1}$ obs	calc
Hexamethylcyclotrisiloxane	$[(CH_3)_2SiO]_3$	64.5°C	···°C	222.384	1434.5	356.5	353.5
Hexaphenylcyclotrisiloxane	$[(C_6H_5)_2SiO]_3$	190	···	594.780	4802.4	232.4	139
Diethylsilanediol	$(C_2H_5)_2Si(OH)_2$	96	···	120.196	771.5	219.5	193.6
Dimethyldiethoxysilane	$(CH_3)_2Si(OC_2H_5)_2$	···	113.5	148.248	1119.2	197.5	174.0
Di-*n*-propyldiethoxysilane	$(n\text{-}C_3H_7)_2Si(OC_2H_5)_2$	···	179–180	204.352	1727.3	240.6	203.6

[1] Moore, Renguist, and Parks, J. Am. Chem. Soc. **62**, 1505 (1940).
[2] H. M. Huffman and E. L. Ellis, J. Am. Chem. Soc. **57**, 41 (1935).
[3] F. R. Bichowsky and F. D. Rossini, *The Thermochemistry of the Chemical Substances* (Reinhold Publishing Corporation, New York, 1936). Wagman, Kilpatrick, Taylor, Pitzer, and Rossini, J. Research Natl. Bur. Standards, **34**, 143 (1945).
[4] Linus Pauling, *The Nature of the Chemical Bond* (Cornell University Press, Ithaca, New York, 1940), second edition.